Remarkable *in vitro* Assemblies of a Bacterial Cytoskeletal Protein, FilP and its Derivatives

Emily Louise Alcock

100039421

A thesis submitted for the degree of Doctor of Philosophy

University of East Anglia

School of Biological Sciences

November 2020

Abstract

Intermediate filaments form a part of the cytoskeleton in eukaryotes. Intermediate filaments can self-assemble into large, non-polar higher order structures and have a characteristic domain architecture. Few homologues of intermediate filaments in bacteria have been identified. The protein FilP from *Streptomyces coelicolor* is thought to be intermediate filament-like and is the focus of this thesis.

In this thesis FilP is compared to eukaryote intermediate filaments to show that FilP does have a great deal of similarity to those and fits the classical definition of intermediate filaments in many ways, although there are a few key differences. A notable difference is the unusual 51-mer repeat sequence seen in its coil 2. Characterisation of FilP higher order assembly *in vitro* reveals the higher order structures formed in varying buffer conditions using transmission electron microscopy. FilP was found to form a rope structure, characteristic of intermediate filaments, and other structures including a striated structure.

A series of FilP variants were generated, expressed and purified which were designed to identify the essential regions for FilP for higher order assembly. The variants were observed by transmission electron microscopy which that the C terminal end of the coil 2 subdomain was essential for the formation of higher order structures. Expression of these FilP variants in *Escherichia coli* yielded surprising results in that the length of the cells when grown on cellophane increased dramatically from a normal length. Intriguingly, cells expressing a small section of 51-mer repeat sequence dramatically affected the morphology of the cells. This suggests that FilP interacts with the cell division machinery within *Escherichia coli*. A FilP knockout strain of *Streptomyces coelicolor* revealed that FilP is involved in the structural integrity of the cell. FilP localisation within *Streptomyces coelicolor* was also observed.

These experiments clearly show that FilP is involved in the cytoskeleton of the cell and displays characteristics of intermediate proteins. However, it does not exactly fit the strict definition of intermediate filaments. This research opens up the discussion what constitutes an intermediate filament.

Table of Contents

List of Figures

List of tables

Acknowledgements

I would like to thank my supervisor Gabriella Kelemen for her support and guidance during my time in her laboratory. I am especially thankful for her moral support when I was losing the plot while staring at a grey screen on the TEM.

To my wonderful friends who have supported me in lab and beyond; Kavana Bywater-Brenna, Gemma Cassettari, Mashael Alanazi, Lucy Clark, Sundeep Kaur and Elena Tan, I don't know how I would have coped without you wonderful crazy people and the sing-alongs to Disney music in lab. Apologies to anyone who heard us. Thanks also goes to my wonderful undergrad students who helped me on parts of this project, particularly to Jess Fong and Masie Greenwood who more than made up for putting restriction enzymes in my plasmid stocks on their first day…

Thanks is also due to my wonderful family and Charel Wohl for supporting, allowing and encouraging me to pursue my research. Many thanks for listening intently when I ramble on about what I have been doing even though you do not know what I am going on about.

1 Introduction

1.1 Cytoskeletal Proteins

The eukaryotic cytoskeleton comprises of three main components: microtubules, microfilaments and intermediate filaments. Microtubules (such as tubulin) have a diameter of ~25 nm, microfilaments (such as actin) have a diameter of ~ 6 nm and intermediate filaments are in between at ~10 nm in diameter (A. a Chernyatina et al., 2015; Herrmann and Aebi, 2004; Parry and Steinert, 1992). They are all polymeric structures which are organised into networks which resist deformation but can reorganise in response to externally applied forces (Fletcher and Mullins, 2010). The eukaryotic cytoskeleton has three broad functions: allowing the cell to indirectly respond to the external environment; arranging and maintaining integrity of intracellular compartments; and generating coordinated forces which allow the cell to move and change shape.

The cytoskeleton is dynamic and adaptive. The polymerisation and depolymerisation of microtubules and microfilaments generate directed forces that drive changes in cell shape and, together with molecular motors, guide organisation of the cellular components. This process is controlled by several classes of regulatory proteins including: nucleation-promoting factors, which initiate filament formation; capping proteins, which terminate filament growth; polymerases, which promote faster filament growth; depolymerisation factors and severing factors which disassemble the filaments; and cross-linkers and stabilisers which organise and reinforce higher-order assemblies (Fletcher and Mullins, 2010).

Microtubules and microfilaments are both polarised polymers with the subunits being structurally asymmetrical. This means that both are suitable as tracks for molecular motors which will move towards one pole or the other. Microtubule molecular motors are mainly from the dynein or kinesin families whereas microfilament molecular motors are often from the myosin family.

1.2 Microfilaments

Microfilaments are much less rigid than microtubules but the presence of high levels of cross-linkers promotes assembly of highly organised, more rigid structures. This allows the formation of highly bundled or branched networks and can aid in processes like supporting the leading edge of most motile cells and generating forces involved in changes in cell shape. Unlike microtubules, microfilaments do not switch between discrete states of polymerisation and depolymerisation. Instead, they elongate steadily in the presence of nucleotide bound monomers which produces the sustained forces required to advance the leading edge of the migrating cell (Pollard and Borisy, 2003). Microfilaments are continually assembled and disassembled in response to local signalling systems unlike microtubules which are organised from one or two organising centres (Fletcher and Mullins, 2010).

Actin, a microfilament, is the most abundant protein in most eukaryotic cells, as well as being involved in more protein-protein interactions than any known protein (Dominguez and Holmes, 2011; Schmidt and Hall, 1998). There are two forms of actin observed, the monomeric G-actin, and the polymerised F-actin. F-actin consists of two protofilaments which are twisted around each other to form a right-handed double helix (van den Ent et al., 2001). These actin polymers are the determinants for the shapes of many eukaryotic cells besides having a range of other functions such as motility, muscle contraction, and contraction of the cell during cell division. Many of these processes are mediated through indirect interaction with the cell membrane (Doherty and McMahon, 2008).

1.3 Microtubules

Microtubules are the stiffest of the three components of the cytoskeleton. It has the most complex assembly and disassembly dynamics. Its persistence length, which is a measure of flexibility, is so large (~5 mm) that single microtubules can span the length of a typical animal cell (Brangwynne et al., 2006) though they are known to buckle under excessive loads. Within eukaryotic cells, microtubules form highways for traffic as well as the mitotic spindles. Microtubules can switch between stably growing and rapidly shrinking forms (Mitchison and Kirschner, 1984). This dynamic instability allows it to rapidly reorganise and allows individual microtubules to quickly search a space, this can be up to 1000 times faster than a polymer which relies on its sensitivity to concentration changes in its constituent subunits or the actions of regulatory proteins (Holy and Leibler, 1994).

Tubulins are globular proteins and α- and β-tubulins polymerise into microtubules. They show dynamic instability and have phases of shrinking and growing. Dimers of α- and β-tubulin polymerise by binding to GTP at the nucleotide exchange site in β-tubulin and it can then assemble on the + end of the microtubule (Howard and Hyman, 2003). Whether the β subunit is bound to GTP or GDP affects the stability of the structure. When GTP is bound, the structure is more stable, when GDP is bound it is less stable and tends to dissociate (Heald and Nogales, 2002). Microtubules function in many processes within eukaryotic cells including structural support, intracellular transport and DNA segregation (Stanton et al., 2011). Microtubules have two distinct ends, a + and - ends with α-tubulin exposed on the - end, and β-tubulin exposed on the + end. In most cells, the dimers associate into 13 parallel protofilaments (Figure 1.3.1) which curl round into a tube shape (McIntosh et al., 2009; Sui and Downing, 2010).

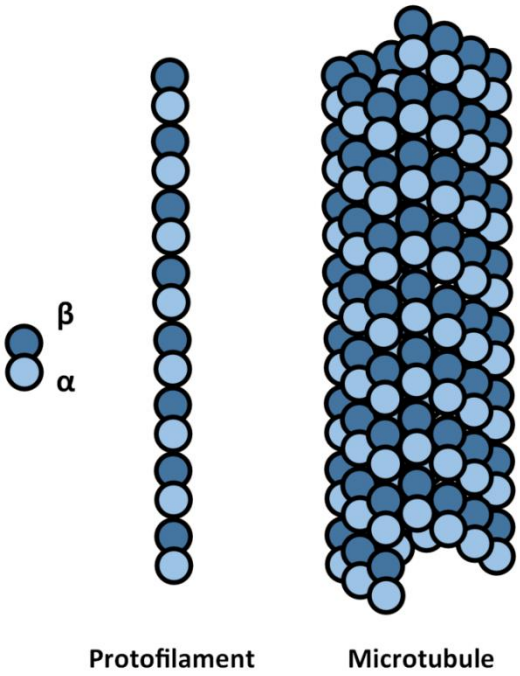

Figure 1.3.1 α and β tubulin form protofilaments and microtubules.

Diagram of tubulin α (light blue) and (dark blue) β tubulin which forms protofilaments and microtubules. Image based on (Pilhofer et al., 2011).

1.4 Intermediate Filaments

Intermediate filaments were first identified as part of the eukaryotic cytoskeleton, along with microfilaments and microtubules. The cytoskeleton has three broad functions: indirectly connecting the cell to the external environment; arranging and maintaining integrity of intracellular compartments; and generating coordinated forces which allow the cell to move and change shape. There are five main families of intermediate filaments in eukaryotes, four cytoplasmic and one nuclear. Acidic and basic keratins in epithelial cells such as in the skin or kidneys form type I and II respectively, vimentin in mesenchymal cells forms type III and neurofilament in neurons forms type IV. These four types are cytoplasmic. Type V intermediate filaments are found in the nucleus of all nucleated cells and are the lamins (Hesse et al., 2001).

Eukaryotic Intermediate filaments are the least stiff of the cytoskeletal components. They resist tensile forces much better than they resist compressive forces. They can be crosslinked to each other, as well as to microtubules and microfilaments, by plectins (Wiche, 1998). Many cell types assemble intermediate filaments in response to mechanical stress (Flitney et al., 2009). Unlike microtubules and microfilaments, intermediate filaments are not polarised and cannot, therefore, support directional molecular motors.

The structure of the intermediate filaments is part of what defines them. Intermediate filaments have a tri-partite structure with a variable head domain at the N-terminus, a variable tail domain at the C-terminus, and a central rod domain which is characterised by domains which form coiled-coils. This rod domain is separated into three sub-domains: coil 1A, coil 1B and coil 2 (Figure 1.4.1). It is typically 310 or 350 amino acids in length for cytoplasmic or nuclear intermediate filaments respectively although there is low sequence conservation between them (A. a Chernyatina et al., 2015; Herrmann and Aebi, 2004).

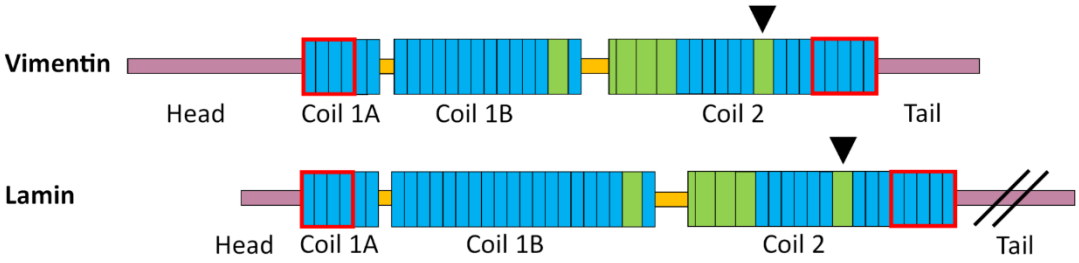

Figure 1.4.1 Vimentin and Lamin C domain architecture.

The blue boxes show α-helical segments predicted or shown to form a heptad coiled-coil repeat sequence, green boxes show segments predicted to form hendecad repeat sequences, the yellow boxes show predicted linker subdomains, purple boxes show head and tail domains. Black arrows show the characteristic stutter (a hendecad motif present in the middle of the coil 2 subdomain) for intermediate filaments. Red outlined box shows conserved subdomains. Proteins shown with N-terminus on the left. Figure based on data from (Kapinos et al., 2010; Köster et al., 2015).

1.5 Coiled-coils

Coiled-coil interactions between helices are ubiquitous in protein in all kingdoms of life (Gruber and Lupas, 2003; Walshaw et al., 2010). The α-helical fold, which makes up the coiled-coil, was first proposed by Linus Pauling as a fundamental part of protein secondary structure (Pauling and Corey, 1951) which was followed by the interpretation by Francis Crick (Crick, 1953). Coiled-coils are characterised by repeat sequences of residue properties. The most common coiled-coil is the canonical heptad repeat whereby the seven positions in the repeat sequence are given the letters a to g (Gruber and Lupas, 2003). Amino acids in positions a and d have hydrophobic properties and are referred to as the 'core' positions. Amino acids at positions e and g have electrostatic properties. When these heptad repeat sequences form an α-helix, there are approximately two turns for every repeat sequence (Figure 1.5.1), with 3.6 amino acid residues per turn (Gruber and Lupas, 2003). This allows the hydrophobic residues (positions a and d) to be located on the same side of the α-helix and a hydrophobic streak is introduced along one side of the α-helix with the electrostatic residue positions flanking it. The 3.6 amino acid residues per turn makes the hydrophobic streak slightly left-handed rather than perfectly straight due to the non-perfect alignment of the hydrophobic residues. When two α-helices interact along the hydrophobic streak, the streak becomes buried at the interface of the interaction. This assembly is called a left-handed coiled-coil (Gruber and Lupas, 2003).

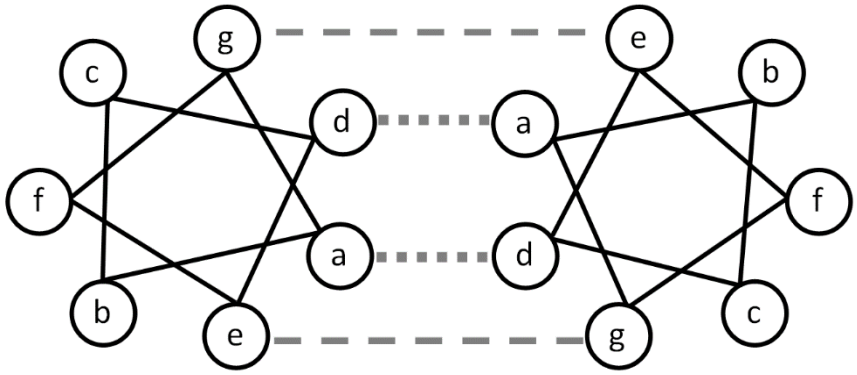

Figure 1.5.1 A heptad repeat sequence in a coiled-coil domain.

Each letter represents a different amino acid repeat position. The square dashed lines between positions a and d are hydrophobic interactions and the elongated dashed lines between positions g and e are electrostatic interactions.

Though the heptad repeat is the most common, it is not the only repeat sequence known for coiled-coils. Other numbers of repeat sequences have been observed (Gruber and Lupas, 2003; Kühnel et al., 2004). With eleven amino acids in the repeat sequence, the hendecad repeat sequence has three helical turns per repeat and the hydrophobic residues are typically found at positions a, d and h. This hendecad repeat sequence generates a slightly right-handed hydrophobic streak (Gruber and Lupas, 2003). When two α-helices of this nature associate, a slight right-handed coil is formed. However this is so slight that the two coils are almost parallel to the axis of the helices with hardly any coiling of the two coils around each other (Nicolet et al., 2010). Because of the lack of coiling, these α-helical assemblies are sometimes referred to as a bundle rather than a coiled-coil.

The positions of the hydrophobic and charged residues do not always follow strictly the rules as described above. Hydrophobic residues can often be found at non-core positions, or core positions can lack hydrophobic residues. Both of these scenarios leads to weaker periods being observed. Local modifications in the repeat sequence can cause supercoiling and are relatively common in canonical coiled-coils (Brown et al., 1996; Gruber and Lupas, 2003; Walshaw et al., 2010). It has also been observed that some coiled-coils switch from one repeat sequence to another in a relatively short space which can switch the handedness of the coil (Parry, 2006).

1.6 Elementary dimer of Intermediate Filaments

The coiled-coil rod domain of intermediate filaments mainly consists of heptad repeat sequences, with six in coil 1A, thirteen in coil 1B, and thirteen also in coil 2. Hendecad sequences are also observed within the rod domains of intermediate filaments. For example, a single hendecad repeat is present towards the C terminal end of coil 1B, and four within coil 2, three of which are at the beginning and the fourth in the middle of coil 2 (Figure 1.4.1). The hendecad motif present in the middle of the coil 2 subdomain is highly conserved and a key characteristic of intermediate filaments and is often referred to as the "stutter" (Arslana et al., 2011; A. A. Chernyatina et al., 2015; Chernyatina et al., 2012; Chernyatina and Strelkov, 2012; Kelemen, 2017; Strelkov et al., 2003). Intermediate filaments form homodimers by the coiled-coil association of the rod domains, but these homodimers readily associate to further higher order assemblies in the absence of any co-factors, the exact mechanism of this is not fully understood.

Structural characterisation of intermediate filaments has been elusive. No full-length intermediate filament has been successfully crystallised. This is due to free intermediate filament dimers only existing in highly denaturing conditions (Harald Herrmann et al., 1996) and the higher order structures which these proteins form have also proven to elude successful crystallisation. Attempts have been made to build up the structure of a full-length homodimer by crystallising small, overlapping fragments and then build the model *in silico*. This approach has been successfully deployed to generate a multitude of structural data (Aziz et al., 2012; Chernyatina et al., 2012; Chernyatina and Strelkov, 2012; Meier et al., 2009; Nicolet et al., 2010; Strelkov et al., 2002, 2001). Using these pieces, a full structure for a parallel, in register, homodimer of vimentin was proposed (A. a Chernyatina et al., 2015). Only coil 1B and coil 2 have been seen to form parallel homodimers. The coil 1A subdomain has been shown to also form an alternative to this 'closed' configuration. An 'open' configuration was seen in a crystallisation of a fragment consisting of coil 1A, L1, and part of coil 1B whereby the coil 1 A helices are spread apart. This arrangement has been proposed to be important in the further assembly of the elementary dimers to form higher order structures. According to this, the N terminus of coil 1A of an elementary dimer has been shown to interact with the C terminus of coil 2 within the adjacent elementary dimer (Chernyatina et al., 2012). Both the

'closed' and 'open' forms might be present at different configurations of the assembly of higher order structures (Meier et al., 2009; Smith et al., 2002).

1.7 Higher order organisations of Intermediate Filaments

Eukaryotic intermediate filaments have two distinct pathways of assembly which have been observed. Coiled-coil homodimers form initially, then two distinct pathways are followed. The vimentin pathway has lateral assembly of the protein into unit-length filaments followed by the longitudinal assembly of these into the long, full filament (H Herrmann et al., 1996). The other pathway, the lamin pathway, has the longitudinal assembly preceding the anti-parallel lateral assembly (Davidson and Lammerding, 2014). The association of dimers laterally and longitudinally (Figure 1.7.1) form the filaments with the axis of the dimers roughly aligned to the filament direction (Bagchi et al., 2008; A. a Chernyatina et al., 2015; Herrmann and Aebi, 2004).

The assembly of intermediate filaments into their higher order structures is not fully understood and the assembly pathways appear to differ between types of intermediate filaments. The most understood assembly pathway is for that of the type III intermediate filament, vimentin (Figure 1.7.1). The vimentin assembly pathway is understood to follow these steps: from the basic building block of the elementary dimer, two dimers come together to form anti-parallel, slightly staggered, tetramers (H Herrmann et al., 1996; Soellner et al., 1985). The staggered tetramers have been seen *in vitro* in buffers of low ionic strength (Herrmann et al., 1999). The lateral association of eight dimers generates rod shaped filaments which are ~60-65 nm long and ~16 nm in diameter, which are termed unit length filaments (Herrmann et al., 1999; Strelkov et al., 2003). These unit length filaments further associate longitudinally in a head to tail manner to produce the filament (Figure 1.7.1). These final filaments have a diameter of around ~11 nm which suggests some rearrangement to obtain the final form (Strelkov et al., 2003). What determines the diameter of these filaments remains unknown.

An alternative intermediate filament assembly pathway has been proposed for the type V intermediate filament family of nuclear lamins, though this is not as well understood (Figure 1.7.1). This assembly pathway also contains steps of lateral and longitudinal assembly, just like that for vimentin, however for lamins the longitudinal interactions occur prior to the lateral ones. This means that no unit length filaments are formed. The elementary dimers undergo longitudinal head to tail assembly into dimer strands of variable length, which is

followed by the lateral association of the dimer strands in an anti-parallel and staggered fashion producing protofilaments of tetrameric strands (Ben-Harush et al., 2009; Dittmer and Misteli, 2011; Stuurman et al., 1998). These can then laterally associate to produce fibres of varying width. Although the pathway is different, the proposed final assembly of the intermediate filament is the same, although the intermediate filaments for the lamins have a characteristic striated pattern when viewed by transmission electron microscopy (Aebi et al., 1986; Heitlinger et al., 1992, 1991, Figure 1.7.2). These highly ordered paracrystals are very different to those seen with vimentin. Initially thought to be *in vitro* artefacts, however, the paracrystals are the dominant structures formed in physiological buffers, as well as in cells naturally expressing lamin (Klapper et al., 1997; Zwerger et al., 2013).

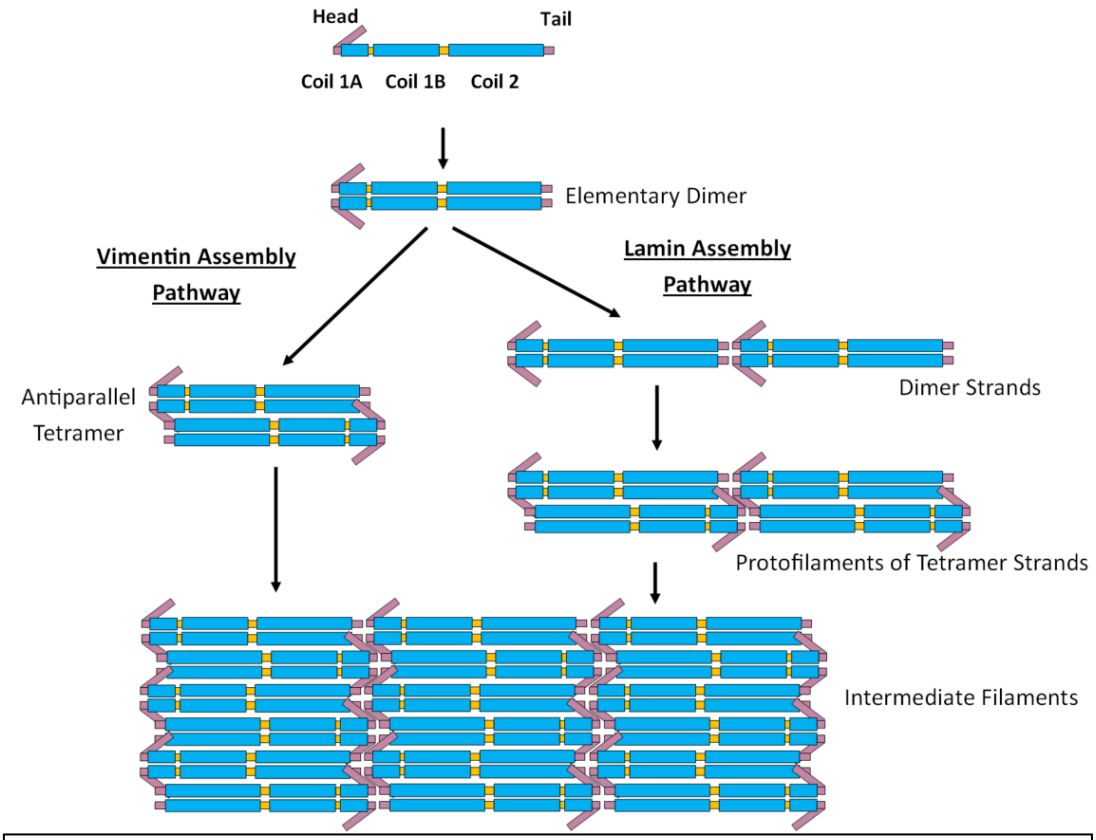

Figure 1.7.1 Eukaryotic intermediate filament assembly pathways.

The characteristic tripartite structure with the head and tail domains flanking the α helical rod domain. The rod domain consists of coil 1A, coil 1B and coil 2 which are connected by linker sequences. The elementary dimer is assembled as a parallel in register dimer. In the vimentin pathway, the elementary dimer associates with another laterally into an antiparallel tetramer. These antiparallel tetramers further associate laterally and longitudinally into intermediate filaments. In the lamin pathway, the elementary dimers associate longitudinally via head to tail associations. These dimer stands form antiparallel tetramer strands called protofilaments. These protofilaments then associate laterally to generate the intermediate filament.

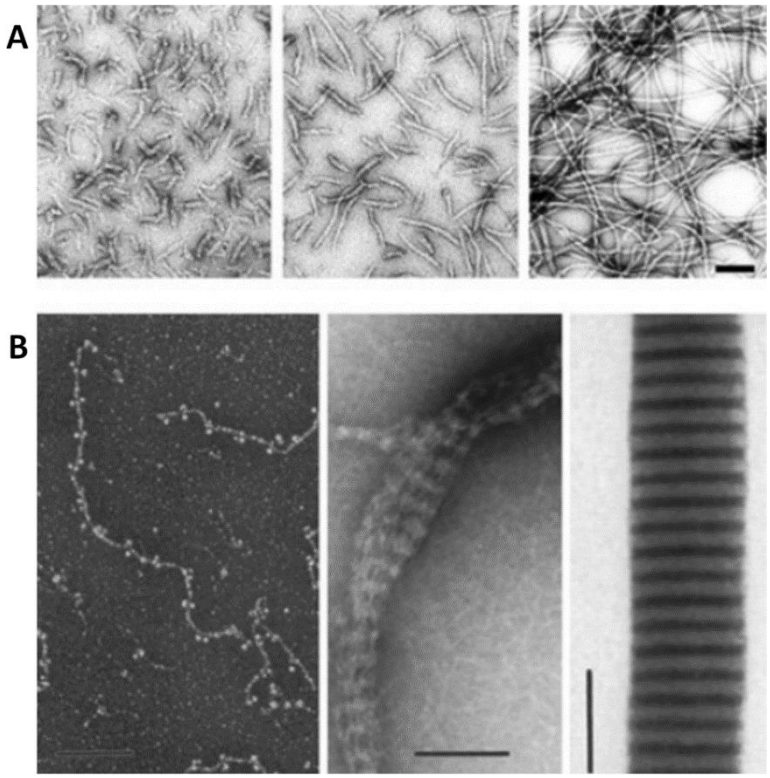

Figure 1.7.2 Intermediate filament formation *in vitro*.

(A) Assembly of vimentin filaments after addition of assembly buffer monitored at 10 seconds (left), 1 minute (middle), and 1 hour (right). Scale bar 100 nm. Images taken from (Herrmann and Aebi, 2004) **(B)** Chicken lamin B_2 filament formation *in vitro*. Dialysed into 25 mM MES, 150 mM NaCl, 1 mM EGTA pH = 6.5 (left), the same buffer in the presence of 25 mM $CaCl_2$ (middle) and finally 25 mM Tris, 25 mM $CaCl_2$, pH8.5 (right). Protein assemblies were monitored using transmission electron microscopy with rotary shadowing (left) or with negative staining (middle and right). Scale bars represent 100 nm. Images from (Heitlinger et al., 1991).

Both the vimentin and lamin pathways of intermediate filament assembly require head to tail assembly. Although there is very low sequence conservation amongst intermediate filaments, there are two highly conserved boxes of residues. One lies at the N-terminus of coil 1A comprising of 26 amino acids, and the other at the C-terminus of coil 2 comprising of 32 amino acids (Figure 1.4.1). So-called "minilamins" have been produced which carry the N-terminal or C-terminal fragments of lamin with a truncated rod domain. These have been used to show that there is coil formation between the ends of coil 1A and coil 2. This suggests that these conserved stretches might play an important role in forming the head to tail interactions needed for higher order assemblies of intermediate filaments (Kapinos et al., 2010; Köster et al., 2015).

Mutations of intermediate filaments have revealed details about the assembly and structure. In its native form, vimentin forms rope-like filaments (long smooth filaments, as opposed to striated filaments which have a dark and light banded pattern) when viewed by TEM. In vimentin where the tail domain had been deleted, no affect was observed on the higher order assemblies but did, however, affect its cellular localisation (Rogers et al., 1995). This suggests that the tail domain of vimentin is not important for the higher order assembly. Removing the characteristic stutter in the centre of the coil 2 domain of vimentin affected the higher order assembly pathway for filament formation. This highlights the importance of the stutter for higher order assembly (Herrmann et al., 1999).

Lamins form rope like structures as well as striated structures under different conditions (Figure 1.7.2). A lamin which lacked the head domain was still able to form dimers and striated structure like the wild-type, but no rope structures were observed. Tail-less lamins form dimers and striated structure which appear like the wild-type, however the propensity for the mutant to form ropes increased. For lamin which lacked both the head and tail domains, dimers were able to form like wild-type, rope was seen to be like wild-type, but was not formed as effectively. Striated structures were readily formed like wild-type in some types of lamin proteins, but the striated structures appeared loosely packed and fuzzy with some other types of lamins as observed with electron microscopy (Heitlinger et al., 1992, 1991; Karabinos et al., 2003; Sasse et al., 1997; Stuurman et al., 1996). This indicates that the head and tail domains are not important for dimer formation or that of the striated structure. However, the head domain is important for the formation of the rope structure, where the removal of the tail also aided the formation of the rope structure.

Further to this, yeast two hybrid screening for loss of function of randomly mutagenized lamin against wild-type lamin fragments showed two areas which were important for the binding of the fragments. These were located at the N and C terminus of the rod domain, which further indicates that it is the rod domain that is important for the assembly within these higher order structures. Interestingly one single point mutation I396V reduced binding by 10 fold (Stuurman et al., 1996).

1.8 Intermediate Filaments in Bacteria

For decades, the assumption was that bacteria were devoid of a cytoskeleton which supports its shape. This was mainly due to the involvement of peptidoglycan in maintaining the shape of bacterial cells. Henning et al (Henning et al., 1973) showed that degradation of the peptidoglycan with lysozyme in an isotonic solution to prevent lysis, resulted in spherical *Escherichia coli*. However, since then, homologues of all three types of cytoskeleton have been observed in bacteria. MreB has a weak sequence similarity to actin and FtsZ is a protein found in bacteria which is homologous to tubulin. These are discussed in further detail later.

1.9 Crescentin

The first bacterial intermediate filament-like protein is crescentin from the bacterium *Caulobacter crescentus*. *C. crescentus* is a vibroid shaped α-proteobacterium, which is mostly found in aquatic environments. The curved shape of this bacterium is consistent throughout its complex lifecycle and the curvature of the cells depends on the presence of crescentin (Ausmees et al., 2003).

Using both immunolocalization and CreS-GFP fusions, crescentin has been shown to form a filament along the inner curvature of the crescent shaped cells from pole to pole (Ausmees et al., 2003). Using the GFP fusion, the C terminally tagged CreS-GFP was shown to be non-functional. Cells expressing only CreS-GFP lost their crescent shape and became straight. Interestingly the CreS-GFP was still shown to be forming filaments within the cells. In older cultures where the cells were still long and straight, the CreS-GFP could be seen to be a helical filament. This helical filament is like that observed in a merodiploid strain carrying both *creS* and *creS-gfp* where the cells maintain their curved nature. This ability of the CreS-GFP only strain to form helical filaments without causing a curvature of the cell indicates that it is not the filament formation in itself that causes the curvature of the cells, instead some feature of the filaments is lost when the GFP is added such as loss of ability to interact with the cell membrane, cell wall or other unknown partner which links crescentin to cell shape (Ausmees et al., 2003).

Crescentin has a similar domain organisation than those of eukaryote intermediate filaments (Figure 1.9.1). The classical tri-partite structure is maintained including the α-helical rod domain and variable head and tail domains flanking it. The sequence identity between eukaryotic intermediate filaments and crescentin is low at around 25% (Ausmees et al., 2003), but this was not unexpected due to the low sequence identity seen within eukaryotic intermediate filaments. Crescentin contains 430 amino acids with the first 80 being the head domain, the last 13 being the tail domain and the 365 amino acids between these being the rod domain. This length of rod domain is comparable, if a bit longer, than the rod domains for eukaryotic intermediate filaments. Cytoplasmic intermediate filaments are typically 310 amino acids in length, or 350 amino acids in length for nuclear intermediate filaments. The rod domain of crescentin is said to consist of four sub-domains named coil 1A, coil 1B, coil 2A and

coil 2B. This is different from the current sub-domain organisation of eukaryotic intermediate filaments. However, at the time of crescentin discovery, there were thought to be four coiled-coil rod sub domains named in the same way, which were linked by short non-helical sequences in intermediate filaments (Parry and Steinert, 1999). This was based on sequence analysis using the assumption that the coiled-coil repeats were only consisting of heptad repeats. However, this has now been shown not to be the case. It was then subsequently changed to a single coil 2 domain when overlapping fragments of coil 2A and coil 2B of human vimentin suggested a continuous single coil 2 domain (Nicolet et al., 2010; Strelkov et al., 2002). Given the lack of crystallographic data for crescentin, combined with its similar biophysical and biochemical properties to that of eukaryote intermediate filaments, it has been speculated that crescentin could also contain 3 rod sub-domains. Crescentin coil 2A and coil 2B could actually be one single coil 2 which contains the "stutter" (Figure 1.9.1) which is characteristic of intermediate filaments (Kelemen, 2017).

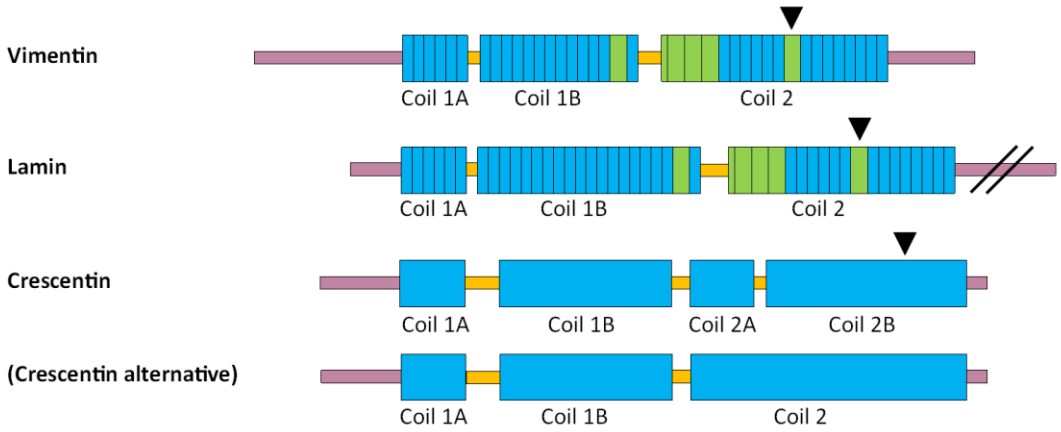

Figure 1.9.1 Vimentin and lamin C domain architecture compared to that of crescentin.

The blue boxes on vimentin and lamin show α-helical segments predicted or shown to form a heptad coiled-coil repeat sequence, green boxes show segments predicted to form hendecad repeat sequences. For crescentin helices assignments are not shown. Yellow boxes show predicted linker subdomains, purple boxes show head and tail domains. Black arrows show the characteristic stutter for intermediate filaments. Proteins shown with N-terminus on the left. Crescentin original coil assignment shown with the proposed alternative coil assignment. Figure based on data from (Ausmees et al., 2003; Kapinos et al., 2010; Kelemen, 2017; Köster et al., 2015).

Variants of crescentin have been made in order to establish the roles of the domains on the higher order assemblies observed. A mutant that lacked the head domain generated filaments like the wild-type *in vitro* rope structures (Figure 1.9.2), but no filaments were seen *in vivo.* Moreover, this head-less mutant allele failed to complement the null mutant (Cabeen et al., 2011). However a mutant that lacked only the first 27 amino acids of the head domain was still not able to compliment the null mutant (Cabeen et al., 2011, 2009). This suggested that these first 27 amino acids, which are positively charged, were important for the attachment of the crescentin filament to the membrane (Cabeen et al., 2009). A mutant which lacked the tail domain formed filaments like wild-type *in vitro* (Figure 1.9.2) and in the null mutant partial complementation was observed with cells having around 25% curvature of that of the wild-type(Cabeen et al., 2011). In a mutant that lacked the linker subdomain between coil 1A and coil 1B, an increase in filament diameter was observed and in a close to physiological buffer, protein aggregates, rather than ordered assemblies were seen (Figure 1.9.2). The linker-less construct failed to complement the null mutant, where aggregates were observed that localised to the poles (Cabeen et al., 2011). This suggests that the linker 1 subdomain may be important for correct lateral assembly and potentially for the alignments of the sub domains. In a crescentin mutant which lacked the stutter motif, no filaments were formed in the close to physiological buffer, however striated structures were formed in low pH buffers in the presence of magnesium ions (Cabeen et al., 2011) (Figure 1.9.2). In the null mutant, short filaments or diffuse signal was observed with no complementation (Cabeen et al., 2011).

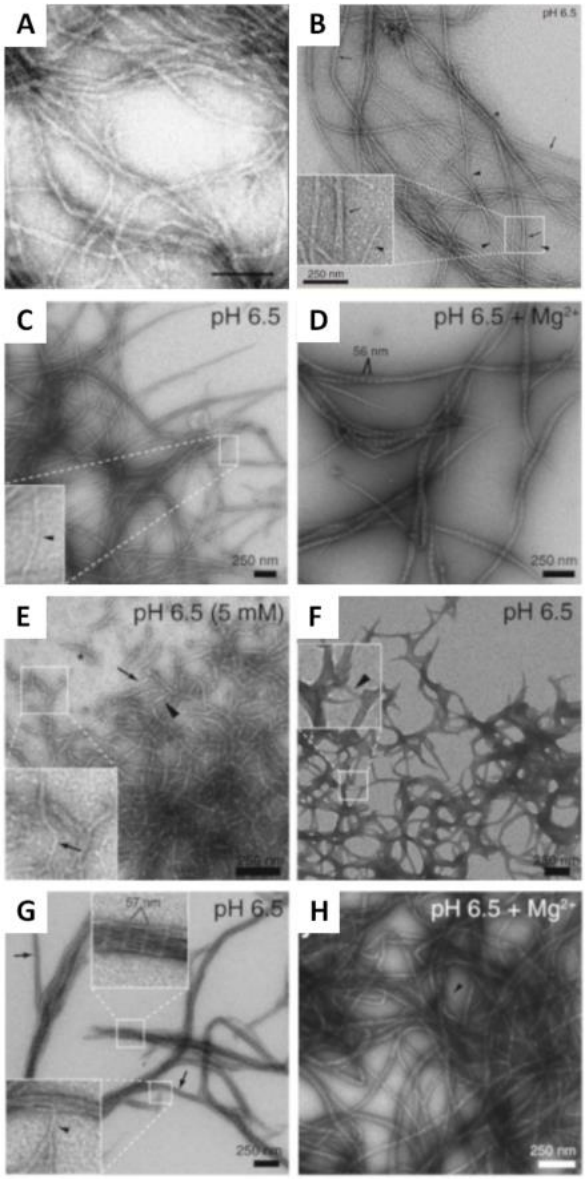

Figure 1.9.2 Crescentin Structures Observed by TEM

Negatively stained crescentin and mutants viewed by TEM. Wild-type crescentin in **(A)** 50 mM Tris pH7.0 **(B)** 50 mM PIPES pH6.5. Crescentin lacking its tail domain in **(C)** 50 mM PIPES pH6.5 and **(D)** 50 mM PIPES pH6.5 5 mM $MgCl_2$. Crescentin lacking the linker subdomain between coil 1A and coil 1B in **(E)** 5 mM PIPES pH6.5 and **(F)** 50 mM PIPES pH6.5. Crescentin with the stutter removed in **(G)** 50 mM PIPES pH6.5 and **(H)** 50 mM PIPES pH6.5 5 mM $MgCl_2$. **(A)** from (Ausmees et al., 2003) **(B-H)** from(Cabeen et al., 2011). Scale bars: 100 nm **(A)**, 250 nm **(B-H)**.

The crescentin mutants produced similar results to the vimentin and lamin mutants in that the mutants lacking the tail domains were the least affected in their higher order assembly with all the structures produced being very similar to wild-type, although addition of Mg caused filament bundling and the appearance of striations (Figure 1.9.2). Although tail-less vimentin was shown to affect its cellular localisation. Tail-less crescentin complemented the null mutant to around 25% curvature of the wild-type suggesting some role for the tail in fully functioning crescentin. The head-less mutants in lamin could form dimers and striated structure but no rope structures, whereas head-less mutant of crescentin formed rope filaments *in vitro* but did not form filaments *in vivo* or complement the null mutant. The mutants that lack the stutter in vimentin and crescentin failed to form higher order structures (although crescentin formed striated structures similar to those observed in lamins in low pH buffers in the presence of magnesium ions). All of this together indicates that, generally, the rod domain is important for the formation of higher order structures.

1.10 FilP and Scy

The proteins Scy and FilP from *Streptomyces coelicolor* are both coiled-coil proteins which have tripartite structures like intermediate filaments. They have non coiled-coil head and tail domains and a central coiled-coil rod domain. This rod domain, however, is not thought to be separated into three sub-domains like that of intermediate filaments. Instead it is proposed to consist of two sub-domains, coil 1 and coil 2 with a linker sequence in between (Holmes et al., 2013; Walshaw et al., 2010, Figure 1.10.1). Although there may also some evidence for the possibility of a flexible motif within coil 2. The structure of Scy and FilP has not been determined using crystallography, but structural predictions have been made using bioinformatic analysis of the primary amino acid sequences of FilP and Scy (Walshaw et al., 2010). The coil 1 sub-domain is composed of six canonical heptad repeat sequences, but the coil 2 sub-domain has a much more unusual repeat sequence. It is predicted to contain a much longer 51 residue repeat sequence, which is essentially made of 7, 11, 11, 11, 11 repeats. It contains partial heptad and hendecad structure forming 14 supercoiled turns in Scy (Walshaw et al., 2010). The simplest oligomers are long coiled-coil dimers formed by two parallel coiled-coil domains. However, there is some evidence of a flexible hinge domain which could make more complex structures possible. Of the smaller heptad domain, the amino acids at positions a and d are compatible with a parallel homo-dimeric assembly to be likely, a trimeric assembly possible and a tetramer unlikely (Harbury et al., 1993; Lupas, 1996; Walshaw et al., 2010). The larger 51-repeat domain is compatible with this as well and also seems to suggest that a dimeric assembly is most likely due to the extreme preference for alanine at positions a and h (but not d or e) (Walshaw et al., 2010).

The *filP* gene (SCO5396) is located adjacent to that of the *scy* gene (SCO5397) in *S. coelicolor*. FilP has a near identical domain organisation to that of Scy except that it has a truncated CC51 subdomain (Bagchi et al., 2008; Bentley et al., 2002; Walshaw et al., 2010) (Figure 1.10.1). FilP has an N-terminal head domain composed of 16 amino acids; coil 1 heptad repeat subdomain composed of 48 amino acids; a central linker composed of 9 amino acids; coil 2 51 repeat subdomain (CC51) composed of 219 amino acids; and a C-terminal tail domain composed of 18 amino acids. This is predicted to form a parallel homodimer (Walshaw et al., 2010).

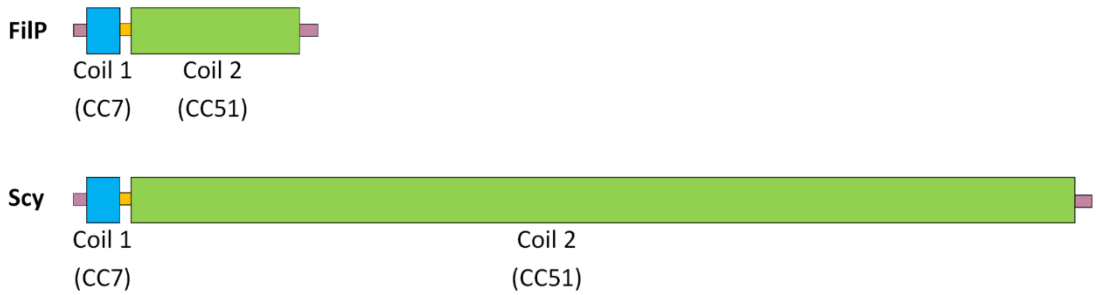

Figure 1.10.1 Domain architecture of FilP and Scy.

Coil 1 which is composed of heptad repeat sequences shown in blue. Coil 2 which is composed of a mix of heptad and hendecad repeat sequences which form a 7, 11, 11, 11, 11 sequence forming a 51 repeat sequence shown in green. Head and tail domains shown in purple. Linker subdomain shown in yellow. Proteins shown with N terminus on the left. Figure based on data from (Walshaw et al., 2010).

Scy

Scy localises to hyphal tips during active growth as well as to sites of future branch points (Holmes et al., 2013). A Scy knockout mutant has very small colonies which are developmentally delayed and have an over branching phenotype in both the vegetative and aerial hyphae. In sporulating hyphae, the septation and chromosome distribution were highly irregular. Wild-type *S. coelicolor*, exhibits apical dominance in that new branch points are inhibited behind the growing apical tip. The Scy knockout did not display this and branching was found close to the growing tip which implicates Scy in the control of apical dominance (Holmes et al., 2013). In this Scy knockout mutant, DivIVA localisation is patchier and more dispersed but the expression levels remain unchanged in comparison to the wild-type. If Scy is overexpressed, it has a hyperbranching phenotype, much like that when DivIVA is overexpressed. Overexpression of Scy influences the localisation of DivIVA, in that it changes to resemble that when DivIVA is overexpressed (Holmes et al., 2013). Scy and DivIVA co-localise at the hyphal apex and sites on the lateral wall. This implicates that both are involved in the selection of sites for de novo tip formation and work together to ensure correct growth and branching (Holmes et al., 2013). DivIVA and Scy have been shown to interact both by bacterial two hybrid assays and with ultracentrifugation pelleting assays with the purified proteins whereby the presence of Scy pulled DivIVA into the pellet fraction where it would

have been found in the supernatant fraction by itself, thereby indicating an interaction. Scy also affects cell division and localisation of FtsZ in the Scy knockout mutant were not the ordered rings of sporulation septa which are normal for the wild-type. Instead, FtsZ had long, loosely curved cables which ran alongside and sometimes parallel to the lateral walls (Holmes et al., 2013). Scy has also been shown to interact with ParA, recruiting it to the tips and regulating the polymerisation of ParA. This interaction is proposed to coordinate the transition from hyphal elongation to sporulation (Ditkowski et al., 2013). Scy which was expressed from *E. coli* when purified was able to form a network of rope like filaments when observed by TEM (Holmes et al., 2013).

FilP

FilP is an intermediate filament like protein. The *filP* gene lies directly downstream to that of *scy* and they are similar except FilP is smaller (311 amino acids) and has a differing role within the cell (Bentley et al., 2002; Walshaw et al., 2010). FilP in *S. coelicolor* was identified initially as a homologue for a protein in *Streptomyces reticuli* which had an affinity to avicel, a crystalline form of cellulose. This led to the name AbpS (avicel binding protein) (Walter et al., 1998). The structure of AbpS was predicted to have a putative transmembrane segment at its C-terminus. Through use of FITC labelling and proteinase K experiments it was shown that AbpS is anchored to the cell wall and protrudes from the surface of the hyphae (Walter et al., 1998). Immunolabelling and microscopic studies further suggested that the N-terminal section protrudes from the cell wall whilst the C-terminus is embedded in it (Walter et al., 1999). The N-terminal section contains avicel binding properties and was shown to form α-helical coiled-coils. A crosslinking experiment suggested that AbpS oligomerises into homotetramers that together could make the functional avicel receptor (Walter and Schrempf, 2003). SCO5396 from *S. coelicolor* has high sequence conservation (93.55%) to AbpS of *S. reticuli*, although it is not clear to what degree the studies of AbpS in *S. reticuli* are relevant to its function in *S. coelicolor* which has been suggested to play a different role. SCO5396 was identified again when looking for proteins similar to Crescentin from *Caulobacter crescentus*. The protein was then characterised by its relationship to growth and cytoskeletal-like properties and so, its name was changed to FilP (filamentous intermediate-like protein) (Bagchi et al., 2008).

***In vivo* FilP**

Streptomyces strains lacking FilP have been observed to have a relatively mild phenotype. When grown on solid media, a FilP knockout has been seen to lag approximately a day behind a wild-type control in terms of when it sporulates (Bagchi et al., 2008). Microscopically, when grown on either solid media or in liquid culture, the hyphae of the FilP knockout mutant appeared much more meandering that the wild-type (Bagchi et al., 2008; Fröjd and Flärdh, 2019, Figure 1.10.2). FilP knockouts have also been shown to have a reduced rigidity of the cell wall at the hyphal tips as was shown by atomic force microscopy and the distorted growth morphology suggests a mechanical role in controlling cell shape (Bagchi et al., 2008). A FilP homologue in *Kitasatospora viridifaciens* has also been shown to be essential for the formation of S-cells in hyperosmotic stress and oxygen limited conditions, as well as for normal the normal mycelium growth under non-hyperosmotic stress conditions (Ultee et al., 2020).

Localisations of FilP have produced some varying results. A FilP-EGFP fusion protein was used to observe its localisation in a FilP knockout background as well as with a wild-type copy present (Bagchi et al., 2008). In the knockout background they observed prominent fluorescent filamentous structures in the vegetative hyphae. FilP was also observed in immature and still growing aerial hyphae but not in mature spore chains (Bagchi et al., 2008). With a copy of the wild-type FilP expressed, the localisation of the FilP-EGFP fusion was seen to be different in that it was observed in nearly all tips of young hyphae as well as a tip distant regions (Bagchi et al., 2008). Immunolocalisation revealed that during early growth nearly all hyphae fluoresced in the apical regions with the signal strongest just behind the tip where DivIVA signal appears (Fuchino et al., 2013; Javadi et al., 2019, Figure 1.10.2). Long cables were also observed asymmetrically along one side of the hyphae as well as sights of new branch points were marked by bright fluorescence. In hyphae which were no longer growing this apical gradient was replaced by a uniform intensity along the hyphae (Fuchino et al., 2013).

Localisation using a FilP mCherry fusion protein in *Streptomyces venezuelae*, with a wild-type copy of FilP present showed that the localisation appeared to be irregular spots or patches along the hyphae with no distinct apical gradients (Fröjd and Flärdh, 2019, Figure 1.10.2). However, treatment with formaldehyde produced distinctive zones of fluorescence just subapical of the tips. The inference from this was that the handling of cells and

interference with its growth was a source of discrepancy between the results observed with immunofluorescence in comparison to those observed with non-fixed samples with fluorescent protein fusions (Fröjd and Flärdh, 2019).

Strains with only the FilP-EGFP or FilP-mCherry and no wild-type copy of FilP displayed a FilP knockout phenotype. However, strains with both the FilP fusion protein and a wild-type copy displayed wild-type characteristics (Bagchi et al., 2008; Fröjd and Flärdh, 2019).

After osmotic upshift, which was achieved by moving hyphae grown on a cellophane onto a plate containing sucrose which *S. coelicolor* cannot catabolise, growth of the hyphae ceased for 2 to 3 hours. After this lag, growth resumed with new branches emerging from the lateral hyphal wall with only 12% restarting growth at the tips and 77% regrowth exclusively at the lateral sites (Fuchino et al., 2016). This affect was also observed with NaCl-containing media. Osmotic downshift and acid stress did not have the same affect with regrowth occurring at the existing tips. FilP and DivIVA were observed to persist at the tips of existing hyphae throughout the lag phase but delocalise from these arrested tips prior to regrowth. Scy was present at the hyphal tips during the lag phase but also persisted at the arrested tips once branching and new growth resumed. Mutants which lacked FilP or Scy still had this same affect and therefore, neither FilP or Scy are thought to be required for the reprogramming of cell polarity (Fuchino et al., 2016).

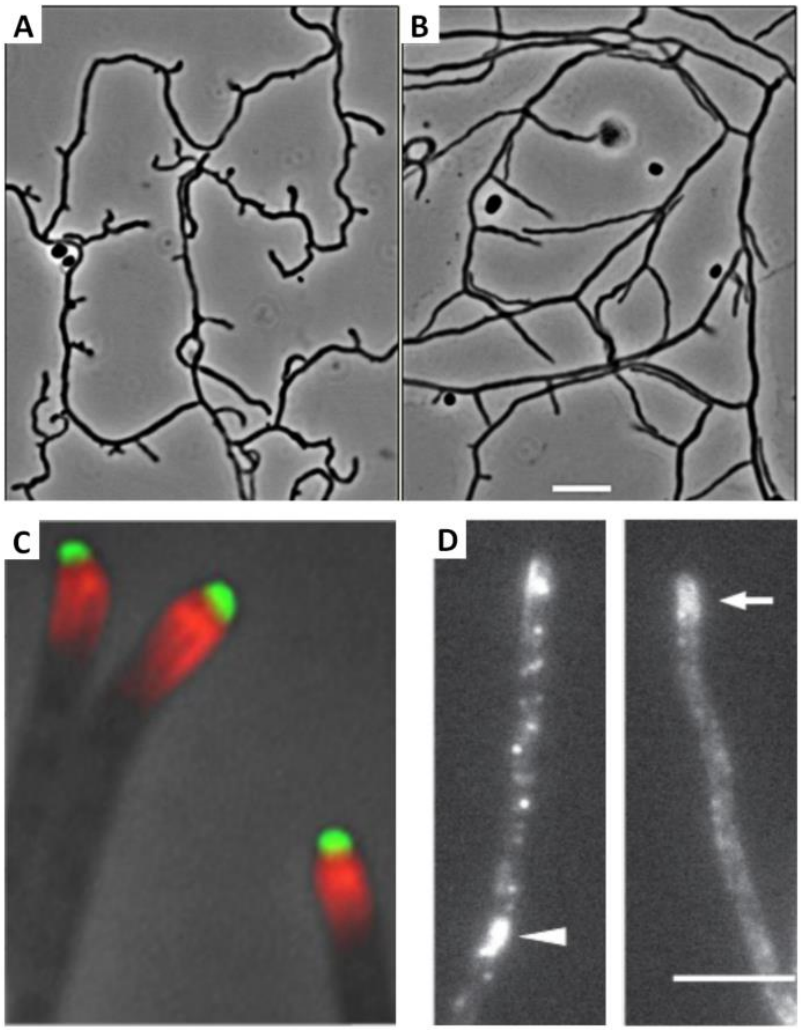

Figure 1.10.2 FilP knockout phenotype and FilP localisation.

FilP knockout strain **(A)** compared to the wild-type strain M145 **(B)** grown for 20 hours in the angle between an inserted coverslip and agar visualised by phase contrast microscopy. (Bagchi et al., 2008). **(C)** Overlay of phase contrast, anti-FilP immunofluorescence (red) and DivIVA-EGFP fluorescence (green). (Fuchino et al., 2013). **(D)** Localisation of FilP-mCherry in *filP+/filP-mCherry* merodiploid *Streptomyces venezuelae*. Left Fluorescence image of living vegetative hyphae mounted directly on agarose coated slides without fixation. White arrowhead indicates example of large foci fluorescence point. Right fluorescence image of hyphae which were fixed with formaldehyde before mounting on agarose coated slides. White arrow indicated apical gradient structures. (Fröjd and Flärdh, 2019). Scale bar represents 5 µm.

In vitro FilP

FilP has been previously purified and visualised *in vitro* using transmission electron microscopy (TEM) and scanning electron microscopy (SEM). The structures which were previously observed included a smooth rope-like filament with a diameter of around 60 nm which constituted the less frequent type, and striated filaments which branched and had a varying diameter(Bagchi et al., 2008) (Figure 1.10.3A, B). These striated filaments visually resembled those seen with nuclear lamins (Stuurman et al., 1998, Figure 1.7.2). The structures initially observed included some striated structures surrounding a dominant lace like structure (Fuchino et al., 2013) (Figure 1.10.3C, D). Recent observations at pH6.8 showed striated structures which closely resembled those previously observed ((Javadi et al., 2019), Bagchi et al., 2008, Figure 1.10.3E). also It was also observed that with addition of both monovalent and divalent cations a hexagonal mesh lacework was observed which more closely resembled what was observed initially (Fuchino et al., 2013, Figure 1.10.3F). These additions of magnesium, potassium and sodium ions increased the solubility of the proteins (Javadi et al., 2019). Differing pHs were also found to alter the appearance of the higher order assemblies of FilP. In citric acid pH3.9 the structures were observed to have the same unit length but vague banding patterns and thin bundles (Figure 1.10.3G). It is speculated that the low pH altered the charge of FilP which could affect the lateral alignment of protofilaments and explain the less pronounced banding pattern (Javadi et al., 2019). FilP in Tris pH8.8 formed fewer and less condensed filaments compared with assembly buffer at pH6.8 (Figure 1.10.3H). FilP in Etanolamine pH11 no filaments were observed but rod-shaped polymer units were seen (Figure 1.10.3I). In a Hepes buffer FilP displays a 'bead on a string' look (Figure 1.10.3J). These are around 60 nm apart and from this it is suggested that the primary stage of assembly is two FilP rods interacting tail to tail (Javadi et al., 2019).

FilP higher order assembly as described above has been seen with an N-terminally histidine tagged FilP. A C-terminally histidine tagged-FilP formed smooth filaments as well as striated filaments which had a smaller unit length to the banding pattern at around 28 nm as opposed to the around 60 nm banding pattern for N terminally histidine tagged FilP (Javadi et al., 2019). This C-terminally histidine tagged FilP failed to complement a FilP knockout strain, where the N-terminally tagged version did (Javadi et al., 2019). The histidine tags associated with the N terminal made major band more defined, where with C terminal histidine tags the

minor band became denser. This gave the appearance of a half unit length (Javadi et al., 2019). Non-tagged FilP was observed at low concentrations to form striated filaments with a unit length of around 19 nm. At higher concentrations it formed striations with a larger unit length of around 54 nm similarly to that of the N-terminally histidine tagged version (Javadi et al., 2019). It is speculated that the additional 18 amino acids which were introduced with the tagged version are likely to be the cause of the 6 nm difference between the tagged and un-tagged versions (Javadi et al., 2019). Use of nano-gold staining to identify where the histidine tag lies within the striated structure revealed that, for the N terminally tagged version, this was in the major band. The C-terminally tagged version had less specific localisation and the addition of the nanogold appeared to disassemble the structures. The non-tagged version of FilP showed a faint affinity for FilP which was also present in the other versions. This indicated that the FilP heads were gathered in the electron dense major band of the striated structure with the C-terminal tail to tail interactions between them (Javadi et al., 2019).

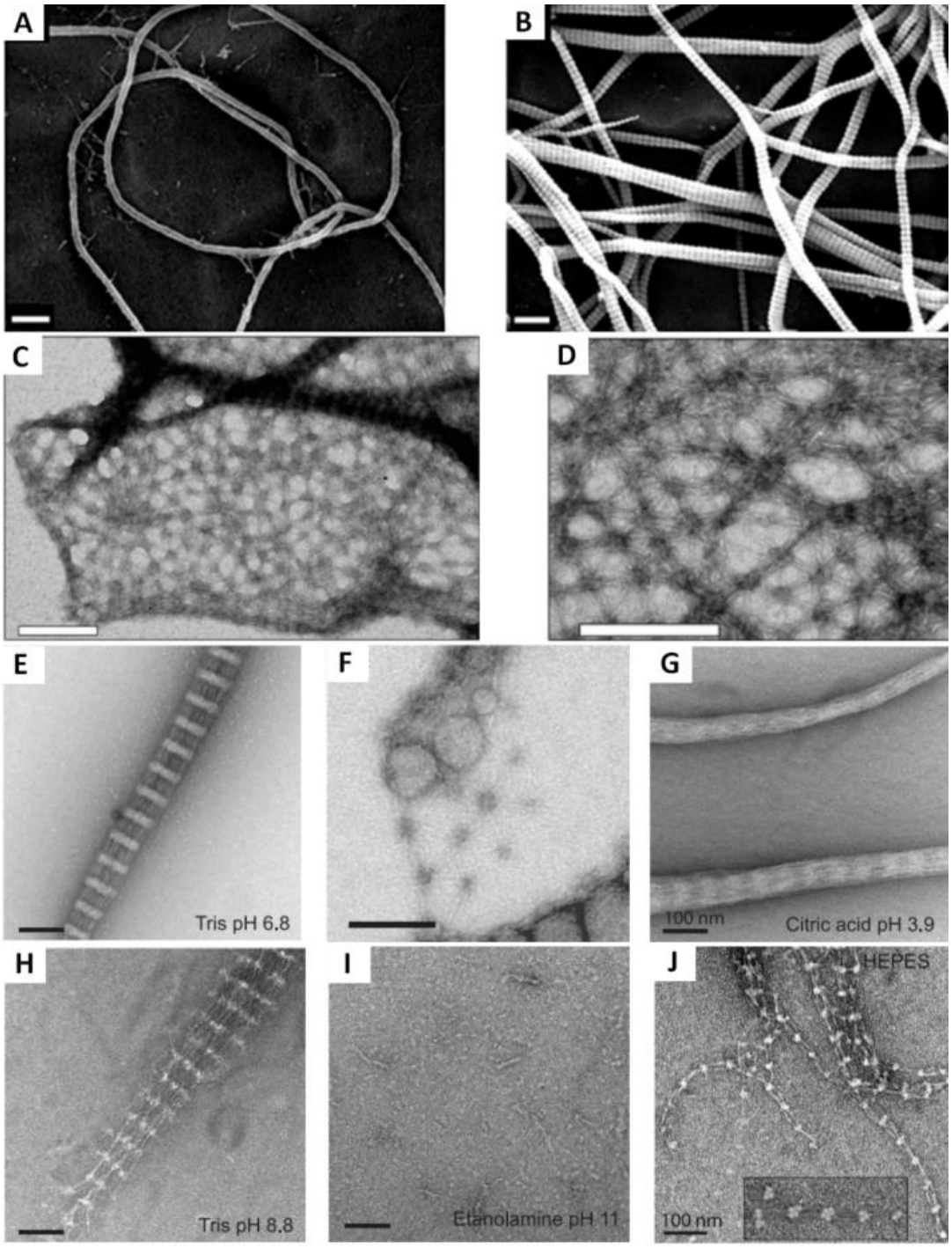

Figure 1.10.3 FilP structures previously observed.

(A), **(B)** Scanning electron micrographs of filaments formed by FilP in 50 mM Tris pH7.0 as observed by (Bagchi et al., 2008). Smooth non-branching filaments shown in **(A)**, striated branching filaments shown in **(B)**. **(C)**, **(D)** Transmission electron microscopy of FilP in 50 mM Tris pH7.0 as observed by (Fuchino et al., 2013). Networks and striated filaments of FilP. **(E)** FilP dialyzed in Tris assembly buffer, pH 6.8. **(F)** FilP meshwork in polymix buffer. **(G)** FilP dialyzed in citric acid, pH 3.9. **(H)** FilP dialyzed in Tris, pH 8.8. **(I)** FilP dialyzed in ethanolamine, pH 11. **(J)** FilP dialyzed in Hepes buffer. **(E-J)** from (Javadi et al., 2019). Scale bars 200 nm **(A-D)**, 100 nm **(E-J)**.

1.11 Bacterial Cell Shape

For bacteria to grow, new peptidoglycan precursors must be inserted into the cell wall (Vollmer et al., 2008). There are three sites of growth in bacteria (Figure 1.11.1). Lateral growth is where new cell wall is inserted along the lateral walls for the elongation of the cell. This is found in organisms such as *E. coli* and *B. subtilis* and is driven by a protein called MreB which is a bacterial homologue of eukaryotic actin. The other form of growth for elongation is polar growth which is found mainly among *Actinomycetes*. This is where new cell wall material is inserted at the poles of the cell. Polar growth is driven by a protein known as DivIVA which is not currently considered to be a homologue of any class of eukaryotic protein (Flärdh, 2003a). The final site of growth is that which occurs during cell division. This is the most common type of growth and is found in all bacteria (Cabeen and Jacobs-Wagner, 2005). This is the only mechanism of growth which is seen in spherical bacteria and mainly occurs at the mid-cell (Cabeen and Jacobs-Wagner, 2005). Growth site of division is driven by FtsZ, a bacterial homologue of eukaryotic tubulin (Carballido-López and Errington, 2003).

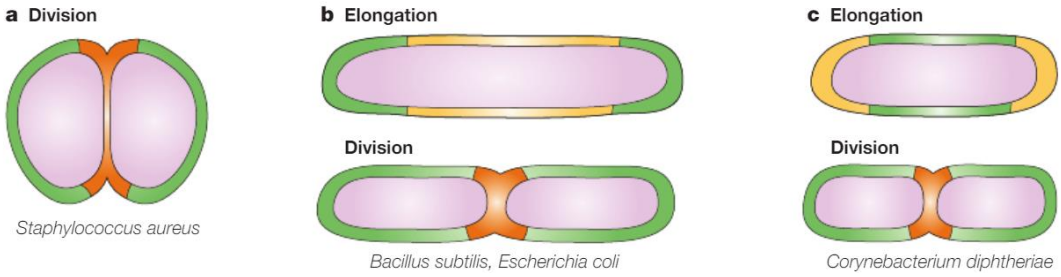

Figure 1.11.1 The Mechanisms of bacterial growth.

Three sites where peptidoglycan precursors are inserted into the cell wall during bacterial growth. **(A)** At the site of division. This is the most common form of bacterial growth and is driven by FtsZ. **(B)** and **(C)** are two mechanisms of growth which leads to the elongation of bacteria. **(B)** MreB dependant lateral growth and **(C)** DivIVA dependant polar growth. Taken from (Cabeen and Jacobs-Wagner, 2005). Green, existing peptidoglycan pre growth. Red, new peptidoglycan at the division site. Yellow, new peptidoglycan along the sidewalls.

1.12 MreB

The majority of known bacteria are characterised as rod-shaped with growth occurring at the lateral walls (Daniel and Errington, 2003). MreB was one of the first proteins identified to contribute to this mode of growth in *E. coli* and *B. subtilis* (Levin et al., 1992; Wachi et al., 1987). MreB is one of the homologues of the cytoskeletal protein actin which have been found in bacteria. These proteins share a conserved actin fold and similar 3D structures and polymerises into filamentous structures similarly to F-actin (Jones et al., 2001; Van den Ent et al., 2001). Filament assembly and disassembly is controlled by ATP binding and hydrolysis. MreB was originally defined as a cell-shape determining factor which led to cell shapes other that spherical. MreB is absent in most coccoid shaped bacteria where most rod shaped bacteria contain at least one MreB homologue (Daniel and Errington, 2003). *B. subtilis*, for example, is a rod shaped bacterium and contains two MreB proteins with Mbl (MreB-like) and MrebH (MreB homologue) (Jones et al., 2001; Varley and Stewart, 1992). It has been shown that both are required for formation of the rod shape however the effect on the shape with the absence of each protein is different. This suggests that they interact with different components of the cell wall synthetic machinery (Carballido-López et al., 2006; Defeu Soufo and Graumann, 2006; Domínguez-Cuevas et al., 2013; Kawai et al., 2009). *E. coli* has only one MreB protein and depletion of this protein within the cell gives rise to spherical cells (Kruse et al., 2005) there are no known conditions where the depletion of MreB in *E. coli* still gives rise to a rod shaped cell (Shi et al., 2018).

The use of a small molecule known as A22 has been useful to study the function of MreB. A22 binds MreB and leads to its depolymerisation and re-localisation (Gitai et al., 2005; Wang et al., 2010). When A22 is present, cell wall construction persists but occurs diffusely across the cell surface including at the poles (Billings et al., 2014; Cho et al., 2014). This diffuse cell wall construction causes a loss of the rod shape over time and eventually cell lysis (Gitai et al., 2005). Interestingly, the A22 caused the MreB to disassemble faster than the cell lost its rod shape leading to the conclusion that polymerised MreB patterns the cell wall growth rather than acts as a structural foundation for it (Errington, 2015).

Point mutations of MreB in *E. coli* have been made and many of these have been seen to alter lots of properties of the cell including the cell width (Ouzounov et al., 2016; Shi et al., 2017) and variation in cell width within individual cells (Morgenstein et al., 2017, 2015).

Localisation of MreB and Mbl in *B. subtilis* revealed helical filaments which wrap around the cell longitudinally from pole to pole (Jones et al., 2001). Localisation of the sites of insertion of new cell wall material were also shown to form a helical pattern, suggesting that

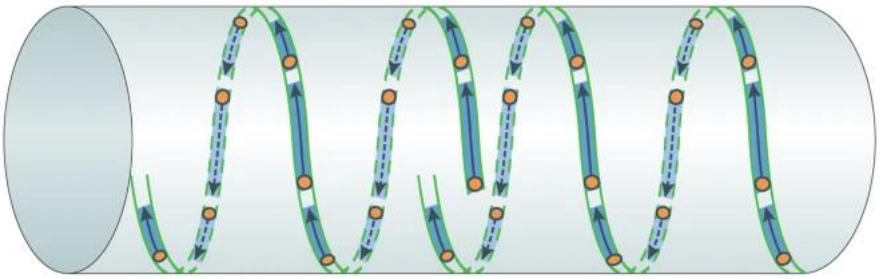

Figure 1.12.1 Model for the role of MreB in shape determination of bacteria.

MreB filaments (solid and dashed lines) elongate in response to the cylindrical shape. The filaments can recruit peptidoglycan synthetic complexes (orange circles) which generate new peptidoglycan strands. Taken from (Errington, 2015)

MreB proteins contribute to the control of the location of cell wall synthesis in bacteria (Daniel and Errington, 2003). These initial localisations were challenged by observations of MreB filaments using electron cryotomography which suggested that MreB localises to discreet patches and that these patches are moved in a helical path through the cell coupled to the cell synthetic machinery (Domínguez-Escobar et al., 2011; Garner et al., 2011; Swulius et al., 2011; Van Teeffelen et al., 2011). More recently, the model has moved back towards the helical filaments with observations of MreB *in vitro*. MreB has been shown to form helical filaments which interact with membranes (Salje et al., 2011; van den Ent et al., 2014). In addition, helical filaments have been once again observed in actively growing cells (Olshausen et al., 2013; Reimold et al., 2013). This all together leads to the current model of MreB (Figure 1.12.1) in which filaments associate to the membrane and elongate in a uniform and cylindrical shape. This recruits cell wall synthetic complexes which creates new peptidoglycan as directed by the motion of the MreB helices (Errington, 2015).

Although MreB is involved in cell shape determination and chromosome segregation in rod-shaped bacteria which grow by lateral growth, it is also present in bacteria which do not exhibit these characteristics such as *Streptomyces*. Here, MreB is not essential for the growth of non-sporulating vegetative mycelium, but functions to aid in the formation of spores which are uniform and environmentally stable. A knockout mutant of MreB produced swollen aerial hyphae and swollen spores (Mazza et al., 2006).

1.13 Polar Growth

Polar growth is not as common as the method for growth in bacteria as that of lateral growth, however a large number of bacteria do exhibit this form of growth. Polar growth is especially prevalent in the Gram-positive *Actinobacteria* and the Gram-negative *Rhizobium* and *Agrobacterium* genera (Brown et al., 2012; Daniel and Errington, 2003). DivIVA is the protein which was the first to be implicated to be driving this mode of growth (Flärdh, 2003a). DivIVA (and homologues of) is thought to be an essential protein for growth in *Actinobacteria* such as *Mycobacterium tuberculosis* (Kang et al., 2008; Nguyen et al., 2007). DivIVA was originally identified in *B. subtilis* where it is located at the poles and plays a role in division rather than growth (Cha and Stewart, 1997). In *S. coelicolor*, DivIVA was identified due to its homology with DivIVA from *B. subtilis* and was therefore named accordingly (Cha and Stewart, 1997; Flärdh, 2003a). DivIVA is localised to the poles in both bacteria where it is involved with division and where it is involved with growth (Flärdh, 2003a; Marston et al., 1998). Due to this, it is thought that the homologues share similar characteristics whether they function for growth or division. In *Actinobacteria* DivIVA is thought to localise cell wall synthesis machinery and has been shown to interact with penicillin-binding protein 3 (PBP3) in *Mycobacterium* (Mukherjee et al., 2009). DivIVA has been implicated for driving growth in numerous *Actinobacteria*, no homologues of DivIVA have been found in Gram-negative bacteria (Oliva et al., 2010). In Gram-negative bacteria which exhibit polar growth, no mechanism has yet been identified (Oliva et al., 2010). Within bacteria which exhibit polar growth, there is a great variety in the way this manifests with the filamentous *Streptomyces*, bi-directional growth in *Corynebacterium*, asymmetrical bi-directional growth in *Mycobacterium*, and uni-directional growth in *Agrobacterium* (Aldridge et al., 2012; Brown et al., 2012; Meniche et al., 2014; Sieger et al., 2013).

1.14 Cell Division

Most bacteria divide by binary fission. This leads to physical cell separation whereby a single septum is formed between two replicated chromosomes in the mid-points of the cells which produces two identical, or near identical, offspring which each contain a single complete chromosome (Adams and Errington, 2009; Wu and Errington, 2012). This is a highly regulated process as initiation of cell division prior to the completion of the chromosome segregation can break the chromosomes (Wu and Errington, 2012). Division of the cell is carried out by a large protein complex known as the divisome which undertake the constriction needed as well as facilitate the septum formation.

FtsZ is a bacterial cell division protein which shares homology with tubulin in eukaryotes (Adams and Errington, 2009). The sequence homology between these is low, however it is the structure and function which provide this homology (Erickson et al., 1996; Nogales et al., 1998). FtsZ proteins are highly conserved among bacteria and archaea (Erickson, 1997; Wang and Lutkenhaus, 1996). FtsZ polymerises similarly to that of tubulin in that it depends on GTP binding (Bramhill and Thompson, 1994). FtsZ acts as a GTPase where FtsZ with bound GTP forms filaments, but when GTP is hydrolysed to GDP, the FtsZ polymers can disassemble (Mukherjee and Lutkenhaus, 1998; Romberg et al., 2017).

FtsZ is associated with cell division in most bacteria. In *E. coli*, for example, the polymerisation is symmetrical and assembles into a Z ring at the midpoint of the cell which circumscribes the interior of the cell in a GTP dependant manor (Adams and Errington, 2009; Erickson, 1995; Mukherjee and Lutkenhaus, 1994). The Z ring constricts to initiate division of the cell (Erickson et al., 2010). FtsZ is an integral part of a protein complex which is known as the divisome. Other components of the divisome are recruited to the Z-ring whereby the divisome constricts and directs the synthesis of new cytoplasmic membrane and cell wall material, producing a cross-wall or septum (Wu and Errington, 2012).

The Z ring is a dense band of short FtsZ filaments at the mid-cell (Holden et al., 2014; Strauss et al., 2012; Yao et al., 2017). These short filaments move by treadmilling. Treadmilling is a motion whereby an asymmetric filament polymerises at the plus end and depolymerises at the minus end. GTP hydrolysis is the rate determining factor for the depolymerisation and treadmilling speed (Bisson-Filho et al., 2017; Loose and Mitchison, 2014; Yang et al., 2017). The

rate of constriction and cell wall synthesis speed is dependant on FtsZ filament treadmilling speed in *B. subtilis* (Bisson-Filho et al., 2017).

The timing and location of the division is of vital importance to the cell, and therefore the divisome is subject to strict regulation. In rod-shaped bacteria, such as *B. subtilis* and *E. coli*, two distinct systems have been described which restrict division to the mid-cell (Adams and Errington, 2009; Barák and Wilkinson, 2007; Harry et al., 2006). The first of these is the Min system (Figure 1.14.1). The Min system prevents division close to the cell poles by inhibiting the polymerisation of FtsZ (Barák and Wilkinson, 2007; Bramkamp and van Baarle, 2009; Lutkenhaus, 2007). MinC inhibits the formation of the Z ring. MinC associates with MinD, a membrane-bound ATPase, and is directed to the cell poles by either DivIVA (in *B. subtilis*) or MinE (in *E. coli*). DivIVA is located at the cell poles and recruits the MinCD complex. MinE oscillates from pole to pole in the cell and is therefore most often in the midpoint of the cell where it excluded the MinCD complex. Both DivIVA and MinE add to the levels of MinCD at the poles, thereby preventing inappropriate Z ring formation at these sites (Barák and Wilkinson, 2007; Bramkamp and van Baarle, 2009; Lutkenhaus, 2007).

The second system which aids in restricting the site of cell division to the mid-cell is nucleoid occlusion (Figure 1.14.1). Nucleoid occlusion inhibits cell division in the vicinity of the chromosome to ensure chromosomes are not guillotined by the septum (Hajduk et al., 2016; Yu and Margolin, 1999). Noc (in *B. subtilus*) and SlmA (in *E. coli*) were the first nucleoid occlusion factors discovered (Bernhardt and De Boer, 2005; Wu and Errington, 2004). SlmA directly interacts with FtsZ on the surface of each nucleoid to inhibit Z ring assembly, whereas the functionally analogous Noc protein does not directly interact with FtsZ (Adams et al., 2015; Cho et al., 2011; Tonthat et al., 2013). Noc has been shown to corral the FtsZ filaments during cytokinesis. Rather then it inhibining *de novo* formation of FtsZ rings over the nucleoid, it inhibits the FtsZ from migrating away from its location at the midcell (Yu et al., 2021).

Division in *noc min* and *slmA min* double mutants was severely inhibited which was unexpected as without these regulatory systems, division could occur anywhere along the cell. Instead, these two negative regulatory systems are required to sequester FtsZ to the mid-cell and in the absence of this, FtsZ levels do not reach sufficiently high levels to form a Z ring (Bernhardt and De Boer, 2005; Wu and Errington, 2012, 2004). Chromosome replication and

segregation may also play a part in this and have direct links with cell division (Hajduk et al., 2016).

FtsZ requires proteins to promote the stabilisation of the Z ring as well as to anchor it to the membrane at sites of future cell division. For Gram-negative bacteria, such as *E. coli*, two proteins are positive regulators of the Z ring and are the transmembrane proteins FtsA and ZipA. Both of these proteins interact directly with FtsZ and provide the interaction between the Z ring and the membrane necessary for division and are essential for the recruitment of the next set of proteins to the divisome (Pichoff and Lutkenhaus, 2005, 2002). The ZipA protein is found exclusively among Gram-negative bacteria while FtsA homologues are also found within Gram-positives. FtsA is an actin-like protein which is able to form actin-like protofilaments (Szwedziak et al., 2012).

In *Streptomyces*, like all bacteria, cell division is driven by FtsZ, however it is not an essential protein in *Streptomyces* as *Streptomycetes* are still viable in the absence of division (McCormick et al., 1994). While viable, it is not capable of producing any spores or compartmentalisation within the hyphae resulting in a strain which does not sporulate nor is it able to grow properly (McCormick et al., 1994). Prior to the formation of spores, FtsZ has been shown to form a series of rings along aerial hyphae which appear as an evenly spaced ladder (Schwedock et al., 1997; Zhang et al., 2016). In an FtsZ null mutant, sporulation septa nor cross-walls in the vegetative hyphae are able to form. This suggests that the entire colony has no compartmentalisation and indeed it has been observed that were lysis in the wild type strain was limited to a small compartment, in an FtsZ knockout mutant the whole colony lysed (Santos-Beneit et al., 2017). However, in the knockout mutant it was sometimes possible to get small sections of the hyphae which survived when the rest of the colony lysed. These are enclosed by a hyphal tip and a branch point which appears to have sealed the hyphae at that point without the presence of FtsZ (Santos-Beneit et al., 2017). This has also been observed in the wildtype and suggests that there is a mechanism by which the membrane can seal itself without the need for FtsZ at the branch points (Santos-Beneit et al., 2017).

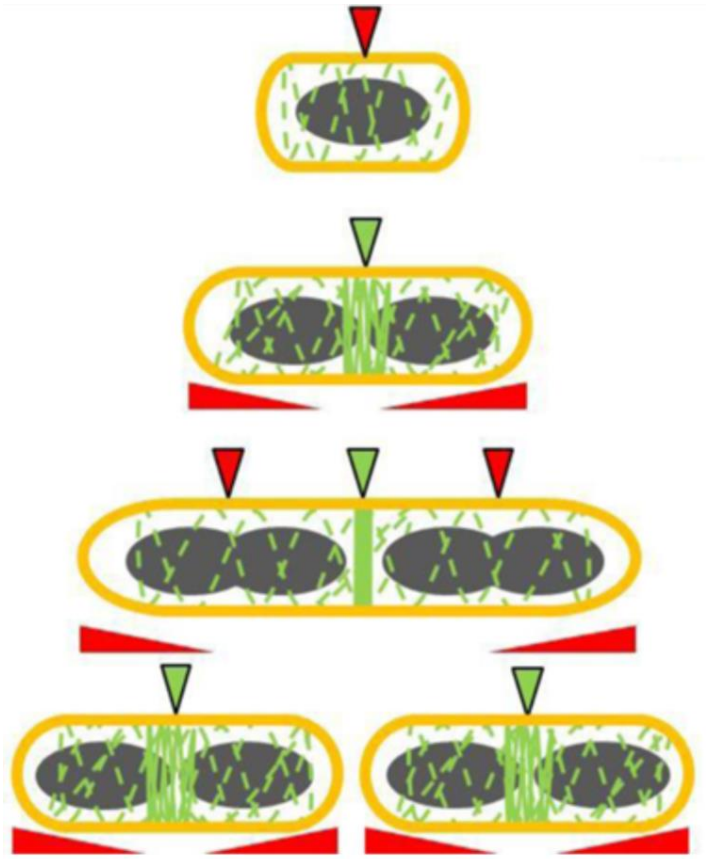

Figure 1.14.1 Z ring formation and nucleoid occlusion.

A mid-cell defining factor marks the position of the future division site at which the Z ring will assemble. At this stage, mid-cell becomes competent for Z ring assembly. However, the early utilization of this division site by the Z ring is blocked by nucleoid occlusion (demonstrated by the red arrow). The mid-cell site becomes unmasked (green arrow) upon segregation of the bulk of the replicated chromosomes (shown in grey). This causes Noc and other nucleoid occlusion factors to clear the central region of the cell. As the cells elongate, other division sites competent for Z ring assembly become available at the cell quarters. These sites are masked (in red) by the combined activity of Noc (and possibly other nucleoid occlusion factors), and Min that acts at a distance from the pole, allowing FtsZ to concentrate to the mid-cell division site only. The red elongated triangles below each cell correspond to the position and concentration of Min (higher at the poles). The quarter (potential) division sites only become available after Z ring constriction is initiated at the first (mid-cell) site, allowing separated daughter cells to initiate a new division cycle. The dashed green lines along the length of the cell indicate the constant dynamic movement of FtsZ throughout the cell. Taken from (Rodrigues and Harry, 2012).

1.15 Streptomyces Development

Streptomyces coelicolor is a model organism for filamentous growth for actinomycetes. *Streptomycetes* are Gram-positive and GC rich. They are soil dwelling bacteria and, unlike most other bacteria, *Streptomyces* have linear chromosomes (Lin et al., 1993) with *S. coelicolor* containing over 7500 genes within its 8.5 Mbp chromosome (Bentley et al., 2002).

Streptomycetes produce a great number of secondary metabolites including over two-thirds of the clinically useful antibiotics of natural origin such as tetracycline, streptomycin, and chloramphenicol (Atta, 2015; Bibb, 2013). Clinically relevant secondary metabolites, other than antibiotics, are also produced: antifungals, including nystatin and amphotericin B (Fjærvik and Zotchev, 2005); anticancer; immune-suppressive; and anthelmintic agents (Baltz, 2007) all contribute to the clinical relevance of *Streptomycetes*. All of the aforementioned antibiotics and antifungals are drugs which are listed by the World Health Organisation as essential medicines (The International Pharmacopoeia, 2015). This gives the study of *Streptomyces* great importance as they produce these secondary metabolites which are advantageous for human health treatments.

Study of *Streptomyces* is also of great importance due to the close relationship with *Mycobacterium tuberculosis*. *M. tuberculosis* is pathogenic and poses a great issue for human health. The World Health Organisation have estimated that, in 2012 alone, 8.6 million people developed TB and 1.3 million died from the disease around the globe (Who, 2013). By gaining a greater understanding of *Streptomyces*, there is greater knowledge which could also be applied to *M. tuberculosis* and could help with the targeting of drugs to treat it. *M. tuberculosis* and *S. coelicolor* are both actinomycetes and grow by polar growth. This close link and growth method commonality mean that by studying the much less dangerous *S. coelicolor* findings from this organism can be applied to the pathogen.

S. coelicolor exhibits a more complex life cycle than most other bacteria, as it does not divide by binary fission, but by filamentous growth (Figure 1.15.1). Initially, ovoid spores which contain a single chromosome begin to germinate and germ tubes are formed (Jyothikumar et al., 2008). These germ tubes contain multiple chromosomes and grow by tip extension and branching events that occur along the lateral wall of the hyphae in a similar way to filamentous fungi (Errington, 2003). Branching is essential for exponential growth of the hyphae as the rate

of single tip extension is limited (Chater, 1993; Flärdh, 2003b). When grown on semisolid agar medium, hyphae first grow across and into the medium forming the vegetative mycelium. In the vegetative mycelium, cell division does not occur. These multi-chromosomal hyphae are occasionally segmented by septation but this is not followed by cell division. This stage of growth is characterised by colonies which appear shiny and bald which is the classic phenotype for mutants which are blocked at this stage of development (Flärdh and Buttner, 2009; McCormick and Flärdh, 2012). In response to lack of nutrients, aerial mycelium are formed by extension into the air (Kelemen and Buttner, 1998). Aerial mycelium grow as multi-genomic hyphae with less branching than in vegetative hyphae. Colonies at this stage of development appear fuzzy and white which is the classic appearance for mutants blocked at this stage of development. Once growth has ceased, septa are placed at equal spacing along the unbranched hyphae with a single chromosome in each pre-spore compartment in these aerial hyphae. The spore chain then matures into unigenomic spores (Figure 1.15.1) and a grey polyketide pigment is produced (Chater, 1993; Flärdh and Buttner, 2009; Kelemen et al., 1998).

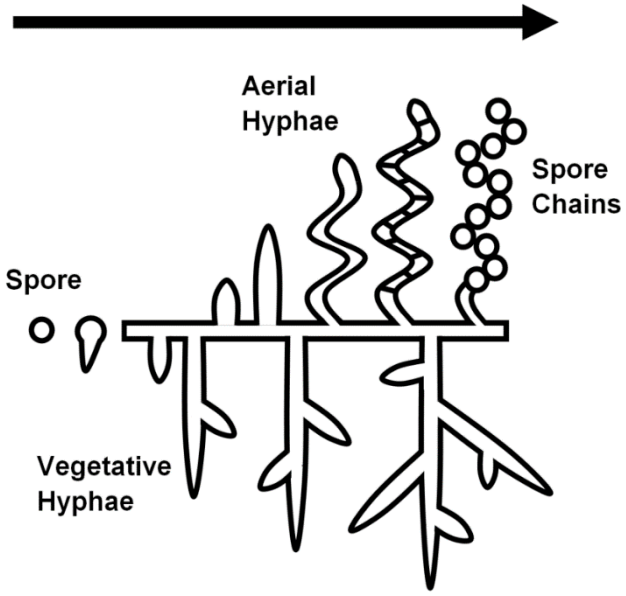

Figure 1.15.1 Life cycle of *Streptomyces coelicolor.*

The life cycle of *S. coelicolor* begins with a single uni-genomic spore which germinates with the protrusion of either one or two germ tubes. *S. coelicolor* then grows and branches forming a network of vegetative hyphae which grow into the media for uptake of nutrients. Upon nutrient depletion, aerial hyphae are erected above the surface of the media. After the cessation of aerial growth, septa are formed along the length of the aerial hyphae creating pre-spore compartments. These compartments then mature into spores from which the life cycle can begin again.

1.16 Comparison of FilP to Eukaryotic Intermediate Filaments and Crescentin

Intermediate Filament Definition and Characterisation

Sequence conservation within eukaryotic intermediate filaments is relatively low. The sequence identities between lamin and vimentin, for example, is around 29%. Therefore, it is not possible to define intermediate filaments based on sequence alone and a combination of factors must be considered. According to the strict definition of intermediate filaments, all intermediate filaments: (i) can self-assemble into higher order structures without the requirement for cofactors; (ii) they have a tripartite structure with a head and tail domain flanking a central rod domain; (iii) the rod domain is coiled-coil in nature; (iv) the rod domain is around 310 or 350 amino acids for a cytoplasmic or nuclear intermediate filament respectively; (v) the rod domain is divided into three sub-domains; (vi) the coil 2 domain contains a characteristic stutter (A. a Chernyatina et al., 2015).

Sequence Comparison of Intermediate Filaments and FilP

Sequence comparison of the two eukaryotic intermediate filaments vimentin and lamin shows that they are not very similar, with only around 29% sequence identity. Comparison of these established intermediate filaments with FilP showed that FilP had around 22% and 23% sequence identity with vimentin and lamin respectively. FilP, however, had a higher sequence identity with that of crescentin at 28% which resembles that of the sequence identities between the cytoplasmic vimentin and the nuclear lamins from eukaryotic intermediate filaments (Table 1.16.1).

As intermediate filaments have a variable head and tail domain which have very low sequence identities, it is perhaps more accurate to look only at the rod domains for the sequence identities. For rod domains only, vimentin and lamin rise to 32% sequence identities whereas FilP compared to vimentin and lamin respectively rose to 24% and 26%. However, comparison of only the rod domains for FilP and crescentin did not change the percentage identity (Table 1.16.1).

Table 1.16.1 Sequence identity of vimentin, lamin, FilP and crescentin.
Sequence identities of FilP (*Streptomyces coelicolor*), vimentin (*Mus musculus*), lamin C (*Homo sapiens*), crescentin (*Caulobacter crescentus*) and the coiled-coil rod domains of these proteins only. Uniprot numbers are indicated in brackets. Compared using the software Clustal Omega (Madeira et al., 2019).

	FilP (A0A0P4R0U8)	**Vimentin** (P20152)	**Lamin** (W8QEH3)	**Crescentin** (Q6IET3)
FilP	100%	21.6%	23.4%	27.9%
Vimentin		100%	29.0%	22.0%
Lamin			100%	24.5%
Crescentin				100%
	FilP rod	**Vimentin rod**	**Lamin rod**	**Crescentin rod**
FilP rod	100%	24.1%	26.1%	27.7%
Vimentin rod		100%	31.8%	23.7%
Lamin rod			100%	26.8%
Crescentin rod				100%

Domain Comparison of Intermediate Filaments and FilP

Comparison of the domain organisation of FilP to that of vimentin, lamin, and crescentin shows that all have the characteristic tripartite structure of eukaryotic intermediate filaments (Figure 1.16.1). However, the rod domain of FilP is shorter than the rod domains of intermediate filaments. Intermediate filaments normally have rod domains of around 310 or 350 amino acids for cytoplasmic or nuclear intermediate filaments respectively. The rod domain of FilP is only 270 amino acids long, crescentin on the other hand has a rod domain which is 365 amino acids long and thus slightly longer than that of the expected length for an intermediate filament rod domain. Following the strict definitions for intermediate filaments as defined by the eukaryotic field, prokaryotic intermediate filaments are not strictly intermediate filaments.

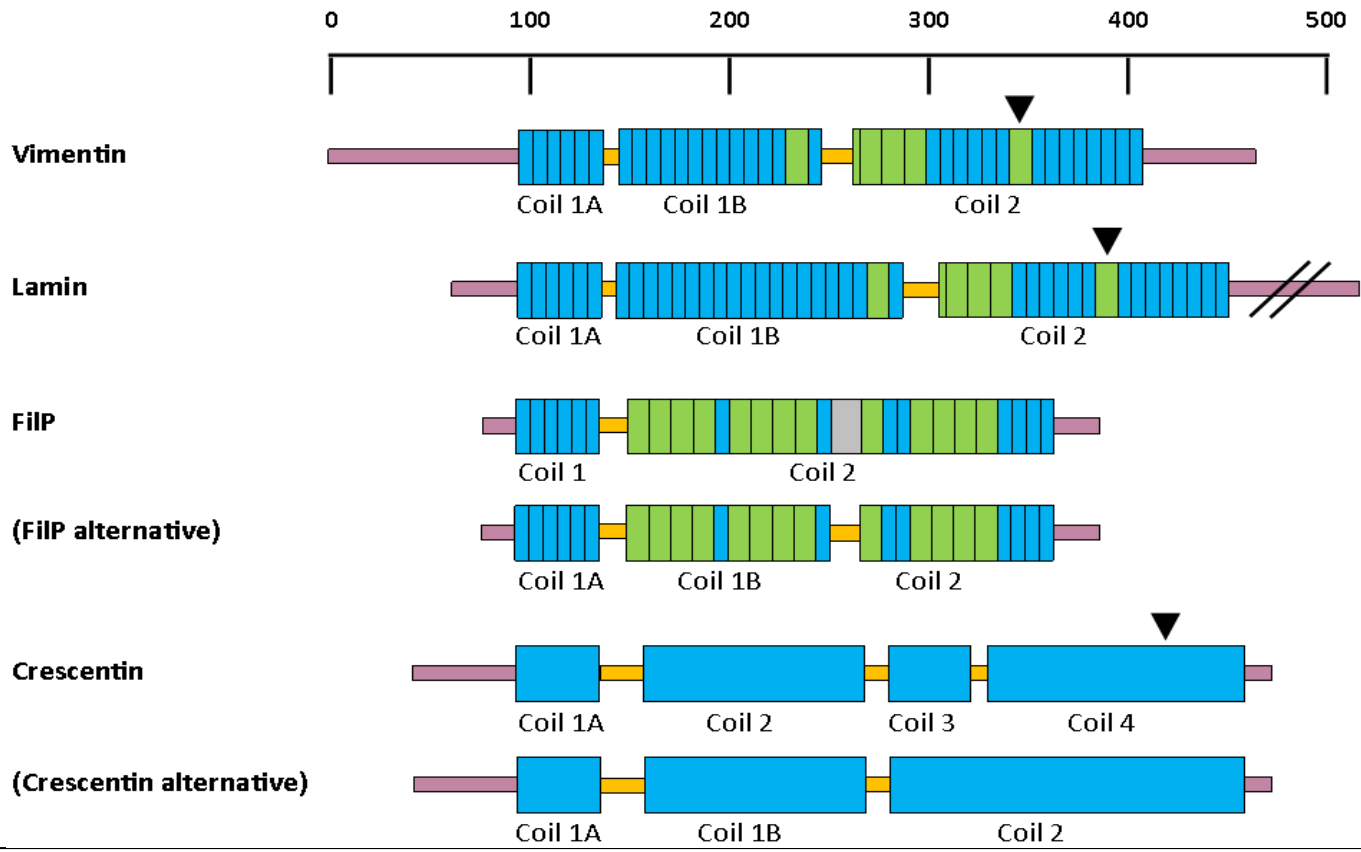

Figure 1.16.1 Comparison of FilP domain organisation to eukaryotic intermediate filaments and crescentin.

The predicted domain architecture of FilP is schematically shown together with that of two IF proteins, cytoplasmic vimentin, nuclear lamin C and crescentin from *Caulobacter crescentus*. The blue boxes show α-helical segments predicted or shown to form a heptad coiled-coil repeat sequence, green boxes show segments predicted to form hendecad repeat sequences, the yellow boxes show predicted linker subdomains, purple boxes show head and tail domains. All proteins shown with N-terminus on the left. Black arrows show the characteristic stutter for intermediate filaments.

Where the rod domains of the eukaryotic intermediate filaments are separated into three subdomains, named coil 1A, coil 1B, and coil 2, the proposed architecture for that of both FilP and crescentin differs (Figure 1.16.1). Heptad and hendecad motifs were assigned to vimentin and lamin as designated by Chernyatina et al (A. a Chernyatina et al., 2015) which were based on predictions of residues buried in the hydrophobic core by the NetSurfP algorithm (Petersen et al., 2009) compared to residues which gave typical 'core-like' signal in SDSL-EPR experiments (Budamagunta et al., 2007). For FilP, the amino acid sequence was used to assign heptad or hendecad motifs depending on the positions of hydrophobic amino acids. For crescentin, we do not have any information on individual motifs.

Crescentin was proposed to have four subdomains however, as discussed earlier, at the time crescentin was discovered, the rod domain of eukaryotic intermediate filaments was also thought to consist of four subdomains. Based on x-ray crystallography of fragments of vimentin, the previously named coil 2A and 2B have been combined into one sub-domain called coil 2, proposing three subdomains for eukaryotic intermediate filaments. In the absence of crystallographic data for crescentin, it is possible that crescentin also has three subdomains instead of four. This would make it more similar to eukaryotic intermediate filaments, but in the absence of structural data, this cannot be established. FilP was proposed to have only two sub-domains of the rod domain, where the second sub-domain is dominated by a novel 51-mer repeats. The two sub-domain structure of FilP does not conform to the definitions for the intermediate filaments (Walshaw et al., 2010). However, there is a motif in the middle of the second sub-domain which lacks clear coiled-coil assignment. It is possible that this could be a second linker, which would in fact divide coil 2 into two separate coils, making the sub-domain organisation of FilP more similar to that of the intermediate filament definitions (Figure 1.16.1).

All four proteins shown in Figure 1.16.1 have very similar coil 1A subdomains. FilP, vimentin and lamin all contain six heptad repeat sequences, data for heptad and hendecad repeat assignment is not available for crescentin. However, the coil 1A subdomain of crescentin contains 42 amino acids which equivalent of six heptad repeats and therefore appears likely to consist of heptad repeat sequence. This would therefore be a useful feature to be used as a definer for intermediate filaments which spans both eukaryotes and prokaryotes.

For coil 1B (if we here compare this to the first half of coil 2 for FilP) vimentin has been seen to contain twelve heptad repeats followed by one hendecad and a final heptad repeat sequence. This is very similar to that of lamin which has 18 heptad repeats followed by one hendecad and a final heptad repeat sequence. However, the coiled-coil architecture of FilP differs from vimentin and lamin. The domain equivalent in FilP contains two 51-mer repeats (four hendecad, one heptad, four hendecad, one heptad). This appears markedly different although this prospective subdomain in FilP contains 102 amino acids which is the same as that for vimentin and 22 amino acids shorter than that of lamin. Intriguingly, the C terminal end of the coil 1B sub-domain of FilP is very similar to that of vimentin and lamin with a hendecad followed by a heptad repeat sequence. The heptad and hendecad component for this domain in crescentin is unclear, however it has 111 amino acids which is in between the lengths for vimentin and lamin (Figure 1.16.1, Figure 1.16.2).

The coil 2 subdomain for vimentin and lamin have the same heptad and hendecad architecture with three and a half hendecad repeats, six heptad repeats, one hendecad repeat (the stutter), and eight heptad repeats. The equivalent part of this in FilP (the second half of coil 2) differs from that of vimentin and lamin again in that it contains one hendecad repeat, two heptad repeats, four hendecad repeats, and four heptad repeats before the tail domain. The similarities in the coil 2 subdomain between FilP and vimentin and lamin include that all start with hendecad repeats and finish with heptad repeat sequences (Figure 1.16.1, Figure 1.16.2).

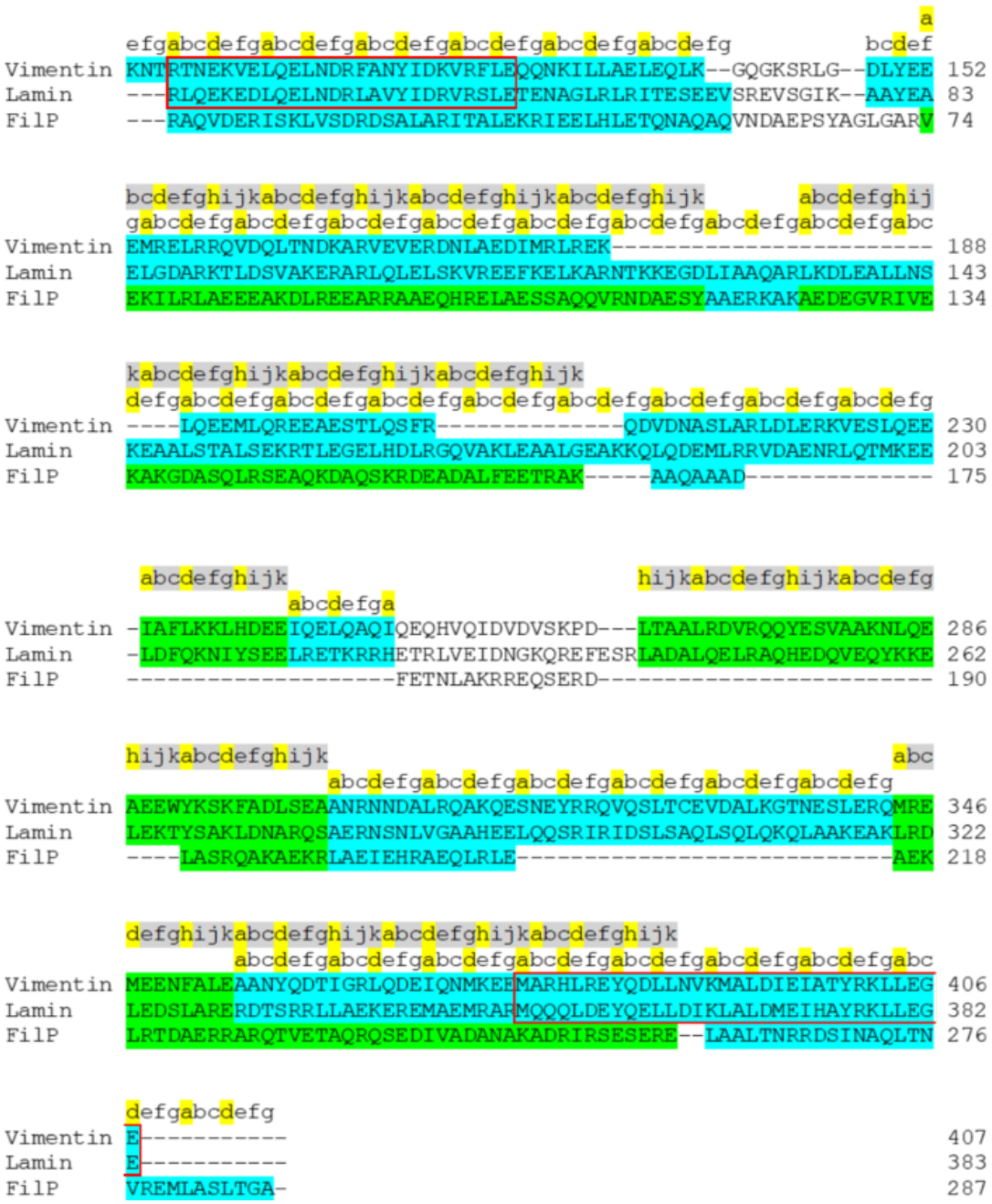

Figure 1.16.2 Sequence alignment of vimentin (*Mus musculus*), lamin (*Homo sapiens*) and FilP(*Streptomyces coelicolor*) rod domains.

Top line (grey highlight) hendecad repeat lettering. Second line heptad repeat lettering. Blue highlight heptad repeat, green highlight hendecad repeat, yellow highlight hydrophobic positions. Heptad and hendecad motifs assigned to vimentin and lamin (A. a Chernyatina et al., 2015). Head and tail domain sequences are not shown. Red boxes on vimentin and lamin indicate areas of highly conserved residues (Kapinos et al., 2010; Köster et al., 2015).

The characteristic stutter which appears in the eukaryotic intermediate filaments is essentially a hendecad repeat surrounded by heptad repeats, hence a slight alteration in the repeat sequence, a stutter. This is present in the eukaryotic intermediate filaments (Figure 1.16.1) as well as in crescentin. FilP on the other hand does not have a stutter identified as it has several hendecad repeats sequences within its coil 2 subdomain. This means that it is difficult to identify a stutter from the other hendecad repeats, or whether they should all be considered stutters.

Summary of Comparison between FilP and Eukaryote Intermediate Filaments

Sequence analysis of FilP, its domain structure and the positions of heptad and hendecad repeats show some similarity but also major differences when compared to eukaryote intermediate filaments, such as vimentin and lamin.

Intermediate filaments are defined by six criteria:

- Intermediate filaments can self-assemble into higher order structures without the requirement for cofactors.
- Intermediate filaments have a tripartite structure with a head and tail domain flanking a central rod domain.
- The rod domain is coiled-coil in nature.
- The rod domain is 310 or 350 amino acids for a cytoplasmic or nuclear intermediate filament respectively.
- The rod domain consists of three sub-domains.
- The coil 2 domain contains a characteristic stutter.

FilP fulfils the first three requirements. It has been shown to self-assemble into higher order structures without the requirement for cofactors, it has a tripartite structure with a head and tail domains flanking the central rod domain and this rod domain is coiled-coil in nature. However, FilP has a slightly shorter rod domain of only 270 aa. Current sub-domain assignment (Walshaw et al., 2010) also suggests that FilP has two sub-domains, and not three.

However, our assignments of heptad and hendecad repeats (Figure 1.16.2) suggested that there is a potentially non coiled-coil motif in the centre of coil 2 which could in fact be a second linker. Only further structural studies will establish the exact sub-domain organisation of FilP. The last criteria of an intermediate filament, the inclusion of a stutter in the middle of coil 2 sub-domain, is difficult to assess due to the many hendecad repeats in the coil 2 subdomain of FilP. Overall, FilP appears to largely fit with the definition of eukaryotic intermediate filaments but does fall short of the strict length characteristics. For the definition to include both eukaryotic and prokaryotic intermediate filaments, the strict length limits for the rod domain should be lifted. The coil 1A similarity across all whereby it contains six heptad repeats should also be included as part of the definition.

1.17 Aims

This thesis aims to analyse the protein FilP from *S. coelicolor* and to assess it in various ways. These include characterisation of higher order structures which FilP can make under varying conditions *in vitro*. A further aim is the generation of a series of truncated FilP proteins to establish which motif within FilP is required for higher order assembly, assessing the higher order character of these truncated FilP proteins, and nanogold staining of FilP and truncated FilP proteins to visualise where the N-terminus of the protein is within the structures. Further to this, FilP and truncated FilP proteins will be expressed in *E. coli* to assess the morphology of the cells using phase contrast and fluorescence microscopy. *S. coelicolor* FilP knockout strains will be generated to characterise these macroscopically and microscopically as well as to generate a C-terminally mCherry tagged FilP in its native location in *S. coelicolor* and to use fluorescence microscopy to assess the localisation of FilP mCherry fusion at varying growth stages in both single and double crossover strains.

2 Materials and Methods

2.1 Bacterial strains and plasmids

E. coli Strains Used in this Study

Table 2.1.1 *E. coli* strains used in this study.

Strain	Genotype	Reference or Source
DH5α	*F-λ- endA1 glnV44 thi-1 recA1 relA1 gyrA96 deoR nupG Φ80dlacZΔM15 Δ(lacZYA-argF)U169 hsdR17(r_K^- m_K^+)*	(Hanahan, 1983)
BW25113/pIJ790	*λ- Δ(araD-araB)567 ΔlacZ4787(::rrnB-4), lacIp-4000($lacI^Q$) rpoS369(Am) rph-1 Δ(rhaD-rhaB)568 hsdR514*	(Datsenko and Wanner, 2000)
ET12567	*F- dam::Tn9 dcm6 hsdM hsdR*	(MacNeil et al., 1992)
BL21 (DE3) pLysS	*F-, dcm, ompT, lon, $hsdS_B$(r_B^- m_B^-), gal, λ (DE3), pLysS(cm^R)*	(Studier and Moffatt, 1986)

S. coelicolor Strains used in this Study

Table 2.1.2 *Streptomyces* strains used in this study

Strain	Genotype	Reference or Source
M145	$SCP1^-$ $SCP2^-$ Pgl^+	(Hopwood et al., 1985)
filP::aac(3)IV	M145 *filP::aac(3)IV*	(Holmes, 2012)
FilP mCherry	M145 *filP:: filP-mCherry-ApraR*	This study

Plasmid and Cosmid DNA used in this Study

Table 2.1.3 Plasmid/Cosmid DNA used in this study.

Plasmid	Genotype	Reference or Source
8F4	Supercos Cosmid with a 33.9 Kbp chromosomal fragment with *filP* and *scy.*	(Redenbach et al., 1996)
8F4/*filP::filP-mCherry-ApraR*	Supercos Cosmid with a 33.9 Kbp chromosomal fragment with 2.1 Kbp cassette insert containing *mCherry* and *ApraR* C terminally to the *filP* gene.	This study
pET28a	*ori* pBR322, T7 Promoter, His•Tag coding sequence, *lacI, kan, ori* f1	Novagen
pET28a-FilP	pET28a with *filP*	(Holmes, 2012)
pET28a-FilPC	pET28a with *filPC*	This work
pET28a-FilPT	pET28a with *filPT*	This work
pET28a-FilPN	pET28a with *filPN*	This work
pET28a-FilP Δlinker	pET28a with *filP Δlinker*	This work
pET28a-2CC51	pET28a with *2CC51*	This work
pET28a-miniFilP	pET28a with *minifilP*	This work
pET28a-FilP Δtail	pET28a with *filP Δtail*	This work
pET28a-FilP Δ4x7	pET28a with *filP Δ4x7*	This work
pET28a-FilP Δ4x7 2x11	pET28a with *filP Δ4x7 2x11*	This work
pET28a-miniFilP Δtail	pET28a with *miniFilP Δtail*	This work
pET28a-miniFilP Δ4x7	pET28a with *miniFilP Δ4x7*	This work
pET28a-FilP-mCherry	pET28a with FilP mCherry	Kelemen Lab, University of East Anglia

2.2 Media

Solid Media

SFM (Soya Flour Mannitol): For general growth and phenotypic analysis of *S. coelicolor* strains.6 g of mannitol was dissolved in 3000 ml of tap water while 6 g soya flour and 6 g agar were measured into 500 ml Duran bottles. The dissolved mannitol media was dispensed in 300 ml aliquots into Duran bottles and twice autoclaved.

Lennox Broth (LB) Agar (Kieser et al., 2000): For growing of *E. coli* strains and spore titres of *S. coelicolor* strains. 16 g tryptone, 8 g yeast extract, 8 g NaCl and 1.6 g glucose were dissolved in 1600 ml dH_2O, while 4 g of agar was measured into 500 ml Duran bottles. The dissolved media was dispensed in 400 ml aliquots into Duran bottles and autoclaved.

Liquid Media

Lennox Broth (LB) (Kieser et al., 2000): For growing *E. coli* strains.10 g tryptone, 5 g yeast extract, 5 g NaCl, and 1 g glucose were dissolved in 1000 ml dH_20. Once dissolved, the media was dispensed, either in 10 ml aliquots into universals or in 50 ml aliquots into 250 ml conical flasks, and autoclaved.

SOB (Super Optimal Broth): For growing *E. coli* BW25113/ pIJ790.10 g tryptone, 2.5 g yeast extract, 1 ml 5 M NaCl, 0.093g KCl, 5 ml 1 M $MgCl_2$, and 3g $MgSO_4$ were dissolved in 500 ml dH_20. Once dissolved, the media was dispensed in 10 ml aliquots into universals and autoclaved.

2.3 Bacterial Growth Conditions and Storage

Streptomyces coelicolor strains

S. coelicolor strains were grown on SFM containing appropriate antibiotics at 30°C for the amount of time required for them to reach the desired developmental stage. For storage and spore preparation spores were streaked onto an SFM plate to generate a confluent lawn and incubated at 30 °C until mature spores developed. Spores were harvested by rubbing spores in a layer of water using a cotton bud and this spore suspension was collected in a falcon tube using a Pasteur pipette. The spore suspension was centrifuged for 10 minutes at 4500g at 4°C and the supernatant removed. Spores were resuspended in 1 ml 20% glycerol and stored at -20°C in a 2 ml screwcap microcentrifuge tube.

Escherichia coli strains

E. coli strains were grown on either solid or liquid LB and incubated at 37°C (with the exception of BW25113/pIJ790 which was grown at 30°C due to the presence of a temperature sensitive plasmid).

Antibiotic concentrations used in this study

Table 2.3.1 Antibiotic concentrations used in this study.

Antibiotic	**Stock (mg/ml)**	***Streptomyces* final concentration** (μg/ml)	***E. coli* final concentration** (μg/ml)
Apramycin	100	50	50
Chloramphenicol	25	-	25
Kanamycin	100	50	50
Nalidixic Acid	25	25	-

2.4 General Molecular Biology Methods

Plasmid DNA isolation from *E. coli*

A single colony of DH5α (or BW25113 for cosmids after cassette targeting) containing the desired plasmid DNA was inoculated into 50 ml LB supplemented with the appropriate antibiotic. The inoculum was grown overnight at 37°C (shaking 250 rpm). The overnight growth was collected in a 50 ml falcon by centrifugation for 5 minutes at 5000 g at 4°C. The cells were washed in 40 ml 50 mM Tris/HCl, 10 mM EDTA pH8.0 and centrifuged for 5 minutes at 5000 g at 4°C. The supernatant was discarded, and cells re-suspended in 1 ml of the same solution before the addition of 2 ml 200 mM NaOH, 1% SDS. The cells were mixed gently by turning the falcon tube and incubated for 4 minutes on ice. After incubation 1.5 ml 3 M potassium acetate pH5.5 was added, and the lysate shaken vigorously. The lysate was incubated for 10 minutes on ice before centrifugation for 10 minutes at 5000 g at 4°C. The supernatant was transferred to a 15 ml falcon and mixed with 500 µl of 1:1 phenol:chloroform. The extract was vortexed for 30 seconds and centrifuged for 5 minutes at 5000 g. After centrifugation the aqueous phase was collected in a fresh 15 ml falcon and 7 µl of 30 mg/ml RNase was added. The extract was incubated for 1 hour at 37 °C. After incubation another phenol: chloroform extraction was performed as before. After collecting the aqueous phase the DNA was precipitated by mixing 1:1 with isopropanol kept at -20°C, the solution was mixed by inversion and incubated on ice for 30 minutes. The precipitated DNA was centrifuged for 15 minutes at 5000 g at 4°C. The supernatant was discarded, and the DNA pellet washed with 2 ml 70% ethanol kept at -20°C. The DNA was centrifuged for 5 minutes at 5000 g at 4°C and the supernatant was discarded. The DNA pellet was allowed to air dry for 5 minutes before re-suspension in 200-400 µl sterile dH20. DNA was stored at -20°C.

Agarose Gel Electrophoresis of DNA

Agarose gels were cast using the Bio-Rad Mini-Sub and Sub-cell trays. Gels were made in a range between 0.7% and 1% agarose in 1x TAE buffer with the addition of 0.5 µg/ml ethidium bromide. DNA was mixed with 1x loading dye and run on gels submerged in 1x TAE buffer. Gels were imaged with UV light using a Bio-Rad trans-illuminator. A size marker of λ DNA digested with HindIII, and EcoRI was used to estimate band sizes.

50x TAE: 2M Tris acetate, 50 mM EDTA, pH8.0

10x loading dye: 50 mM Tris, 50 mM EDTA, 50% glycerol, pH7.4. This was autoclaved and 0.05% xylene cyanol, 0.05% bromophenol blue were added.

PCR

PCR reactions were performed using a BioRad T100 Thermo Cycler.

Hi-fidelity PCR

Phusion High-Fidelity DNA Polymerase was used for the generation of PCR fragments used for cloning. Reactions were performed under the following conditions:1x Phusion GC Buffer, 200 µM of each of the four dNTPs, 1.5 mM $MgCl_2$, 3% DMSO, 1 µM of each primer, and 0.02 U/µl Phusion DNA polymerase. These were subject to initial denaturation at 98°C for 2 mins, denaturation 98°C for 20 seconds, primer annealing *°C for 30 seconds, extension 72°C for ** seconds. Denaturation, primer annealing, and extension steps are repeated for 25 cycles. Final extension 72°C for 5 minutes and cool down 20°C for 20 minutes. (*primer annealing temperature set according to melting temperature calculator at www.thermoscientific.com/pcrwebtools. Calculated temperature was adjusted down by 5°C due to presence of DMSO. ** Extension time was proportional to length of the product as calculated at 30 seconds per 1 Kbp.)

Low-Fidelity PCR

Go Taq DNA Polymerase (Invitrogen) was used for low-fidelity PCR for diagnostic purposes. Reactions were performed under the following conditions: 1 x Go Taq polymerase buffer, 200 µM of each of the four dNTPs, 2.5 mM MgCl2, 5% DMSO, 1 µM of each primer, and0.02 U/µl Go Taq DNA polymerase. These were subject to initial denaturation at 96°C for 5 mins, denaturation 98°C for 20 seconds, primer annealing 55°C* for 30 seconds, extension 72°C for ** seconds. Denaturation, primer annealing, and extension steps are repeated for 30 cycles. Final extension 72°C for 5 minutes and cool down 20°C for 5 minutes. (*Primer annealing temperature was initially set at 55°C, but altered if no product visible. ** Extension time was proportional to length of the product as calculated at 30 seconds per 0.5 Kbp.)

Oligonucleotide Sequences used in this Study

Table 2.4.1 Oligonucleotide sequences	
Primer	**5' – 3' Sequence**
pET28 Xba FRW	CACTATAGGGGAATTGTGAGCGG
FilP Eco UT REV	GGTCAGAATTCGAGCGGGACTGCTGGGCCGGGACC
FilP Trunc Eco UT REV	GGTCAGAATTCCGCTTCGACTGCGCGTCCTTCTGC
FilP ∆tail Eco REV	GGA TCA AAG CTT TCA GGC GCC CGT GAG CGA CGC CAG C
FilP ∆4x7 Eco REV	GGA TCA GAA TTC TCA CTC GCG CTC CGA CTC CGA ACG G
FilP ∆4x7 2x11 Eco REV	GGA TCA GAA TTC TCA CTG GCG CTG CGC CGT CTC CAC G
FilP Eco UTC REV	
THAbps FRW	GGATCATCTAGAGCATATGAGCGACACTTCCCCCTACG
FilPC Xba Nde FRW 2	GGT CAT CTA GAG CAT ATG TCG TAC GCG GGT CTC GGC GC
THAbps REV	GGATCAGAATTCTCAGCGGGACTGCTGGGCCG
FilPN Eco UT REV	GGTCAGAATTCTCTGCGTCGTTGACCTGGGC
FilP FP Pro NOV FRW	GAGTCGGTCTCCCGCGGGGTCCCGGCCCAGCAGTCCCGCCCGGT CGCCACCAGCAAGG
FilP FP KO REV	CCCATGTTCGTACGGATTCGGCAGGCGTACCCCCCGCGCCCGCAT ATGTGTAGGCTGG

Restriction Digests

For the purposes of analysis plasmids containing recombinant DNA, the plasmids were digested with 10 U of the appropriate restriction enzymes from Roche in 1x the recommended digestion buffer in 20 µl total volume. Digests were incubated for 4 hrs or overnight at 37°C. Digests were stopped by heating to 65°C for 10 minutes then cooled on ice. The digested DNA was then loaded onto an agarose gel and analysed by electrophoresis.

Restriction digests for the purposes of preparing the DNA for cloning were digested with 20 U of the appropriate restriction enzyme from Roche in 1x the recommended digestion buffer in 150 µl total volume. Digests were incubated overnight at 37°C. Digests were stopped by heating to 65°C for 10 minutes then cooled on ice. The digested DNA was then loaded onto an agarose gel and separated by electrophoresis.

Isolation of DNA Fragments by Agarose Gel Electrophoresis

Post preparative restriction digest and separation of the fragments by electrophoresis, the agarose gels were visualised using long-wavelength UV light at 310 mm. Required fragments were excised using a scalpel and purified using the Qiagen QIAquick Gel Extraction kit. Fragments were stored in sterile water and stored at -20°C.

Ligation of DNA Fragments

Linearised vector and insert fragments were mixed in approximately 1:3 molar ratio in 11.5 µl volume made up with deionised water. This mix was incubated at 65°C for 2 minutes to denature any unspecific base-pairing then cooled on ice. 3 µl of ligation buffer and 0.5 µl of T4 ligase from Invitrogen was then added and the ligation mix was incubated at 4°C overnight.

Electroporation Transformation of Competent *E. coli* Cells

A single colony of the appropriate *E. coli* strain was inoculated into 10 ml LB with appropriate antibiotics and incubated overnight at 37°C or 30°C depending on the strain and shaken at 250 rpm. This overnight culture was subcultured, using 1% of the new volume, into either 10 ml or 50 ml fresh LB with appropriate antibiotics. This was incubated at the appropriate temperature until an OD600 of around 0.7. These cells were then collected by centrifugation for 5 minutes at 5000 g at 4°C. The supernatant was removed and the cells were washed twice in 10% glycerol centrifuging at 5000g for 5 minutes at 4°C. After the second wash, the pellet was resuspended in a final volume of around 100 µl per 10 ml initial culture 10% glycerol. For transformation, 45 µl cells were mixed with 1 µl plasmid or cosmid DNA. Electroporation was conducted in an ice cold 0.2 cm electroporation cuvette using a BioRad Gene Pulser 2 set to 200 Ω, 25 µF and 2.5 kV. After electroporation, cells were mixed with 500 µl ice cold LB and incubated for 1 hr at either 30°C or 37°C before plating onto LB agar plates with appropriate antibiotics. Plates were incubated overnight at either 30°C or 37°C.

Chemical Transformation of Competent *E. coli* Cells

A single colony of the appropriate *E. coli* strain was inoculated into 10 ml LB with appropriate antibiotics and grown overnight at either 30°C or 37°C depending on the strain. These overnights were subcultured, 500 µl into 50 ml fresh LB with appropriate antibiotics and incubated at the appropriate temperature until the culture reached an OD600 of around 0.4-0.6. Cells were collected by centrifugation at 5000 g for 5 minutes at 4°C. The supernatant was discarded, and the cells washed with 10 mM NaCl centrifuging in the same way as before. The supernatant was removed, and the pellet resuspended in 30 mM $CaCl_2$, 10 mM $RbCl_2$ and incubated on ice for 1 hr at 4°C. After this incubation, the cells were centrifuged as before and the pellet resuspended in 500 µl 30 mM $CaCl_2$, 10 mM $RbCl_2$. For transformation, 50 µl cells were mixed with 1 µl plasmid or cosmid DNA or 5 µl ligation mix and incubated for 30 minutes on ice. The cells were then heat shocked at 42°C for 1 minute, 1 ml ice cold LB was added and placed in ice to cool after heat shock. This was then placed at 30°C or 37°C for 1 hour before plating on to LB agar plates with appropriate antibiotics. Plates were incubated overnight at 30°C or 37°C.

Conjugation into *S. coelicolor*

Conjugation of vectors containing *oriT* into *S .coelicolor* was achieved using the *E. coli* strain ET12567/pUZ8002. A single colony of ET12567/pUZ8002 containing the desired plasmid or cosmid for conjugation was inoculated into 10 ml LB containing kanamycin, chloramphenicol and the antibiotic for which the plasmid or cosmid confers resistance. These were grown overnight at 37°C, 250 rpm. These overnights were subcultured by transferring 100 µl into fresh 10 ml LB with the appropriate antibiotics. The fresh culture was incubated with shaking at 37°C until it achieved an OD600 ~0.4-0.6. The cells were collected by centrifugation for 5 minutes at 5000 g at 4°C. The supernatant was removed and the cells washed twice with 10 ml LB centrifuging as before. The pellet was re-suspended in 250 µl LB and kept on ice. Approximately 10^8 spores of the desired *S. coelicolor* strain were added to 500 µl LB and germination activated by heating at 50°C for 10 minutes before cooling on ice. After cooling, the germinating spores were mixed with the ET12567/pUZ8002 cells containing the plasmid/cosmid and centrifuged for 2 minutes at 16,000 g at 4°C. The supernatant was removed, and the pellet re-suspended in 300 µl sterile water. A dilution series was set up in which three 10x dilutions were made. The stock and 3 dilutions were then plated onto SFM containing 10 mM MgCl2 and incubated at 30°C. After overnight incubation the plates were overlaid with 500 µl sterile dH20 containing nalidixic acid and the appropriate antibiotics. The plates were then incubated at 30°C until the appearance of colonies which had developed mature spores (5-8 days). Successful ex-conjugants were selected and streaked for single colonies on SFM supplemented with nalidixic acid and the appropriate antibiotics and grown at 30°C until spores were produced. Spore preparations of the strain were then generated, originating from a single colony of the streaked plate.

Replica plating

Determination of double crossover ex-conjugants during the generation of mutant strains of *S. coelicolor* was achieved through replica plating. Double crossover events lead to strains that are apramycin resistant but kanamycin sensitive. Spores were transferred from the SFM conjugation plate to first a LB plate containing kanamycin and nalidixic acid and then immediately an LB plate containing apramycin and nalidixic acid using a single sterile velveteen cloth such that both LB plates become a replica of the original SFM plate. The replica plates were incubated for 2 days at 30°C before being analysed for colonies present on the apramycin containing plate that were absent from the kanamycin containing plate. These colonies were identified on the original SFM conjugation plate and picked and streaked for single colonies on SFM supplemented with nalidixic acid and apramycin and grown at 30°C until spores were produced. Another round of replica plating was performed on the streaks once they had produced spores for confirmation by colony PCR and sequencing, after which spore preparations were generated for the successful double crossover strain.

2.5 Microscopy of *S. coelicolor* and *E. coli*

Coverslip Microscopy for *S. coelicolor*

Approximately 10^5 spores of *S. coelicolor* strains or *E. coli* cells were plated in a 1 cm^2 confluent patch (0.5 cm by 2 cm) on SFM or LB agar containing the appropriate antibiotics and IPTG if required. A glass coverslip, 22x22 mm with a thickness of 0.13-0.17 mm, was inserted into the patch at an approximate angle of 70˚ to the horizontal plane of the medium. Plates were incubated at 30°C for *S. coelicolor* or 37°C for *E. coli*. Coverslips removed at regular intervals in order to visualise the developmental stages of *S. coelicolor* or to visualise the development of the *E. coli* cells.

Cellophane microscopy for *S. coelicolor*

A cellophane was placed on the surface of SFM containing the appropriate antibiotics and IPTG if required. A spore dilution, such that approximately 1000 colonies per cm^2 would be plated, was made using spores of the desired *S. coelicolor* strain. The spores were plated onto the cellophane covered SFM plate and spread across the surface. The plates were incubated at 30°C for approximately 16-18 hours after which a 1 cm^2 cellophane patch was cut using a scalpel and stained.

Microscopy of *E. coli*

E. coli strains which required IPTG induction were inoculated from a single colony into 10 ml LB with appropriate antibiotics and incubated overnight at 37°C 250 rpm. This overnight culture was subcultured into fresh 10 ml LB with appropriate antibiotics and grown for 3 hours at 37°C 250 rpm after which they were plated for microscopy as detailed below.

Microscopy of *E. coli* on coverslips

E. coli cells were plated in a 1 cm^2 confluent patch (0.5 cm by 2 cm) on LB agar containing the appropriate antibiotics and IPTG. A glass coverslip, 22x22 mm with a thickness of 0.13-0.17 mm, was inserted into the patch at an approximate angle of 70˚ to the horizontal plane of the medium. Plates were incubated 37°C and coverslips removed at regular intervals in order to visualise the development of the *E. coli* cells.

Microscopy of *E. coli* on cellophane

A cellophane was placed on the surface of LB agar containing the appropriate antibiotics and IPTG. *E. coli* cells were plated at varying concentrations dependant on time between plating and visualisation. These plates were incubated for either 2 hours or overnight after which a 1 cm^2 cellophane patch was cut using a scalpel and stained.

Microscopy of *E. coli* in liquid media

For liquid microscopy of *E. coli,* after the 3-hour subculture instead of plating the cells, IPTG was added to the subculture and incubated for a further 2 hours or overnight. A sample was then taken for staining or live viewing.

Coverslip Staining

Plates with *S. coelicolor* grown on coverslips were dried for 30 minutes by opening them to sterile air. This ensured that the aerial hyphae stuck to the surface of the coverslip. Coverslips were removed from the media and placed on filter paper with the sample face up. The sample was fixed with 100% methanol (kept in the freezer) for 1 minute, after which the excess methanol was removed, and the remainder allowed to evaporate. The sample was stained with the application of WGA Alexa Fluor® 488 conjugate (50 µg/ml) and/or propidium iodide (25 µg/ml) to each coverslip on the growth line. The samples were incubated for 30 minutes in total darkness at room temperature. The coverslips were washed 4 times by pipetting 1 ml phosphate buffer solution onto the surface before allowing the slides to dry.

After drying the slides were mounted face down onto microscope slides (76 x 26mm (thickness 1.0 – 1.2mm) with an 8 µl drop of 20% glycerol on the surface (if DAPI staining used, this was used as the mounting liquid instead of 20% glycerol). Excess liquid was removed from the edge of the coverslip before it was sealed with a fine coat of nail varnish applied around the edge.

Staining cells grown on cellophane

Cut out cellophane squares were placed with the sample face up onto a glass microscope slide that had been wettened with sterile water. The sample was fixed with 100% methanol (kept in the freezer) for 1 minute, after which the excess methanol was removed, and remainder washed with phosphate buffer solution. The sample was stained with the application of WGA Alexa Fluor® 488 conjugate (50 µg/ml) and/or propidium iodide (25 µg/ml) to each cellophane such the surface was covered. The samples were incubated for 30 minutes in total darkness at 4°C. The cellophanes were washed 4 times by pipetting 1 ml phosphate buffer solution onto the surface before tipping the excess buffer onto filter paper. After washing, the cellophanes were mounted face up onto microscope slides (76 x 26mm (thickness 1.0 – 1.2mm) with a 5 µl drop of 20% glycerol on the surface. An 8 µl drop of 20% glycerol was deposited onto the surface of the cellophane and a glass coverslip, 22x22 mm with a thickness of 0.13-0.17 mm, was placed on top (If DAPI staining was used, this replaced the 8 µl drop of 20% glycerol onto the cellophane). Excess liquid was removed from the edge of the coverslip before it was sealed with a fine coat of nail varnish applied around the edge.

Staining cells grown in liquid culture

For *E. coli* cells, liquid staining was achieved by taking an aliquot of the growing culture into an Eppendorf tube and centrifuging for 2 minutes to pellet the cells. The supernatant was discarded and the cells washed in phosphate buffer solution before resuspending in 100% methanol (kept in the freezer) to fix. This was immediately centrifuged and the supernant removed. The cells were washed with phosphate buffer solution twice before suspension in 10 µl WGA Alexa Fluor® 488 conjugate (50 µg/ml) and/or propidium iodide (25 µg/ml) and

incubation in darkness at 4°C for 30 minutes. Cells were then washed a further three times with phosphate buffer solution and finally resuspended in a desired volume of phosphate buffer solution. A 5 µl aliquot of the stained cells was pipetted onto the microscope slides (76 x 26mm (thickness 1.0 – 1.2mm) and a glass coverslip, 22x22 mm with a thickness of 0.13-0.17 mm, was placed on top. Excess liquid was removed from the edge of the coverslip before it was sealed with a fine coat of nail varnish applied around the edge.

Visualisation of Microscope Slides

Samples were visualised using an Axioplan 2 Imaging E (Carl Zeiss) Universal microscope with an AxioCamMR camera. A Plan Apochromatic 100x/1.40 Oil (440780) objective was used in combination with FS 38 GFP and FS 45 TxR filters. AxioVs40x64 V 4.9.1.0 software was used for image capture.

2.6 Protein Purification

Cell Lysis

Protein expression was carried out according to the optimal conditions as set out in the results section. Once cells with over production of the target protein were generated, for large scale purification they were collected in a 500 ml Beckmann centrifuge tube and centrifuged for 7 minutes at 7000 g using a Beckmann Avanti J20 centrifuge and a Beckmann JA 10 500 rotor. For small scale purification, they were collected in a 50 ml falcon tube and centrifuged at 4000 g for 10 minutes. The supernatant was discarded, and the cells were re-suspended in approximately 50 ml (or 5 ml) of the appropriate binding buffer. The cells that contain protein to be purified under denaturing conditions were re-suspended in Tris binding buffer and native lysis was performed first. Cell lysis was achieved using a high pressure homogeniser french press at a pressure of 1000 psi for large scale, or sonicated for the small scale. After lysis, the lysate was deposited in a 50 ml Beckmann centrifuge tube and centrifuged for 30 minutes at 20000 g using a Beckmann Avanti J20 centrifuge and a Beckmann JLA 25 50 rotor or at g in a benchtop centrifuge for 30 minutes at 4°C. For proteins that were purified under native conditions the supernatant was collected and used for purification. For proteins purified under denaturing conditions, the supernatant was discarded, and the pellet was re-suspended using denaturing binding buffer.

Protein Purification Under Native Conditions

Binding buffer 50 mM Tris, 300 mM NaCl, 20 mM MgCl2, 10 mM imidazole pH8

Washing buffer 50 mM Tris, 300 mM NaCl, 20 mM MgCl2, 20 mM imidazole pH8

Elution buffer 50 mM Tris, 300 mM NaCl, 20 mM MgCl2, 300 mM imidazole pH8

Cleaning buffer 50 mM Tris, 300 mM NaCl, 20 mM MgCl2, 500 mM imidazole pH8

Large Scale Protein Purification Under Native Conditions

Large scale purification was carried out using a 2 ml Ni-Sepharose pre-packed gravity column from Novagen. The column was washed with 5 column volumes of first deionised water and then binding buffer to equilibrate. After centrifugation the supernatant was applied to the column and allowed to drip through, with the flow through collected in a single fraction. The column was then washed with 10 ml binding buffer which was collected in a single fraction. After the initial wash the column was washed with 10 ml washing buffer which was collected in a single fraction. The protein was then eluted with 12 ml elution buffer which was collected in twelve 1 ml fractions. The column was then cleaned to ensure all protein had passed through using 12 ml cleaning buffer collected first as two 1 ml fractions then the subsequent 10 ml as one fraction. Fractions containing purified protein were identified using SDS-PAGE.

Small Scale Protein Purification Under Native Conditions

Small scale purification was achieved using a QIAGEN Ni-NTA spin column kit. The column was equilibrated by addition of 600 µl binding buffer and centrifuging at 4°C with the lid open for 2 minutes at 2800 rpm. The sample was then loaded in the same way in 600 µl aliquots until it had all gone through the column and collected as a single fraction, centrifuging in the same way as previously. Washing buffer was applied in two 600 µl aliquots and collected as separate fractions. Elution buffer was applied as three 300 µl aliquots and collected as separate fractions. Fractions containing purified protein were identified using SDS-PAGE.

Protein Purification Under Denaturing Conditions

Denaturing binding buffer	8 M Urea, 0.1 M NaH_2PO_4, 0.01 M Tris-HCl, pH 8.0
Denaturing washing buffer	8 M Urea, 0.1 M NaH_2PO_4, 0.01 M Tris-HCl, pH 6.3
Denaturing elution buffer	8 M Urea, 0.1 M NaH_2PO_4, 0.01 M Tris-HCl, pH 4.5

Large Scale Protein Purification Under Denaturing Conditions

After removing soluble proteins using the native cell lysis protocol as described above, the pellet was re-suspended in approximately 20 ml of denaturing binding buffer. The suspension was mixed for one hour using gentle stirring to solubilise the target protein. The lysate was subsequently deposited in a 50 ml Beckmann centrifuge tube and centrifuged for 30 minutes at 20000 g using a Beckmann Avanti J20 centrifuge and a Beckmann JLA 25 50 rotor. Purification was carried out using a 2 ml Ni-Sepharose pre-packed gravity column from Novagen. The column was washed with 5 column volumes of first deionised water and then denaturing binding buffer to equilibrate. After centrifugation the supernatant was applied to the column and allowed to drip through, with the flow through collected in a single fraction. The column was then washed with 10 ml denaturing binding buffer which was collected in a single fraction. After the initial wash the column was washed with 10 ml denaturing washing buffer which was collected in a single fraction. The protein was then eluted with 22 ml denaturing elution buffer which was collected first in twelve 1 ml fractions and then in one 10 ml fraction. Fractions containing purified protein were identified using SDS-PAGE.

Small Scale Protein Purification Under Denaturing Conditions

Small scale purification was achieved using a QIAGEN Ni-NTA spin column kit. The column was equilibrated by addition of 600 µl denaturing binding buffer and centrifuging at room temperature with the lid open for 2 minutes at 2800 rpm. The sample was then loaded in the same way in 600 µl aliquots until it had all gone through the column and collected as a single fraction, centrifuging in the same way as previously. Denaturing washing buffer was applied in two 600 µl aliquots and collected as separate fractions. Denaturing elution buffer was applied as three 300 µl aliquots and collected as separate fractions. Fractions containing purified protein were identified using SDS-PAGE.

Dialysis

Dialysis was carried out using Spectra/Por® molecularporous membrane tubing with a molecular weight cut off of 3500 Da. Dialysis was set up in either a small scale for volumes less than 1 ml. For small scale the tubing was cut open and 5 cm^2 squares were cut and equilibrated in the target buffer for 10 minutes. The protein was aliquoted into a 2 ml microcentrifuge tube with the lid removed. The O-ring from the lid was removed and used to secure the membrane over the top of the microcentrifuge tube by fixing it to the underside of the lip. The membrane was pulled tight across the opening to ensure a flat surface. The tube was secured in a float and placed upside down in the target buffer such that the membrane separated the internal solution from the dialysis buffer. The buffer was gently stirred at for at least 2 hours at a time. The buffer was replaced twice so that dialysis was carried out three times.

Determining the concentration of protein solutions

To measure protein concentration the Bradford assay was performed. A standard curve was generated using known concentration of reactions containing BSA. Tubes were set up in 200 µl volume such that the final concentration of BSA in a 1 ml volume was as follows: 0 µg/ml, 1 µg/ml, 2.5 µg/ml, 5 µg/ml, 7.5 µg/ml and 10 µg/ml. Bio-Rad protein assay reagent was diluted in a 1:3 ratio with deionised water and mixed. The reagent was then used to make the standard curve reactions 1 ml in volume. The reactions were incubated for 5 minutes at room temperature before their absorbance measured at 595 nm in a Jenway 7205 spectrophotometer. The protein of unknown concentration was measured first by diluting a small volume (1-5 µl) to 200 µl with deionised water. This was then treated the same way as the reactions used to generate the standard curve. The absorbance of the unknown protein was then compared to the standard curve and protein concentration estimated.

SDS-PAGE

For SDS-PAGE, gels were cast using the ATTO system. The percentage acrylamide in the resolving gel varied between 8 and 15% depending on the size of the protein that was being analysed. The protein loading dye was added to protein samples such that it diluted to a 1x buffer. The protein was heated at 95°C for 5 minutes to denature before being cooled on ice. The gel was placed in the ATTO tank and submerged with 1x SDS-PAGE running buffer. Samples were loaded and subjected to electrophoresis for between 45 minutes and 1 hour at 200 V. After running the gels were stained with Colloidal Coomassie blue R250 for a minimum of 1 hour with gentle agitation. Gels were de-stained in 50% ethanol, 2% acetic acid for 2 x 1 hr. The gels were then viewed with white light illumination using a Bio-Rad trans-illuminator.

2.7 Preparing Samples for Transmission Electron Microscopy

Preparing Grids for Transmission Electron Microscopy with Negative Staining

Grids were prepared for TEM using Carbon Film 400 Mesh Copper Grids from agar Scientific. Using tweezers which just touched the edge and not the grid, the grids were placed on parafilm in a petri dish. To the upper face of the grid, 5 µl of the protein was added and left to settle for 2 minutes then the liquid removed using whatman paper to draw it off. The grid was then washed by addition of 5 µl of sterile water which was left for 1 minute. A 5 µl aliquot of 2% ammonium molybdate pH7.0 (centrifuged just prior) was added as a negative stain for 2 minutes and the liquid removed in the same way as before. The grid was them transferred onto Whatman paper in petri dish for complete drying and storage.

Preparing Grids for Transmission Electron Microscopy with Nanogold staining

Grids were prepared for TEM using Carbon Film 400 Mesh Copper Grids from agar Scientific. Using tweezers which just touched the edge and not the grid, the grids were placed on parafilm in a petri dish. To the upper face of the grid, 5 µl of the protein was added and left to settle for 2 minutes then the liquid removed using whatman paper to draw it off. The grid was then washed by addition of 5 µl of sterile water which was left for 1 minute. A 5 µl aliquot of 5 nm Ni-NTA-Nanogold® was then dropped onto the parafilm, and the grid was placed upside down onto this drop and left for minutes. The grid was then washed with 5 µl sterile water and 5 µl of NanoVan® was added as the negative stain for 2 minutes before removal of the liquid. The grid was them transferred onto Whatman paper in petri dish for complete drying and storage.

TEM

Transmission Electron Microscopy was performed using a JEOL 2010 TEM which was usually operated at 160 kV.

3 *In vitro* Analysis of FilP Higher Order Assemblies

3.1 Introduction

Transmission Electron Microscopy

Transmission electron microscopy (TEM) allows for the visualisation at many times greater resolution than that of light microscopes. This is because, instead of light, TEM uses a beam of electrons which have a much smaller wavelength than that of light. An electron gun produces these electrons and the electron beam is focussed by the condenser lens. When the electron beam hits the sample and is transmitted through the sample depending on the thickness and material of the sample. Transmitted electrons are focussed by the objective lens onto a phosphor screen. When the electrons hit the phosphor screen, light is generated, and this allows visualisation to the human eye with darker areas having fewer electrons passed through the sample. A camera coupled to the TEM allows capture of images of the sample in monochrome. Inside the TEM the sample is in a vacuum which helps with image resolution as it stops the collision of electrons with gas molecules and facilitates the straight movement of the electron beam towards the sample (Fultz and Howe, 2008; Williams and Carter, 1996).

Negative staining is where the background is stained but leaves the sample untouched and visible. Ammonium molybdate is one such negative stain which strongly scatters electrons as well as adsorbing well to biological matter (Hayat, 2000). This makes the image appear with the protein sample as white as the electrons can pass through, and the surroundings as black. As the stain adsorbs strongly around the protein, the blank background can also often appear as white.

Intermediate Filament Structure Observed by TEM

The vimentin higher-order assembly pathway is understood to be as follows: from the basic building block of the elementary vimentin dimer, two dimers come together to form an anti-parallel slightly staggered tetramer (H Herrmann et al., 1996; Soellner et al., 1985). The anti-parallel nature of the organisation was suggested due to the structure of the elementary dimer, and the model was proposed whereby the coil 1Bs align anti-parallel and the lateral interactions are formed by charged or polar residues on the outer of the dimers allow these lateral interactions of the two dimers (Chernyatina et al., 2012). These tetramers have been

seen *in vitro* in buffers of low ionic strength. Increasing the ionic strength of the buffer increases the lateral associations (Herrmann et al., 1999). The lateral association of eight dimers generates rod shaped filaments which are ~60-65 nm long and ~16 nm in diameter, these are termed unit-length filaments (Herrmann et al., 1999; Strelkov et al., 2003). These unit length filaments further associate longitudinally in a head to tail manner to produce the filament (Figure 1.7.1). These filaments have a diameter of ~11 nm which suggests some rearrangement for these filaments to form (Strelkov et al., 2003).

Another intermediate filament assembly pathway has been proposed for the type V intermediate filament family of nuclear lamins, though this is less understood. This assembly pathway contains steps of lateral and longitudinal interaction of the dimers, just like the pathway for vimentin, however they are in a different order. For lamins, the longitudinal interactions occur before the lateral interactions and, therefore, no unit length filaments have been shown to be formed. The first stage of association is the longitudinal head to tail assembly of the dimers into dimer strands of variable length. This is followed by the lateral association of the dimer strands in an anti-parallel and staggered fashion producing protofilaments of tetrameric strands (Ben-Harush et al., 2009; Dittmer and Misteli, 2011; Stuurman et al., 1998). These protofilaments can further associate via lateral interaction to produce fibres of varying width which have a characteristic striated pattern when viewed using transmission electron microscopy using negative staining (Aebi et al., 1986; Heitlinger et al., 1992, 1991, Figure 1.7.2). These highly ordered paracrystals are very different to the filaments seen with vimentin and other intermediate filaments. These paracrystals were thought to be *in vitro* artefacts, however, further experiments have shown that they are the dominant structures formed in physiological buffers, as well as in cells expressing lamin (Klapper et al., 1997; Zwerger et al., 2013).

FilP Structures Observed by TEM

FilP has been previously purified and visualised *in vitro* using transmission electron microscopy (TEM) and scanning electron microscopy (SEM). Structures observed included a smooth rope-like filament with a diameter of around 60 nm which constituted the less frequent type, and striated filaments which branched and had a varying diameter (Bagchi et al., 2008*;* Figure 1.10.3). These striated filaments visually resembled those seen with nuclear lamins (Stuurman et al., 1998). Other structures observed (Fuchino et al., 2013) included some striated structures surrounding a dominant lace like structure (Figure 1.10.3). Recent observations (Javadi et al., 2019) at pH6.8 showed striated structures which closely resembled those observed by Bagchi et al., 2008. They also observed that with addition of both monovalent and divalent cations a hexagonal mesh lacework was observed which more closely resembled what was observed by Fuchino et al., 2013.

Aims

As highlighted in the introduction, it is unclear to what degree FilP fits into the definition of being an intermediate filament. Previous studies of FilP have also appeared inconsistent with their findings as to the appearance of the higher order structures. To address this, I aim to characterise the appearance of the higher order structures of FilP and to assess under which conditions it can make them.

To achieve this, I will express and purify a histidine-tagged FilP protein. This purified protein will be dialysed into a variety of buffers of differing pH and salt concentrations. This will lead to further clarification of the higher order structures which FilP can make and under which conditions it forms which structures.

3.2 Strategy for the generation of His-FilP

The vector that was used to overproduce FilP in this investigation was pET28. The pET28 plasmid is a high copy number vector for overexpression of a desired protein in *E. coli*. It carries a kanamycin resistance gene, a T7 polymerase promoter upstream of the gene of interest, meaning that expression is driven by T7 polymerase. The *E. coli* strain BL21 (DE3) pLysS was used as a host for overexpression, as this contains a T7 polymerase gene which is under the regulation of a LacI repressor. This blocks RNA polymerase from transcribing the T7 polymerase gene in the absence of its inducer and therefore, there is no leaky expression of the gene of interest. Furthermore, the *pLysS* strain encodes a *pLysS* gene which codes for a T7 lysozyme which is constitutively expressed at low levels to stop any T7 polymerase from activating the gene of interest before induction. Induction of gene of interest expression can be achieved by inactivating the LacI repressor by addition of isopropyl β-D-1-thiogalactopyranoside (IPTG) (Doherty et al., 1995; Pan and Malcolm, 2000; Schlicke and Brakmann, 2005).

The vector for the expression of His-FilP in *E. coli* was a vector previously generated (Holmes et al., 2013). It is a pET28a based vector with the *filP* gene inserted between the *Nde*I and *Eco*RI restriction sites. The insertion of *filP* between the *Nde*I and *Eco*RI restriction sites allows the expressed protein to contain a polyhistidine tag N-terminally attached to the protein (Figure 3.2.1).

This pET28 FilP plasmid was transformed by electroporation into the *E. coli* strain BL21 (DE3) pLysS and large quantities of these cells were grown up. Expression of FilP using this vector had previously been optimised (Holmes et al., 2013) so the established protocol for FilP expression and purification was followed. Cells were grown at 37°C until early exponential phase when production of the His-FilP protein was induced by the addition of 1 mM IPTG. Cells were harvested after 24 hrs incubation at 37°C following induction and lysed using a french press.

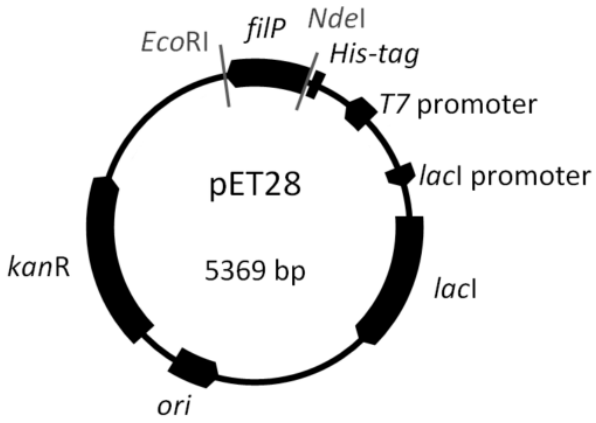

Figure 3.2.1 pET28 FilP construct

FilP has been inserted between the *Eco*RI and *Nde*I restriction sites. pET28 encodes the T7 promoter, *lac*I promoter, *lac*I gene, *ori*, and the kanamycin resistance gene *kan*R. (Holmes et al., 2013).

Purification of His-FilP was achieved using a gravity flow nickel-affinity chromatography column (Figure 3.2.2). Nickel affinity chromatography was chosen as the purification technique to be used due to the presence of the his-tags which are on the N-terminus of the protein. His-tagged proteins are able to bind to the nickel immobilised in the column which allows for the other proteins from the cells to be washed through. Elution of the his-tagged protein of interest, in a native purification, can be achieved by the addition of a buffer solution containing imidazole which competitively binds to the nickel whereas in a denaturing purification, a decrease in the pH to 4.5 protonates the imidazole nitrogen of the histidine residue, due to the pKa of 6.0, and disrupts the interaction between the histidine and the nickel (Bornhorst and Falke, 2000).

Both FilP and eukaryote intermediate filament proteins have intrinsic properties that promote higher order assemblies as soon as the proteins are made in high concentration. This means that both overexpressed intermediate filament proteins and FilP are always found in the insoluble pellet fraction. Hence, eukaryotic intermediate filaments are routinely purified under denaturing condition and their assembly monitored during dialysis. FilP was also purified from the insoluble pellet fraction of lysed cells. Denaturing conditions (8 M urea) were used to solubilise these higher order assemblies which would interfere with the purification process.

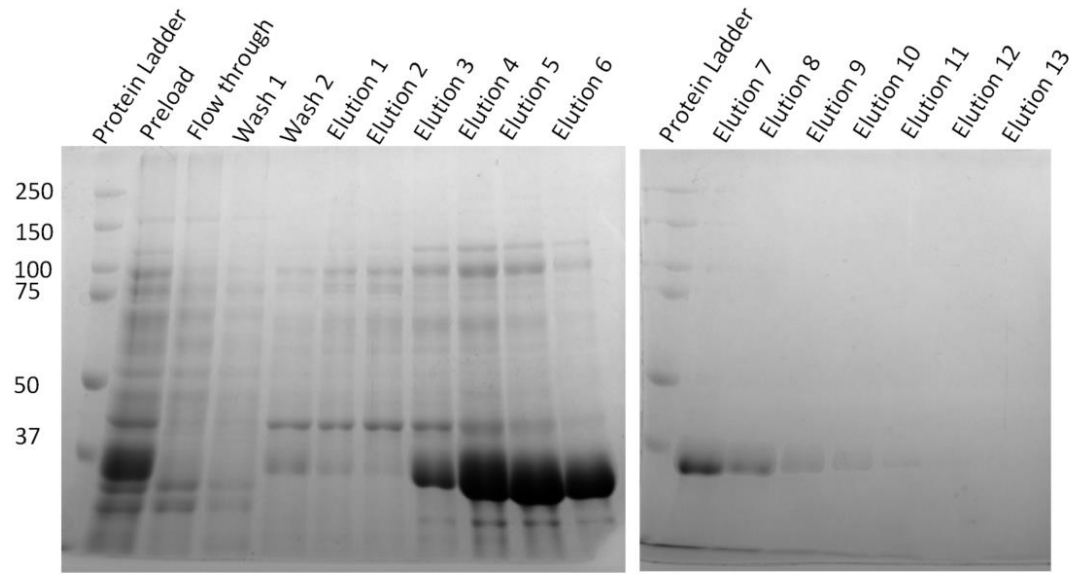

Figure 3.2.2 FilP purification

Purification of His-FilP from BL21 pLysS after 22 hrs induction with 1 mM IPTG at 37°C under denaturing conditions using a Ni-NTA gravity flow column. Samples included the preload, flow through, washes and elution fractions. Molecular weight standard marker is shown in the first lane on the left. Sizes shown in kDa. 10% SDS PAGE visualised by Coomassie staining. The 37 kDa His-FilP was eluted in fractions 3-7.

Following successful purification (Figure 3.2.2), His-FilP was dialysed into various buffers. For testing a range of pHs, buffers were chosen for whether the chosen pH fell within its buffer range. This is the pH range where a buffer effectively neutralizes added acids and bases, while maintaining a relatively constant pH.

The successfully purified and dialysed proteins were subsequently spotted onto Carbon Film 400 Mesh Copper Grids and negatively stained using 2% ammonium molybdate pH7.0. Visualisation was achieved by transmission electron microscopy (TEM) using a JEOL 2010 normally run at 160 kV (80 kV and 200 kV on occasion). Images taken were analysed using ImageJ software and data charts were generated using Microsoft Excel.

3.3 TEM and analysis

Eukaryotic intermediate filaments are known to form higher order structures that are dependent on pH. Therefore, the purified His-FilP protein was dialysed into buffers of varying pHs. His-FilP has a pI of 5.82. As different buffers have varying pH optimum we have used the following buffers, 10 mM Tris pH8.5, 10 mM HEPES pH7.5 and 10 mM PIPES pH6.5 when FilP was dialysed and first screened by TEM. All three conditions showed large, highly organised, striated structures (Figure 3.3.1) with lighter bands of denser protein alternating with darker bands of less dense protein. The negative staining procedure means that the stain appears black on the images and the protein appears white. However, the stain aggregates around the proteins so the background can also often appear white. Thus, areas denser in protein will appear whiter.

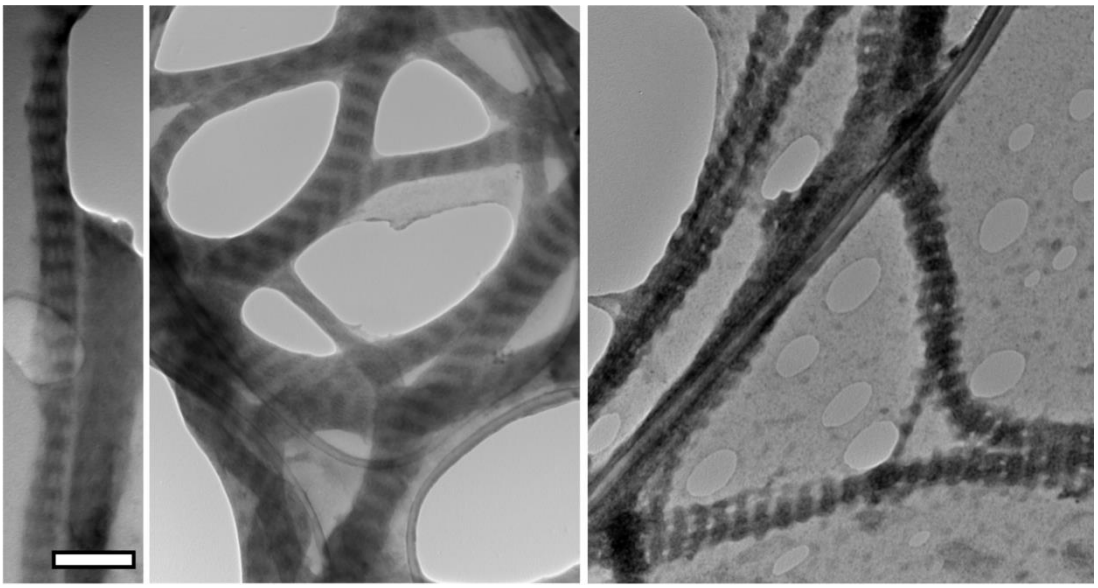

Figure 3.3.1 His-FilP in varying pHs.

His-FilP in 10 mM Pipes pH6.5 (left), 10 mM Hepes pH7.5 (middle), and 10 mM Tris pH8.5 (right). Filaments were negatively stained using 2% ammonium molybdate pH7.0 and visualized by transmission electron microscopy. (Scale bar: 200 nm for all panels)

Interestingly, a lace-like structure had previously been observed in 50 mM Tris pH7.0 (Fuchino et al., 2013) where protein lines connect nodes (Figure 1.10.3 C,D). Thus, His-FilP was also dialysed into 50 mM Tris pH7.0, negatively stained with 2% Ammonium Molybdate pH7.0, and the structures were observed by TEM, however, I could not observe any lace structure. Instead, a filamentous smooth rope-like structure was readily seen (Figure 3.3.2) which resembles that of the eukaryotic intermediate filaments higher order structures such as those observed by (Herrmann and Aebi, 2004) with vimentin after 1 hour in assembly buffer (Figure 1.7.2). This has not been shown for FilP before. An occasional small striated section was also sometimes observed, though the rope structure was by far the most common (Figure 3.3.2). The average width of intermediate filament rope structures is around 10 nm (Herrmann and Aebi, 2004). To establish whether FilP ropes are comparable to those of eukaryotic intermediate filaments we measured the widths of the FilP ropes. The average width of these FilP rope filaments in 50 mM Tris pH7.0 was 15.5 nm, which is comparable to the width of eukaryotic intermediate filaments. The rope structure observed with His-FilP in 50 mM Tris pH7.0 (Figure 3.3.2) is visually similar to those rope structures which have been observed in eukaryotic intermediate filaments (Figure 1.7.2). This indicates that FilP is similar to the eukaryotic intermediate filaments with this rope form produced by both intermediate filaments and FilP, which supports the idea that FilP is an intermediate filament like protein.

The striated structure that was also observed which resembles that of the 'paracrystaline' structure which has been observed with the type V intermediate filaments (lamins) (Figure 1.7.2). The lamins also show an ability to form both the rope structures and a striated structure. This further lends itself to the idea that FilP is an intermediate filament like protein and that it is potentially more like that of the lamin family than the other, cytoplasmic, intermediate filaments.

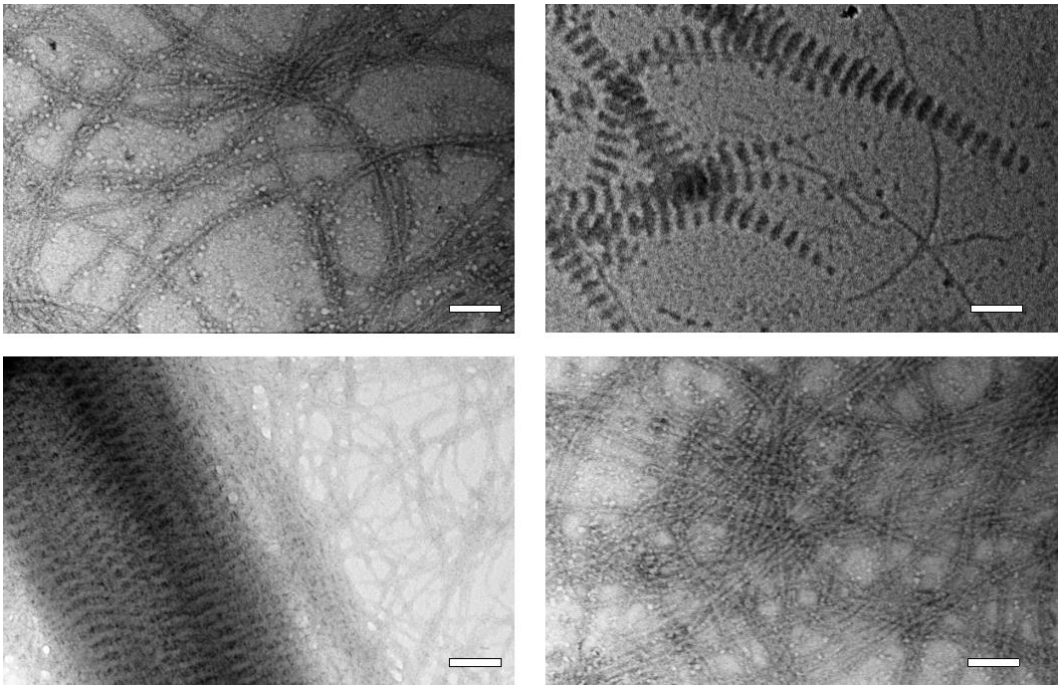

Figure 3.3.2 TEM FilP in 50 mM Tris pH7.0 buffer

His-FilP in 50 mM Tris pH7.0. Filaments were negatively stained using 2% ammonium molybdate pH7.0 and visualized by transmission electron microscopy. (Scale bars: 200 nm.)

Following from the analysis of FilP in pH7.0 buffers, pH8.0 and 8.5 buffers were analysed to assess whether differences of pH with a tris buffer had any effect on the higher order assemblies of FilP. Whilst at pH7.0 FilP formed smooth ropes (Figure 3.3.2), the structures observed in 50 mM Tris at both pH8.0 and pH8.5 were predominantly striated structures (Figure 3.3.3). No rope filament formation was observed for these conditions. Some potential lace like structure was observed where faint lace-like structures were typically observed to surround a large striated area. The lace structure was observed in 50 mM Tris pH8.0 and pH8.5 (Figure 3.3.3). This is contrary to observations where a lace structure was observed in 50 mM Tris pH7.0 (Fuchino et al., 2013). The structure observed also differs in its appearance in that the previously observed lace structure has defined nodes with obvious protein connections between them. We were able to observe nodes, but very little linking protein or clear definition. It is unclear why there are these discrepancies between the pH at

which the lace structure was found and the appearance of the lace structure. In 50 mM Tris pH7.0, where the lace structure was previously found (Fuchino et al., 2013), our observations were of rope and striated structures. This variation in structures seen under the same conditions highlights that the protein is likely to be sensitive in its nature of forming higher order structures to a factor which is yet unknown. The protein concentration could also affect the formation of the lace structure. In the lace structure, there appears to be fewer lateral interactions of elementary dimers than in the striated or rope structures.

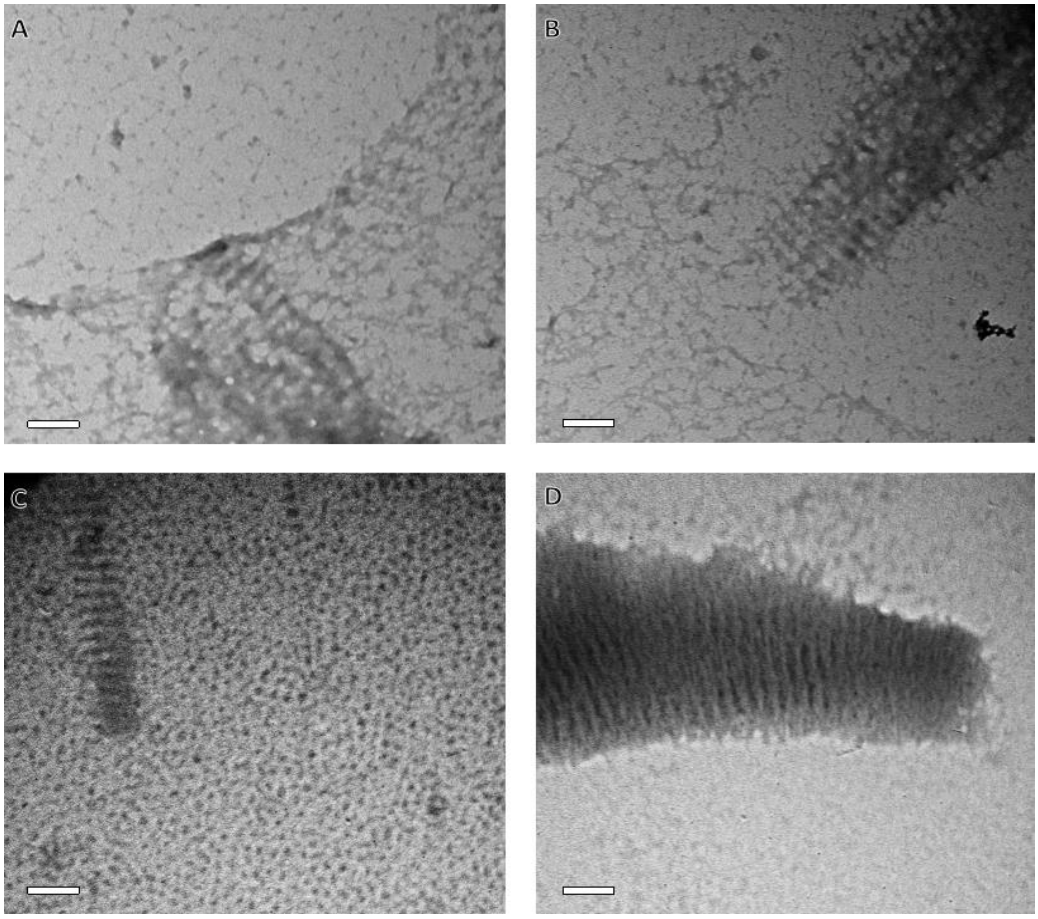

Figure 3.3.3 TEM 50 mM Tris pH8.0 and pH8.5

His-FilP in 50 mM Tris pH8.0 (**A-B**) and pH8.5 (**C-D**) Samples negatively stained using 2% ammonium molybdate pH7.0 and visualized by transmission electron microscopy. (Scale bars: 200 nm.)

Analysis of the striated structures was much more complex than for the rope structure. To characterise the striated patterns, we needed to introduce some terminology (Figure 3.3.4). The protein dense white stripes which are perpendicular to the direction of the filament are termed the stripe (or white stripe). A unit length is deemed to comprise of one white stripe and one darker area of striation. The width of the filament is measured from one side to the other (Figure 3.3.4). Measurements of the unit lengths of the striations of FilP from the TEM images were undertaken to assess the repeated nature of the striated structure. For 50 mM Tris pH8.0 the average unit length was 63.4 nm compared to 62.6 nm for pH8.5 (Figure 3.3.5). To test for statistical significance, measurements were compared using a two-tailed T-test with a 95% confidence level. These are not statistically different, which shows that the pH difference has not affected the unit length of the structure.

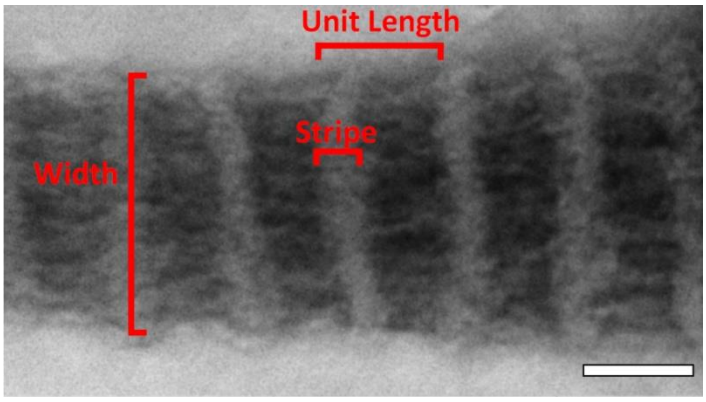

Figure 3.3.4 Striated structure measurement diagram

His-FilP measurement example. The stripe (white), unit length and width of filament indicated. Image from 50 mM tris pH7.0, 5 mM $MgCl_2$ and 150 KCl. Filaments were negatively stained using 2% ammonium molybdate pH7.0 and visualized by transmission electron microscopy. The negative staining procedure means that the stain appears black on the images and the protein appears white. However, the stain aggregates around the proteins so the background can also often appear white. Thus, areas denser in protein will appear whiter. (Scale bars: 50 nm.)

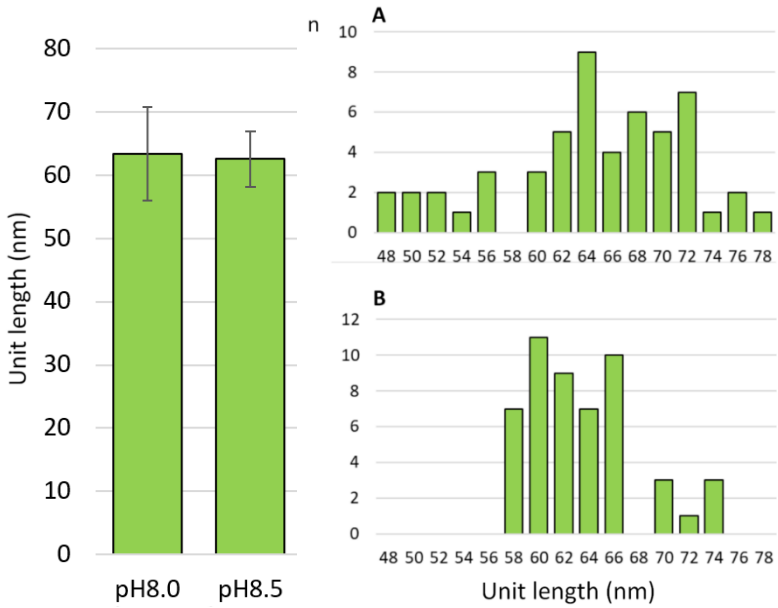

Figure 3.3.5 Analysis of the unit length of the striated FilP patterns in 50 mM Tris pH8.0 and 8.5.

Average unit lengths (nm) of His-FilP striated structures in 50 mM Tris pH8.0 (mean 63.3 nm standard deviation 7.35, n 53) and pH8.5 (mean 62.59 standard deviation 4.35 n 51). Error bars represent standard deviation. Histograms 50 mM Tris pH8.0 (A) and pH8.5 (B).

Addition of Cations Affects the Lateral Interactions of FilP

Next, we tested the effect of the presence of positively charged cation for FilP assembly as we speculated that this would change the width of the filaments. Dialysis of His-FilP into 50 mM Tris pH7.0 with the addition of the cations magnesium or potassium were tested by TEM (Figure 3.3.6). The divalent cation $MgCl_2$ was added at 2 mM and 5 mM concentrations and the monovalent cation KCl was added at 50 mM, 100 mM and 150 mM concentrations. These cations were used on their own and in combination to observe the effects they would have on the higher order assembly of FilP (Figure 3.3.6).

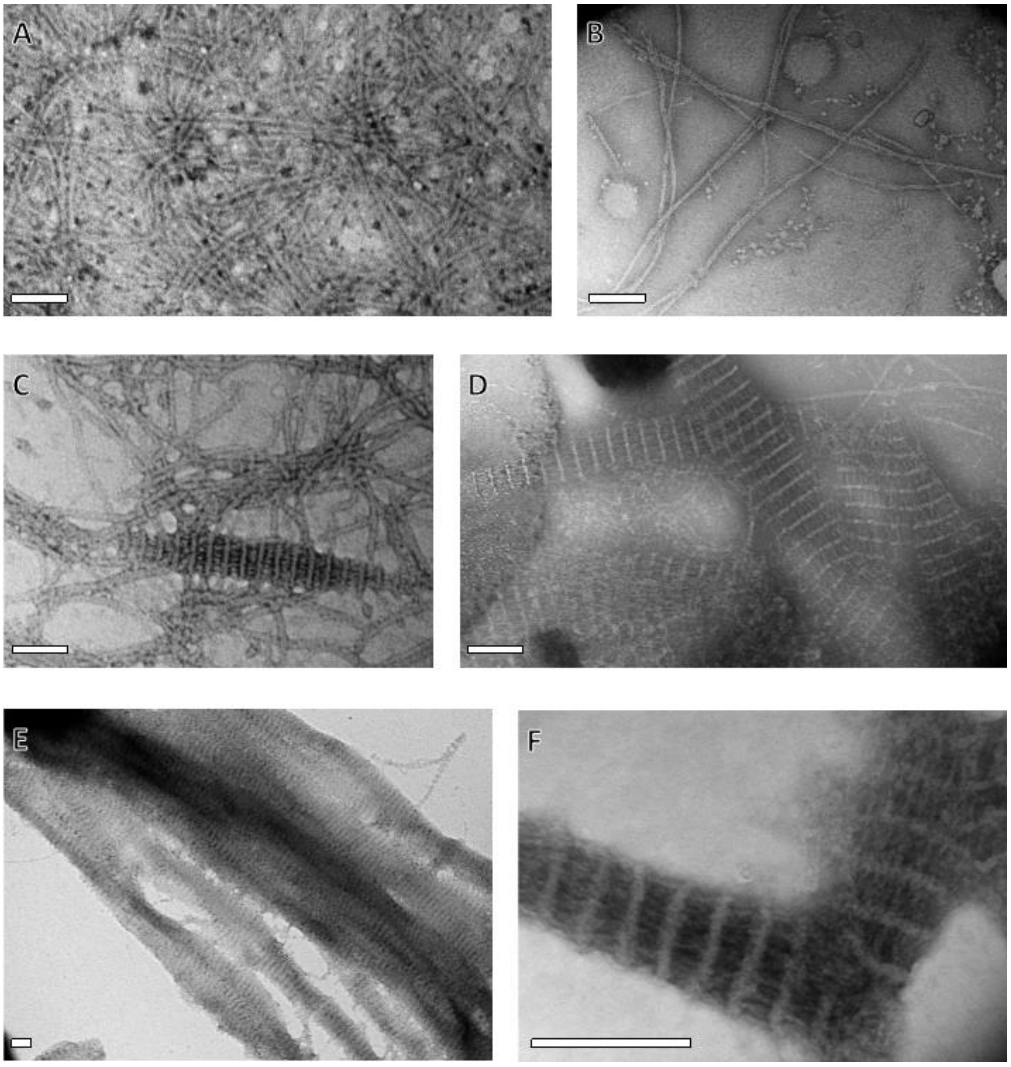

Figure 3.3.6 FilP in 50 mM Tris pH7.0 buffers with cation additions

His-FilP in 50 mM Tris pH7.0 including **(A)** 2 mM $MgCl_2$, **(B)** 5 mM $MgCl_2$, **(C)** 50 mM KCl, **(D)** 100 mM KCl, **(E)** 150 mM KCl, **(F)** 5 mM $MgCl_2$ and 150 KCl. Filaments were negatively stained using 2% ammonium molybdate pH7.0 and visualized by transmission electron microscopy. (Scale bars: 200 nm.)

In 50 mM Tris pH7.0 with the addition of both 2 mM and 5 mM $MgCl_2$, the structures observed were almost exclusively the rope like structure, similarly than without the cation addition. However, with the addition of 50 mM KCl, 100 mM KCl and with both 150 mM KCl and 5 mM $MgCl_2$ some of the rope filaments were still observed. However striated structures were also observed (Figure 3.3.6). The combination of both 150 mM KCl and 5 mM $MgCl_2$ was observed to have a much larger amount of the striated structure, though a few rope filaments were still observed (Figure 3.3.6). To see whether the width of these ropes were consistent with the width of rope in 50 mM Tris pH7.0 without cation addition, they were measured. FilP in 50 mM Tris pH7.0 showed rope structures in the presence and absence of $MgCl_2$ at both 2 mM and 5 mM concentrations (Figure 3.3.6) and the rope structure remained the dominant structure in the samples (Figure 3.3.11). The widths of these rope filaments remained the same with or without cations at 15.5 nm (standard deviation 6.41), 13.6 nm (standard deviation 3.50) and 14.42 nm (standard deviation 4.75) for FilP in 50 mM Tris pH7.0 without cations, with 2 mM $MgCl_2$, and 5 mM $MgCl_2$ respectively (Figure 3.3.7). To test for statistical significance, measurements were compared using a two-tailed T-test with a 95% confidence level. This revealed that these measurements had no statistical difference between them.

In the presence of KCl in 50 mM Tris pH7.0 the striated structures of FilP became more common although some rope structures were still found. The rope width in the presence of 100 mM KCl was 14.49 nm (standard deviation 3.68) which is statistically the same as FilP in 50 mM Tris without cation addition. However, in the presence of 50 mM KCl, and also with 150 mM KCl and 5 mM $MgCl_2$, the rope width was statistically larger than without cation addition at 19.00 nm (standard deviation 8.31) and 22.16 nm (standard deviation 6.09) respectively compared to 15.5 nm without cation addition. This indicates that, generally, the presence of the monovalent cation potassium increases the width of these rope structures, although why 100 mM KCl would not be included in this trend is unknown. The addition of the divalent cation magnesium did not appear to affect the width of the ropes at the concentrations tested here. The increase in width with the positively charged cations could be due to these cations aiding the lateral interactions by acting as a bridge between the negatively charged rods, thus allowing greater lateral association. Here, it seems that the monovalent cation potassium is more effective at the concentrations tested compared to the divalent cation magnesium at increasing these lateral interactions with regards to the rope structure.

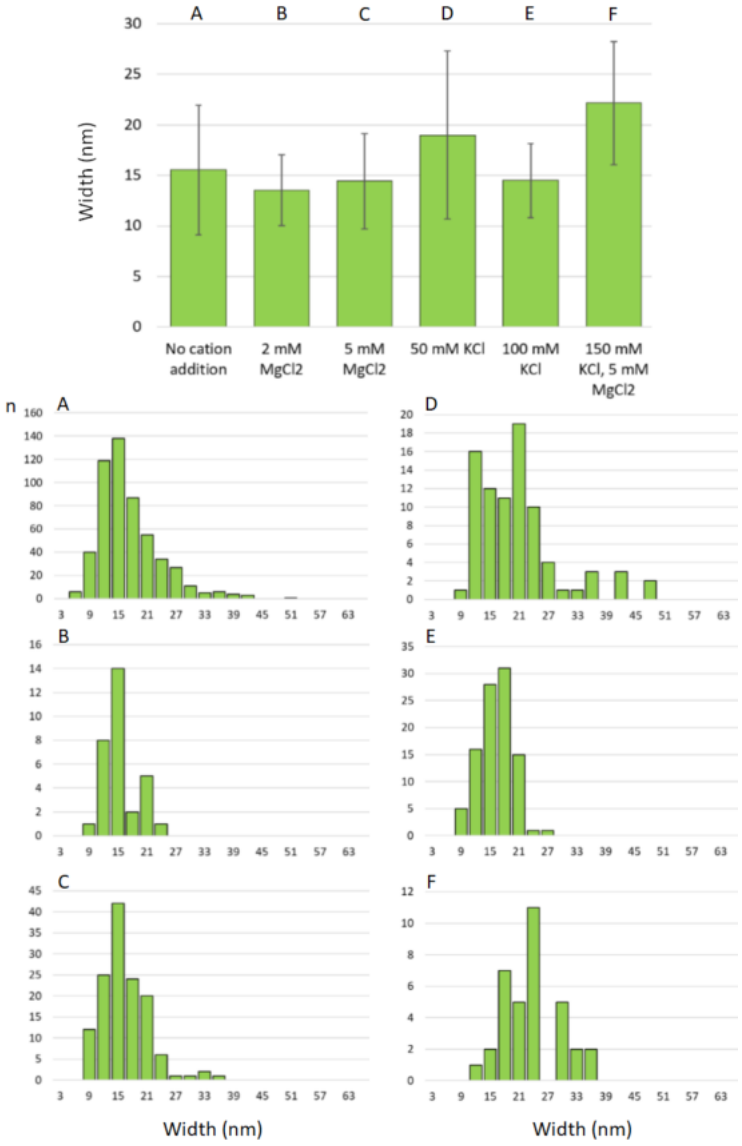

Figure 3.3.7 Widths of His-FilP rope structures in 50 mM Tris pH7.0

Average widths (nm) of His-FilP rope structures in **(A)** 50 mM Tris pH7.0 (mean 15.5 nm, standard deviation 6.41, n 536), **(B)** 50 mM Tris pH7.0 2 mM $MgCl_2$ (mean 13.6 nm, standard deviation 3.50, n 31), **(C)** 50 mM Tris pH7.0 5 mM $MgCl_2$ (mean 14.42 nm, standard deviation 4.75, n 136), **(D)** 50 mM Tris pH7.0 50 mM KCl (mean 19.00 nm, standard deviation 8.31, n 83), **(E)** 50 mM Tris pH7.0 100 mM KCl (mean 14.49 nm, standard deviation 3.68, n 97), **(F)** 50 mM Tris pH7.0 5 mM $MgCl_2$ 150 mM KCl (mean 22.16 nm, standard deviation 6.09, n 35). Error bars represent standard deviation. Histograms no addition **(A)**, 2 mM Mg **(B)**, 5 mM Mg **(C)**, 50 mM K **(D)**, 100 mM K **(E)** and 150 mM K 5 mM Mg **(F)** respectively.

Analysis of the striated structures observed in the presence of cations showed that the unit length of this striation was 62.6 nm (standard deviation 5.00) for 50 mM Tris pH7.0 with 50 mM KCl and 61.1 nm (standard deviation 2.54) with 100 mM KCl (Figure 3.3.8). There were insufficient measurements for 50 mM Tris pH7.0 with 150 mM KCl and 5 mM $MgCl_2$ to calculate an average unit length. To test for statistical significance, measurements were compared using a two-tailed T-test with a 95% confidence level. Results from this revealed that there is no statistical difference between each other or to the unit length of 63.7 nm for FilP in 50 mM Tris pH7.0 without the presence of cations.

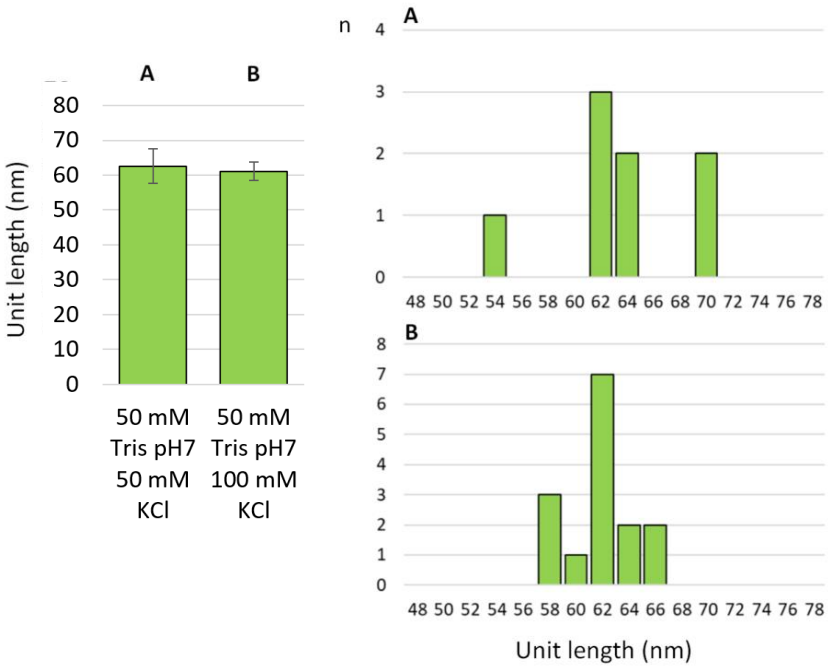

Figure 3.3.8 Analysis of the unit length of the striated FilP patterns in Tris pH7.0 including KCl.

Average unit lengths (nm) of His-FilP striated structures in 50 mM Tris pH7.0 with 50 mM (mean 62.6 nm, standard deviation 5.00, n 8) or 100 mM (mean 61.1 nm, standard deviation 2.54, n 15) KCl. Error bars represent standard deviation. Histograms 50 mM Tris pH 7.0 with 50 mM KCl (A), 100 mM KCl (B).

Addition of cations to 50 mM Tris pH8.5 caused the size of the structures to become visually larger (Figure 3.3.9) and therefore darker and more difficult to image. Analysis of the images and measurement of the unit lengths (where possible) revealed that the average unit lengths in the presence of 2 mM and 5 mM $MgCl_2$ were 60.3 nm and 63.2 nm respectively

(Figure 3.3.10). To test for statistical significance, measurements were compared using a two-tailed T-test with a 95% confidence level. The unit lengths were statistically the same in in 50 mM Tris pH8.5 with and without 5 mM $MgCl_2$. The unit length was found to be shorter in the presence of 2 mM Mg Cl_2. However, the number of measurements taken for this condition was low (35), therefore this data is likely to be unreliable.

This fact that the unit length in the striated structure stayed the same under varying conditions indicated that the unit length is likely to depend on an intrinsic property of the protein, and thus directly linked to the size of the protein. FilP homodimers are predicted to be around 46.5 nm in length (assuming the full length is canonical heptad repeat coiled-coil) or around 40 nm according to COILS prediction (Javadi et al., 2019; Lupas et al., 1991), which means that the unit length is larger than the length of an elementary dimer. This suggests that the unit length is comprised of more than one FilP dimer length, and likely indicates further associations between FilP dimers to build up the striated higher order structure.

The striated structure also increased in the volume and became denser in the presence of cations in 50 mM Tris pH8.5 (Figure 3.3.9). Some of the structures were so large and dense (particularly in 50 mM Tris pH8.5 5 mM $MgCl_2$ 150 mM KCl) that the image was very dark and therefore difficult to measure and image the striations (Figure 3.3.9). The apparent increase in the density of the structure indicates that cations aid lateral interactions of FilP, presumably by allowing larger structures to be formed by electrostatic interaction between the cations and the negatively charged rods. However, these observations are somewhat contrary to what was observed by (Javadi et al., 2019) who observed an increase in solubility of the protein with increased cations as well as a shifting from a striated structure to an hexagonal meshwork lace. Where cations appear to increase interactions for us, it decreases it for them. Why there would be this discrepancy is unclear.

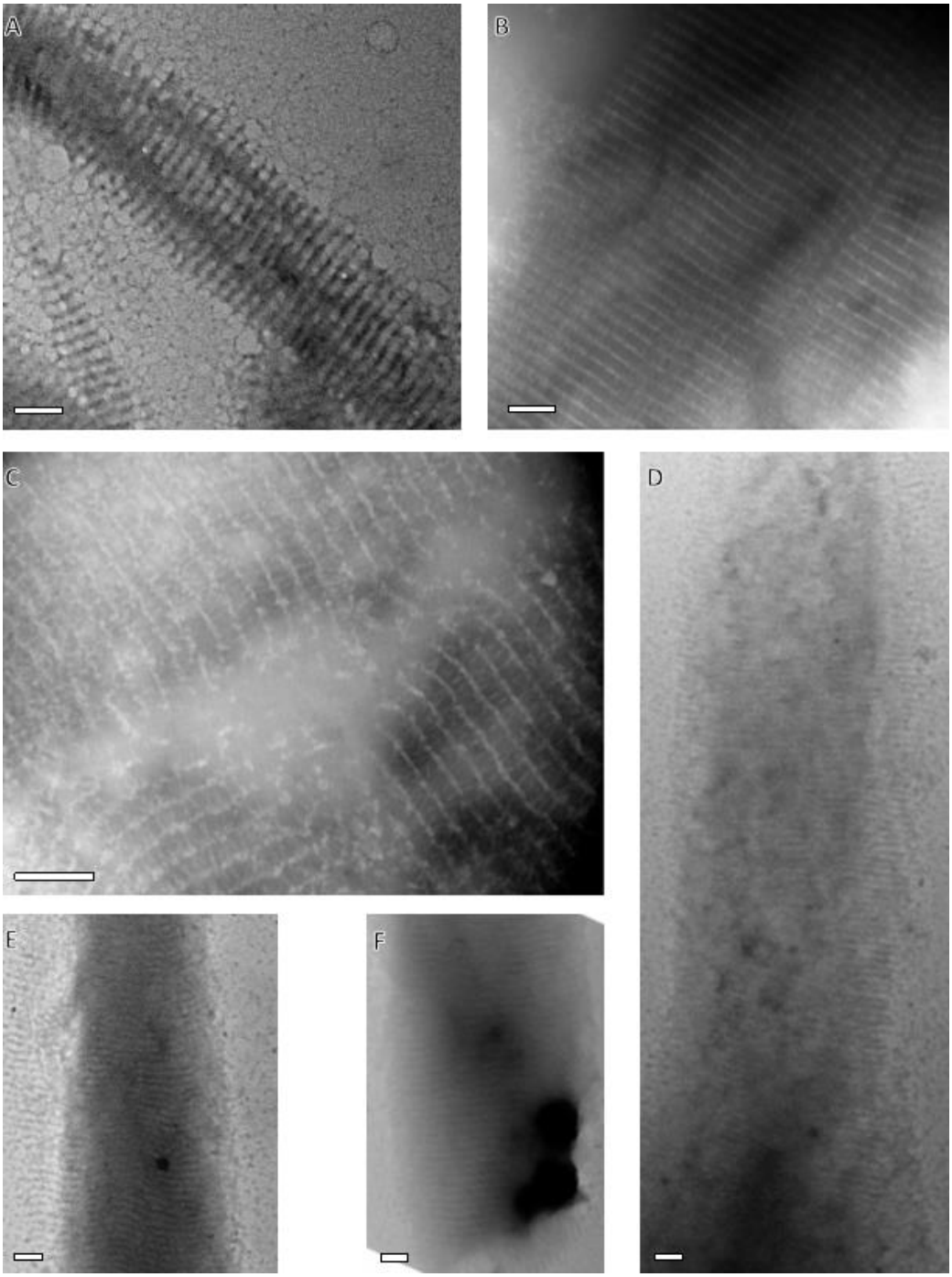

Figure 3.3.9 FilP in Tris pH8.5 in the presence of different cations.

His-FilP in **(A)** 50 mM Tris pH8.5 with 2 mM $MgCl_2$, **(B),(C)** 5 mM $MgCl_2$, **(D)** 50 mM KCl, **(E)** 100 mM KCl, **(F)** 150 mM KCl. Samples negatively stained using 2% ammonium molybdate pH7.0 and visualized by transmission electron microscopy. (Scale bars: 200 nm.)

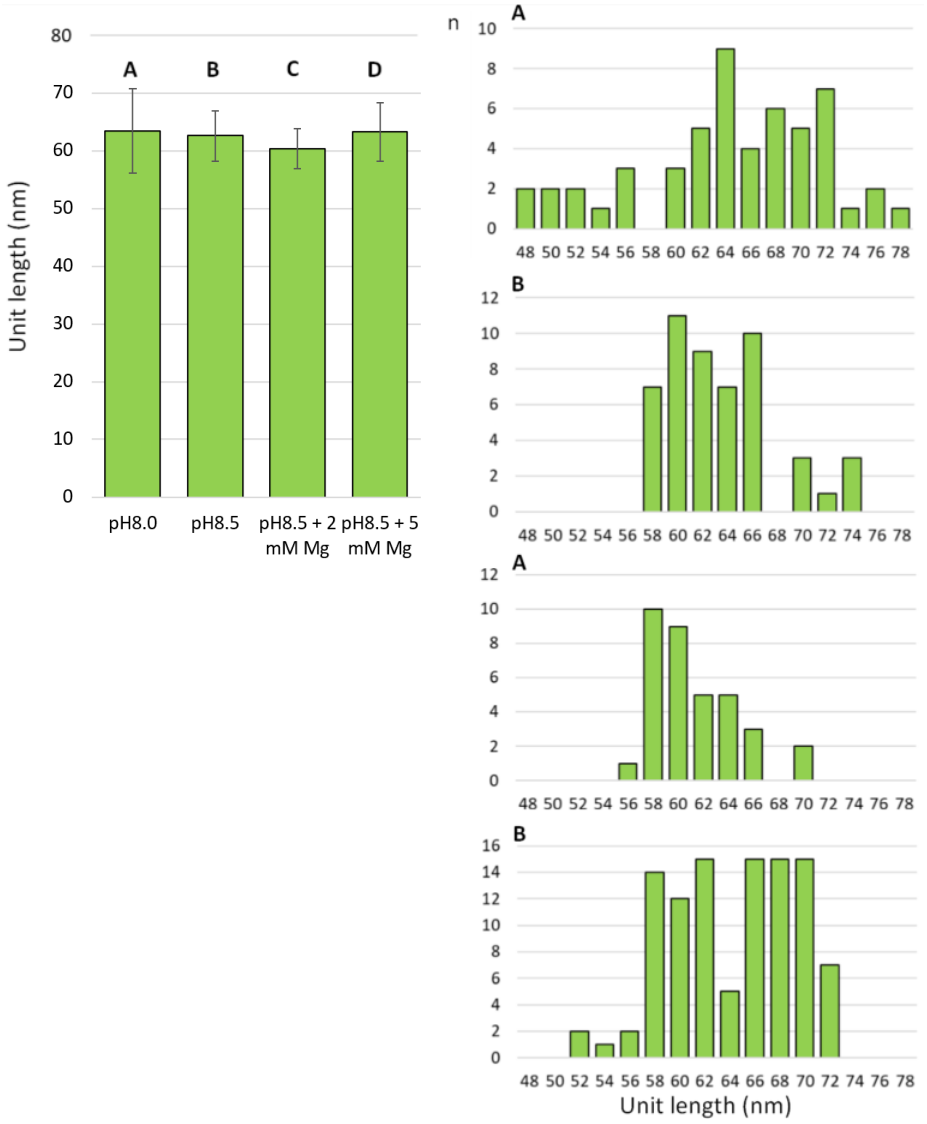

Figure 3.3.10 Analysis 50 mM Tris pH8.0 and 8.5 with cations

Average unit lengths (nm) (left) of His-FilP striated structures in **(A)** 50 mM Tris pH8.0 (mean 63.3 nm standard deviation 7.35, n 53); **(B)** pH8.5 (mean 62.59 standard deviation 4.35 n 51); **(C)** pH8.5 with 2 mM $MgCl_2$ (mean 60.3 nm standard deviation 3.49 n 35); and **(D)** pH8.5 with 5 mM $MgCl_2$ (mean 63.2 nm standard deviation 5.12 n 103). Error bars represent standard deviation. Histograms 50 mM Tris pH8.0 **(A)** and pH8.5 without additions **(B)**, with 2 mM $MgCl_2$ addition **(C)**, and with 5 mM $MgCl_2$ addition **(D)**.

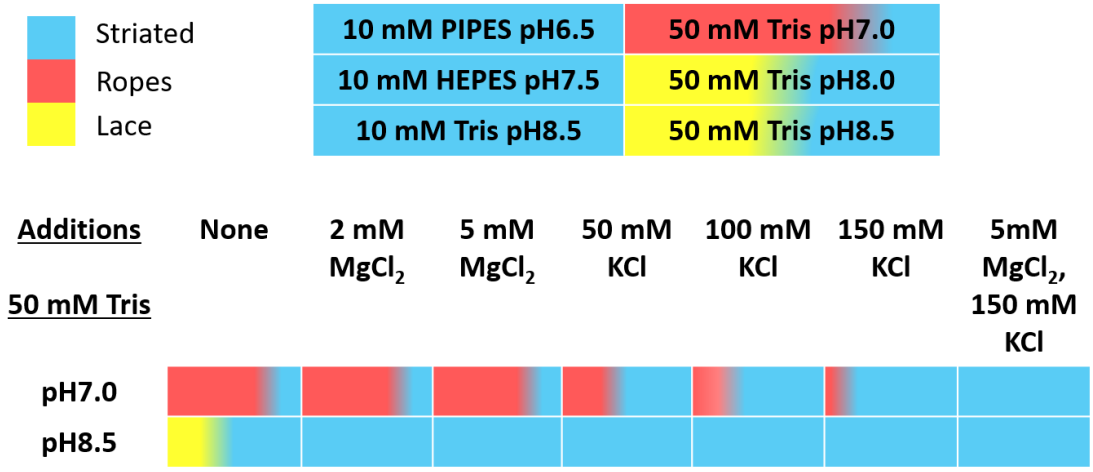

Figure 3.3.11 Summary of FilP higher order assemblies observed.

Blue striation. Red ropes. Yellow potential lace. Where the conditions have multiple types of FilP higher order assembly observed the box is shared in roughly proportional to abundance of those structures.

Repeating FilP in 50 mM Tris pH7.0 and Other pHs

To further confirm the results, and check for reproducibility, selected conditions were repeated along with new conditions using both the same protein batch, and new protein batches (the results did not very between the different batch lots). The results from these experiments follow

FilP dialysed into 50 mM Tris pH7.0 revealed that striated structures were dominant under this condition, and rope structures were only observed once more following the initial experiments described previously (Figure 3.3.12). TEM visualisation and measurement analysis of FilP in 50 mM Tris pH7.0 revealed that the average unit length was 63.7 nm (Figure 3.3.13).

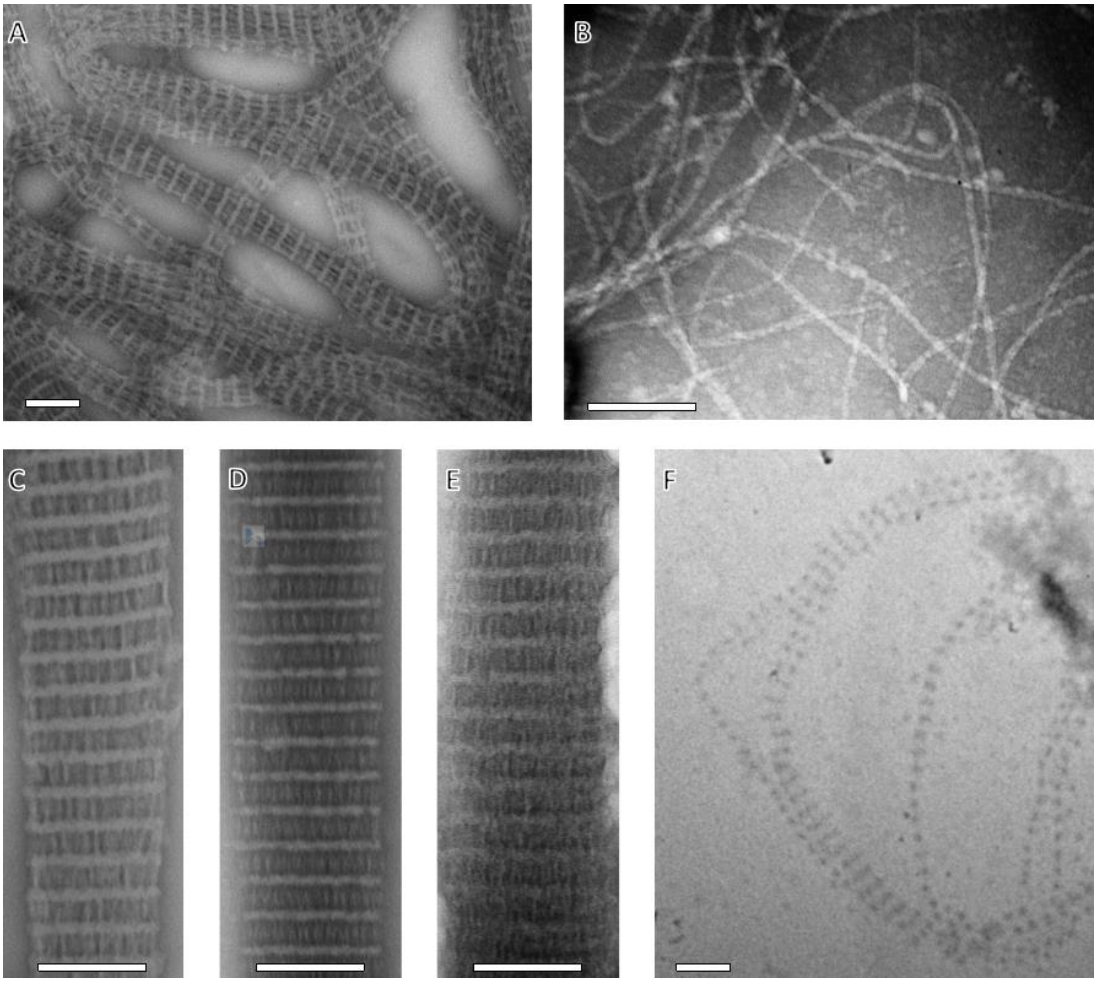

Figure 3.3.12 TEM 50 mM Tris pH7.0

His-FilP in 50 mM Tris pH7.0. Samples at 30 µM (**A-C**), 20 µM (**D**), and 2 µM (**E-F**). Samples negatively stained using 2% ammonium molybdate pH7.0 and visualized by transmission electron microscopy. (Scale bars: 200 nm.)

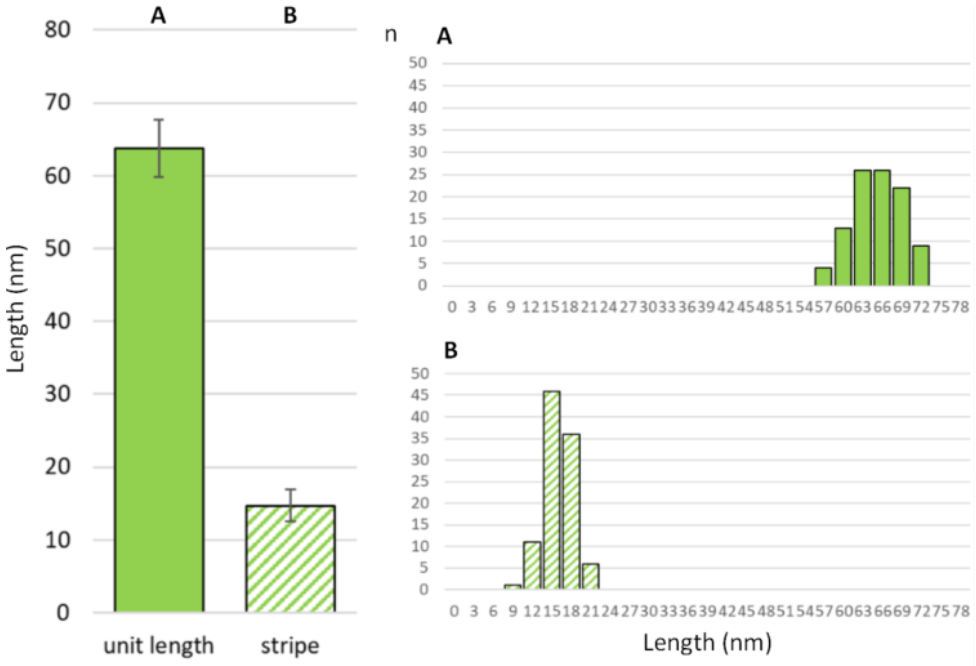

Figure 3.3.13 Analysis of the striation pattern of FilP in 50 mM Tris pH7.0 buffer

Average unit lengths and stripe measurements for striations in 50 mM Tris pH7.0 His-FilP. Unit length **(A)** mean 63.7 nm, standard deviation 3.92, n 100. Stripe **(B)** measurement mean 14.7 nm, standard deviation 2.19, n 100. Error bars represent standard deviation. Histograms of His-FilP 50 mM Tris pH7.0 unit length **(A)** and stripe length **(B)**.

FilP was also analysed in a wider variety of pHs. 20 mM Tris was used without cation addition at pHs 6.0, 6.5, 7.0, 7.5, 8.0 and 8.5 to assess whether the rope or lace structure might be more dominant at any of these pHs. Visualisation by TEM revealed that, at this time, all structures observed were of the striated structure (Figure 3.3.14). Analysis of the measurements revealed that the unit length for these was slightly lower than that for 50 mM Tris pH7.0. Where for 50 mM Tris pH7.0 the unit length was 63.7 nm, the unit lengths for these were 61.3 nm, 60.1 nm, 60.8 nm, 60.5 nm, 58.1 nm, and 60.3 nm for pH 6.0, 6.5, 7.0, 7.5, 8.0, and 8.5 respectively (Figure 3.3.15). To test for statistical significance, measurements were compared using a two-tailed T-test with a 95% confidence level. This revealed that they are all significantly different from the measurements for FilP in 50 mM Tris at all pHs tested without cation addition although, the reason for this is unknown. The difference is small, if significant. The 20 mM Tris pH8.0 unit length of 58.1 nm is significantly lower than for all the other measurements with 20 mM Tris again, why this would be is unknown.

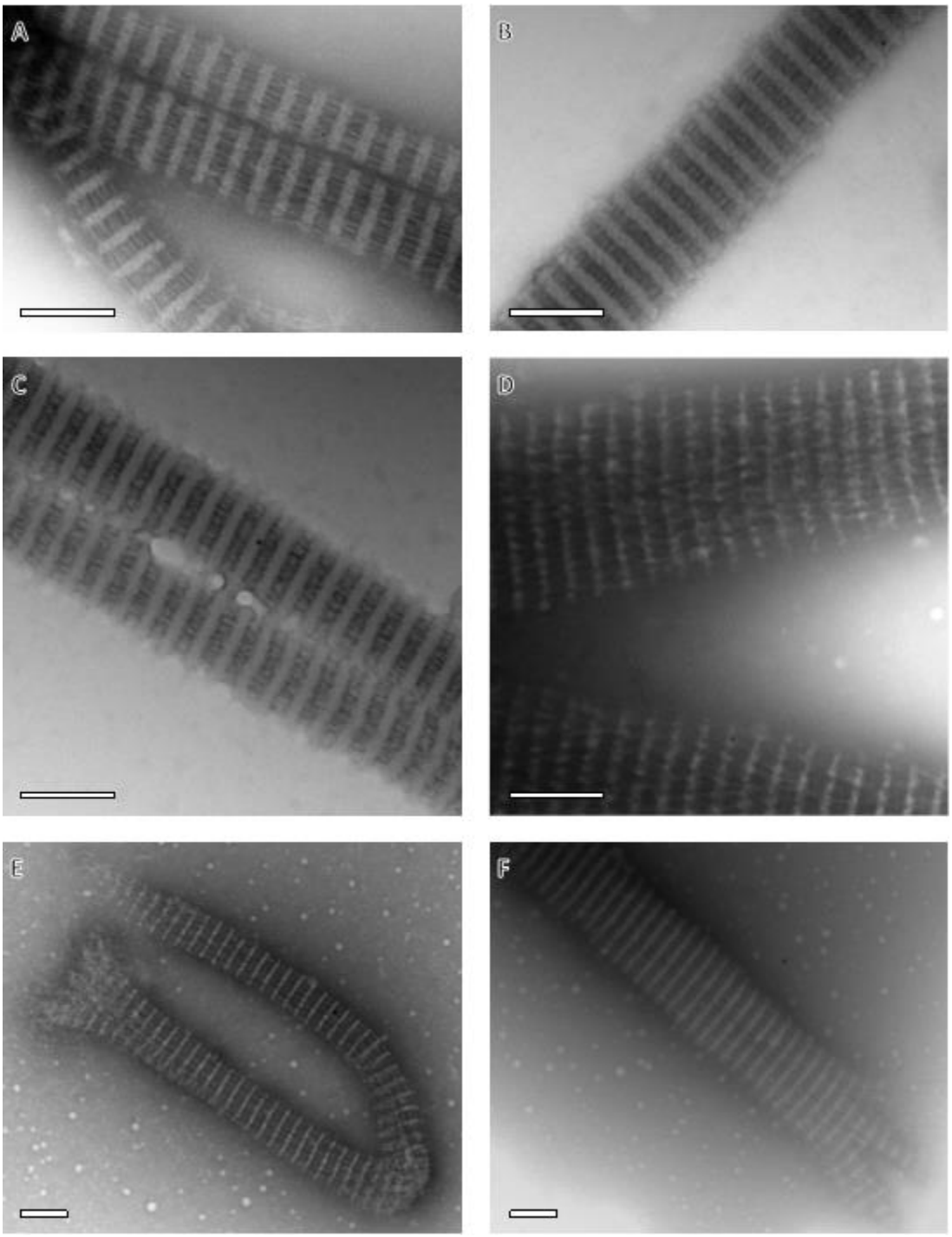

Figure 3.3.14 TEM of FilP in 20 mM Tris buffers

His-FilP in 20 mM Tris pH6.0 (**A**), pH6.5 (**B**), pH7.0 (**C**), pH7.5 (**D**), pH8.0 (**E**), and pH8.5 (**F**). Protein concentrations 30 µM. Samples negatively stained using 2% ammonium molybdate pH7.0 and visualized by transmission electron microscopy. (Scale bars: 200 nm.)

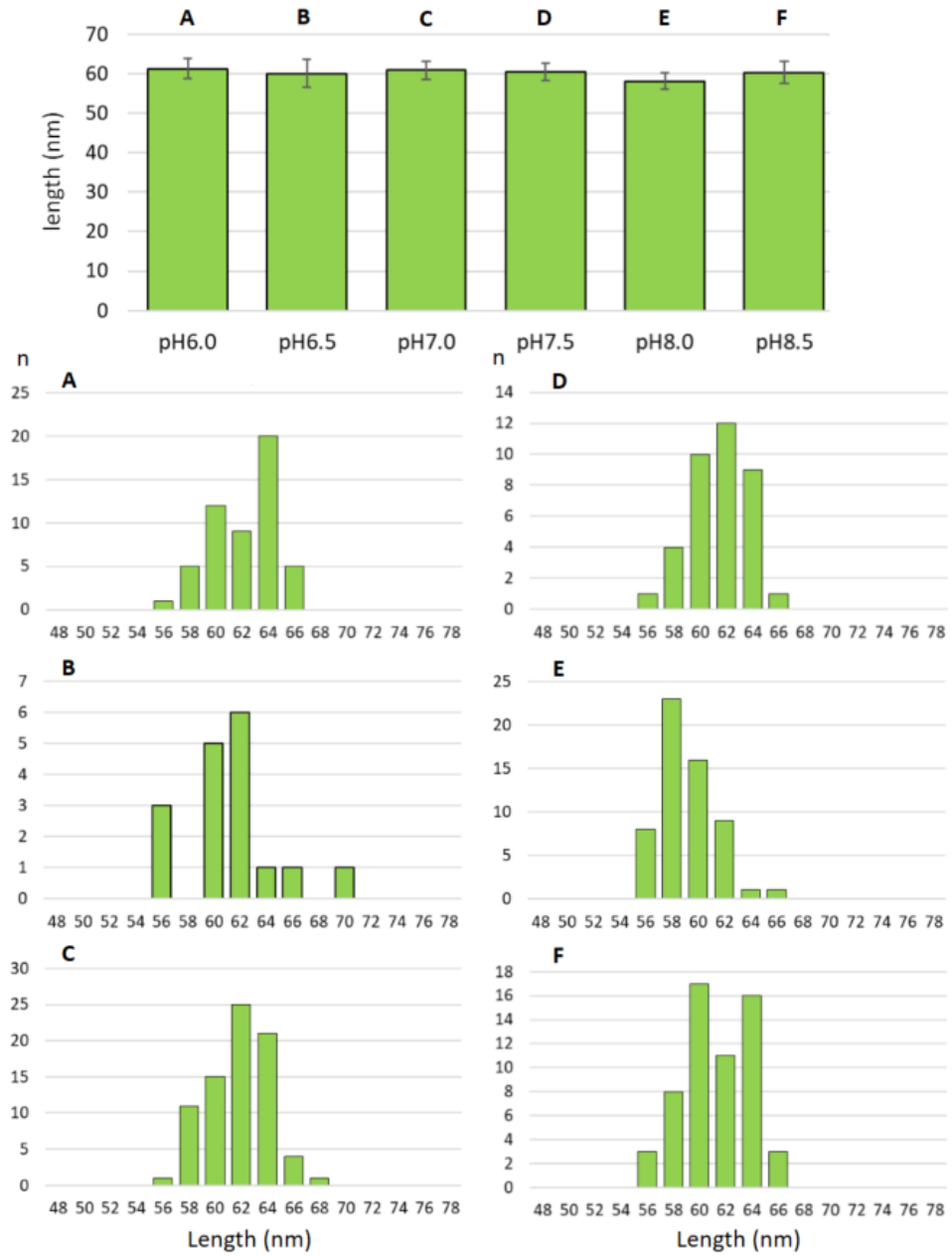

Figure 3.3.15 Analysis of the striation patterns of FilP in 20 mM Tris buffers

Average unit lengths of His-FilP in **(A)** 20 mM Tris pH6.0 (mean 61.3 nm standard deviation 2.56 n 52), **(B)** pH6.5 (mean 60.1 nm standard deviation 3.64 n 17), **(C)** pH7.0 (mean 60.8 nm standard deviation 2.30 n 78), **(D)** pH7.5 (mean 60.5 nm standard deviation 2.10 n 37), **(E)** pH8.0 (mean 58.1 nm standard deviation 2.05 n 58), **(F)** pH8.5 (mean 60.3 nm standard deviation 2.75 n 58). Error bars represent standard deviation. Histograms of His-FilP 20 mM Tris pH6.0 **(A)**, pH6.5 **(B)**, pH7.0 **(C)**, pH7.5 **(D)**, pH8.0 **(E)**, pH8.5 **(F)**.

In FilP, the analysis of the striated structure shows that the pH of the buffer does not affect the unit length of the striation, nor does the addition of cations (Figure 3.3.8, Figure 3.3.10, Figure 3.3.13). Only buffer concentration appeared to change the unit length (Figure 3.3.15). In all conditions tested with 50 mM Tris with and without cation addition, the unit length was around 63 nm (Figure 3.3.6, Figure 3.3.8, Figure 3.3.10). However, using 20 mM Tris, the unit length changed to being around 60 nm (with pH8.0 being lower at 58 nm). These differences, though statistically significant, are very small and potentially an error in measurement or imaging as opposed to a real difference in the unit length of the structure.

3.4 Summary

In conclusion, the rope structure observed indicates that FilP is like the eukaryotic intermediate filaments. Both appearance and the width of the rope structures are concordant with the width in eukaryotes (Figure 1.7.2, Figure 3.3.2, Figure 3.3.7) . This further aids to the argument that FilP is intermediate filament-like in its nature. This rope structure is also similar to that which has been observed with crescentin. However, this is the first time the rope structure has been reported for FilP.

The striated structure closely resembles the paracrystal structure which has been observed for the eukaryotic intermediate filament type lamins (Figure 1.7.2, Figure 3.3.2, Figure 3.3.8). This suggests that FilP resembles the type V lamins more closely than it does other types of intermediate filaments. This could suggest that FilP might also follow the assembly pathway that is established for lamins and we investigate this in the next chapter. The unit lengths of the striations in FilP remain constant, despite changes pH and salt concentration. This suggests that the unit length is an intrinsic property of the protein which does not alter when the conditions do. This unit length of 63.7 nm for FilP (50 mM Tris pH7.0) suggests that the unit length is comprised of more than one elementary dimer.

The rope and striated structures suggest strong lateral interactions but the way they are aligned must be different to give the different appearance. The lace structure is different. It is likely that the lateral interactions are less favoured in this structure and it would be interesting to establish how the lateral interactions are forming. The lace structure which we observed for FilP was not as defined as that observed by others.

The reliability of FilP to form these structures under the same conditions is questionable. In our first round of observations in 50 mM Tris pH7.0 we reliably saw rope structures as the main structure with some striations (Figure 3.3.2), however in a second round of observations separated by time, we observed striated filaments in vast majority and only saw rope structures once more (Figure 3.3.12). This is again different to what was observed by Fuchino et al (Fuchino et al., 2013) where a lace structure was observed in 50 mM Tris pH7.0. Javadi et al (Javadi et al., 2019) also observed a striated structure at pH6.8. This variation in structures seen under the same conditions highlights that the protein is likely to be sensitive in its nature of forming higher order structures to a factor which is as yet unknown.

Also confusingly, (during the time when we were able to see ropes and lace) addition of cations pushed the structures towards the striated structure and appeared to increase the lateral associations (Figure 3.3.6, Figure 3.3.9). This is again contrary to findings by Javadi et al (Javadi et al., 2019) who observed an increase in solubility of the protein with increased cations as well as a shifting from a striated structure to an hexagonal meshwork lace. Where cations appear to increase lateral interactions for us, it decreases it for them. Why there would be this discrepancy is unclear and further highlights that there is likely to be a factor which affects structure of higher order assemblies of FilP which we have not yet elucidated.

4 Assessing What is Required for Successful Higher Order Assembly of FilP- Construct Designs, Protein Overexpression and Purification

4.1 Aims

To generate a series of truncated FilP proteins to establish which motif is required for higher order assembly. Optimisation of protein overexpression and purification.

4.2 Variant Design Rational

To identify the motifs which were essential for the ability of FilP to form higher order assemblies we designed, created and tested a large variety of FilP variants which lacked distinct FilP fragments. FilP variants known as FilPC, FilPN and FilPT were designed to lack the head domain and coil 1 subdomain; the coil 2 subdomain and tail domain; and half of the coil 2 subdomain and tail domain respectively (Figure 4.2.1). The rationale behind this was to establish whether abolishing any of these important features would abolish the ability of FilP to form higher order structures. A variant known as miniFilP was designed to lack an internal part of the coil 2 domain (Figure 4.2.1). MiniFilP was designed to maintain all of the features of FilP while just shortening the coil 2 subdomain to assess whether this construct was still able to form higher order assemblies like the full length FilP and if so, whether the unit length of the assembly was altered. FilP Δlinker was designed to just lack the linker which joins coil 1 and 2 (Figure 4.2.1). This was designed to see if the deletion of the linker would change propensity for FilP to form higher order structures even if the flexibility in the centre of the coils was removed and essentially formed one long coil. The small construct known as 2CC51 is a small part of coil 2 and contains two complete 51 repeats (Figure 4.2.1). This was designed to see if the unusual 51 repeat on its own could form higher order assemblies.

Sequential shortenings of FilP from the C terminus were designed to test which part of the C terminal was essential to for forming higher order assemblies. This was based on the results that FilPT was not able to form higher order assemblies, but miniFilP was, even though it lacked a large part of the coil 2 domain suggesting that the C-terminus of FilP is important for higher order assemblies such as the striated assembly. Sequential shortening of FilP was

designed (Figure 4.2.1) starting with a variant lacking the tail domain, known as FilP Δtail. FilP Δ4x7 then lacks the tail domain and the last 4 heptad repeats of the coil 2 subdomain. FilP Δ4x7 2x11 lacks the tail domain, the last 4 heptad repeats of the coil 2 subdomain and the last 2 hendecad repeats of the coil 2 domain. This sequential shortening was also applied to the miniFilP construct in the same way with the exception that the 2x11 was not removed as that would have created a variant without the end section of the coil 2 domain of miniFilP and would therefore have been a shorter version than FilPT which was already known not to form higher order structures (Figure 4.2.1).

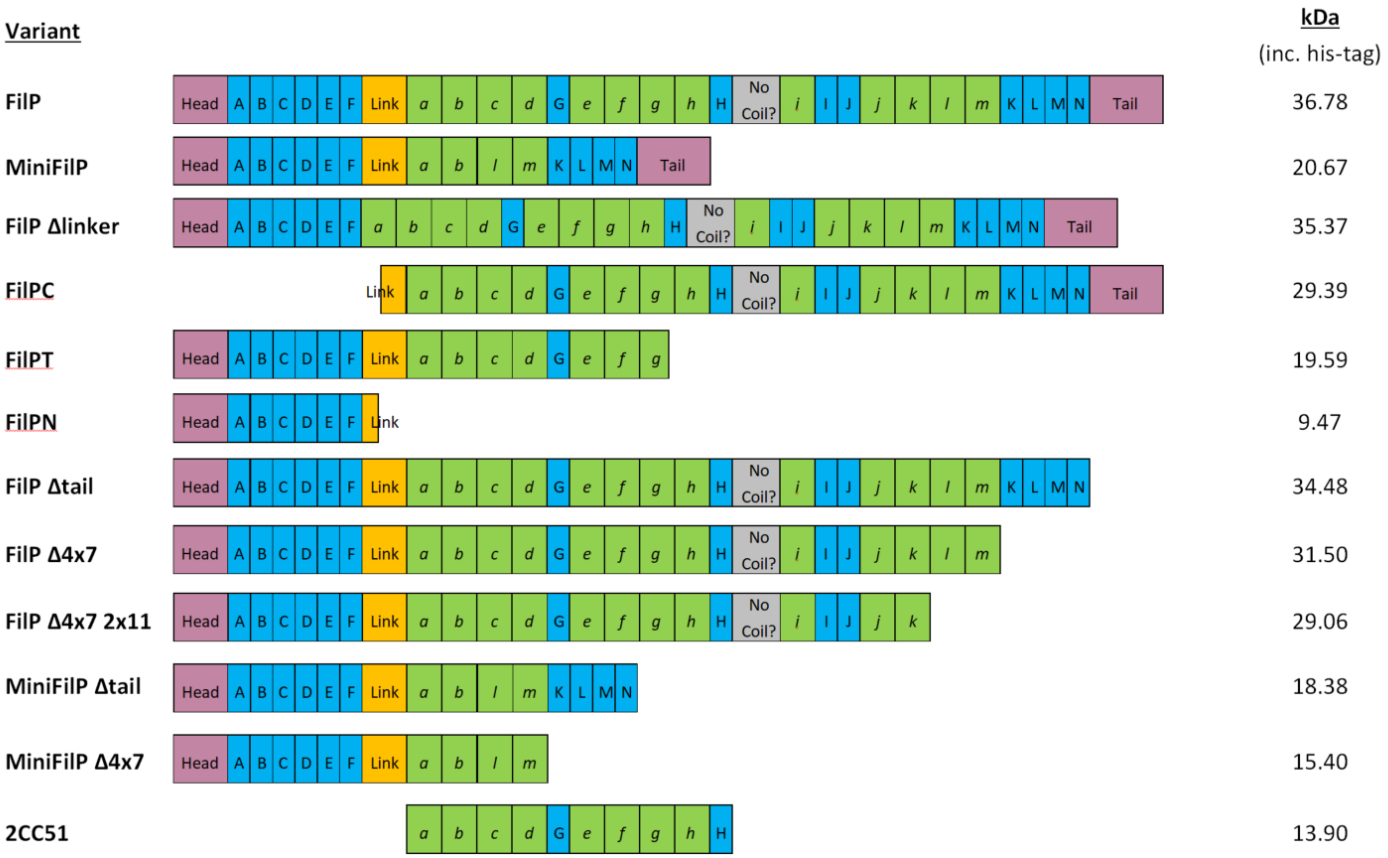

Figure 4.2.1 FilP variants diagram
Diagram showing the FilP variants generated. The non-coiled head and tail domain are shown in purple, the linker subdomain is shown in yellow, heptad repeats are shown in blue and hendecad repeats are shown in green. Sizes are to scale for the number of amino acids without the his-tag. Mass in kDa is shown as calculated with Hi-tag included as computed using the ExPASy - Compute pI/Mw tool (Swiss Institute of Bioinformatics, 2015).

4.3 Strategy for the Generation of Variants

For large scale protein overproduction, we used the plasmid pET28. The pET28 plasmid is a high copy number vector for overexpression of a desired protein within *E. coli*. It carries a kanamycin resistance gene, a T7 polymerase promoter for the gene of interest means that expression is driven by T7 polymerase. The *E. coli* strain BL21 (DE3) pLysS was used as a host for overexpression as this contains a T7 polymerase gene which is under the control of the LacI repressor. This blocks RNA polymerase from transcribing the T7 polymerase gene in the absence of its inducer, here IPTG, and therefore, there is no expression of the gene of interest. Furthermore, the *pLysS* plasmid encodes a *lysS* gene which codes for a T7 lysozyme which is constitutively expressed at low levels to stop any T7 polymerase from activating the gene of interest prior to induction. Induction of gene of interest expression can be achieved by removing the LacI repressor from its operator sites by the addition of isopropyl β-D-1-thiogalactopyranoside (IPTG) (Doherty et al., 1995; Pan and Malcolm, 2000; Schlicke and Brakmann, 2005).

In order to introduce the different FilP variants, the pET28 plasmid was digested with EcoRI and NdeI, or EcoRI and XbaI, following dephosphorylation with alkaline phosphatase. Alkaline phosphatase was added to the digested plasmids to dephosphorylate the ends for ligation and prevent vector regeneration (Dale and Greenaway, 1985). This was then gel extracted which produced a single band which ran to the expected size on an agarose gel, indicating that this was successful (Figure 4.3.6).

FilPC, FilPN and FilPT Constructs

First we designed constructs carrying the N terminal region of FilP (coil 2 and the tail), the C terminal region (the head and coil 1), and a truncated FilP (head, coil 1, linker and half of coil 2) (Figure 4.3.1). Generation of the constructs for the FilP variants FilPC, FilPT and FilPN was achieved by previously in lab by Matthew Stephens by Phusion PCR using the pET28 FilP plasmid as a template. Phusion PCR was carried out using the primer pairs FilPC Xba Nde FRW2 and FilP Eco UT REV, THAbps FRW and FilP Trunc Eco UT REV, THAbps FRW and FilPN Eco UT REV for FilPC, FilPT and FilPN respectively (Figure 4.3.1). The forward primers for these added n *Nde*I restriction site overlapping the start codon, ATG, for each construct, and the reverse primers added an *Eco*RI restriction site downstream of the construct for cloning purposes. These PCR products were subsequently digested with *Eco*RI and *Nde*I restriction enzymes and gel extracted prior to ligation and transformation into *E. coli* DH5α.

Transformants were selected on LB agar plates containing kanamycin and colony PCR was used to identify transformants carrying the expected inserts. This was carried out using the same primer pairs that were used to generate the constructs: FilPC Xba Nde FRW and FilP Eco UT REV; THAbps FRW and FilP Trunc Eco UT REV; THAbps FRW and FilPN Eco UT REV for FilPC, FilPT and FilPN respectively. One of the positive colonies was then taken forward for large scale plasmid preparation. Sequencing of the cloned fragments was used to confirm the successful generation of the plasmids pET28 FilPC, pET28 FilPT and pET28 FilPN.

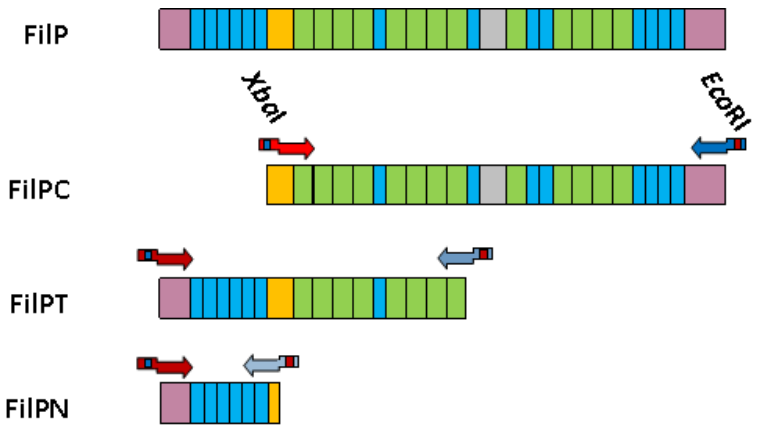

Figure 4.3.1 Generation of FilP variants FilPC, FilPT and FilPN by PCR

Generation of the FilP variant constructs FilPC, FilPT, and FilPN by PCR. Template for all pET28 FilP. FilPC forward primer, FilPC Xba Nde FRW2 (red arrow) truncates the gene such that it starts at the linker subdomain of FilP and adds an *Xba*I restriction site upstream, the reverse primer, FilP Eco UT REV (dark blue arrow) binds to the very end of the *filP* gene and adds an *Eco*RI restriction site downstream. The forward primers for FilPT and FilPN are the same primer, THAbps FRW (dark red arrow), which binds to the start of the *filP* gene and adds an *Xba*I restriction site upstream. The reverse primers for FilPT and FilPN vary to truncate in differing places, the FilPT reverse primer, FilP Trunc Eco UT Rev (medium blue arrow), truncates in the middle of the coil 2 domain and the FilPN reverse primer, FilPN Eco UT REV (light blue arrow), truncates in the middle of the linker subdomain, both add an *Eco*RI restriction site downstream of the gene.

Diagram shows primers (arrows) with *Xba*I restriction site (dark blue box), *Eco*RI restriction site (dark red box), and FilP (multicoloured boxes– light purple for the N terminal head and C terminal tail domains, light blue for heptad repeat sequences, green for hendecad repeat sequences and yellow for the linker domain).

MiniFilP, FilP Δlinker, and 2CC51 Constructs

A variant known as miniFilP was designed to lack an internal part of the coil 2 domain (Figure 4.2.1). MiniFilP was designed to maintain all of the features of FilP while just shortening the coil 2 subdomain to assess whether this construct was still able to form higher order assemblies like the full length FilP and if so, whether the unit length of the assembly was altered. FilP Δlinker was designed to just lack the linker which joins coil 1 and 2 (Figure 4.2.1). This was designed to see if the deletion of the linker would change propensity for FilP to form higher order structures even if the flexibility in the centre of the coils was removed and essentially formed one long coil. The small construct known as 2CC51 is a small part of coil 2 and contains two complete 51 repeats (Figure 4.2.1). This was designed to see if the unusual 51 repeat on its own could form higher order assemblies.

For miniFilP, FilP Δlinker, and 2CC51 the constructs were commercially synthesised including a fragment of the plasmid pET28a containing the promoter site and including the His-tag, enabling us to use *Xba*I for cloning instead of the two nucleotide overhang, and therefore less reliable *Nde*I cloning. This ensured and EcoRI restriction site downstream of the sequence, and an *Xba*I restriction site upstream of the sequence (Figure 4.3.2). This also meant that all proteins contain an N-terminal His-tag which allows purification.

These commercially synthesised constructs were then liberated from the surrounding vector using *Eco*RI and *Xba*I restriction enzymes (Figure 4.3.2) with a common band at around 2000 bp which corresponds to the vector used for the synthetic constructs. The expected size of the construct 2CC51 425 bp, FilP Δlinker 998 bp, miniFilP 614 bp were confirmed (Figure 4.3.2B) and these fragments were gel extracted (Figure 4.3.2C) prior to ligation inot the pET28 vector. Following chemical transformation of *E. coli* DH5α, transformants were selected on LB agar containing kanamycin (Figure 4.3.3). Transformants were then screened using colony PCR using primers pET28 Xba FRW and FilP Eco UT REV for miniFilP and FilP Δlinker. For FilP 2CC51 primers pET28 Xba FRW and FilP Trunc Eco UT REV were used (Figure 4.3.4). One of the positive colonies was subsequently used for large scale plasmid preparation. Sequencing of the cloned fragments was used to confirm the successful generation of the plasmids pET28 miniFilP, pET28 FilP Δlinker and pET28 2CC51.

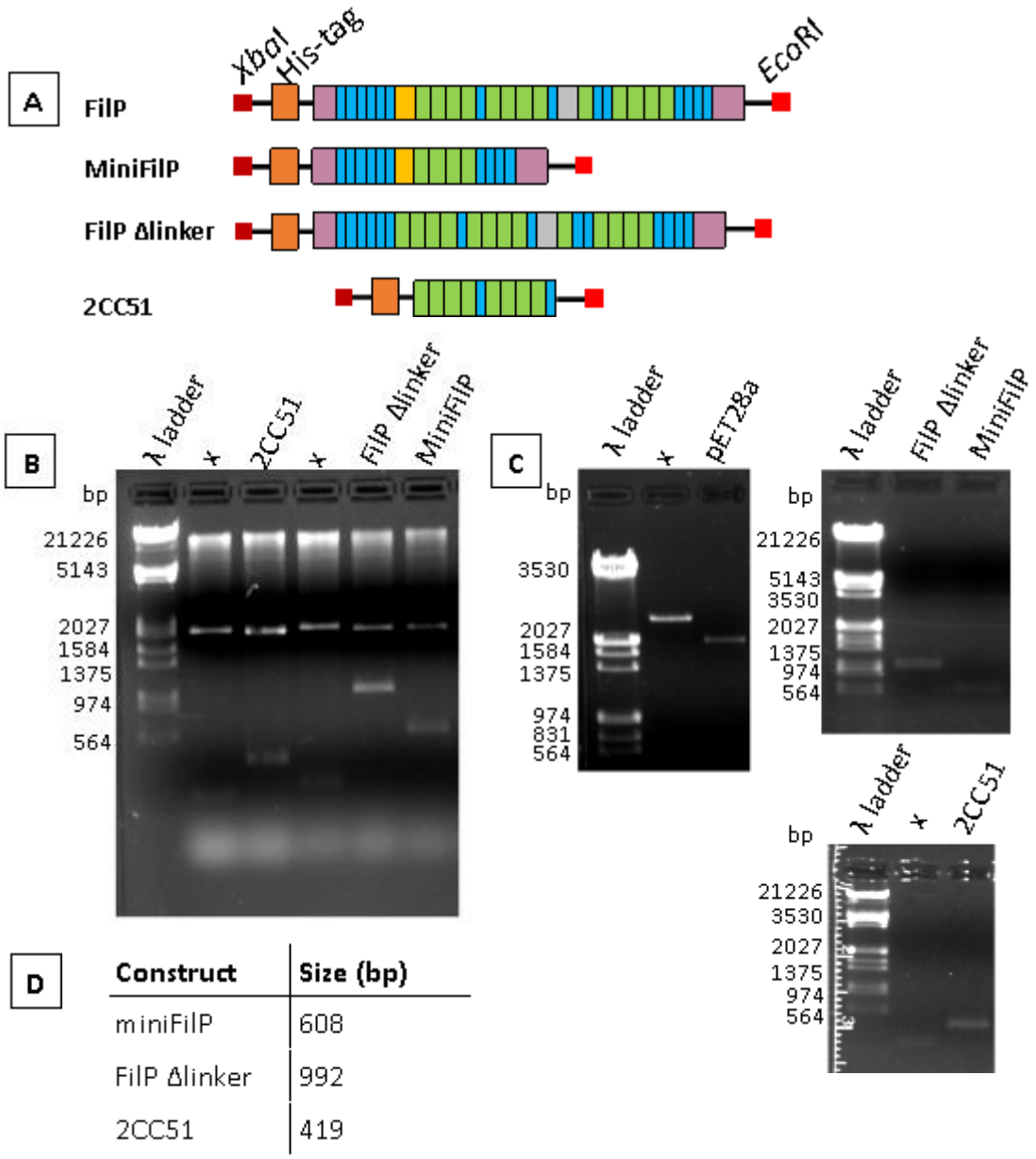

D

Construct	Size (bp)
miniFilP	608
FilP Δlinker	992
2CC51	419

Figure 4.3.2 miniFilP, FilPΔlinker, and 2CC51 digest

Commercially synthesised MiniFilP, FilP Δlinker and 2CC51 with small sections of pET28 either side were digested. **(A)** FilP variants genes commercially synthesised with pET28 flanking subdomains to incorporate the His-tag and EcoRI and XbaI sites. Head and tail domains indicated in purple. Yellow denotes the linker subdomain. Grey is a section where there is potentially no coil. Blue sections are heptad repeat sequences. Green sections denoted are hendecad repeat sequences. Dark red boxes are XbaI sites and light red are EcoRI restriction sites. **(B)** Agarose gel electrophoresis for analysing test digest of synthetic plasmids containing 2CC51, FilP Δlinker and MiniFilP. Digested with EcoRI and XbaI. Band at ~2000 bp is the vector which the synthetic fragments were contained within. **(C)** Agarose gel electrophoresis of pET28, miniFilP, FilP Δlinker, and 2CC51 digested with EcoRI and XbaI restriction enzymes and gel extracted. λ ladders shown to the left of each gel. Lanes marked with an x are not relevant here. **(D)** Sizes of constructs digested with *Eco*RI and *Xba*I.

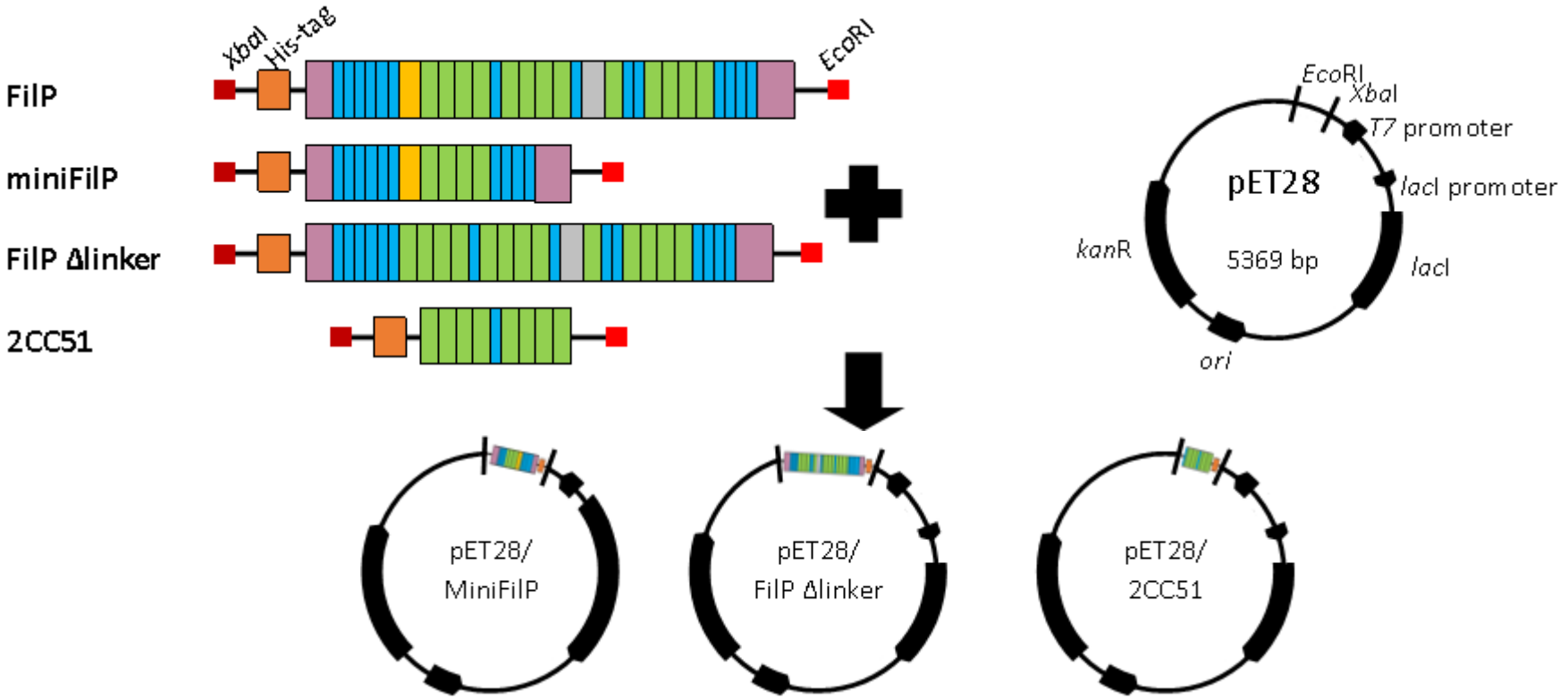

Figure 4.3.3 Construct design for miniFilP, FilP Δlinker and 2CC51
Commercially synthesised FilP variants and pET28 digested (top) then ligated together to produce the plasmids (bottom). Head and tail subdomains indicated in purple. Yellow denotes the linker subdomain. Grey is a section where there is potentially no coil. Blue sections are heptad repeat sequences. Green sections denoted are hendecad repeat sequences. Dark red boxes are *Xba*I sites and light red are *Eco*RI restriction sites. pET28 contains the *Eco*RI and *Xba*I restriction sites, the T7 promoter, *lac*I promoter, *lac*I gene, *ori*, and the kanamycin resistance gene *kan*R.

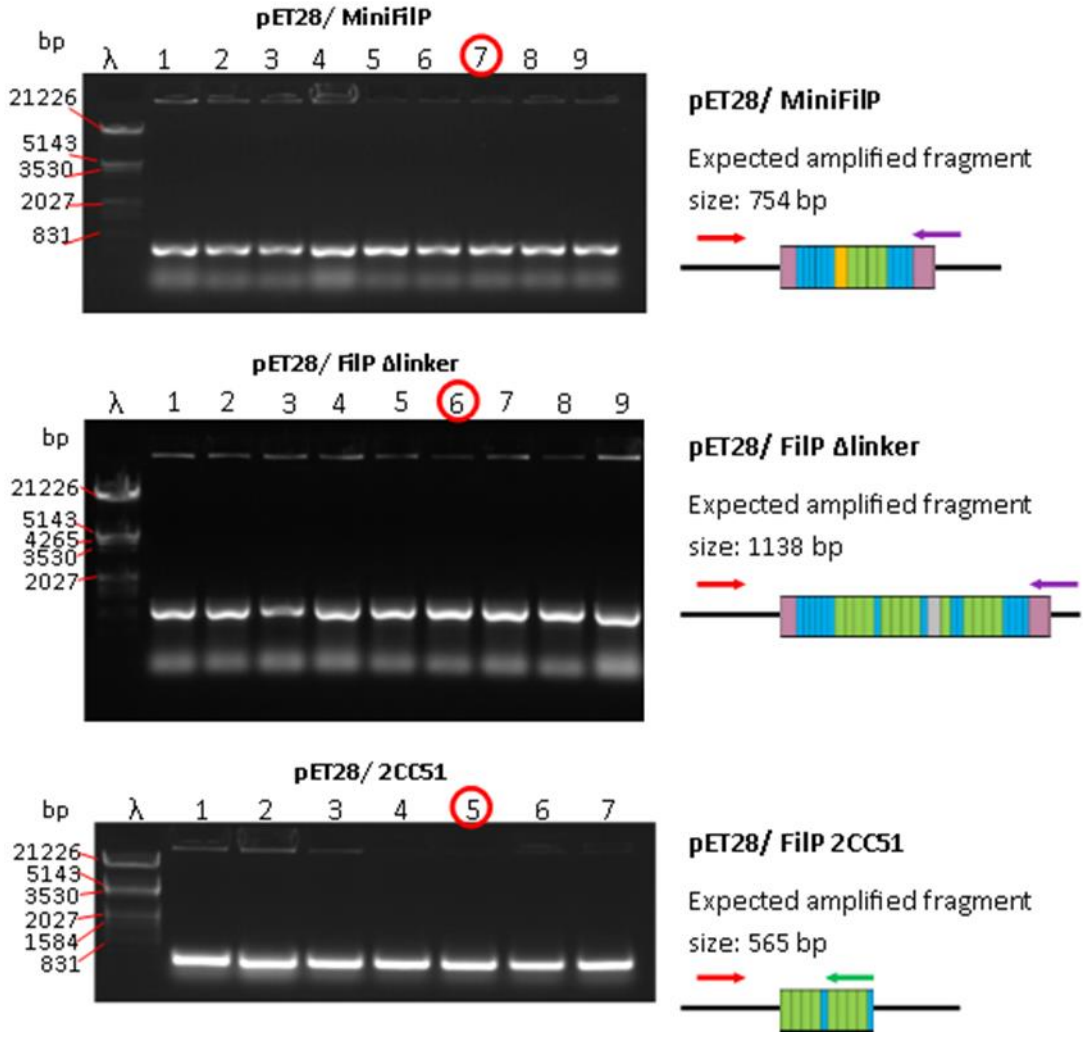

Figure 4.3.4 Colony PCR confirmation of miniFilP, FilP Δlinker, 2CC51

Colony PCR for testing the transformants. Colony PCR products run on agarose gels. Lane λ: λ EcoRI HindIII ladder; lane 1-9: each lane represents a PCR product from a single colony. Right: depiction of colony PCR of each construct and expected bp size amplified by PCR. Arrows on image represent primers used. Purple primer: FilP Eco UT REV. Green primer: FilP Trunc Eco UT REV. Red primer: pET28 Xba FRW. The positive colonies that were selected are circled.

FilP Δtail, FilP Δ4x7, FilP Δ4x7 2x11, miniFilP Δtail, miniFilP Δ4x7 Constructs

In order to test the effect of the heptad or hendecad repeats at the C-terminus of FilP we designed a set of constructs which were successively shortened at the C-terminus. First lacking the tail domain, then the first four heptad sequences, then the following two hendecad sequences for FilP. MiniFilP was also shorted by removal of the tail domain, then the last four hendecads of the coil 2 domain of FilP (Figure 4.2.1).

Generation of the constructs for the C-terminal shortening FilP variants by PCR was achieved by using either pET28 FilP or pET28 miniFilP as a template. PCR was carried out using a universal forward primer pET28 Xba FRW which binds upstream of the *Xba*I restriction site on pET28 upstream of the His-tag for the gene of interest. The reverse primers differed according to the constructs but added an *Eco*RI restriction site downstream of the gene of interest for cloning purposes (Figure 4.3.5). The PCR products were then digested with *Eco*RI and *Xba*I and subsequently gel extracted (Figure 4.3.6) prior to ligations with pET28 (Figure 4.3.7) and transformation into *E. coli* DH5α.

Colony PCR was used to screen the transformants using the universal pET28 primer pET28 Xba FRW and an internal FilP primer FilP Eco UTC Rev (Figure 4.3.8). Plasmids from selected positive colonies were prepared and confirmed using sequencing producing the following plasmids: pET28 FilP Δtail, pET28 FilP Δ4x7, pET28 FilP Δ4x7 2x11, pET28 miniFilP Δtail, and pET28 miniFilP Δ4x7.

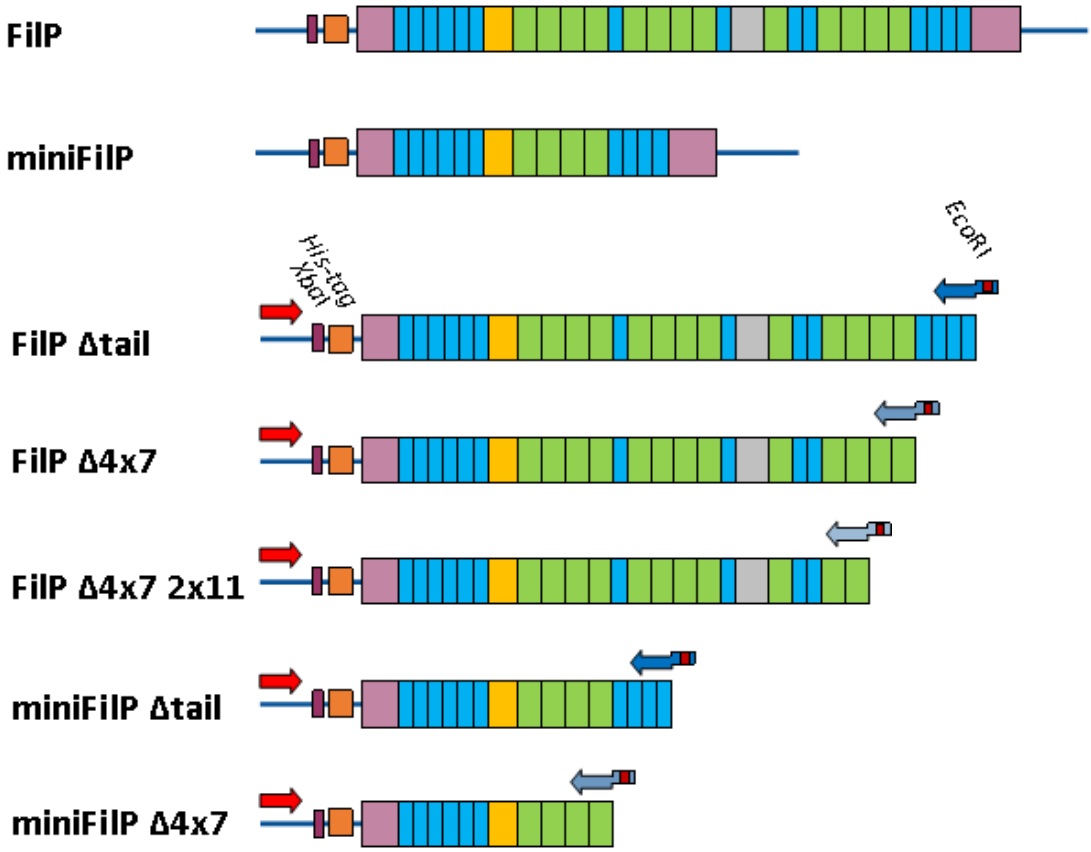

Figure 4.3.5 PCR generation of FilP Δtail, FilP Δ4x7, FilP Δ4x7 2x11, miniFilP Δtail, miniFilP Δ4x7

Generation of the FilP variant constructs FilP Δtail, FilP Δ4x7, FilP Δ4x7 2x11, MiniFilP Δtail and MiniFilP Δ4x7 by PCR using primer pET28 Xba FRW (red arrow) which binds upstream of the gene of interest and an *Xba*I restriction site on the pET28 vector and a specific primer which truncates the gene at the desired point and adds an *Eco*RI restriction site downstream of the gene of interest. Primer FilP Δtail Eco REV primer for Δtail constructs (dark blue arrow), FilP Δtail Eco REV for Δ4x7 constructs (medium blue arrow) and FilP Δ4x7 2x11 Eco REV for Δ4x7 2x11 construct (light blue arrow). Template for FilP Δtail, FilP Δ4x7 and FilP Δ4x7 2x11 use pET28 FilP as a template. MiniFilP Δtail and miniFilP Δ4x7 use pET28 miniFilP as a template. Diagram shows primers (arrows) on the pET28 vector (blue line) with *Xba*I site (dark purple rectangle), His-tag (orange box), and FilP (multicoloured boxes– light purple for the N terminal head and C terminal tail domains, light blue for heptad repeat sequences, green for hendecad repeat sequences and yellow for the linker domain.

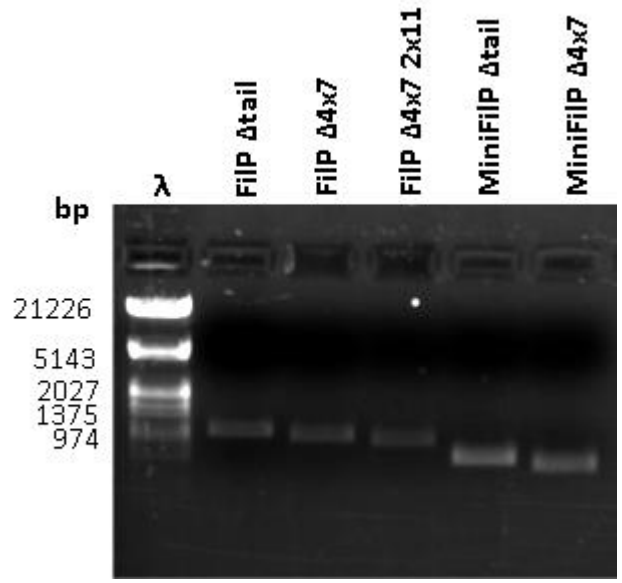

Construct	Size (bp)
FilP Δtail	1006
FilP Δ4x7	922
FilP Δ4x7 2x11	856
miniFilP Δtail	580
miniFilP Δ4x7	496

Figure 4.3.6 PCR generated fragments of FilP Δtail, FilP Δ4x7, FilP Δ4x7 2x11, miniFilP Δtail, miniFilP Δ4x7 prior to ligation.

Agarose gel electrophoresis of PCR product of FilP Δtail, FilP Δ4x7, FilP Δ4x7 2x11, MiniFilP Δtail and MiniFilP Δ4x7 digested with *Eco*RI and *Xba*I restriction enzymes and gel extracted. λ ladders shown to the left of gel. Sizes of constructs (bp).

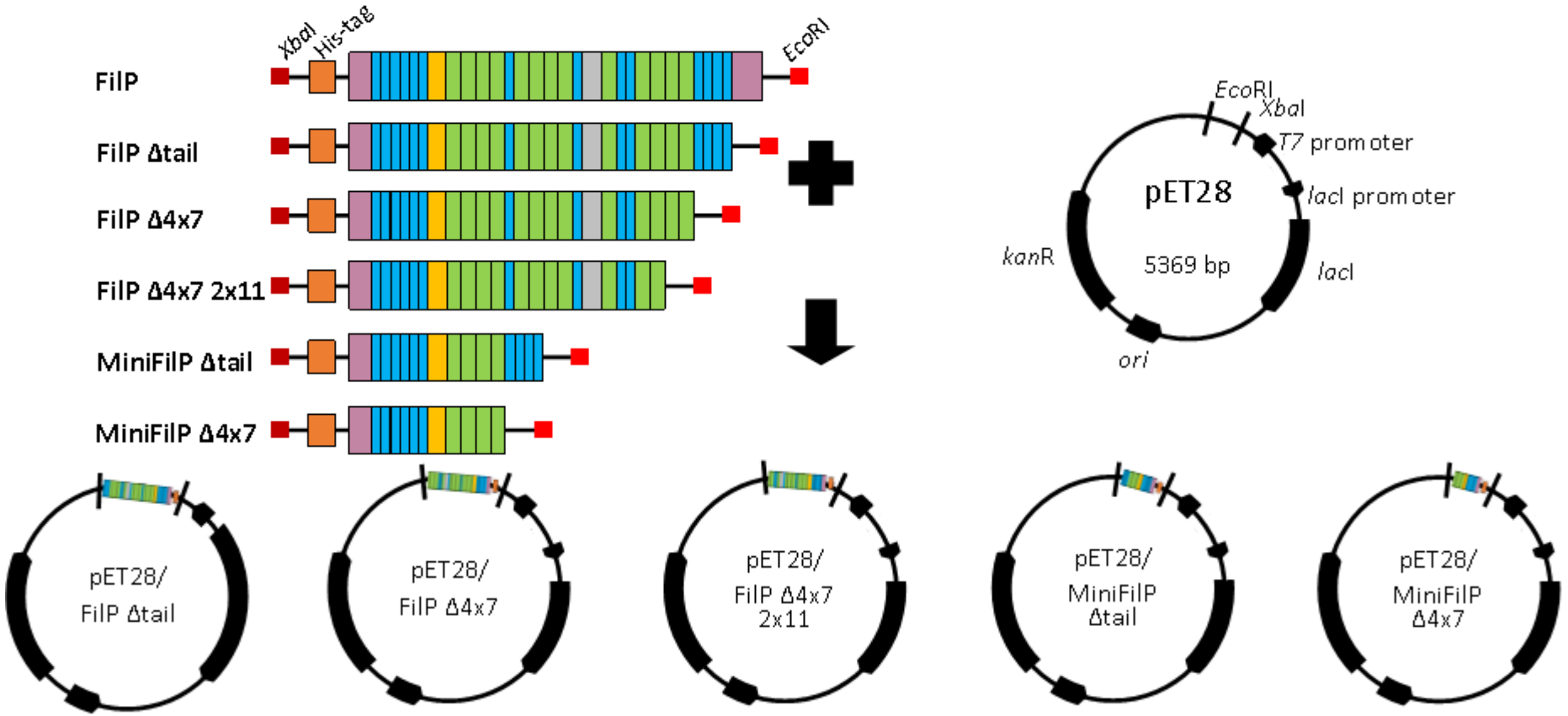

Figure 4.3.7 Ligation plan for FilP Δtail, FilP Δ4x7, FilP Δ4x7 2x11, miniFilP Δtail, miniFilP Δ4x7

FilP variants generated by PCR and pET28 digested (top) then ligated together to produce the plasmids (bottom). Head and tail subdomains indicated in purple. Yellow denotes the linker subdomain. Grey is a section where there is potentially no coil. Blue sections are heptad repeat sequences. Green sections denoted are hendecad repeat sequences. Dark red boxes are *Xba*I sites and light red are *Eco*RI restriction sites. pET28 contains the *Eco*RI and *Xba*I restriction sites, the T7 promoter, *lac*I promoter, *lac*I gene, *ori*, and the kanamycin resistance gene *kan*R.

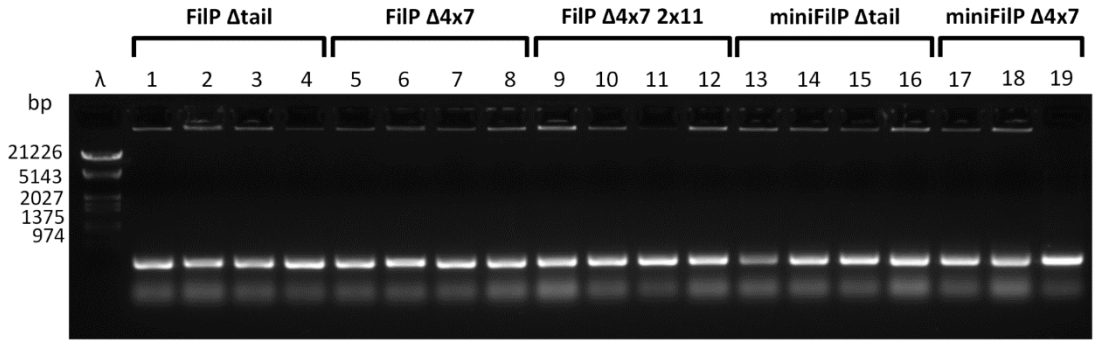

Figure 4.3.8 Colony PCR of FilP Δtail, FilP Δ4x7, FilP Δ4x7 2x11, miniFilP Δtail, miniFilP Δ4x7.

Colony PCR of FilP Δtail, FilP Δ4x7, FilP Δ4x7 2x11, miniFilP Δtail, miniFilP Δ4x7. Colony PCR products run on agarose gels. Lane λ: λ EcoRI HindIII ladder; lane 1-4: FilP Δtail; lane 5-8 FilP Δ4x7; lanes 9-12 FilP Δ4x7 2x11; lanes 13-16 miniFilP Δtail; lanes 17-19 miniFilP Δ4x7. Each lane represents a PCR product from a single colony.

4.4 Expression Trials of FilP Variants

Following the successful generation and confirmation of the plasmids carrying the different FilP variants, samples of the large-scale plasmid stocks were used to transform the *E. coli* strain BL21 (DE3) pLysS using electroporation. Successful transformants were selected for LB agar containing both chloramphenicol and kanamycin.

To confirm and optimise the overproduction of the different FilP variant proteins we tested different temperatures for growth after induction using IPTG and different lengths of time for incubation after induction. Expression trials were carried out to determine the optimum conditions for each construct. A freshly transformed colony was used to inoculate a starter culture. This was subsequently subcultured and grown for 3.5 hrs at 37°C when a 1 ml sample was taken as an uninduced control and 1 mM IPTG was added to the remaining culture to induce expression of the proteins. Cultures were incubated further at either 25°C or 37°C for 4 hrs and 22 hrs whereupon a 1 ml sample was taken for analysis. The 1 ml samples were centrifuged, and the pelleted cells were resuspended in 20 mM Tris buffer 10 mM MgCl pH8.0 and the cells lysed by sonication. Lysates were centrifuged and both supernatant and pellet fractions were analysed by SDS-PAGE (Figure 4.4.1, Figure 4.4.2, Figure 4.4.3).

The expression trials revealed that FilPC was expressed in the pellet fraction at 24 hrs 37°C post induction with IPTG (Figure 4.4.1) therefore this was the condition chosen for large-scale denaturing purification of FilPC (Figure 4.5.1). FilPT expressed in both the supernatant and pellet fractions at 24 hrs 37°C (Figure 4.4.1), although more was visible in the supernatant fraction the large-scale purification was chosen to be done under denaturing conditions from the pellet fraction (Figure 4.5.2). FilPN was expressed in the supernatant fractions at 37°C at both 4 hrs and 22 hrs as well as at 25°C for 22 hrs (Figure 4.4.1). For large-scale native purification of FilPN, 37°C for 4 hrs was chosen as the condition (Figure 4.5.3). MiniFilP was expressed in the pellet fractions for both 25°C and 37°C after 22 hrs, and at lower levels after 4 hrs at 37°C (Figure 4.4.2). 37°C for 22 hrs was chosen as the condition for the large-scale denaturing purification of miniFilP (Figure 4.5.2). FilP Δlinker was expressed in both supernatant and pellet fractions and due to the large band seen in the supernatant fraction at 25°C after 22 hrs (Figure 4.4.2), these were the conditions chosen for the large-scale native purification of FilP Δlinker (Figure 4.5.5). 2CC51 expressed in the supernatant fractions at 37°C

for 4 hrs and 25°C for 22 hrs (Figure 4.4.2). However, purifications at these conditions proved unsuccessful and 2CC51 was purified on a small scale by denaturing of the total cell contents and purified (Figure 4.5.6). FilP Δtail was expressed in the pellet fraction after 22 hrs at 37°C Figure 4.4.3) and small scale purified under denaturing conditions (Figure 4.5.7). FilP Δ4x7 was expressed in the supernatant fraction after 22 hrs at 37°C (Figure 4.4.3) and small scale purified under denaturing conditions (Figure 4.5.8). FilP Δ4x7 2x11 was expressed in the supernatant fraction after 22 hrs at 37°C (Figure 4.4.3),however this proved to have low yield and the total cell contents were small-scale purified under denaturing conditions (Figure 4.5.9). MiniFilP Δtail expressed after 22 hrs at 37°C in the pellet fraction (Figure 4.4.3) and these conditions were used for large-scale purification (Figure 4.5.10). MiniFilP Δ4x7 was expressed at low levels in the supernatant after 22 hrs at 37°C (Figure 4.4.3) however using these conditions for the purification did not have a good yield, so the total cell contents were small-scale purified under denaturing conditions (Figure 4.5.11).

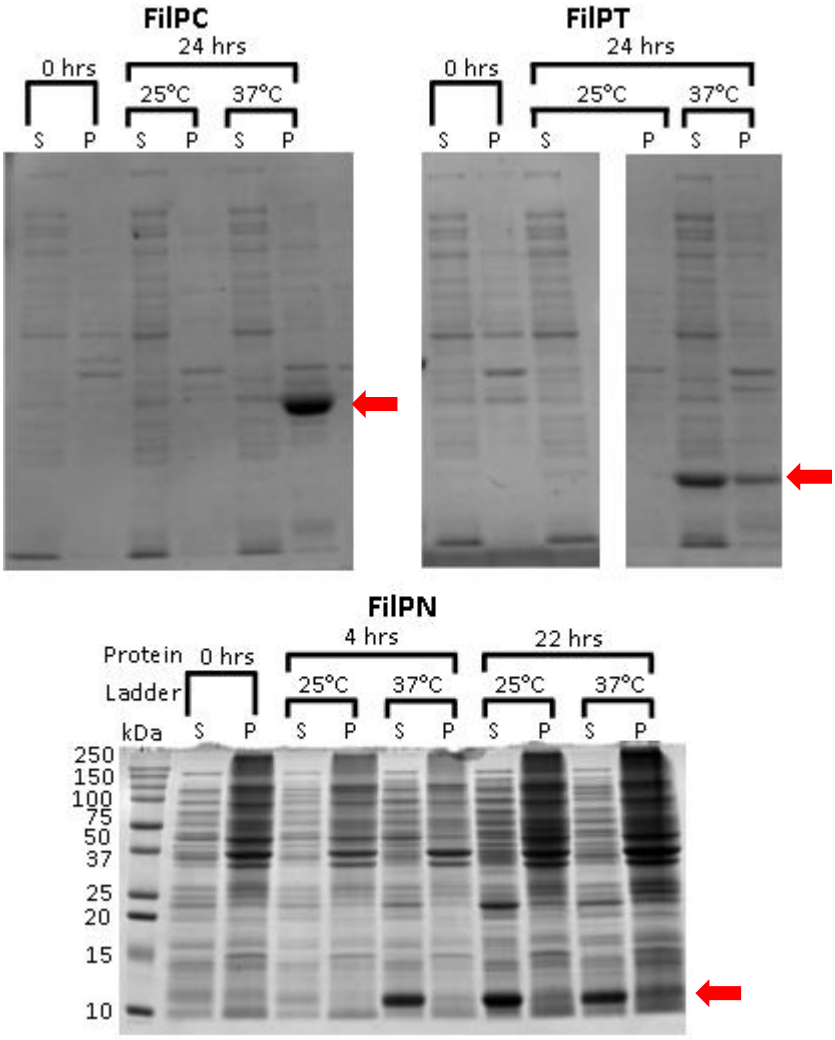

Figure 4.4.1 FilPC, FilPT and FilPN expression trials

Supernatant and pellet fractions from the FilPC, FilPT and FilPN expression trials in *E. coli* were analysed using 15% SDS-PAGE and visualised by Coomassie staining. Samples were collected following 4 or 22 hrs growth either at 25°C or 37°C after induction using 1 mM IPTG. Molecular weight marker is shown in lane 1. Red arrow indicates correct protein band.

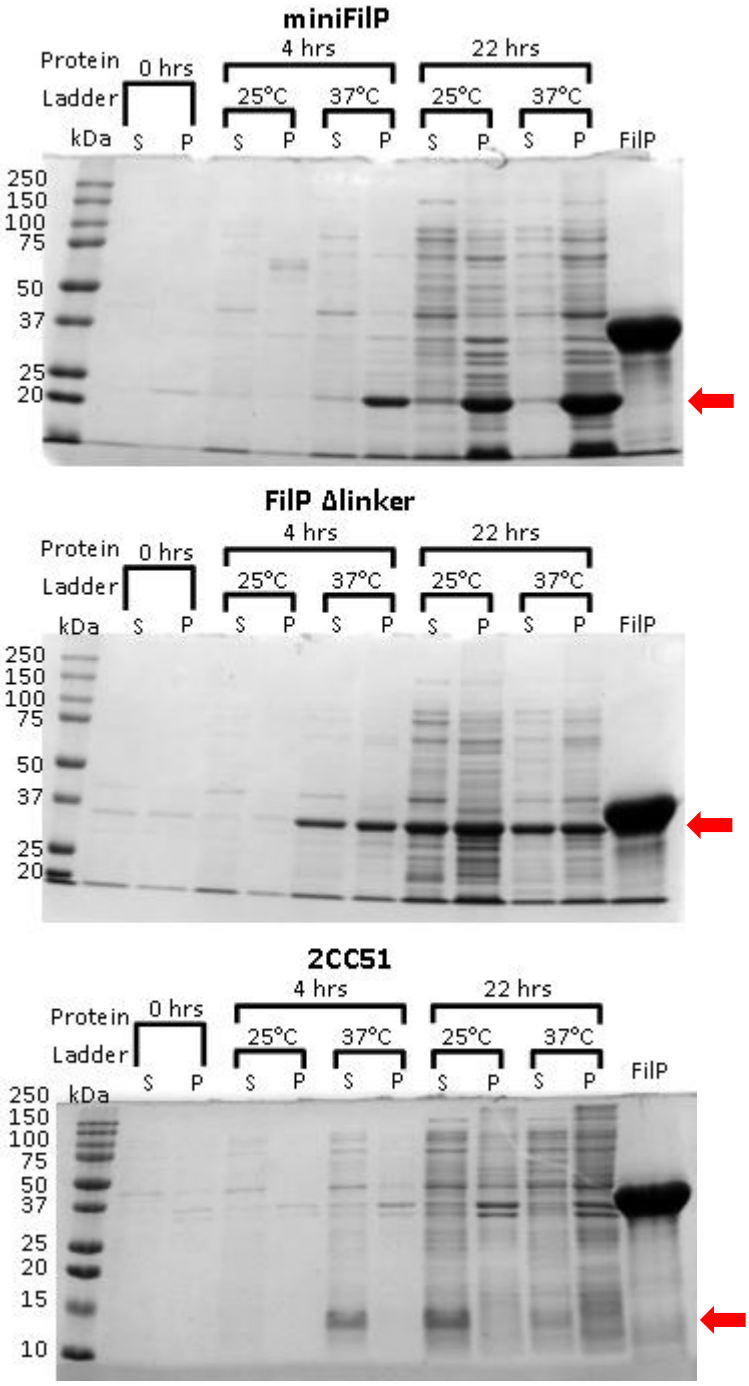

Figure 4.4.2 miniFilP, FilP Δlinker, 2CC51 expression trials

Supernatant and pellet fractions from the miniFilP, FilP Δlinker, 2CC51 expression trials in *E.coli* were analysed using 15% SDS-PAGE and visualised by Coomassie staining. Samples were collected following 4 or 22 hrs growth either at 25°C or 37°C after induction using 1 mM IPTG. Molecular weight marker is shown in lane 1. Red arrow indicates protein overexpression of the FilP variant.

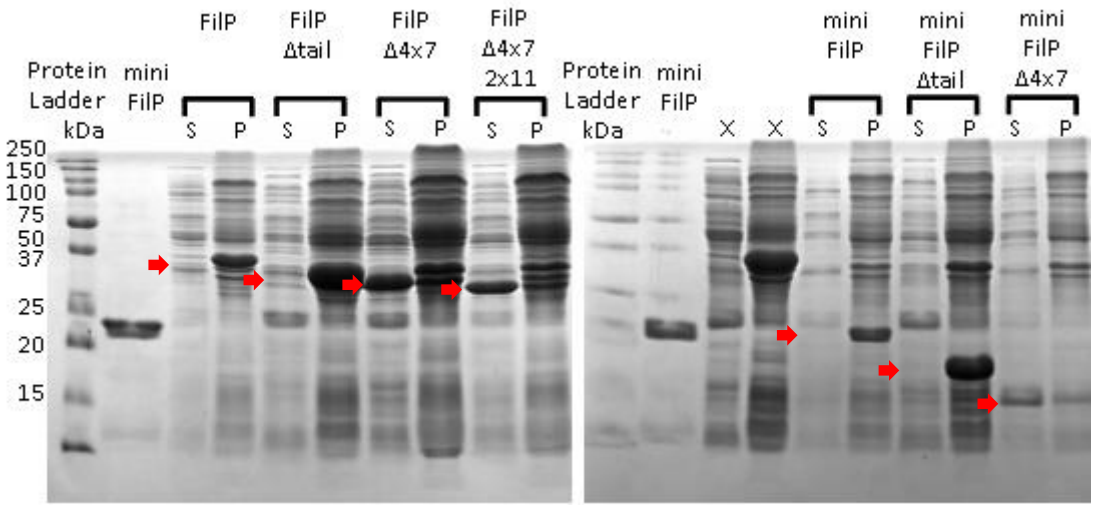

Figure 4.4.3 FilP Δtail, FilP Δ4x7, FilP Δ4x7 2x11, miniFilP Δtail, miniFilP Δ4x7 expression trials

Supernatant and pellet fractions from the FilP Δtail, FilP Δ4x7, FilP Δ4x7 2x11, miniFilP Δtail and miniFilP expression trials in *E.coli* were analysed using 15% SDS-PAGE and visualised by Coomassie staining. Samples were collected following 4 or 22 hrs growth either at 25°C or 37°C after induction using 1 mM IPTG. Molecular weight marker is shown in lane 1. Red arrow indicates protein overexpression of the FilP variant. Lanes marked with an X are not relevant here.

4.5 Large Scale Expression of FilP Variants

After the overexpression trials, large scale overproduction of the relevant FilP variant protein was performed. Routinely 200 ml of transformed BL21 (DE3) pLysS were grown up in the conditions indicated as optimum from the expression trials (Table 4.5.1).

Table 4.5.1 Summary of FilP Variants Expression Conditions

Variant	Ni-NTA mini spin columns or Ni-NTA gravity flow column	Native or Denaturing Conditions	Growth Temperature	Growth Time
FilPC	Gravity flow	Denaturing	37°C	22 hrs
FilPT	Gravity flow	Denaturing	37°C	22 hrs
FilPN	Gravity flow	Denaturing	37°C	4 hrs
FilP Δlinker	Gravity flow	Native	37°C	22 hrs
miniFilP	Gravity flow	Denaturing	37°C	22 hrs
2CC51	Mini spin	Denaturing	37°C	22 hrs
FilP Δtail	Mini spin	Denaturing	37°C	22 hrs
FilP Δ4x7	Mini spin	Native	37°C	22 hrs
FilP Δ4x7 2x11	Mini spin	Denaturing	37°C	22 hrs
miniFilP Δtail	Gravity flow	Denaturing	37°C	22 hrs
miniFilP Δ4x7	Mini spin	Denaturing	37°C	22 hrs

Purification was carried out using Ni affinity chromatography using either Ni-NTA mini spin columns or Ni-NTA gravity flow columns. Nickel affinity chromatography was chosen as the purification technique to be used due to the presence of the his-tags which are on the N-terminus of the proteins. His-tagged proteins are able to bind to the nickel immobilised in the column which allows for the other proteins from the cells to be washed through. Elution of the his-tagged protein of interest, in a native purification, can be achieved by the addition of a

buffer solution containing imidazole which competitively binds to the nickel whereas in a denaturing purification, a decrease in the pH to 4.5 protonates the imidazole nitrogen of the histidine residue, due to the pKa of 6.0, and disrupts the interaction between the histidine and the nickel (Bornhorst and Falke, 2000).

Cultures were collected and resuspended in a low volume of native buffer A which contains 10 mM imidazole. Cells were lysed using a French Press at 1000 kPsi and lysates were centrifuged. For proteins found in the supernatant, the supernatant was passed through a 0.45 µm filter before being loaded onto the column for purification. For proteins which were purified from the pellet fraction, the pellets were resuspended in Urea buffer A which contains 8M urea pH8.0 to solubilise the protein. To aid solubilisation, the suspension was sonicated and centrifugation was used to separate the solubilised proteins. The supernatant was passed through a 0.45 µm filter and loaded onto the column. Purification was either carried out using native or denaturing conditions based on whether the protein was seen to be in the pellet (denaturing conditions) or supernatant fraction (native conditions).

During native purifications, after loading the samples onto the Ni-NTA column several wash steps were introduced using the native buffer A (10 mM imidazole) then native buffer B (20 mM imidazole) to elute any non-specific binding. Native buffer C (300 mM imidazole) is used to elute the His-tagged protein of interest. With the gravity flow columns, a final elution buffer (native buffer D) is used for the final elution and contains 500 mM imidazole. For denaturing purifications, washing is with urea buffer B which is at pH6.3 and elution are performed with urea buffer C which is pH4.5.

Analysis of the fractions collected during the purification process were analysed by SDS-PAGE (Figure 4.5.1, Figure 4.5.2 Figure 4.5.3, Figure 4.5.4, Figure 4.5.5, Figure 4.5.6, Figure 4.5.7, Figure 4.5.8, Figure 4.5.9, Figure 4.5.10, Figure 4.5.11).These show that the proteins were successfully purified and that the protein bands in the elution fractions correspond to the expected size of the His-tagged proteins (Figure 4.2.1).

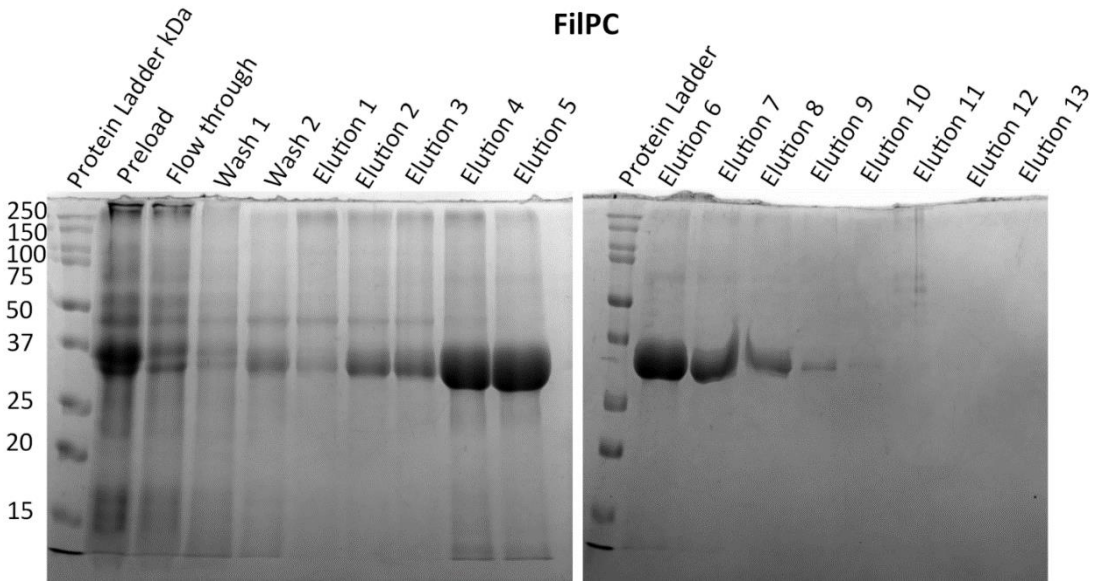

Figure 4.5.1 Purification of FilPC.

Purification of FilPC from BL21 pLysS after 22 hrs induction with 1 mM IPTG at 37°C. Denaturing purification using Ni-NTA gravity flow column. Samples loaded include the preload, flow through, washes and elution fractions. 5 µl standard was loaded into the first lane. Molecular weight markers shown in kDa. All samples were analysed using 15% SDS PAGE and visualised by Coomassie staining.

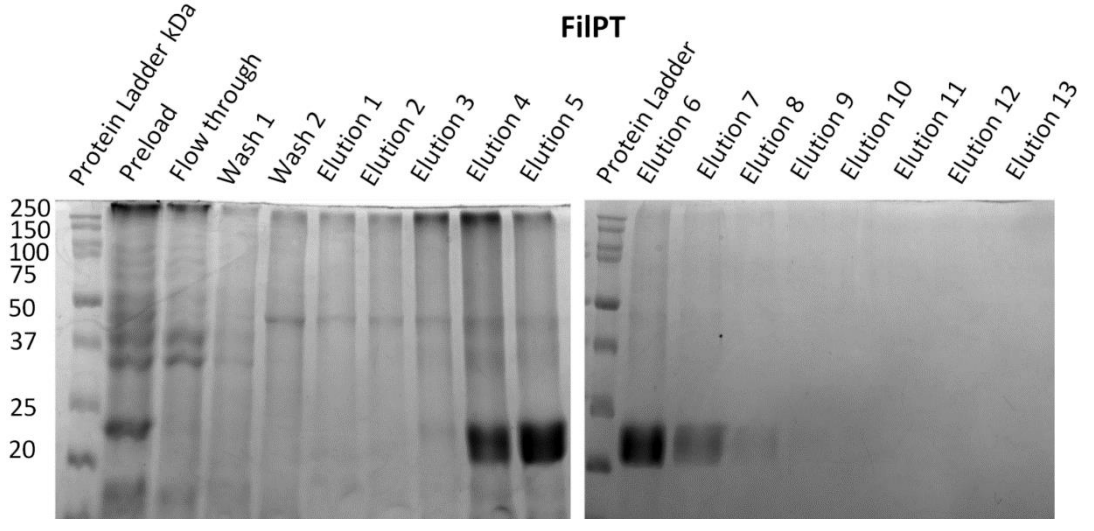

Figure 4.5.2 Purification of FilPT.

Purification of FilPT from BL21 pLysS after 22 hrs induction with 1 mM IPTG at 37°C. Denaturing purification using Ni-NTA gravity flow column. Samples loaded include the preload, flow through, washes and elution fractions. 5 µl standard was loaded into the first lane. Molecular weight markers shown in kDa. All samples were analysed using 15% SDS PAGE and visualised by Coomassie staining.

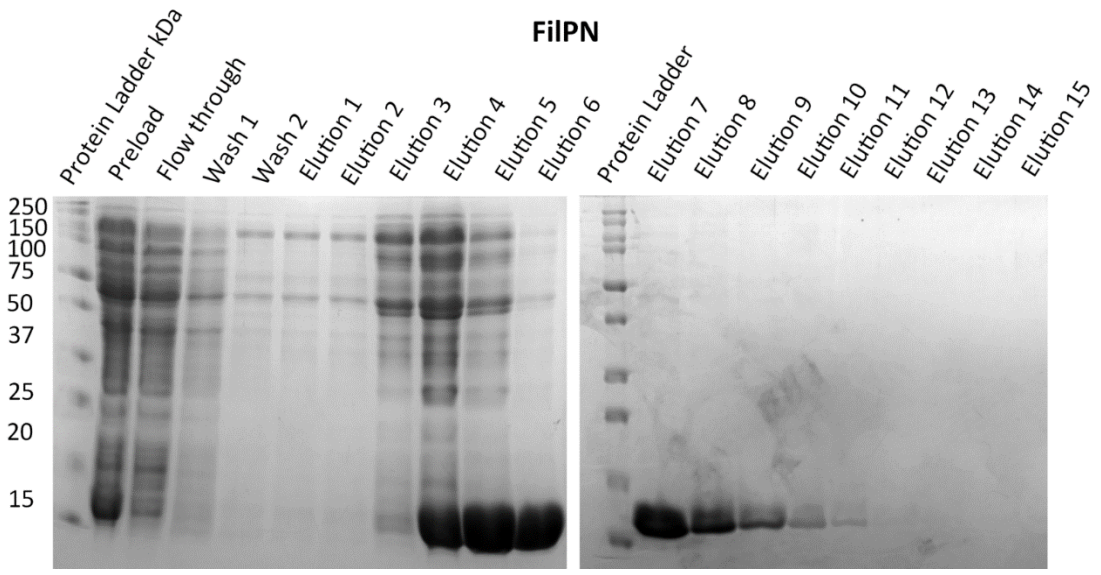

Figure 4.5.3 Purification of FilPN.

Purification of FilPN from BL21 Rosetta pLysS after 4 hrs induction with 1 mM IPTG at 37°C. Denaturing purification using Ni-NTA gravity flow column. Samples loaded include the preload, flow through, washes and elution fractions. 5 µl standard was loaded into the first lane. Molecular weight markers shown in kDa. All samples were analysed using 15% SDS PAGE and visualised by Coomassie staining.

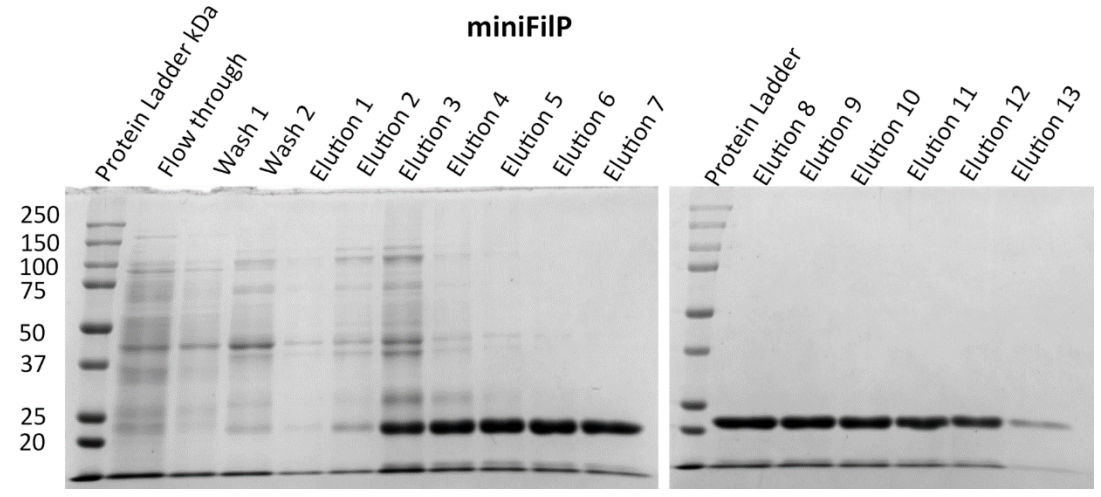

Figure 4.5.4 Purification of miniFilP.

Purification of miniFilP from BL21 pLysS after 22 hrs induction with 1 mM IPTG at 37°C. Denaturing purification using Ni-NTA gravity flow column. Samples loaded include the preload, flow through, washes and elution fractions. 5 µl standard was loaded into the first lane. Molecular weight markers shown in kDa. All samples were analysed using 10% SDS PAGE and visualised by Coomassie staining.

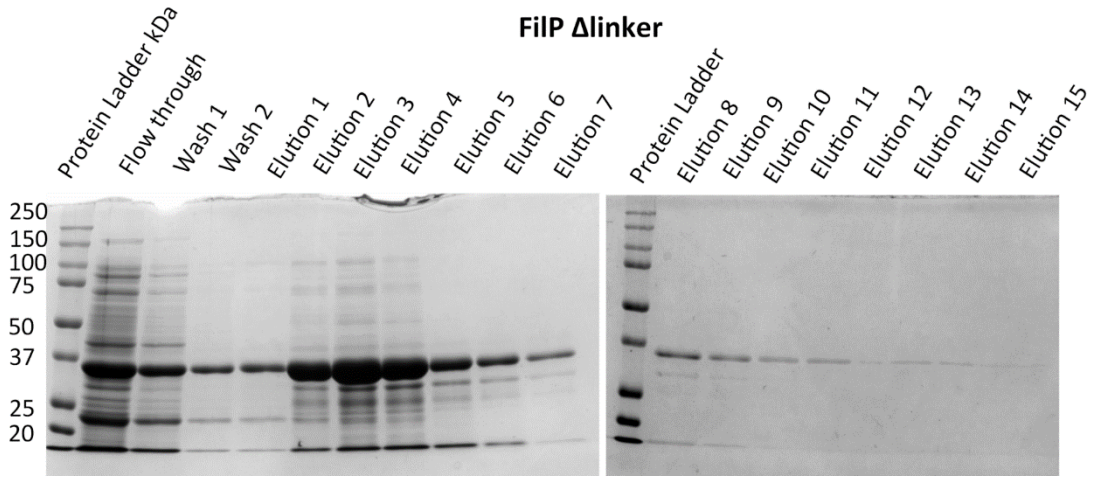

Figure 4.5.5 Purification of FilP Δlinker.

Purification of FilP Δlinker from BL21 pLysS after 22 hrs induction with 1 mM IPTG at 37°C. Native purification using Ni-NTA gravity flow column. Samples loaded include the preload, flow through, washes and elution fractions. 5 µl standard was loaded into the first lane. Molecular weight markers shown in kDa. All samples were analysed using 10% SDS PAGE and visualised by Coomassie staining.

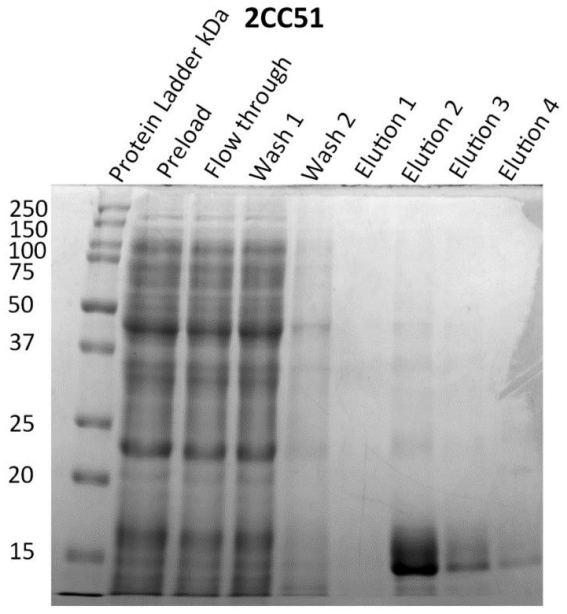

Figure 4.5.6 Purification of 2CC51.

Purification of 2CC51 from BL21 pLysS after 22 hrs induction with 1 mM IPTG at 37°C. Denaturing purification using Ni-NTA mini spin column. Samples loaded include the preload, flow through, washes and elution fractions. 5 µl standard was loaded into the first lane. Molecular weight markers shown in kDa. All samples were analysed using 15% SDS PAGE and visualised by Coomassie staining.

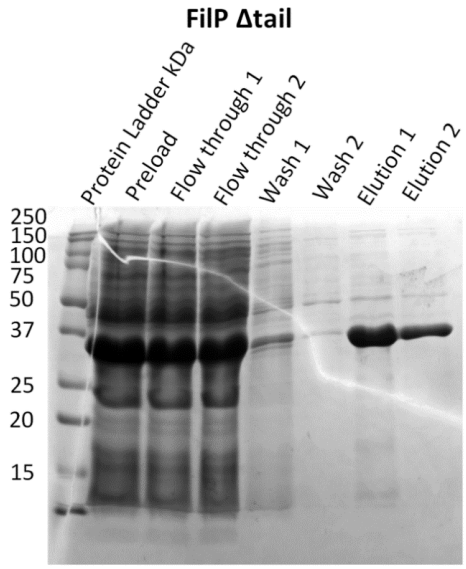

Figure 4.5.7 Purification of FilP Δtail.

Purification of FilP Δtail from BL21 pLysS after 22 hrs induction with 1 mM IPTG at 37°C. Denaturing purification using Ni-NTA mini spin column. Samples loaded include the preload, flow through, washes and elution fractions. 5 µl standard was loaded into the first lane. Molecular weight markers shown in kDa. All samples were analysed using 15% SDS PAGE and visualised by Coomassie staining.

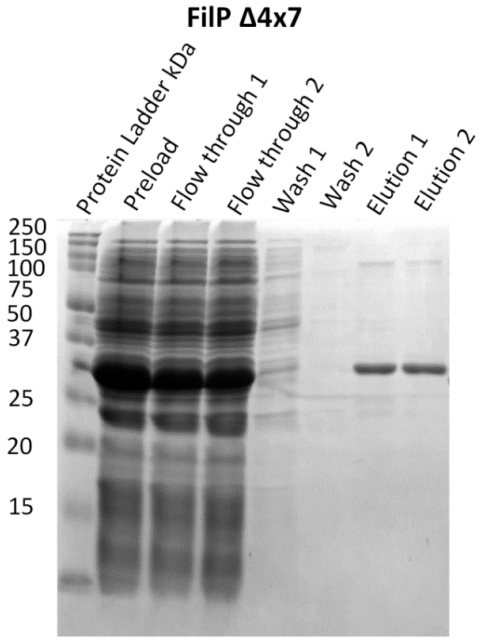

Figure 4.5.8 Purification of FilP Δ4x7.

Purification of FilP Δ4x7 from BL21 pLysS after 22 hrs induction with 1 mM IPTG at 37°C. Native purification using Ni-NTA mini spin column. Samples loaded include the preload, flow through, washes and elution fractions. 5 µl standard was loaded into the first lane. Molecular weight markers shown in kDa. All samples were analysed using 15% SDS PAGE and visualised by Coomassie staining.

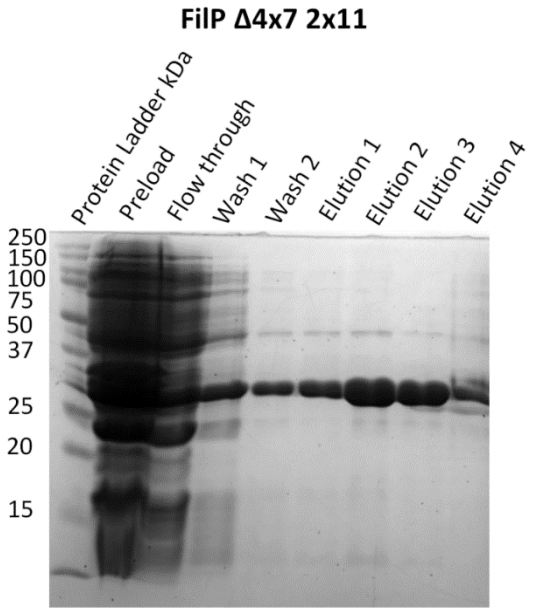

Figure 4.5.9 Purification of FilP Δ4x7 2x11

Purification of FilP Δ4x7 2x11 from BL21 pLysS after 22 hrs induction with 1 mM IPTG at 37°C. Denaturing purification using Ni-NTA mini spin column. Samples loaded include the preload, flow through, washes and elution fractions. 5 µl standard was loaded into the first lane. Molecular weight markers shown in kDa. All samples were analysed using 15% SDS PAGE and visualised by Coomassie staining.

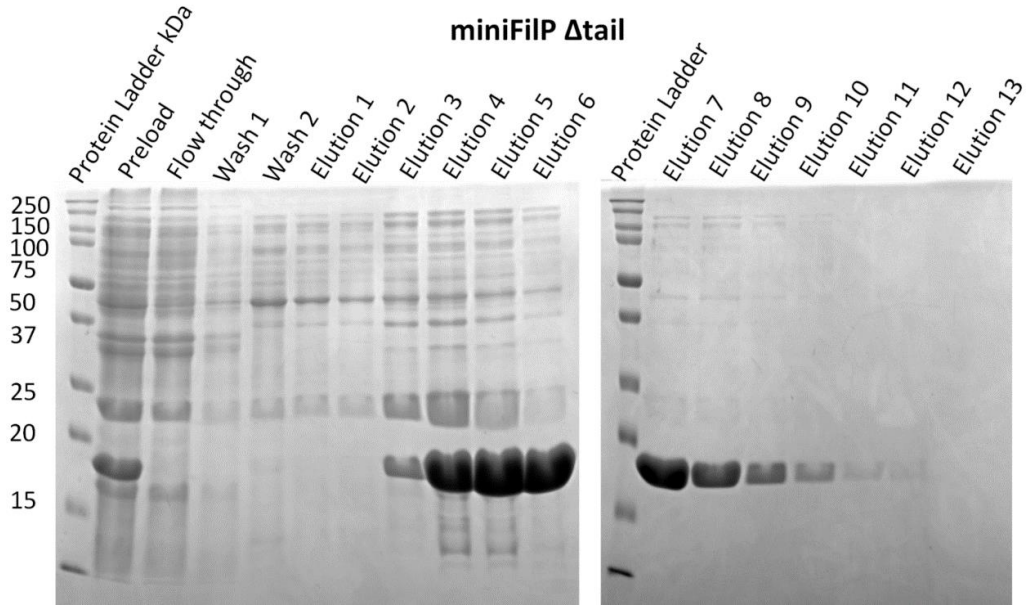

Figure 4.5.10 Purification of miniFilP Δtail.

Purification of miniFilP Δtail from BL21 pLysS after 22 hrs induction with 1 mM IPTG at 37°C. Denaturing purification using Ni-NTA gravity flow column. Samples loaded include the preload, flow through, washes and elution fractions. 5 µl standard was loaded into the first lane. Molecular weight markers shown in kDa. All samples were analysed using 15% SDS PAGE and visualised by Coomassie staining.

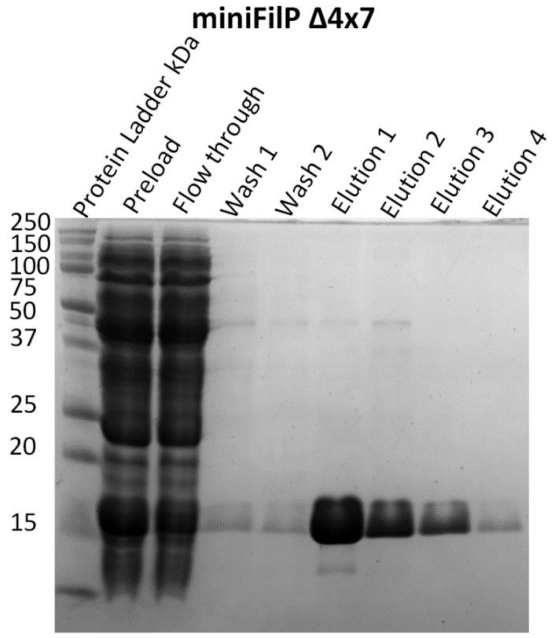

Figure 4.5.11 Purification of miniFilP Δ4x7.

Purification of miniFilP Δ4x7 from BL21 pLysS after 22 hrs induction with 1 mM IPTG at 37°C. Denaturing purification using Ni-NTA gravity flow column. Samples loaded include the preload, flow through, washes and elution fractions. 5 µl standard was loaded into the first lane. Molecular weight markers shown in kDa. All samples were analysed using 15% SDS PAGE and visualised by Coomassie staining.

5 Assessing What is Required for Successful Higher Order Assembly of FilP- TEM Including Nanogold Staining

5.1 Introduction

TEM with Nanogold

Nanogold particles can be used to visualise the locations of histidine tags attached to the N terminus of the proteins. Nanogold particles have multiple nickel-nitrilotriacetic acid functionalities incorporated into the ligands on the surface of gold particles. These nickel-nitrilotriacetic acid functionalities bind to the histidine tags. The gold particles appear black when viewed with TEM due to not allowing any electrons to pass through them, whereas any protein also stained with a negative stain appears white. This, combined with the knowledge of where the histidine-tag is attached to the protein, allows for the localisation of the histidine tag within a structure and, thus, the end of the protein to which it is attached.

Aims

To use TEM to test the higher order assemblies formed by truncated FilP proteins to establish which motifs are required for higher order assembly. Then to use nanogold staining to localise the N terminal histidine tag within these structures to establish how the proteins are organised within these structures.

5.2 TEM

Our purified proteins were dialysed into various buffers (outlined for each variant independently) and spotted onto Carbon Film 400 Mesh Copper Grids and negatively stained using 2% ammonium molybdate pH7.0. Visualisation was achieved by transmission electron microscopy (TEM) using a JEOL 2010 run at 160 kV. Images taken were measured using software ImageJ and data was analysed using Microsoft Excel.

5.3 FilPC, FilPT and FilPN

FilP variants known as FilPC, FilPN and FilPT were designed to lack the head domain and coil 1 subdomain; the coil 2 subdomain and tail domain; and half of the coil 2 subdomain and tail domain respectively (Figure 5.3.1). The rationale behind this was to establish whether abolishing any of these important features would abolish the ability of FilP to form higher order structures.

FilPN and FilPT

FilPN and FilPT purified under denaturing conditions, were dialysed into our standard FilP assembly buffer 50 mM Tris pH7.0. Visualisation by TEM showed protein aggregates but no higher order structure.

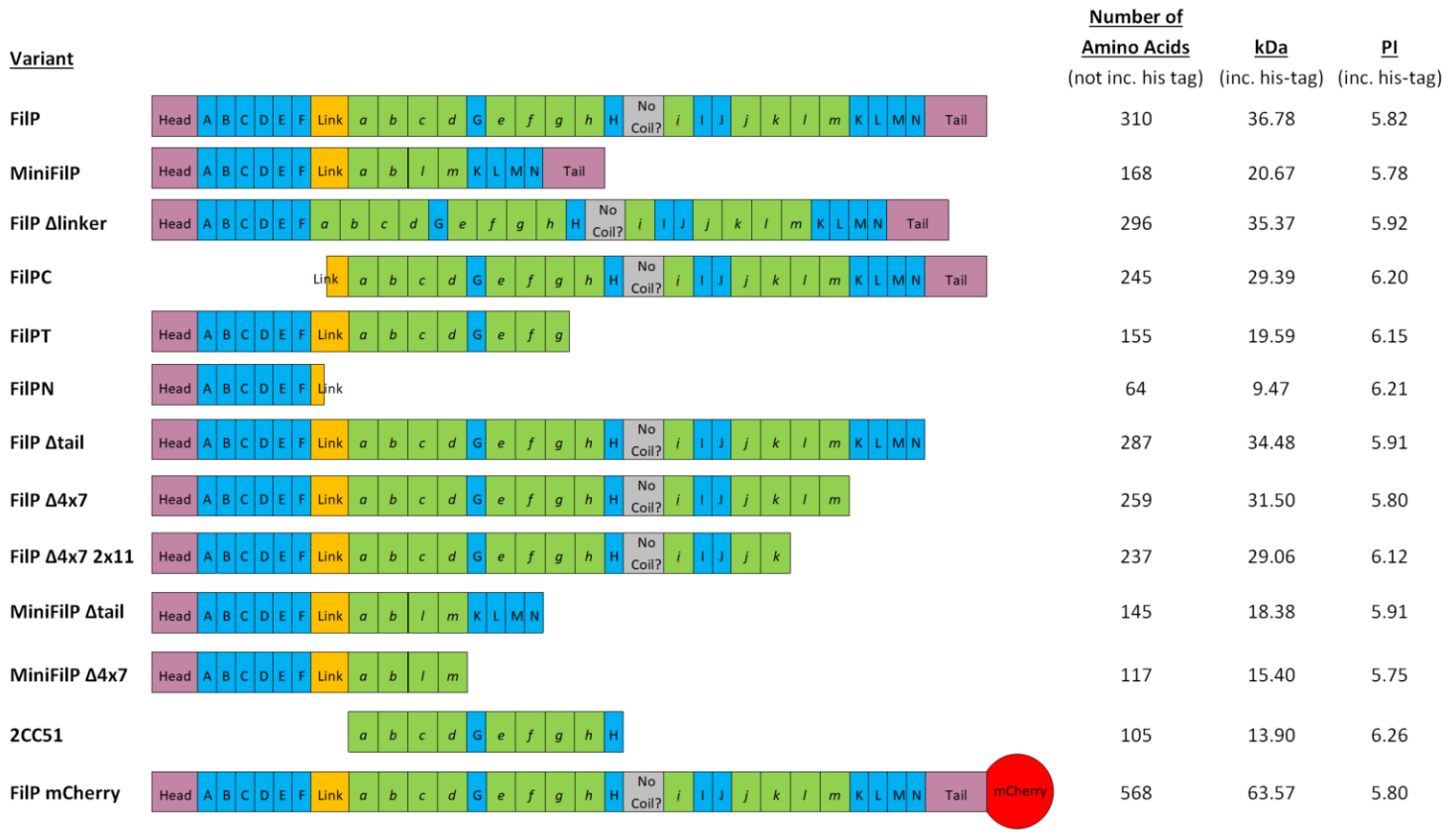

Figure 5.3.1 FilP variants diagram

Diagram showing the FilP variants generated. The non-coiled head and tail domain are shown in purple, the linker region is shown in yellow, heptad repeats are shown in blue and hendecad repeats are shown in green. Sizes are to scale for the number of amino acids. Number of amino acids is shown not including the histidine tag (his-tag is 20 amino acids). Mass in kDa and PI of the FilP variants is shown as calculated with Hi-tag included. kDa and PI computed using the ExPASy - Compute pI/Mw tool (Swiss Institute of Bioinformatics, 2015).

FilPC

FilPC, purified under denaturing conditions, was renatured by dialysis into our standard FilP assembly buffer 50 mM Tris pH6.0, pH6.5, pH7.0, and pH8.5. At pH6.0 and pH6.5 FilPC formed an interconnected lace-like structure which was observed as the predominant structure (Figure 5.3.2). This interconnected lace-like structure is very intricate and includes white 'nodes' where the protein is dense and therefore excluding the negative stain. These nodes appear to be interconnected with white, protein dense, lines. These are unlike any structure which we managed to observe for FilP and is much clearer than any of the structures we previously thought could be a lace like structure (Figure 3.3.3). This lace structure observed for FilPC appears very similar to what was observed in 50 mM Tris pH7.0 (Fuchino et al., 2013) and also with a polymix buffer containing lots of salts (Javadi et al., 2019, Figure 1.10.3). Alongside this interconnected lace-like structure, small sections of striated structure were also observed (Figure 5.3.2). FilPC formed striated structures at pH7.0 and pH8.5 which were very similar to those observed with FilP, as well as large, smooth rope-like structures which had occasional striated patterning within them (Figure 5.3.2).

Measurement of TEM images revealed that the average unit length for FilPC striation at pH7.0, striation at pH6.0, and lace at pH6.0 were 62.5 nm (standard deviation 4.0, n 55), 62.1 nm (standard deviation 5.1, n 90) and 60.8 nm (standard deviation 6.6, n 93) respectively. To test for statistical significance, measurements were compared using a two-tailed T-test with a 95% confidence level. This revealed that these are all statistically the same as each other in addition to being statistically the same as the striation unit length for FilP in 50 mM Tris pH7.0 (Figure 5.3.3). This suggests that removal of the head domain and coil 1 subdomain of FilP had no effect on the unit length of the higher order structures observed. It should also be noted that the pH6.0 buffer is below the PI of FilPC (Figure 5.3.1).

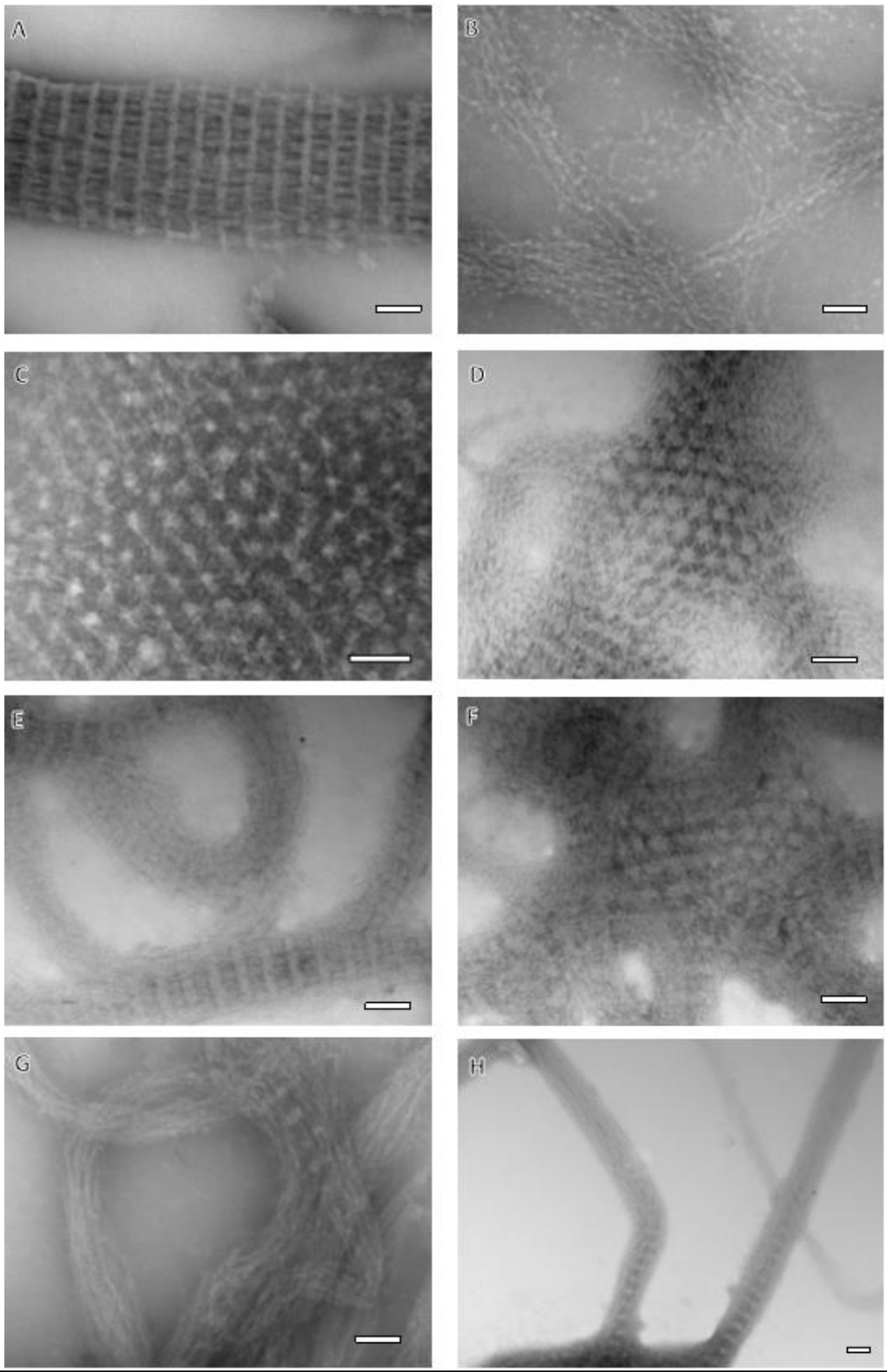

Figure 5.3.2 FilPC TEM images.
Transmission electron microscope images of the higher order assembly structure of FilPC **(B-H)** in comparison with FilP striation **(A)** 50 mM Tris pH7. FilPC purified under denaturing conditions and renatured by dialysis into 20 mM Tris pH6 **(B-D)**, 50 mM Tris pH6.5 **(E), (F)**, 50 mM Tris pH7 **(G)**, 50 mM Tris pH8.5 **(H)**. Scale bars 100 nm.

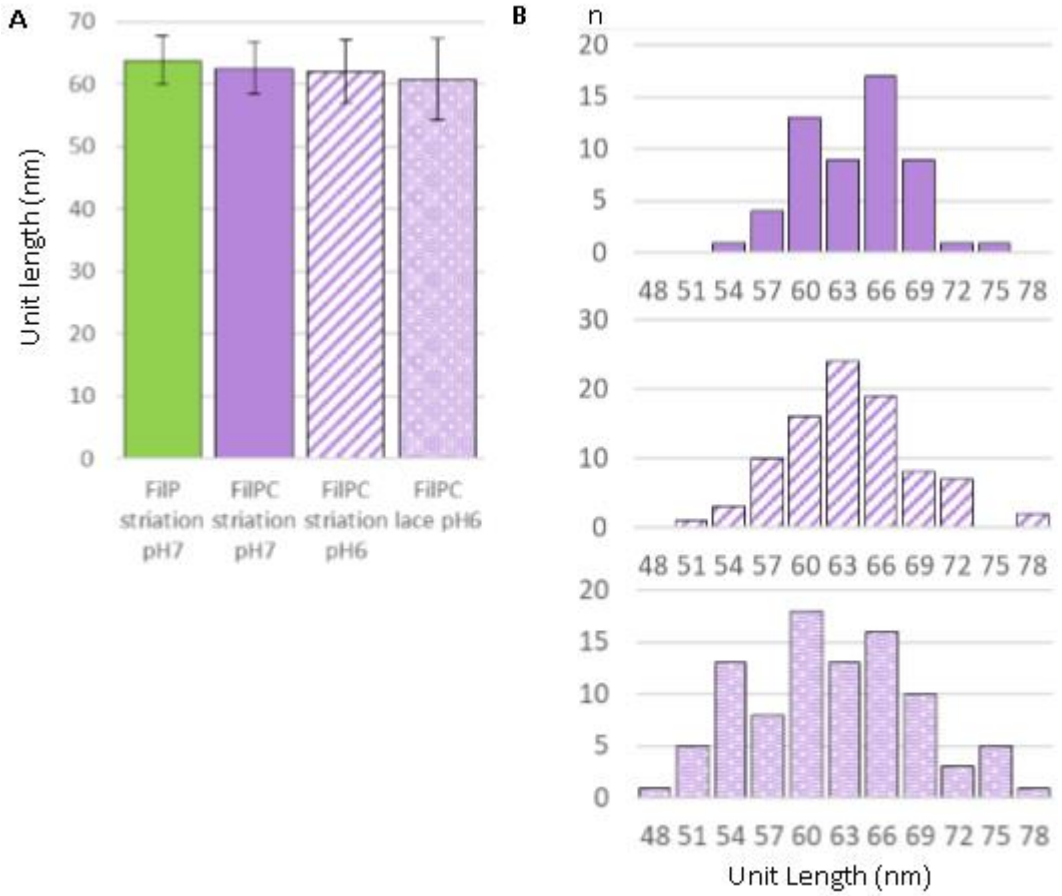

Figure 5.3.3 FilPC Unit Length Analysis.
(A) Average unit length comparison of FilP striation pH7.0, FilPC striation pH7.0, FilPC striation pH6.0, FilPC lace pH6.0. Mean unit lengths: FilP striation pH7 63.8 nm (standard deviation 3.9, n 100); FilPC striation pH7 62.5 nm (standard deviation 4.0, n 55); FilPC striation pH6 62.1 nm (standard deviation 5.1, n 90); FilPC lace pH6 60.8 nm (standard deviation 6.6, n 93). Conditions 50 mM Tris. All unit lengths are statistically identical at the 95% confidence interval. Error bars show standard deviation. **(B)** Histogram of the striation unit lengths of FilPC in 50 mM Tris pH7 (top, solid purple), FilPC striations in 50 mM Tris pH6 (middle, purple stripe), and FilPC lace 50 mM Tris pH7 (bottom, light purple dots).

5.4 TEM and Analysis of FilP Δlinker, miniFilP, and 2CC51

A variant known as miniFilP was designed to lack an internal part of the coil 2 domain (Figure 5.3.1). MiniFilP was designed to maintain all of the features of FilP while just shortening the coil 2 subdomain to assess whether this construct was still able to form higher order assemblies like the full length FilP and if so, whether the unit length of the assembly was altered. FilP Δlinker was designed to just lack the linker subdomain which joins coil 1 and 2 (Figure 5.3.1). This was designed to see if the deletion of the linker would change propensity for FilP to form higher order structures even if the flexibility in the centre of the coils was removed and essentially formed one long coil. The small construct known as 2CC51 is a small part of coil 2 and contains two complete 51 repeats (Figure 5.3.1). This was designed to see if the unusual 51 repeat on its own could form higher order assemblies.

MiniFilP

MiniFilP, purified under denaturing conditions, was renatured by dialysis into our standard FilP assembly buffer 50 mM Tris pH7.0, as well as with added KCl and $MgCl_2$ and a pH8.5 buffer. For all conditions tested, when MiniFilP was visualised by TEM, it appeared striated similarly to that of FilP with white stripes of higher protein density running perpendicular to the direction of the filament (Figure 5.4.1). This suggests that this shortening of the coil 2 domain has not hindered its ability to form higher order assemblies. Occasionally, white lines of high protein density were observed running in the same direction as the filament creating an almost lattice like appearance.

Measurement of TEM images revealed that the average unit length for MiniFilP in pH7.0 was 19.2 nm (Figure 5.4.2). To test for statistical significance, measurements were compared using a two-tailed T-test with a 95% confidence level. This revealed that the unit length (19.2 nm, standard deviation 1.7, n 71) is statistically different to FilP (63.8 nm). This confirmed that the deletion of a large part of the coil 2 domain had indeed maintained the ability of miniFilP to form striated higher order structures although these were different to those of FilP. The shortening of the coil 2 domain has significantly shortened the unit length of these striations by 44.6 nm. Measurement of miniFilP striation unit lengths in varying buffers (with the addition of $MgCl_2$ and/or KCl pH7 or pH8.5) revealed that the unit length of miniFilP does not change in these different conditions (Figure 5.4.2).

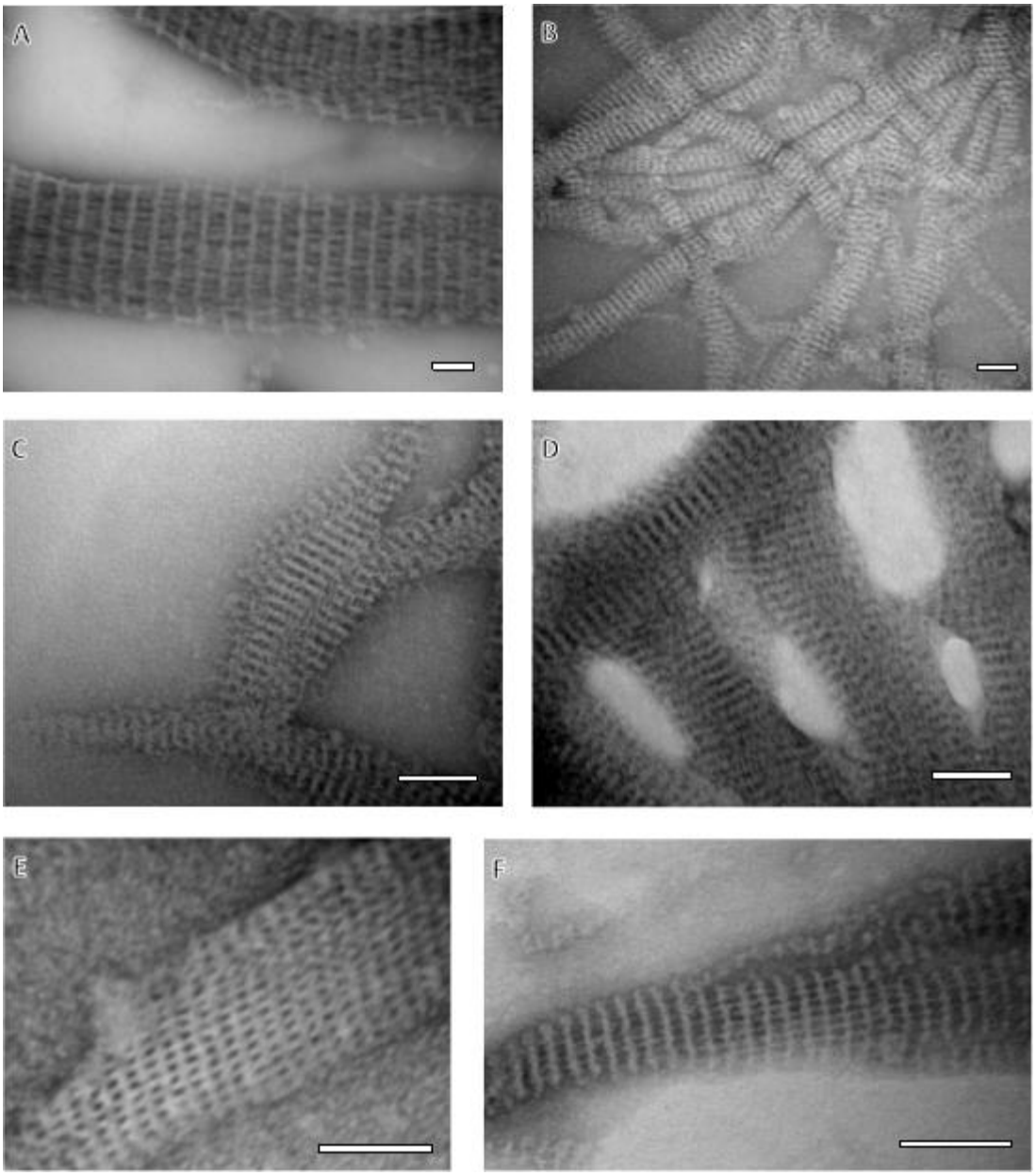

Figure 5.4.1 miniFilP TEM.
Transmission electron microscope images of the higher order assembly structure of MiniFilP **(B-F)** in comparison with FilP striation **(A)** 50 mM Tris pH7. Protein purified under denaturing conditions and renatured by dialysis into 50 mM Tris pH7 **(B, C)**, 50 mM Tris 150 mM KCl 5 mM $MgCl_2$ **(D, E)**, and 50 mM Tris pH8.5 **(F)**. Scale bars 100 nm.

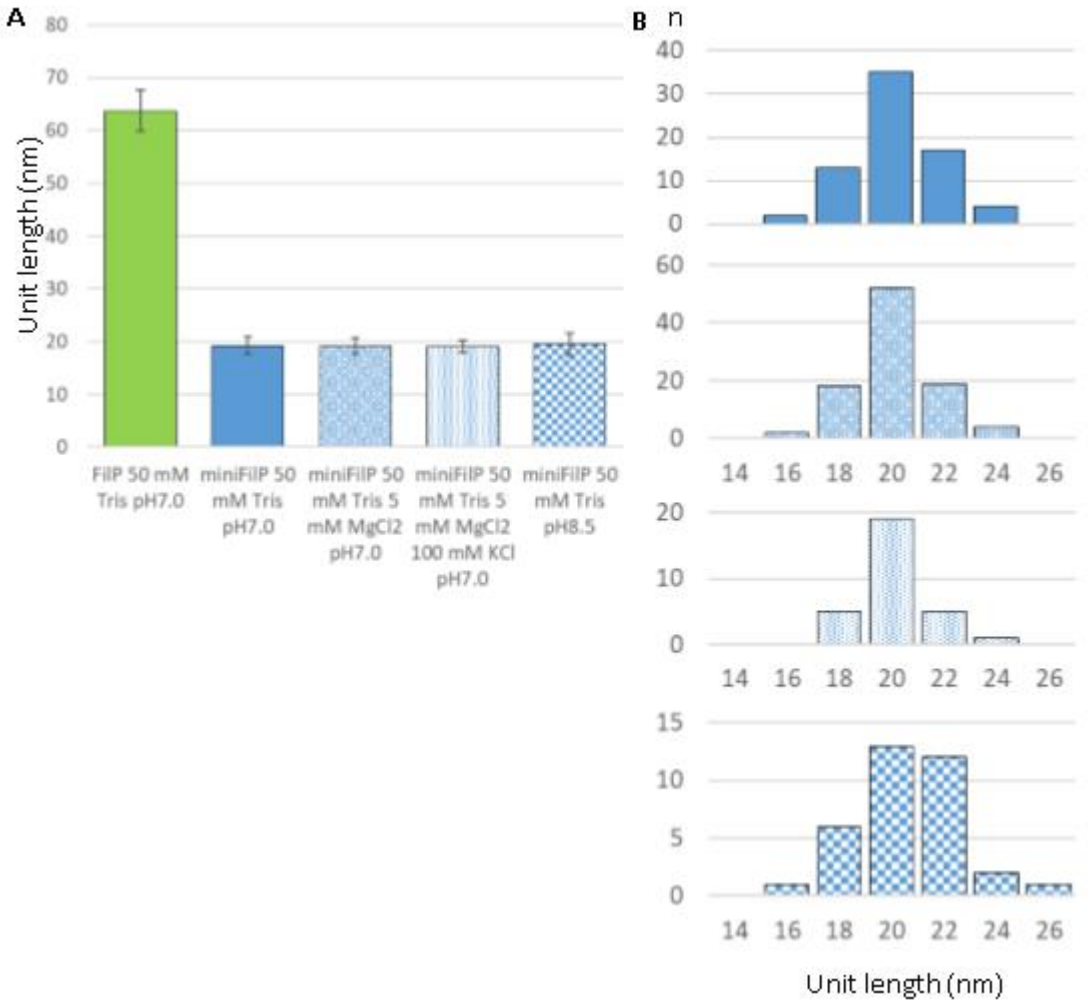

Figure 5.4.2 MiniFilP Unit Length Analysis.
(A) Average unit length comparison of FilP striation 50 mM Tris pH7.0, miniFilP striation 50 mM Tris pH7.0, miniFilP striation 50 mM Tris 5 mM $MgCl_2$ pH7, miniFilP striation 50 mM Tris 5 mM $MgCl_2$ 100 mM KCl pH7, and miniFilP striation 50 mM Tris pH8.5. Means: FilP pH7 63.7 nm (standard deviation 3.9, n 100); miniFilP pH7 19.2 nm (standard deviation 1.7, n 71); miniFilP $MgCl_2$ pH7 19.2 nm (standard deviation 1.5, n 95); miniFilP $MgCl_2$ KCl pH7 19.1 nm (standard deviation 1.2, n 30); miniFilP pH8.5 19.5 nm (standard deviation 2.1, n 35). Error bars standard deviation. **(B)** Histogram of the unit lengths of miniFilP striations in miniFilP pH7 (top, solid blue), miniFilP $MgCl_2$ pH7 (blue diamonds), miniFilP $MgCl_2$ KCl pH7 (blue rectangles), and miniFilP pH8.5 (bottom, blue white checked). There is a significant difference between the FilP striation unit length and all the unit lengths for miniFilP in all conditions. Striation unit lengths of miniFilP in all conditions are statistically the same.

FilP Δlinker

FilP Δlinker, purified under denaturing conditions, was renatured by dialysis into our standard FilP assembly buffer 50 mM Tris pH7.0, as well as with added cations. For all conditions tested, when FilP Δlinker was visualised by TEM, a geometric hexagonal lace-like pattern was observed with white nodes of higher protein density connected by white lines (Figure 5.4.3) which appeared similar to that seen with FilPC (Figure 5.3.2). In 50 mM Tris pH7.0, the predominant lace structure converged into a loose striated pattern in some areas similar to the striated pattern shown by full length FilP. For FilP Δlinker in 50 mM Tris pH7.0 + 5 mM $MgCl_2$ + 100 mM KCl, a larger protein aggregate was observed, this appeared to be structured similarly to the conditions without the salt additions, though it was much denser. The lace structure was not as distinct or as easy to see the associations and had more distinct striations around the edges. Surprisingly, measurement of TEM images revealed that the average unit length for FilP Δlinker striations in pH7.0 was 68.5 nm. To test for statistical significance, measurements were compared using a two-tailed T-test with a 95% confidence level. This revealed that FilP Δlinker unit length is significantly longer than the smaller striation unit length measurement of 63.8 nm for FilP both in 50 mM Tris pH7 (Figure 5.4.4). Comparison between FilP Δlinker unit lengths for the striated structure and the lace structure in 50 mM Tris pH7 revealed that there was a small but significant difference between the unit lengths of the two structures with the striation mean being 68.5 nm and the slightly larger unit length of 71.4 nm for the lace structure (Figure 5.4.4). However, when comparing this to striations and lace unit length measurements in 50 mM Tris 5 mM $MgCl_2$ pH7 the striation unit length mean is 67.3 nm compared to 68.1 nm for the lace structure which are statistically the same. Comparison between the two conditions revealed that striations in both conditions and lace in both conditions were statistically the same (Figure 5.4.4). This reveals that, although there is a small statistical difference between the striation and lace at pH7.0 only, it might not be a true difference.

Even though the protein has shortened in length by the removal of the linker subdomain, the striation unit length measurement increased by around 4.7 nm (7.4%). This could potentially be explained by a reduction in the flexibility of the protein with the removal of the linker subdomain and essentially creating one long coil with only the small head and tail domains flanking it. This reduction in the flexibility of the protein could force the unit length to

be longer. This might also provide some suggestion as to why the lace structures were more dominant here than in the FilP structures. It may be that the forced rigidity of the protein makes the formation of lateral interactions between the proteins less favourable and so, the striated pattern is not seen as frequently as in FilP. When the striated structure is seen in FilP Δlinker, it often flanks areas with a dense lace covering. Thus, the large volume of proteins could allow the striated structure to be seen.

2CC51

The small FliP fragment 2CC51, purified under denaturing conditions, was renatured by dialysis into our standard FilP assembly buffer 50 mM Tris pH7.0. Visualisation by TEM showed protein aggregates but no higher order structure. This suggested that the small 2CC51 fragment, though coil-coiled, cannot form these higher order assemblies on their own.

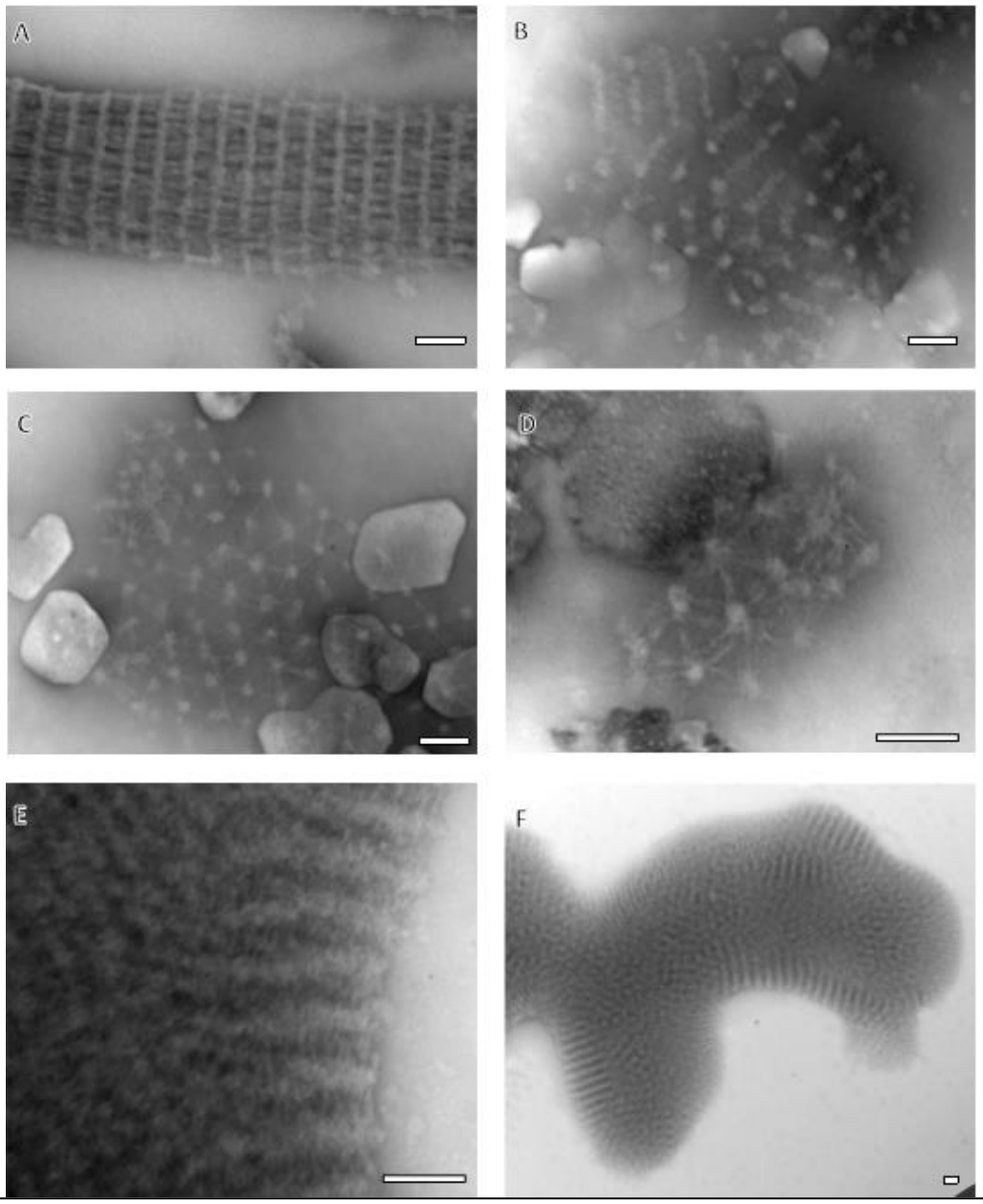

Figure 5.4.3 FilP Δlinker TEM.
Transmission electron microscope images of the higher order assembly structure of FilP Δlinker **(B-F)** in comparison with FilP striation **(A)** 50 mM Tris pH7. FilP Δlinker purified under denaturing conditions and renatured by dialysis into 50 mM Tris pH7 **(B), (C), (D)** and 50 mM Tris 5 mM $MgCl_2$ **(E), (F)**. Scale bars 100 nm. The lighter blobs on **B** and **C** are artefacts which are caused by overexposure to the electron beam during the TEM imaging process.

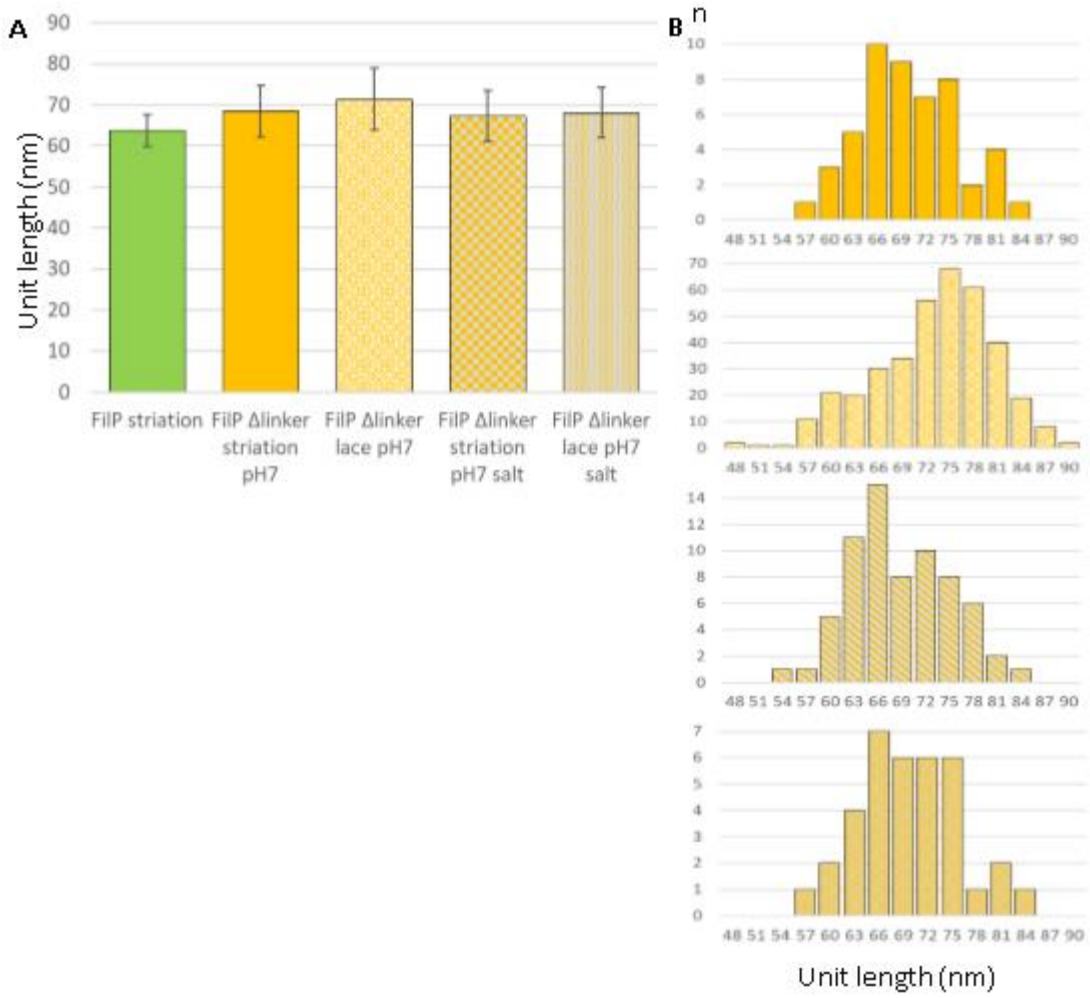

Figure 5.4.4 FilP Δlinker Unit Length Analysis.
(A) Average unit length comparison of FilP striation in 50 mM Tris pH7, FilP Δlinker striation in 50 mM Tris pH7, FilP Δlinker lace in 50 mM Tris pH7, FilP Δlinker striation in 50 mM Tris 5 mM MgCl2 100 mM KCl pH7, and FilP Δlinker lace in 50 mM Tris 5 mM MgCl2 100 mM KCl pH7. Means: FilP 63.8 nm (standard deviation 3.9, n 100); FilP Δlinker pH7 striation 68.5 nm (standard deviation 6.2, n 50); FilP Δlinker pH7 lace 71.4 nm (standard deviation 7.5, n 374); FilP Δlinker pH7 + salt striation 67.3 nm (standard deviation 6.2, n 68); FilP Δlinker pH7 + salt lace 68.1 nm (standard deviation 6.2, n 36). Error bars standard deviation. **(B)** Histogram of the unit lengths of FilP Δlinker pH7 striation (top, solid orange), FilP Δlinker pH7 lace (dotted orange), FilP Δlinker pH7 + salt striation (orange and grey stripes), FilP Δlinker pH7 + salt lace (orange and grey dotted, bottom).

5.5 TEM and Analysis of FilP Δtail, FilP Δ4x7, FilP Δ4x7 2x11, miniFilP Δtail, and miniFilP Δ4x7

Sequential shortenings of FilP from the C terminus were designed to test which part of the C terminal was essential to for forming higher order assemblies. This was based on the results that FilPT was not able to form higher order assemblies, but miniFilP was, even though it lacked a large part of the coil 2 domain suggesting that the C terminus of FilP is important for higher order assemblies, such as the striated assembly. Sequential shortening of FilP was designed (Figure 5.3.1) starting with a variant lacking the tail domain, known as FilP Δtail. FilP Δ4x7 then lacks the tail domain and the last 4 heptad repeats of the coil 2 subdomain. FilP Δ4x7 2x11 lacks the tail domain, the last 4 heptad repeats of the coil 2 subdomain and the last 2 hendecad repeats of the coil 2 domain. This sequential shortening was also applied to the miniFilP construct in the same way with the exception that the 2x11 was not removed also as that would have created a variant without the end section of the coil 2 domain of miniFilP and would therefore have been a shorter version than FilPT which was already known not to form higher order structures (Figure 5.3.1).

FilP Δtail

FilP Δtail is the FilP variant which simply lacks the tail domain of FilP. FilP Δtail, purified under denaturing conditions, was renatured by dialysis into our standard FilP assembly buffer 50 mM Tris pH7.0, and a pH8.5 buffer. For all conditions tested, when FilP Δtail was visualised by TEM, it appeared striated similarly to that of FilP although, some smooth, rope like filaments were also observed at pH7.0 (Figure 5.5.1). Measurement of TEM images revealed that the average unit length for FilP Δtail in pH7.0 was 64.6 nm (Figure 5.5.2). To test for statistical significance, measurements were compared using a two-tailed T-test with a 95% confidence level. This revealed that FilP Δtail is statistically the same as the unit length measurements for FilP and indicates that the removal of the tail domain of FilP does not affect its ability to form striated structures and importantly, does not alter the unit length of the striated pattern.

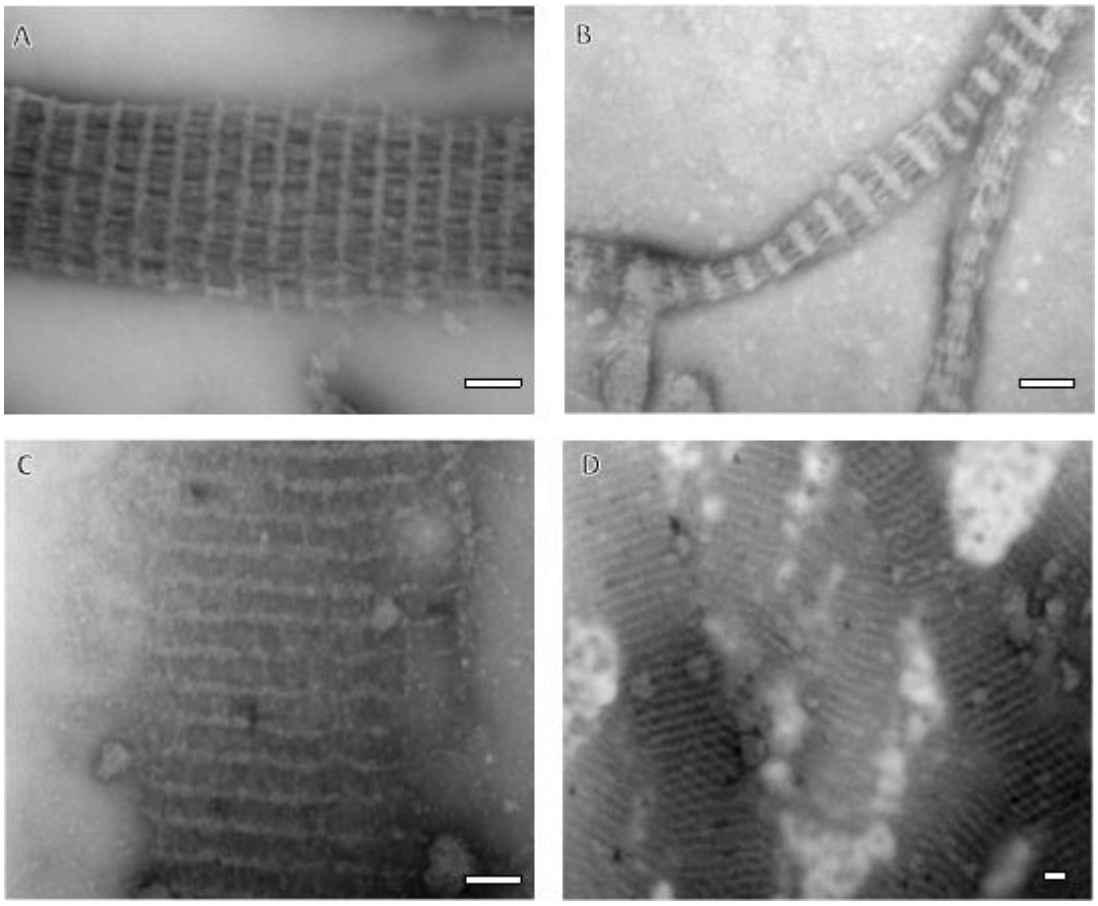

Figure 5.5.1 FilP Δtail TEM.
Transmission electron microscope images of the higher order assembly structure of FilP Δtail **(B-D)** in comparison with FilP striation **(A)** 50 mM Tris pH7. FilP Δtail purified under denaturing conditions and renatured by dialysis into 50 mM Tris pH7 **(B)** and 50 mM Tris pH8.5 **(C), (D).** Scale bars 100 nm.

FilP Δ4x7

FilP Δ4x7 is the FilP variant which lacks the tail domain and the last 4 heptad repeats of the coil 2 subdomain. FilP Δ4x7, purified under denaturing conditions, was renatured by dialysis into our standard FilP assembly buffer 50 mM Tris pH7.0. When FilP Δ4x7 was visualised by TEM, higher order structures were very infrequently observed. When present, the higher order structures appeared striated similarly to that of FilP (Figure 5.5.3). Measurement of TEM images revealed that the average unit length for FilP Δ4x7 in pH7.0 was 34.4 nm (Figure 5.5.2). To test for statistical significance, measurements were compared using a two-tailed T-test with a 95% confidence level. This revealed that FilP Δ4x7 unit length is significantly shorter than that of FilP and indicates that this deletion does affect the unit length of the striations and that they were very infrequently observed indicates that this deletion of the tail and the last four heptad repeats is still able to form higher order structures, but that they differ from those in the full length FilP.

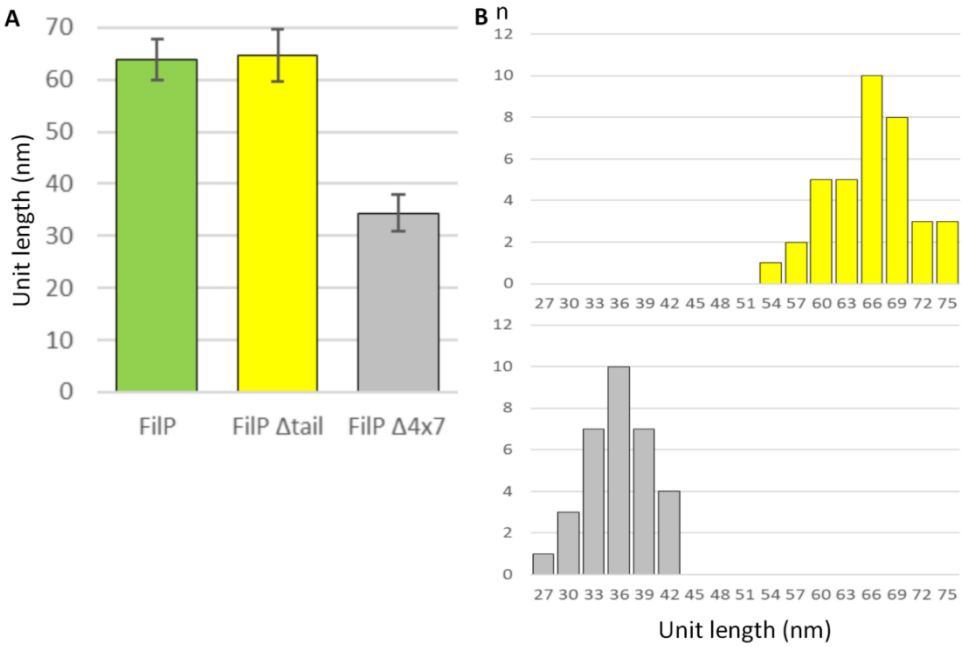

Figure 5.5.2 FilP Δtail and FilP Δ4x7 Unit Length Analysis.
FilP Δtail and FilP Δ4x7 unit length analysis. **(A)** Average unit length comparison of FilP striation, FilP Δtail and FilP Δ4x7 striation in 50 mM Tris pH7. Means: FilP 63.8 nm (standard deviation 3.9, n 100); FilP Δtail 64.6 nm (standard deviation 5.0, n 37); FilP Δ4x7 34.4 nm (standard deviation 3.6, n 32). Error bars represent standard deviation. **(B)** Histogram of the striation unit lengths of FilP Δtail in 50 mM Tris pH7 (top, yellow) and FilP Δ4x7 in 50 mM Tris pH7 (bottom, grey).

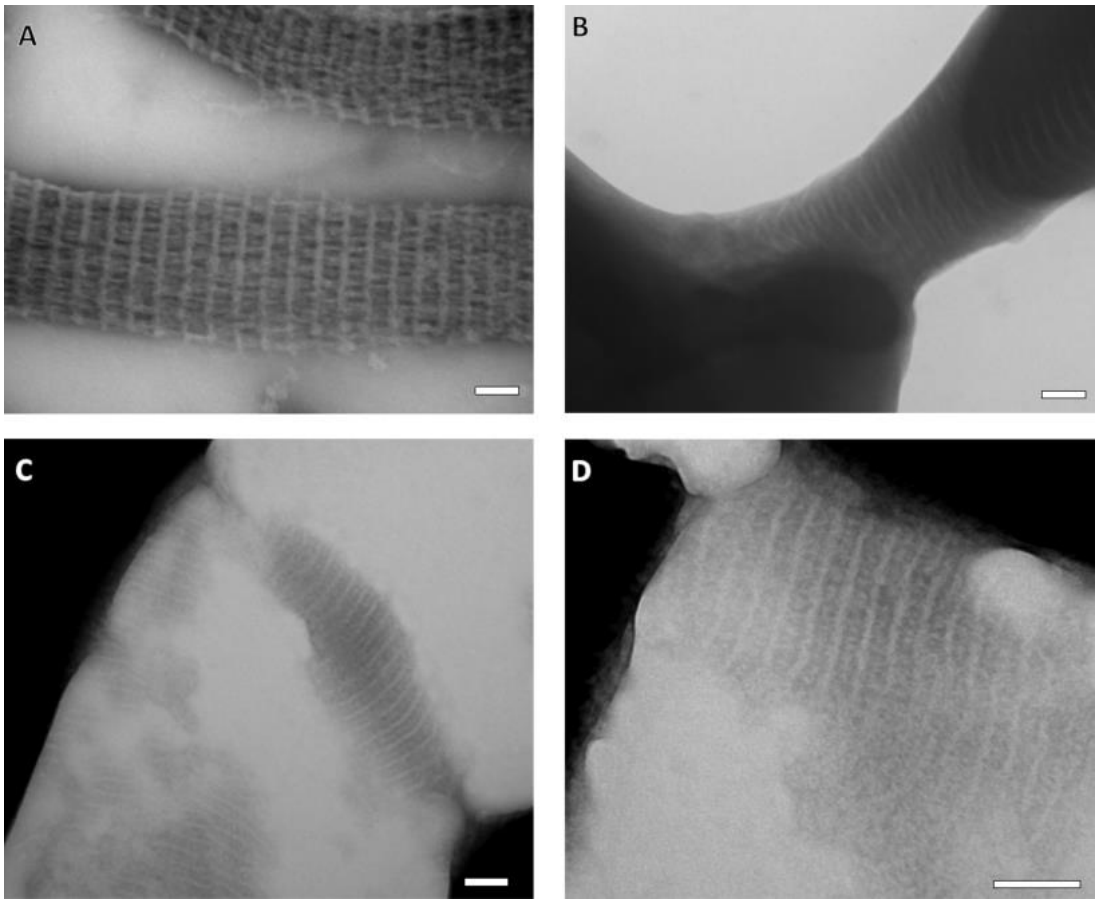

Figure 5.5.3 FilP Δ4x7 TEM.
Transmission electron microscope images of the higher order assembly structure of FilP Δ4x7 **(B-D)** in comparison with FilP striation **(A)** 50 mM Tris pH7. FilP Δ4x7 purified under denaturing conditions and renatured by dialysis into 50 mM Tris pH7 **(B-D)**. Scale bars 100 nm.

FilP Δ4x7 2x11

FilP Δ4x7 2x11 is the FilP variant which lacks the tail domain, the last 4 heptad repeats and the last 2 hendecad repeats of the coil 2 domain. FilP Δ4x7 2x11, purified under denaturing conditions, was renatured by dialysis into our standard FilP assembly buffer 50 mM Tris pH7.0. Visualisation by TEM showed protein aggregates but no higher order structure.

MiniFilP Δtail

MiniFilP Δtail is the FilP variant which has the shortening of the coil 2 subdomain in MiniFilP as well as lacking the tail domain. MiniFilP Δtail, purified under denaturing conditions, was renatured by dialysis into our standard FilP assembly buffer 50 mM Tris pH7.0. While absence of the tail domain did not affect the assemblies of FilP into striated patterns, surprisingly, removal of the tail domain from miniFilP had a major effect of the assemblies generated. Instead of the striated patterns of miniFilP (Figure 5.4.1), amazing spiral structures were observed (Figure 5.5.4). How these structures are achieved by this protein is unknown and would need further investigation.

MiniFilP Δ4x7

MiniFilP Δ4x7 is the FilP variant which has the shortening of the coil 2 subdomain in MiniFilP as well as lacking the tail domain and the last 4 heptad repeats of the coil 2 subdomain. MiniFilP Δ4x7 purified under denaturing conditions was renatured by dialysis into our standard FilP assembly buffer 50 mM Tris pH7.0. Visualisation by TEM showed protein aggregates but no higher order structure. This suggests that removing the large internal section of the coil 2 subdomain and also the tail and last four heptad repeats of the coil 2 subdomain, stops the formation of higher order assemblies.

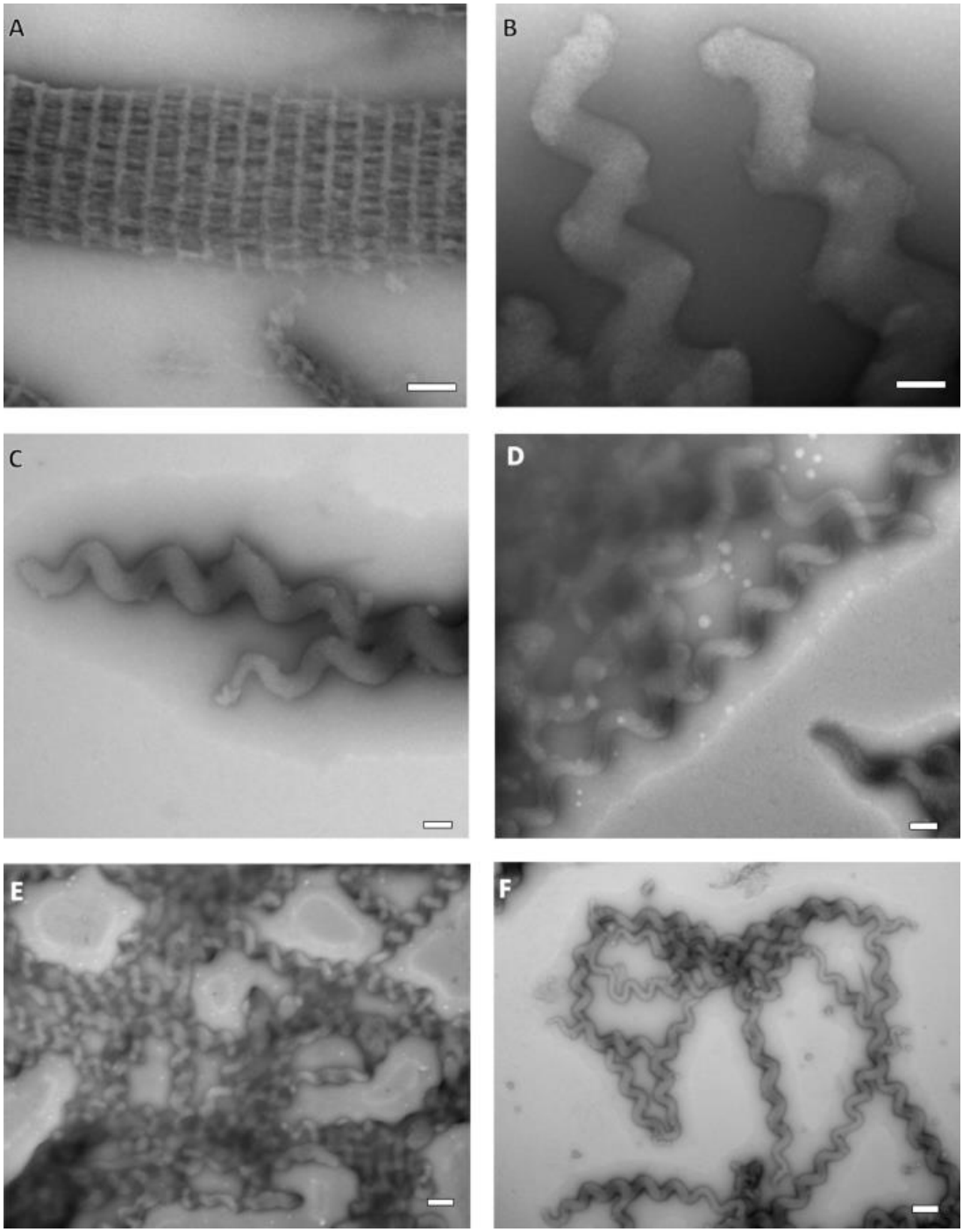

Figure 5.5.4 miniFilP Δtail TEM
Transmission electron microscope images of the higher order assembly structure of MiniFilP Δtail (B-F) in comparison with FilP striation (A) 50 mM Tris pH7. MiniFilP Δtail purified under denaturing conditions and renatured by dialysis into 50 mM Tris pH7 (B-F). Scale bars 100 nm (A-D), 200 nm (E-F).

5.6 TEM and Analysis of FilP mCherry

FilP mCherry was designed to have the mCherry fluorescent tag at the C terminal end of FilP (Figure 5.3.1) in the same way as when expressed for localisation experiments in *S. coelicolor*. We included FilP mCherry in our TEM analysis for several reasons. First, we wanted to establish whether the presence of the large fluorophore had any effect on the ability of FilP to form higher order assemblies. Second, the large C-terminal mCherry tag could give us some indication where the C terminal end of FilP is located within the higher order structures if higher order structures were formed. FilP mCherry was purified under denaturing conditions using a Ni-NTA gravity flow column (Figure 5.6.1) and renatured by dialysis into 50 mM Tris pH7.0. Visualisation by TEM shows that FilP mCherry formed striated structures very similar to that of FilP (Figure 5.6.2). Interestingly, the striation lines show alternating wider and thinner lines, which could be consistent with the mCherry tag generating an extra line in the striated pattern (Figure 5.6.2). It was therefore important to measure the distance between these striations.

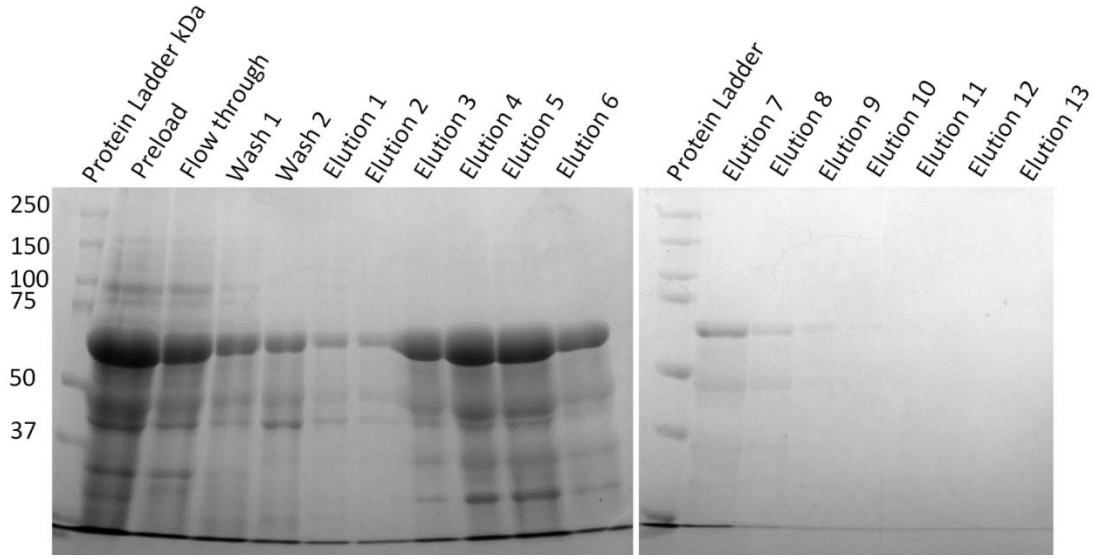

Figure 5.6.1 FilP mCherry purification.

Purification of FilP mCherry purified from BL21 pLysS after 22 hrs induction with 1 mM IPTG at 37°C under denaturing conditions using a Ni-NTA gravity flow column. Samples loaded include the preload, flow through, washes and elution fractions. 5 µl standard was loaded into the first lane. Molecular weight markers shown in kDa. All samples analysed using 10% SDS PAGE and visualised by Coomassie staining.

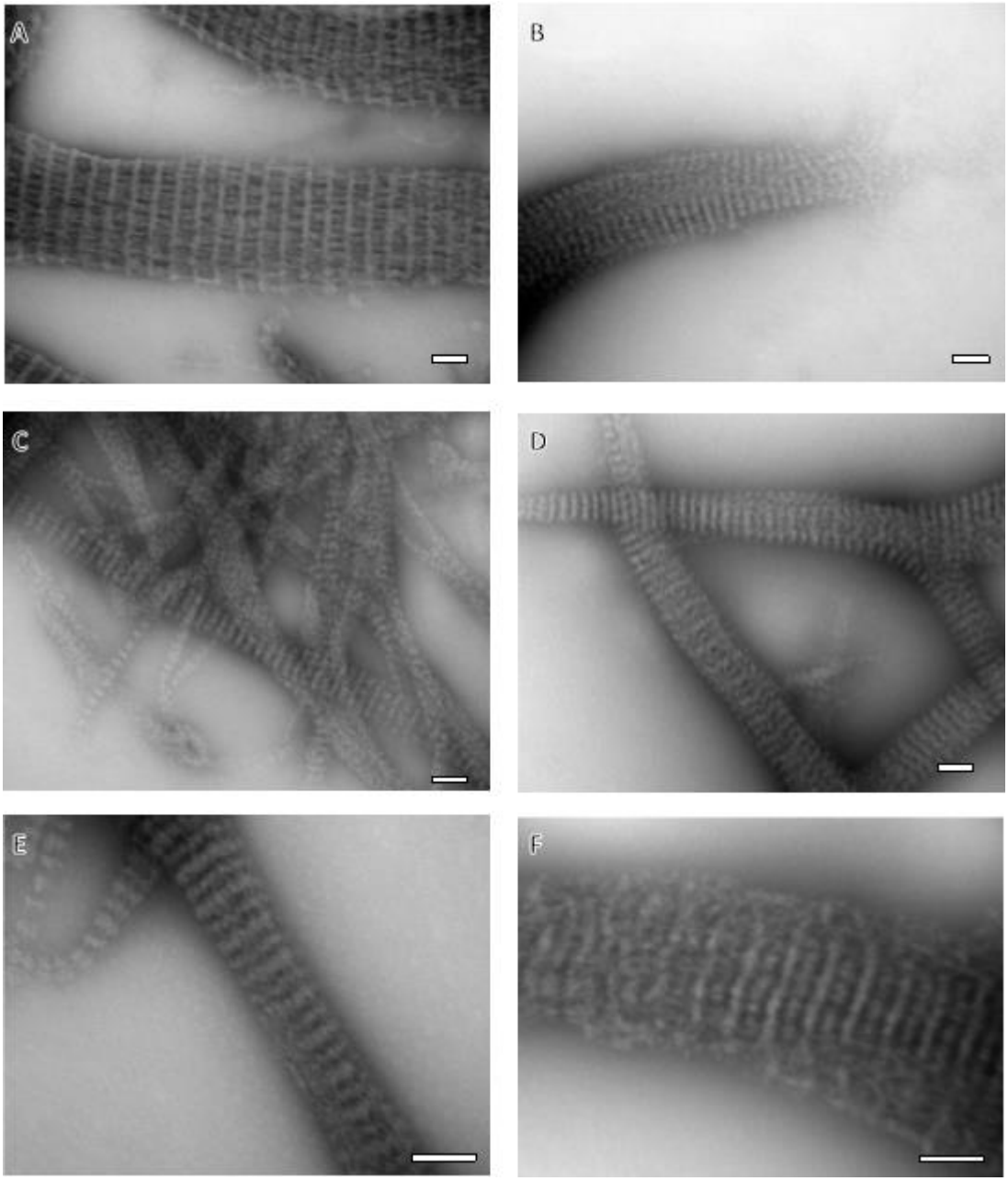

Figure 5.6.2 FilP mCherry TEM.
Transmission electron microscope images of the higher order assembly structure of FilP mCherry **(B-F)** in comparison with FilP striation **(A)** 50 mM Tris pH7. FilP mCherry purified under denaturing conditions and renatured by dialysis into 50 mM Tris pH7 **(B-F)**. Scale bars 100 nm.

The unit length of FilP mCherry striations in 50 mM Tris pH7 was 62.9 nm. To test for statistical significance, measurements were compared using a two-tailed T-test with a 95% confidence level. This revealed that the unit length of FilP mCherry is statistically the same as that of FilP (63.8 nm) (Figure 5.6.3). This unit length is measured between the wider white stripes. This same striation unit length for FilP and FilP mCherry indicates that the addition of the fluorophore has not altered the ability of FilP for higher order assembly, and importantly, nor has it altered the unit length of the striations. However, the observation of minor stripes showed that the addition of the large fluorophore was altering the appearance of the striations. The effect of this was that the striation appeared to have two white stripes per unit length as opposed to the one which is observed for FilP (Figure 5.6.2, Figure 5.6.3). For these stripes in FilP mCherry, there appeared to be an alternating pattern of a wider and not as defined stripe and a narrower but very prominent stripe. This were named the major and minor stripe respectively (Figure 5.6.3). Comparison of these major and minor stripes of FilP mCherry to that of the FilP stripe, revealed that there was a significant difference between that of FilP mCherry minor stripe and that of FilP stripe. However, the FilP stripe and the FilP mCherry major stripe were statistically the same. This implies that the major stripe of FilP mCherry originates from the FilP itself, and the minor stripe originates from the mCherry tag. This also gives us an indication as to the orientation of FilP in the striated structure as the mCherry tag was attached to the C terminus of FilP and appeared on the TEM images to lie in between the stripes of FilP. This indicates that the stripes of FilP are created by the N terminus of FilP.

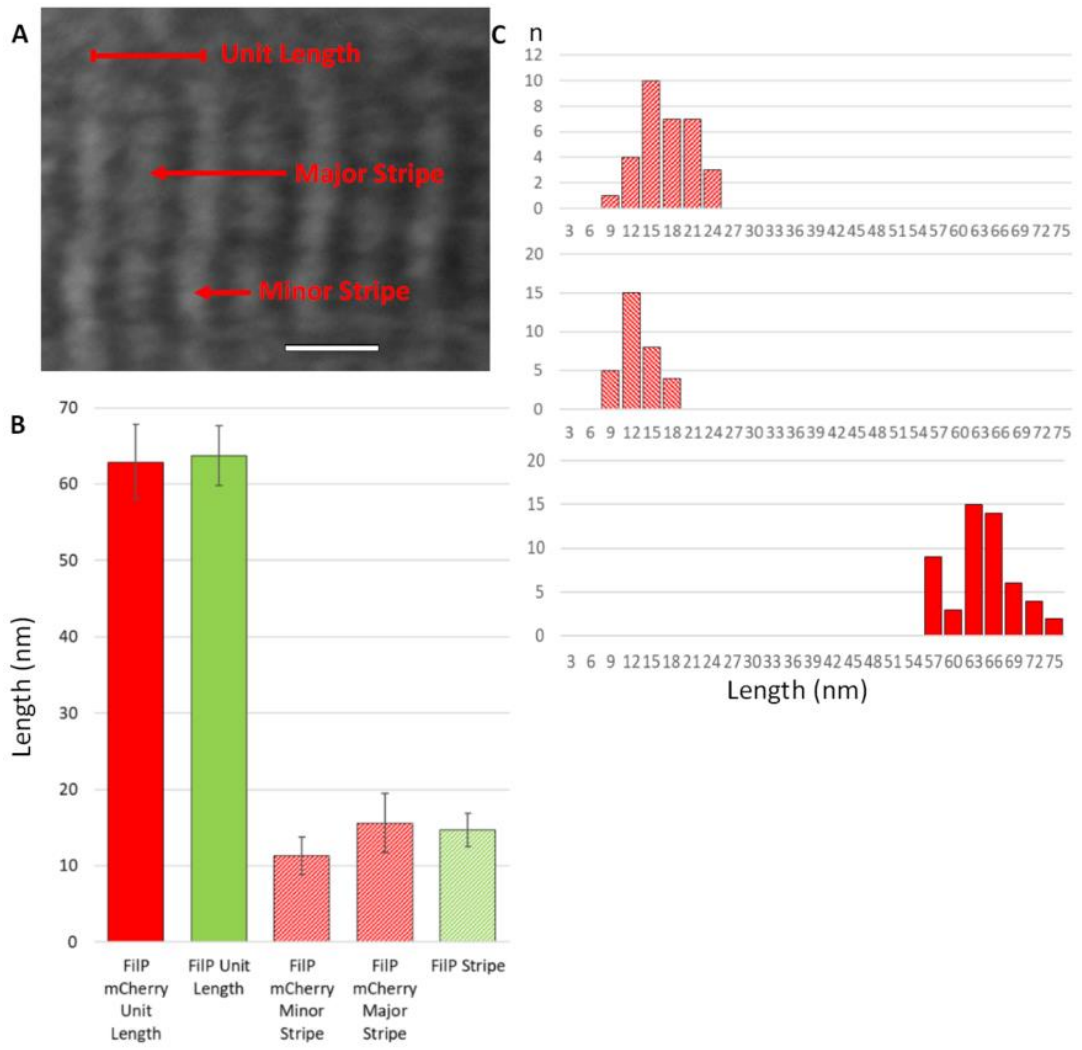

Figure 5.6.3 FilP mCherry Unit Length Analysis.
(A) Diagram showing FilP mCherry striation as observed by TEM negatively stained with 2% Ammonium Molybdate pH7. Unit length, minor stripes and major stripes are indicated. Scale bar 50 nm. **(B)** Average unit lengths for striations in 50 mM Tris pH7 of FilP mCherry and FilP and lengths of FilP mCherry major and minor stripes and length of FilP stripe. Means: FilP mCherry unit length 62.9 nm (standard deviation 4.9, n 53); FilP unit length 63.8 nm (standard deviation 3.9, n 100), FilP mCherry minor stripe 11.3 nm (standard deviation 2.5, n 32); FilP mCherry major stripe 15.6 nm (standard deviation 3.9, n 32); FilP stripe 14.7 nm (standard deviation 2.2, n 100). Error bars standard deviation. Error bars represent standard deviation. **(C)** Histogram of the striation length of FilP mCherry major stripe, minor stripe, and unit length (top to bottom) in 50 mM Tris pH7.

5.7 Conclusions from FilP Variant Measurements

Analysis of the measurements of the striation unit lengths of the FilP variants revealed that the FilPC, FilP Δtail and FilP mCherry variants have the same unit length as FilP in 50 mM Tris pH7.0 (Figure 5.7.1). This indicates that the deletions of the head domain and coil 1 subdomain, and the tail domain does not abolish FilP striations forming (Figure 5.3.2, Figure 5.5.1, Figure 5.6.2) with the same unit length as the full length FilP and hints that these regions are not involved in the formation of these striations. The C terminus of FilP was shown to be important in the formation of higher order assembly structures by the absence of them with the FilPN and FilPT variants which lack the coil 2 subdomain and tail domain, and the second

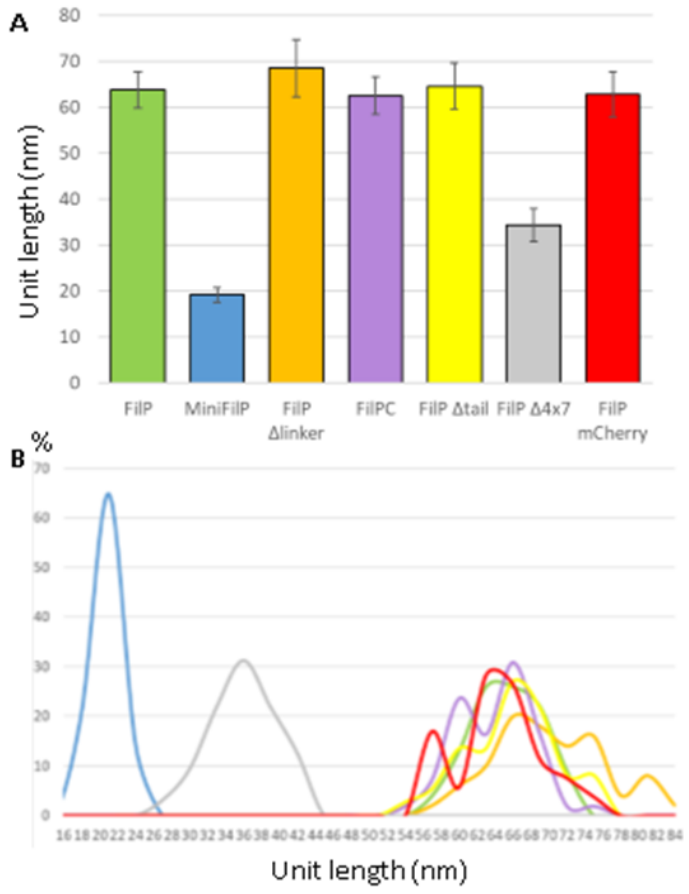

Figure 5.7.1 FilP Variant Average Unit Lengths.

(A) Average striation unit length in 50 mM Tris pH7 of FilP, miniFilP, FilP Δlinker, FilPC, FilP Δtail, FilP Δ4x7, and FilP mCherry. Error bars standard deviation. **(B)** Line representation of histogram of each FilP variant with percentage in each bin for each variant. FilP (green), miniFilP (blue), FilP Δlinker (orange), FilPC (purple), FilP Δtail (yellow), FilP Δ4x7 (grey), and FilP mCherry (red).

half of the coil 2 subdomain and tail domain respectively (Figure 5.3.1). FilP Δtail appears the same as FilP, however, FilPΔ4x7 shows a marked difference from that of FilP. FilP Δ4x7 is still able to form large higher order assemblies but they mostly appeared unstriated, and the occasional striation observed had a much smaller unit length than that of FilP (Figure 5.5.3, Figure 5.5.2). This indicates that the last four heptad repeats of the coil 2 subdomain are important for the formation of the striated structure observed in FilP in some way, but the deletion of this does not abolish the higher order structure completely. Deletion of the further two hendecads from the end of this however (FilP Δ4x7 2x11) did completely abolish the ability to form higher order structures and none were observed. This indicates that an interaction which is crucial for the formation of the higher order structures of FilP occurs within this motif (Figure 5.7.2).

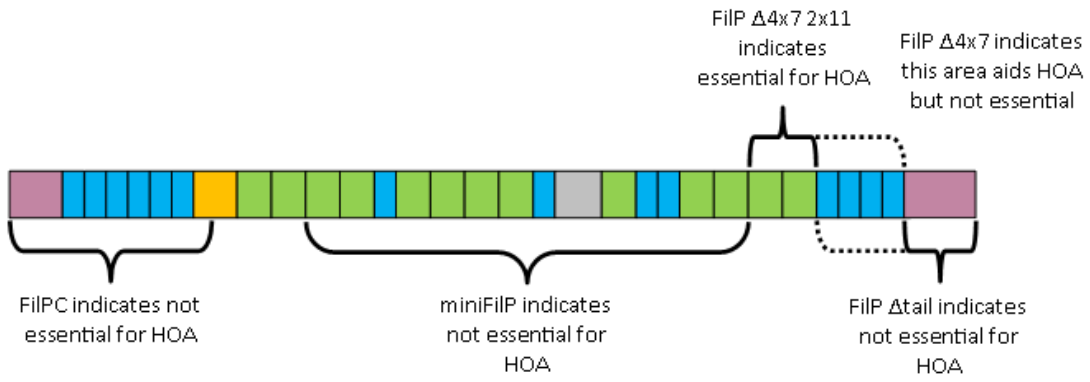

Figure 5.7.2 Essential parts of FilP for higher order assembly

Diagram of FilP indicating which parts of FilP are essential for the higher order assembly of FilP based on the analysis of the FilP variants generated. FilP shown with the N terminus shown on the left. Head and tail domains shown in purple, linker region shown in yellow, heptad repeat shown in blue, hendecad repeat shown in green, uncoiled region shown in grey. Regions which are essential for higher order assembly (HOA) indicated.

The miniFilP construct revealed that the design of this variant was successful, and it did maintain its ability to form higher order structures and striations with the unit length of these being much smaller than that of FilP (Figure 5.4.1, Figure 5.4.2). Therefore, the length of the coil 2 subdomain does affect the unit length of the striated structure but does not affect its ability to form higher order structures.

The C terminally truncated miniFilPs did not, however, have the same effect as these truncations did on FilP. MiniFilP Δtail, instead of appearing identical to miniFilP (as FilP Δtail appeared to FilP), it appeared very different and generated a new structure which has not been seen with any other construct (Figure 5.5.4). This spiralling structure indicates that the loss of the tail domain and internal coil 2 fragment combined allows the protein to form this very different structure. This is unclear why this would be the case. Furthermore, when the next four heptads were removed (miniFilP Δ4x7), no structures were observed. This indicates that when it is lacking a large part of the coil 2 subdomain, the last four heptad repeats are essential for the formation of higher order assembly.

The unit length of the lace structure observed with FilPC was measured to be statistically the same as that of the FilPC striated structure and also that of FilP (Figure 5.3.3). Lace structure was more readily observed with FilPC in pH6.0 as opposed to pH7.0, although it was present in both (Figure 5.3.2). The unit lengths of both lace and striations in pH6.0 and pH7.0 were all statistically identical to the unit length of FilP. This indicates that the loss of the head and coil 1 subdomain increases the propensity of the protein to form lace but does not stop it from forming striations either. It also indicates that the head and coil 1 are not essential in the formation of the lace structure (Figure 5.7.2).

The FilP mCherry construct also raised some very interesting observations. FilP mCherry appeared with an extra stripe per unit length (Figure 5.6.2). This indicates that the C terminal (where the mCherry tag is present) is in between the stripes of FilP and that, potentially, the stripes are comprised of the N terminal head domain of FilP (or N terminal region of coil 2).

The data obtained from the FilP variants generated indicates regions of FilP which are important for its ability to form higher order structures (Figure 5.7.2). The ability of FilPC to form striated structures, and more often lace structures, indicates that the head domain and coil 1 subdomain of FilP is not essential for the higher order assembly of FilP (Figure 5.3.2, Figure 5.3.3). The miniFilP variants ability to generate higher order assemblies despite the lack of a large section of the coil 2 subdomain of FilP indicates that that central part of the rod domain was also not essential for the higher order assembly of FilP (Figure 5.4.1, Figure 5.4.2). FilP Δtail was also able to form higher order assemblies which indicates that the tail domain is not essential for the higher order assembly of FilP (Figure 5.5.1, Figure 5.5.2).

The last two hendecad repeats in the coil 2 subdomain of FilP were indicated to be essential to the higher order assembly of FilP with the FilP Δ4x7 2x11 variant being unable to form higher order structures. The final four heptad repeats of FilP were shown to not be essential for the higher order assembly of FilP as some striations were observed (Figure 5.5.3, Figure 5.5.2). However, these were very infrequent, and of an unusual smaller size. This indicates that this region, may not be essential for the formation of higher order assemblies. However, is important as it increases the propensity for higher order assembly. This indicates that this region aids the higher order assembly of FilP (Figure 5.7.2).

5.8 Nanogold Staining for C Terminal Histidine Tag Visualisation

Nanogold particles were used to visualise the locations of the histidine tags, attached to the N terminus of the proteins, within the higher order structures. Nanogold particles have multiple nickel-nitrilotriacetic acid functionalities incorporated into the ligands on the surface of gold particles. These nickel-nitrilotriacetic acid functionalities bind to the histidine tags and the gold beads appear visible when viewed with TEM. Negative staining was also required alongside the nanogold staining for visualisation of the protein. The negative staining employed here was methylamine vanadate pH8.0. Methylamine vanadate pH8.0 was used rather than our usual stain of ammonium molybdate pH7.0 as per the recommendations of the manufacturer of the nanogold stain for optimum visualisation of both the nanogold and the protein.

FilP striations in 50 mM Tris pH7.0 with 30 µM protein showed that dots were visible in a pattern which flanked the protein dense white stripe on either side, as well as a smattering of nanogold beads throughout the images (Figure 5.8.1). All nanogold staining generated a smattering of nanogold particles which appeared all over the images. These could be due to the particles not binding and just being present on the sample. Alternatively, it could also be due to free FilP protein which is not in the larger higher-order structures and is not visible as it is with the negative staining. The implications from the nanogold particles flanking the protein dense white stripe is that the N-terminal histidine tags lie very close either side of this white stripe. This could imply that the N-terminal head of FilP and/or the coil 1 subdomain of FilP is implicated in generating the protein dense white stripe with the N-terminal histidine tag protruding either side.

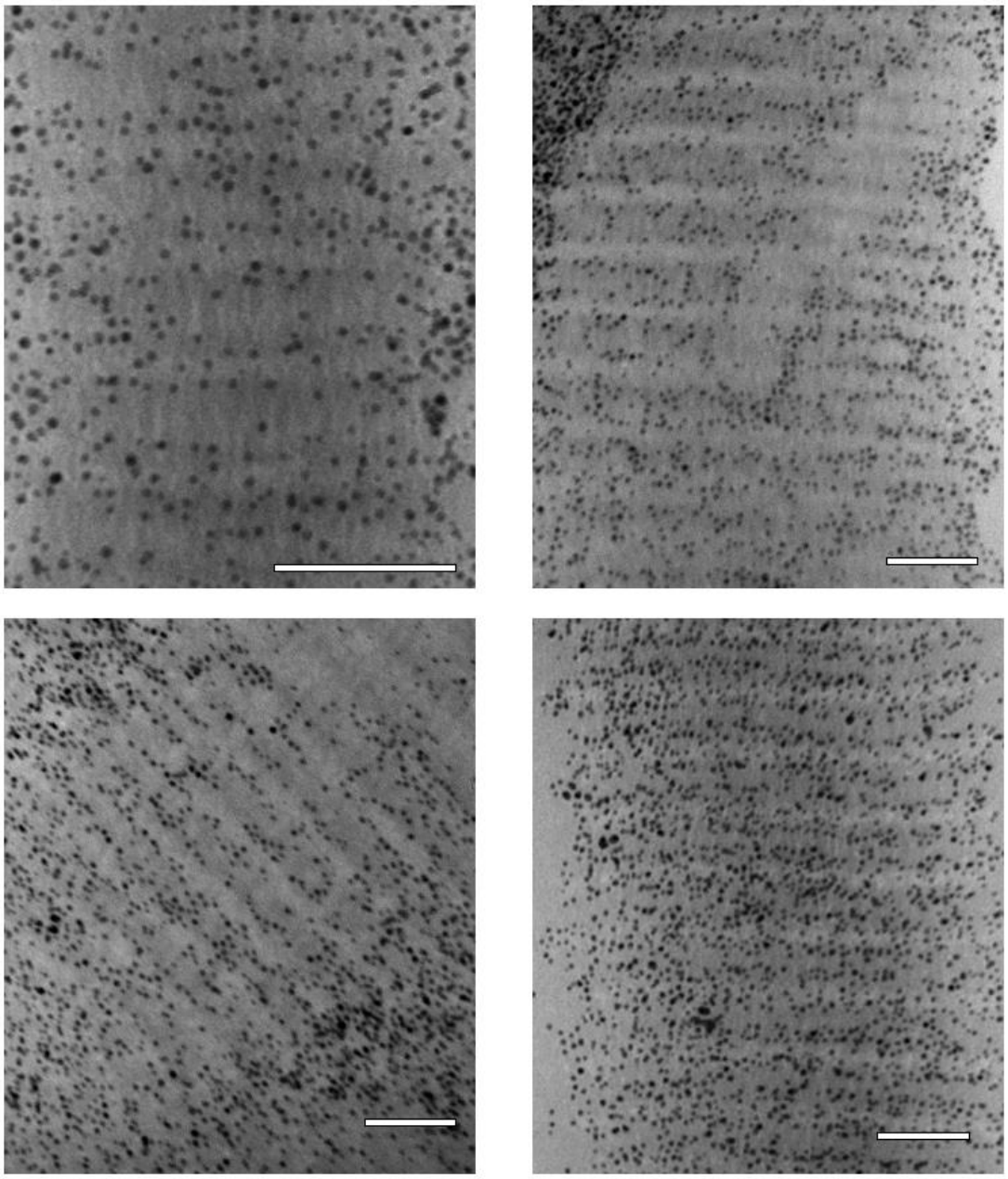

Figure 5.8.1 Nanogold particle staining of FilP.

TEM images of His-FilP striations in 50 mM Tris pH7.0 with nanogold particles (black dots) and methylamine vanadate pH8.0 staining. Scale bars: 100 nm

Nanogold staining with 1.8 nm nanogold beads has previously been imaged with cryo-EM (Javadi et al., 2019). They observed that their N terminally histidine tagged FilP showed nanogold localisation specifically in the vicinity of the white band (Figure 5.8.2). They also found that in a C terminally tagged FilP, the localisation was less specific and appeared to disassemble the structure. A non-tagged FilP also showed a faint affinity for the nanobeads with a smattering present across the structure (Javadi et al., 2019). The difference between our findings and theirs is that our nanogold appeared to flank the stripe where theirs localised

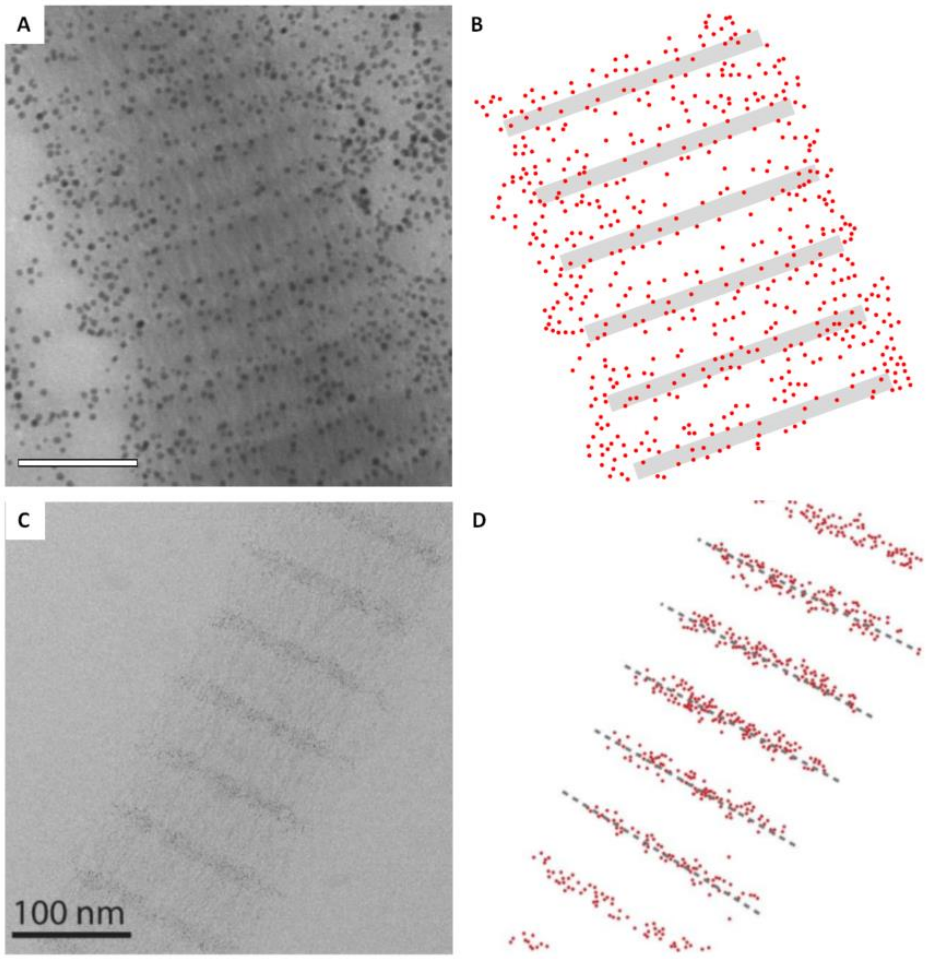

Figure 5.8.2 Comparison of FilP striation with nanogold staining.

A) TEM images of His-FilP striations in 50 mM Tris pH7.0 with nanogold particles (black dots) and methylamine vanadate pH8.0 staining. **B)** The same field of view as (A) as a model, where detected gold nanobeads are shown as red dots and the striation stripes are identified as grey lines. **C)** Image from (Javadi et al., 2019) showing cryo-EM of N-terminally histidine tagged FilP stained with 1.8 nm gold nanobeads. **D)** Image from (Javadi et al., 2019) showing the same field of view as (C) as a model, where detected gold nanobeads are shown as red dots and the striation stripes are identified as grey dashed lines. Scale bars: 100 nm.

to it. This is a subtle difference which could be due to the different sized nanogold beads used, although both our findings indicate that this protein dense white stripe is the location of the N-terminal histidine tag.

Nanogold staining of FilPC was hoped to confirm whether the nanogold lying either side of the white stripe was due to the N-terminal head and/or coil 1 lying within this white stripe, and the histidine tags sticking out either side. Due to the FilPC variant lacking the head and coil 1 (Figure 5.3.1), but still forming occasional striations, it was thought that the nanogold beads might lie directly onto of the white stripe here. However, FilPC when stained with nanogold appeared in several different ways (Figure 5.8.3). Areas where there was no obvious pattern to the nanogold particles where the filament formed also showed no striations with the negative staining. Areas of filaments which did not appear striated with the negative staining also had some lines of pattern for the nanogold particles. These lines of the nanogold particles, however, were not always a consistent width apart and sometimes appeared to be around the unit length for the striation and sometimes were considerably closer together. Where the FilPC striations were visible from the negative stain, the patterning of the nanogold particles was not clear (Figure 5.8.3). This, unfortunately, did not help answer the question of the composition of the white stripes.

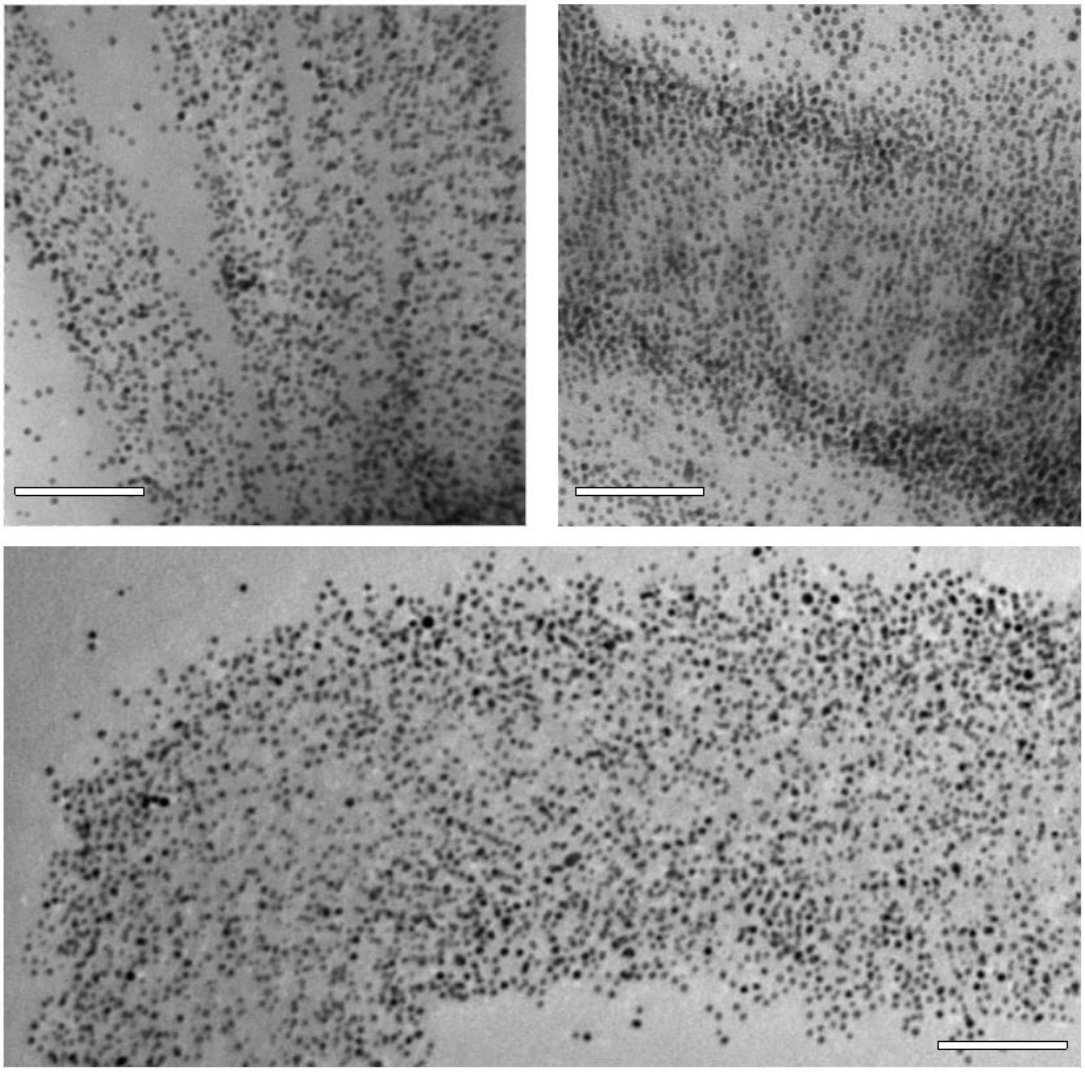

Figure 5.8.3 Nanogold particle staining of FilPC.

TEM images of His-FilP striations in 50 mM Tris with nanogold particles (black dots) and Methylamine vanadate pH8.0 staining. Top left and right pH6.0, bottom pH7.0. Scale bar 100 nm

By staining FilP mCherry with nanogold particles, it was hoped that we would get further confirmation as to which white stripe is the same as the one from FilP and which is from the mCherry tag. Analysis of FilP mCherry TEM with negative staining only showed that an extra stripe appeared between the normal stripes of FilP (Figure 5.6.2). Analysis of the measurements of these white stripes revealed that the larger and slightly less dense stripe (major) was the same width as the one from FilP and that the narrower but slightly denser protein stripe belonged to that of the mCherry tag (Figure 5.6.3). Nanogold staining was hoped to further confirm this following on from the observation with FilP that the nanogold particles

stained either side of the white stripe there (Figure 5.8.1). It was hoped that the same thing would happen with FilP mCherry and that the major white stripe would have nanogold particles flanking either side whereas the minor stripe would not, thus indicating that the minor stripe belonged to the mCherry tag which does not have affinity for the nanogold. However, nanogold staining of FilP mCherry revealed that these particles appeared to lie mostly between the major and minor stripes, though a lot of scattered particles also appeared throughout the sample (Figure 5.8.4). This is not particularly helpful as the nanogold particles cannot be assigned as to which stripe they are lying beside due to the proximity of them.

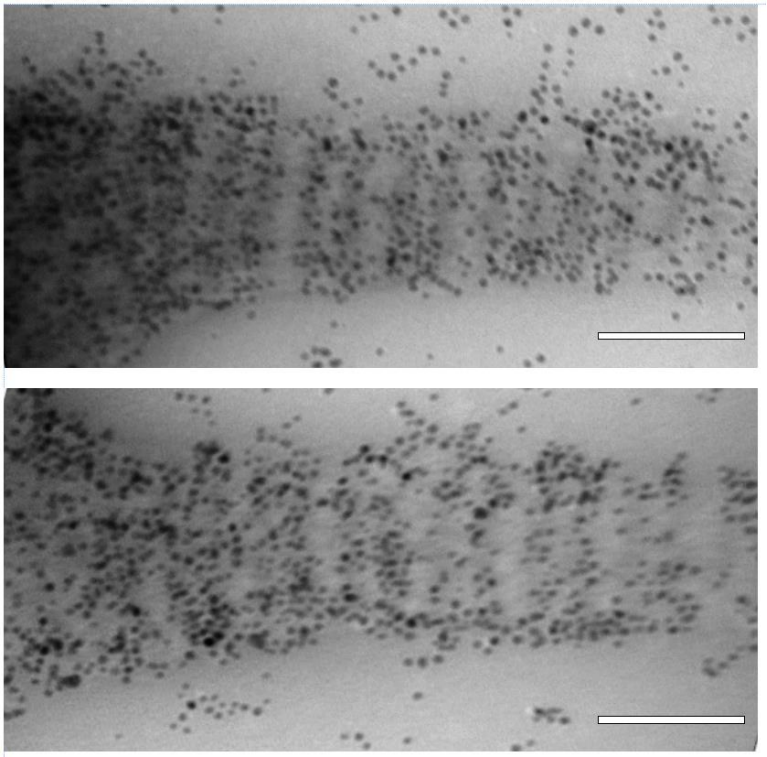

Figure 5.8.4 Nanogold particle staining of FilP mCherry.

TEM images of His-FilP mCherry striations in 50 mM Tris pH7.0 with nanogold particles (black dots) and Methylamine vanadate pH8.0 staining. Scale bar 100 nm.

5.9 Summary

The FilP variants generated were successful in increasing our understanding of the way in which FilP forms higher order assemblies. From FilPC, which lacks the head domain and coil 1 subdomain, and FilP Δtail it was shown that these variants have the same unit length as FilP and the striations appear similar (Figure 5.3.2, Figure 5.3.3, Figure 5.5.1, Figure 5.5.2). This indicates that the head domain, coil 1 subdomain, and tail domain are not essential for the formation of higher order assemblies and does not affect the striation. However, FilPC did also form a lace network structure as well as some smoother filaments which appeared unstriated (Figure 5.3.2). This perhaps indicates that this variant has weaker lateral interactions and could perhaps suggest that the head domain or coil 1 subdomain aids lateral interactions within FilP.

FilPN and FilPT, which lack the coil 2 subdomain and tail, and second half of coil 2 subdomain and tail respectively failed to form higher order structures. This indicates that the second half of coil 2 is essential for the formation of higher order assemblies.

FilP Δ4x7, which lacks the tail domain and the last four heptad repeats of coil 2, formed large assemblies with some observable striation which was much shorter in unit length than that of FilP (Figure 5.5.3, Figure 5.5.2). This indicates that the last four heptad repeats of coil 2 are important for the striation of FilP, but that higher order structures are possible without it. FilP Δ4x7 2x11 which lacks the tail domain, the last four heptad and two hendecads of coil 2 was not able to form higher order assemblies and indicates that the two hendecad repeats at the end of coil 2 are important for the formation of higher order assemblies.

MiniFilP, which lacks an internal section of the coil 2 subdomain, successfully showed that shortening of the coil 2 subdomain shortened the unit length of the striation (Figure 5.4.1, Figure 5.4.2) and shows that we can change the unit length of the striation without affecting its ability to form higher order assemblies. MiniFilP Δtail, which lacks and internal section of the coil 2 subdomain and the tail domain, was no longer able to form striations but instead formed large curled structures (Figure 5.5.4). It is unclear why or how this is the case.

FilP mCherry, which is C terminally attached, revealed an extra stripe which ran between the normal white protein dense stripe seen with FilP (Figure 5.6.2, Figure 5.6.3). This extra stripe was originating from the mCherry tag and indicates that the C terminal of FilP lies

between the stripes whereas the N-terminus (head domain and/or coil 1 subdomain) lies within the protein dense white band. Nanogold staining of FilP striations supported this when the nanogold particles, which bind to the N terminal histidine tag, were seen to localise just either side of the white stripe (Figure 5.8.1), hinting that the N terminus of FilP lies within this.

6 FilP and its Variants Change the Shape of *E. coli*

6.1 Introduction

Escherichia coli is a rod-shaped, Gram-negative bacterium. It is typically around 2 µm in length and around 0.5 - 0.8 µm in width (El-Hajj and Newman, 2015; Takeuchi et al., 2005). *E. coli* reproduces by binary fission. Cells double in length before dividing at the mid-cell producing two identical daughter cells. The elongation of *E. coli* is achieved by lateral growth. Lateral growth is where new cell wall material is inserted along the lateral walls of the cells and is found in bacteria such as *E. coli* and *Bacillus subtilis.* This lateral growth is driven by the MreB protein which is a homologue of the eukaryotic actin. Polar growth in the *Actinomycetes* is another method of growth, where growth mainly occurs at the poles of the cell. It is found mainly in *Actinomycetes* and is not present in *E. coli*. Polar growth is driven by the protein DivIVA, which is not considered to be a homologue of any class of eukaryotic protein (Flärdh, 2003a). In *Streptomyces,* a multi-protein assembly, the tip organising centre (TIPOC), including DivIVA is responsible for establishing and maintaining polar growth (Holmes et al., 2013). The fact that *E. coli* does not contain homologues of these TIPOC proteins is consistent with lack of polar growth in *E. coli.*

The TIPOC is a multiprotein assembly which is present at the tip of actively growing hyphae and orientates the cytoskeletal filaments (Holmes et al., 2013). There are three main proteins involved in the TIPOC: DivIVA, Scy and FilP (Holmes et al., 2013). All three of these proteins have been implicated in growth and branching. DivIVA in *S. coelicolor* localises to the poles as well as to the sites of new tip formation prior to the actual formation of the tips, which indicates that it is a growth marker and a future branch sites marker (Hempel et al., 2008). Scy localises to growing tips during active growth and co-localises with DivIVA both at tips and also at lateral sites preceding new branch formation (Holmes et al., 2013). FilP is an intermediate filament-like protein and was originally found to localise to the tip and to inner curvatures of the hyphae when FilP-EGFP was monitored but recent studies using immunolocalisation have shown that a FilP network extends along the hyphae from just behind the tip (Bagchi et al., 2008; Fuchino et al., 2013). However, its role in growth and branching remains unclear. It has been suggested that FilP could play a role in strengthening the wall behind the growing tip or establishing new polarity centres in response to stress (Bagchi et al., 2008; Fuchino et al.,

2016). It was proposed that FilP could enable the non-motile *S. coelicolor* to grow away from areas of high osmolality using the branching mechanism to move.

Scy and FilP are coiled-coil intermediate filament like proteins with an unusual repeat sequence within their rod domain as previously discussed (chapter 1). FilP and variants of it have been shown to self-assemble into large structures *in vitro* (chapter 3, 5).

E. coli extends its cell wall on its lateral side as governed by MreB (Shi et al., 2018). It lacks any homologous proteins to DivIVA, Scy or FilP. To test the biological role of FilP, we introduced FilP into *E. coli* to establish if FilP alone is sufficient to alter the morphology of *E. coli*.

Aims:

1. Generate constructs for the expression of FilP variants within *E.coli*
2. Express the FilP variants successfully in *E. coli*
3. Assess *E. coli* expressing the FilP variants using phase contrast and fluorescence microscopy to observe any morphological changes

6.2 Generation of Constructs

Generation of FilP and FilP variant constructs are detailed in chapters 4 and 5. The genes encoding these proteins are expressed in the pET28 plasmid and the expression is inducible by Isopropyl β-D-1-thiogalactopyranoside (IPTG). pET28 also adds an N-terminal histidine tag to the proteins when expressed in *E. coli.* In chapter 6 we presented the characterisation of the FilP variants purified using these overexpression constructs, while here we show the effect of these proteins on the physiology of *E.* coli. A control strain of *E. coli* carried the pET28 plasmid without any construct insert. All plasmids were introduced into the *E. coli* BL21 strain using electroporation. *E. coli* cells containing the pET28 FilP constructs were grown in liquid LB broth for three and a half hours at 37°C. For observation in liquid medium, 1 mM IPTG was added followed by a further two hours growth at 37°C. For observation on a solid medium, following the three and a half hours growth in liquid medium, an aliquot of the liquid culture was taken and plated onto a solid LB agar plate containing 1 mM IPTG and topped with a cellophane disk. This was then incubated at 37°C for two hours before viewing.

FilP variants were initially designed for expression and purification from *E.coli* and to test the ability of these variants to form higher order assemblies. FilP Δlinker was designed to lack the linker which joins coil 1 and 2 (Figure 5.3.1). This was designed to see if the deletion of the linker would change propensity for FilP to form higher order structures when its is removed, linking the N-terminal heptad and the C-terminal coiled-coil dominated by hendecads interspersed with heptads. The removal of the linker generates essentially one long coiled-coil. When observed *in vitro* by TEM it formed higher order structures which resembled a lace structure most frequently and the unit length of this was longer than that of FilP (Figure 5.4.3, Figure 5.4.4). A variant known as miniFilP was designed to lack an internal part of the coil 2 domain such that the terminal ends of the coiled-coil structures are maintained (Figure 5.3.1). MiniFilP was designed to maintain all the features of FilP while just shortening the coil 2 subdomain to assess whether this construct was still able to form higher order assemblies like the full length FilP and, if so, whether the unit length of the assembly was altered. Observation by TEM showed that this variant formed higher order structures which resembled that of FilP but with a shortened unit length (Figure 5.4.1, Figure 5.4.2). Sequential shortenings of FilP from the C terminus were designed to test which part of the C terminal was

essential to for forming higher order assemblies (Figure 5.3.1). This was based on the results that FilPT was not able to form higher order assemblies, but miniFilP was, even though it lacked a large part of the coil 2 domain. Sequential shortening of FilP was designed starting with a variant lacking just the tail domain, known as FilP Δtail. FilP Δ4x7 then lacks the tail domain and the last 4 heptad repeats of the coil 2 subdomain (Figure 5.3.1). FilP Δ4x7 2x11 lacks the tail domain, the last 4 heptad repeats and 2 hendecad repeats of the coil 2 sub-domain (Figure 5.3.1). Analysis of the higher order structures these by TEM revealed that FilP Δtail was able to form higher order structures in much the same way as FilP (Figure 5.5.1, Figure 5.5.2). FilP Δ4x7 was able to form large structures but these were mainly unstriated, however a smaller unit length striation was sometimes observed (Figure 5.5.3, Figure 5.5.2). FilP Δ4x7 2x11 was unable to form higher order structures under the conditions we tested. This sequential shortening was also applied to the miniFilP construct in the same way with the exception that the 2 hendecad repeats were not removed due to removing the 2x11 fragment from miniFilP would have created a variant would have been shorter than FilPT. FilPT was already known not to form higher order structures. MiniFilP Δtail was observed to form a strange higher order structure which was large spirals and unlike anything else seen with any other FilP variants (Figure 5.5.4). MiniFilP Δ4x7 was unable to form any higher order assemblies under the conditions tested. FilP variants known as FilPC, FilPN and FilPT were designed to lack the head and coil 1 sun-domain; the coil 2 sub-domain and tail domain; and half of the coil 2 sub-domain and tail domain respectively (Figure 5.3.1). The rationale behind this was to establish whether abolishing any of these important features would abolish the ability of FilP to form higher order structures. FilPN and FilPT were not able to form higher order structures under conditions tested. FilPC was able to form large higher order structures which were sometimes unstriated, striated or lattice-like. The unit length of the FilPC structures were the same as that of FilP (Figure 5.3.2, Figure 5.3.3). FilP-mCherry was designed to have the mCherry fluorescent tag C terminally attached to FilP in the same way that it is when expressed for localisation experiments in *S. coelicolor* (Figure 5.3.1). When this was observed *in vitro* by TEM it appeared striated like that of FilP but with an additional stripe between that of the normal FilP bands which corresponded to the mCherry tag. The unit length of these striations was the same as that with FilP (Figure 5.6.2, Figure 5.6.3). Finally, the small construct known as 2CC51 is part of coil 2 and contains two complete 51 repeats (Figure 5.3.1). This was designed to see if the unusual 51 repeat on its own could form higher order assemblies. Observation by TEM did not

reveal that this fragment could generate visible higher order structures in the conditions tested.

The *E. coli* samples overexpressing the different FilP variants were either observed live, by mounting an aliquot of liquid culture onto the microscope slide or cutting a square of cellophane taken from the surface of a solid LB medium for viewing using microscopy. Some samples were stained using WGA (wheat germ agglutinin- Alexa 488 fluorescent conjugate, a cell wall stain), and PI (propidium iodide, a chromosomal stain which emits red fluorescence). Staining of cellophane samples required washing cells off using PBS buffer, while a direct sample of the liquid cultures could be taken, all cells were subsequently washed with PBS before fixation with methanol and staining with WGA and PI in a microcentrifuge tube. Staining of cells containing FilP-mCherry were stained using WGA only and mounted with DAPI (4',6-diamidino-2-phenylindole, a chromosomal stain emits blue fluorescence).

6.3 Expression of FilP in *E. coli*

The effect of expression of His-tagged FilP in *E. coli* was first tested in liquid culture. Samples were taken at 2 hrs and 20 hrs post induction with IPTG, and it was observed that the presence of FilP within the *E. coli* cells appeared to cause a slight increase in cell length compared to the control, where *E. coli* carried the plasmid pET28 (Figure 6.3.1). Subsequent measurement and analysis revealed that the cells length increased by around 20% after 2 hrs growth post induction compared to the control. To test for statistical significance, measurements were compared using a two-tailed T-test with a 95% confidence level. This revealed that these measurements had a statistical difference between them. The average length of the control cells was 2.09 µm (SD=0.54, n=47) whereas the cells expressing FilP averaged at 2.52 µm in length (SD=0.62, n=131).

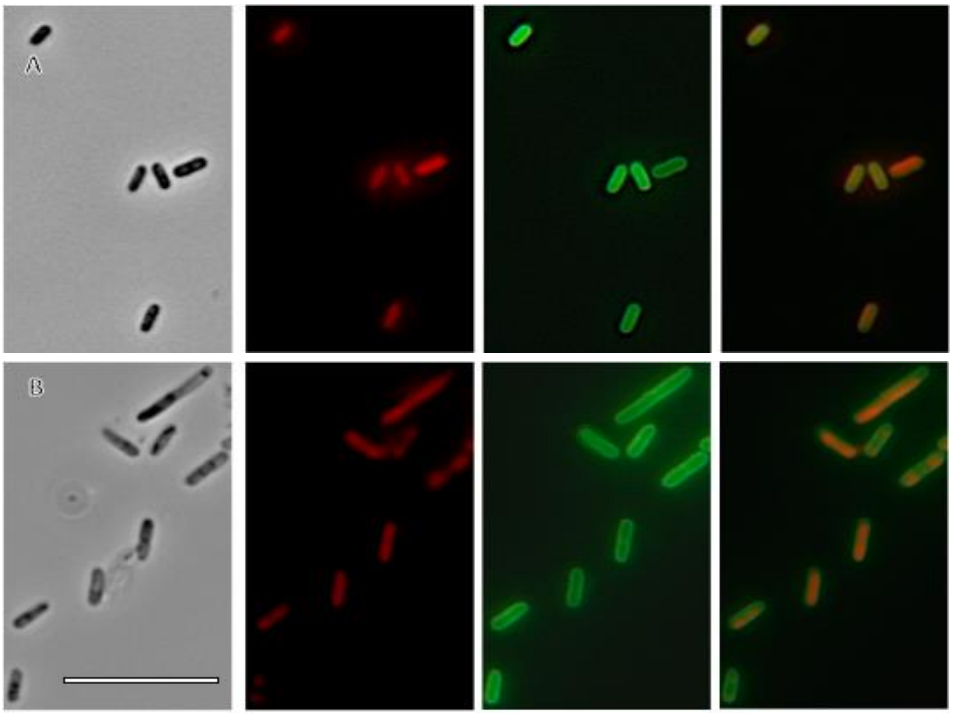

Figure 6.3.1 Monitoring of *E. coli* control cells and *E. coli* cells expressing FilP grown in liquid culture using epi-fluorescence microscopy.

E. coli cells grown in liquid culture for 2 hrs with 1 mM IPTG induction to express His-FilP vs the control and compared to those grown on cellophane. **(A)** phase contrast and fluorescence microscopy images of control *E. coil* BL21 pLysS pET28 grown in liquid culture. **(B)** Phase contrast and fluorescence microscopy images of control *E. coil* BL21 pLysS pET28 FilP grown in liquid culture. Left phase contrast image, red propidium iodine (PI) stain for chromosomes, green wheat germ agglutinin (WGA) stain for cell wall, right PI and WGA overlayed. Scale bars 10 µm for all images.

To test whether the same length increase could be detected when grown on solid media we tested cells that were grown in liquid culture prior to induction but were plated onto cellophane membranes over solid LM medium containing IPTG. Here, the cellophane acts as a barrier between *E. coli* and the medium. The porous nature of the cellophane allows nutrients from the media to be accessed by the *E. coli* cells. The cellophane provided a solid surface for the *E. coli* cells to grow on, and also provided an easily accessible way to view the results as squares could be cut from it and directly mounted for microscopy viewing.

Results from the cellophane experiment revealed that the control *E. coli* cells carrying pET28 grown on cellophane (2.17 µm, SD=0.93, n=366) (Figure 6.3.2) were comparable in length to those grown in liquid culture (2.09 µm, SD=0.54, n=47) (Figure 6.3.1). To test for statistical significance, measurements were compared using a two-tailed T-test with a 95% confidence level. This revealed that these measurements had no statistical difference between them. However, cells expressing FilP were much longer just 2 hrs growth on cellophane after induction (10.88 µm, SD=7.95, n=218) compared to both the control (2.17 µm) and to the FilP expressing cells grown in liquid culture (2.52 µm). The lengths of cells expressing FilP on cellophane varied widely between 2.74 µm and 80.13 µm (Figure 6.3.2).

Observation of the *E. coli* cells expressing FilP grown on cellophane by microscopy revealed that not all of the cells appeared exactly the same (Figure 6.3.2). The ghost of lysed cells could often be observed as well as very circular cells which sometimes appeared to burst. Long cells could also frequently be seen to have an almost banded appearance with fainter and lighter areas observed, as well as un-banded smoother appearing long cells (Figure 6.3.2). When stained with PI (chromosomal stain, red) and WGA (cell wall stain, green) these banded appearance cells, showed uneven distribution of chromosome and cell wall incorporation. Areas which appeared fainter than the rest on the phase contrast image appeared to be the sites of chromosome aggregation within these abnormally elongated cells. In the elongated cells there are multiple chromosomal foci suggesting replication generating multiple chromosomes but lack off division in these cells. The cell wall stain WGA stains sites where new cell wall is incorporated more strongly. The WGA stained these cells unlike for the control or for how WGA normally stains. Here, it did not stain in a nice ring around the cell (Figure 6.3.1), here (Figure 6.3.2) the WGA stain is not solely around the outside of the cell, but in the centre. The WGA sometimes stained in higher intensity the areas where the light image

appears darker and where the chromosomal material appears weaker, and sometimes the WGA stained along the cell wall evenly, even when the banding pattern was not visible. Where the cells appeared smooth, non-banded, the chromosomal stain was sometimes shown to be uniform along the length of the elongated cell, although it was more frequently observed to be localised to several foci along the length of the cell (Figure 6.3.2). Growth of the *E. coli* cells expressing FilP overnight on cellophane appeared to have much longer cells than those observed after two hours growth. However, these became so dense that they were difficult to image, and individual cells were not on a single plane and so could not be imaged for measurement.

The exact reason for the increase in cell length when expressing FilP remains unclear. It seems likely that the ability of FilP to form large higher order structures would potentially physically limit the cells from undergoing cell division if the large protein structures were physically blocking the site of cell division. N-terminally his tagged FilP has been shown to be present in the striated form of higher order assembly when within an *E. coli* cell (Javadi et al., 2019). However, the increased FilP levels are resulting in large protein structures in liquid grown samples too, but they do not inhibit cell division. FilP could also be interacting with native *E. coli* proteins in some way to limit cell division and allow the cells to continue extending to lengths not normally seen with *E. coli* cells. What determines cell size is quite complex, but it is feasible that an internal scaffolding of FilP might enable cells with an increased cell size and not by inhibiting cell division.

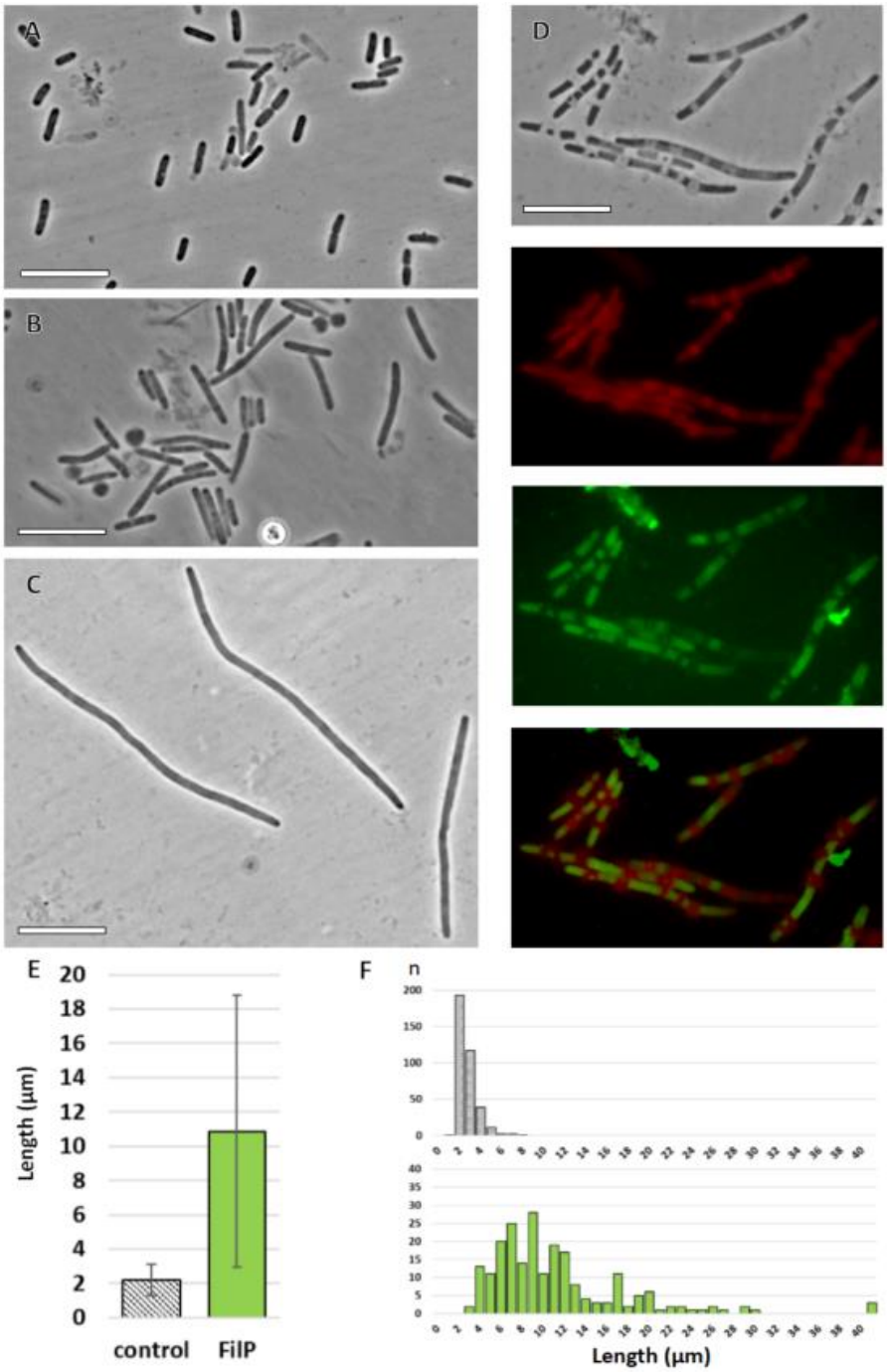

Figure 6.3.2 Monitoring of *E. coli* control cells and *E. coli* cells expressing FilP grown on cellophane using epi-fluorescence microscopy.

E. coli cells grown for 2 hrs after they were placed on cellophane covered solid LB media containing 1 mM IPTG to express His-FilP vs the control. **(A)** Phase contrast image of control *E. coil* BL21 pLysS pET28. **(B), (C)** phase contrast image of *E. coil* BL21 pLysS pET28 FilP. **(D)** phase contrast and fluorescence microscopy images of *E. coil* BL21 pLysS pET28 FilP. Top phase contrast image, red propidium iodine (PI) stain for chromosomes, green wheat germ agglutinin (WGA) stain for cell wall, bottom PI and WGA overlayed. Scale bars 10 µm. **(E)** Comparisons of the average lengths of cells of the control and of the cells expressing FilP. Error bars represent standard deviation. **(F)** Histograms of the length of cells in the control (top) and cells expressing FilP (bottom).

6.4 *E. coli* cells expressing FilP Δlinker

Following from the observations made whereby *E. coli* cells expressing FilP increased in cell length when grown on cellophane, epi-fluorescence microscopy was undertaken with several of the FilP variants. Variants were used which were generated for a previous chapter (chapter 4) and for overexpression for purification purposes.

E. coli cells expressing FilP Δlinker grown on cellophane were shown to behave in much the same way as *E. coli* cells expressing the full FilP protein (Figure 6.3.2, Figure 6.4.1). The lengths of the cells increased after induction compared to those of the control strain carrying the pET28 plasmid. The cell length of *E. coli* expressing FilP Δlinker appeared to be more uniform in length than those expressing full-length FilP (Figure 6.4.1). There were fewer cells which were of extremely long length. However, the average length of *E. coli* expressing FilP Δlinker and FilP were very similar with 8.83 µm (SD=3.85, n=74) and 10.88 µm (SD= 7.95, n=218) in length respectively. Interestingly, we only observed a few cells showing the banded pattern which was commonly observed when FilP was overexpressed. Those cells where the banding pattern was detected in the phase contrast image showed PI staining at places that were phase bright. The cell wall uniformly stained with WGA stain without having un-stained patches as was seen in *E. coli* expressing FilP (Figure 6.3.2, Figure 6.4.1). In the majority of cells, PI stained the chromosomes uniformly along the length og the cell. Intriguingly, there were some cells where the WGA staining was brighter at the poles than along the lateral edges of the cells (Figure 6.4.1).

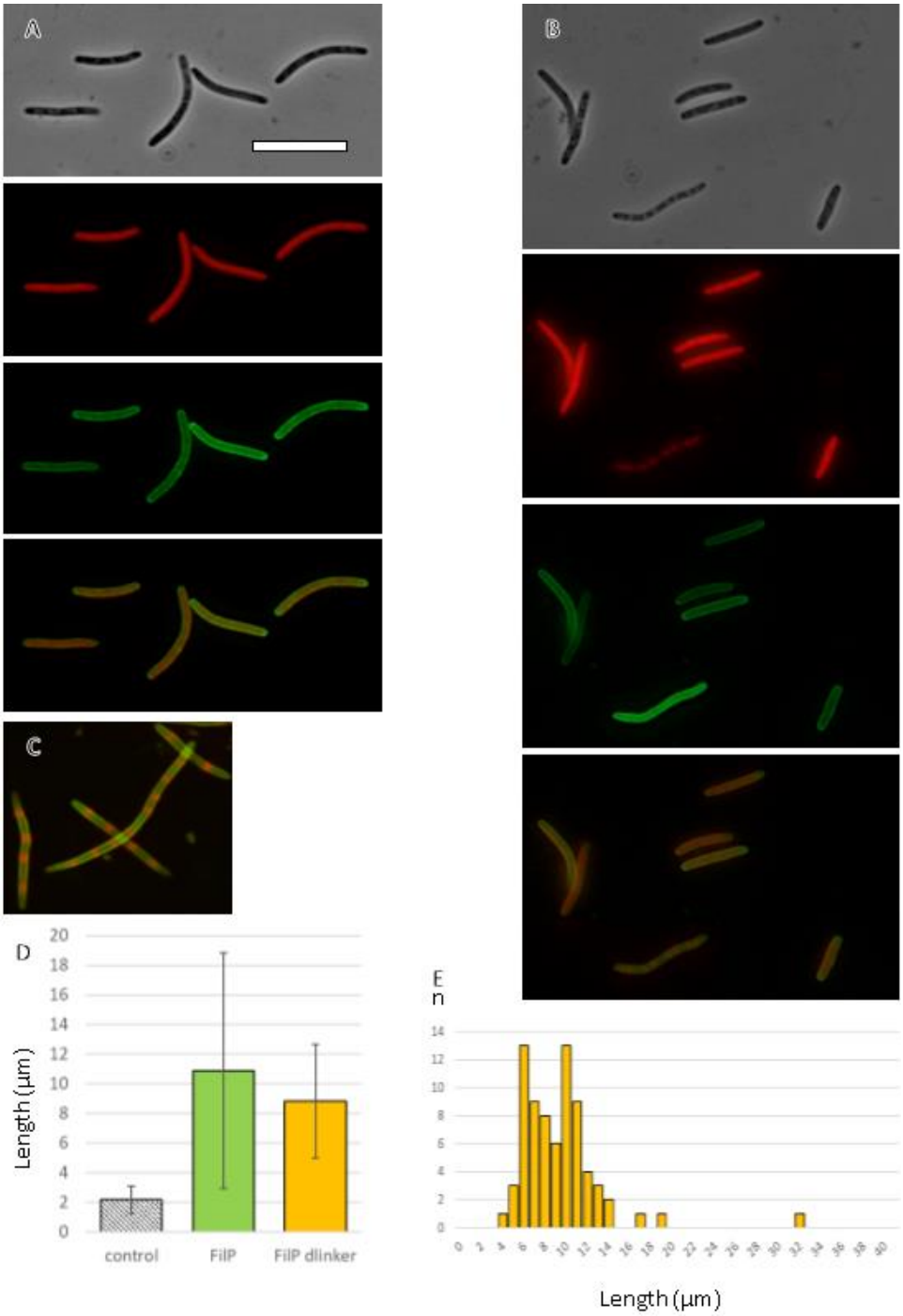

Figure 6.4.1 Monitoring of *E. coli* cells expressing FilP Δlinker grown on cellophane using epi-fluorescence microscopy.

E. coli cells grown for 2 hrs after they were placed on cellophane covered solid LB media containing 1 mM IPTG to express His-FilP Δlinker. **(A)**, **(B)** phase contrast and fluorescence microscopy images of *E. coil* BL21 pLysS pET28 FilP Δlinker. Top phase contrast image, red propidium iodine (PI) stain for chromosomes, green wheat germ agglutinin (WGA) stain for cell wall, bottom PI and WGA combined. Scale bars 10 µm. **(C)** Fluorescence microscopy images of *E. coil* BL21 pLysS pET28 FilP Δlinker. PI and WGA overlayed. Scale bars 10 µm applies to all images. **(D)** Comparisons of the average lengths of cells of the control, cells expressing FilP, and cells expressing FilP Δlinker. Error bars represent standard deviation. **(E)** Histogram of the length of cells expressing FilP Δlinker.

6.5 *E. coli* cells expressing FilP Δtail, FilP Δ4x7 and FilP Δ4x7 2x11

E. coli cells expressing FilP variants that were shortened at the C terminus, FilP Δtail, FilP Δ4x7 and FilP Δ4x7 2x11 were also analysed using phase contrast microscopy to assess whether they were also elongated when grown on cellophane covered LB medium.

E. coli cells expressing FilP Δtail, FilP Δ4x7 and FilP Δ4x7 2x11 grown on cellophane for 2 hrs after induction with IPTG were longer than the control carrying pET28 plasmid (Figure 6.5.1). Average length of the cells grown on cellophane expressing FilP Δtail (12.46 µm, SD=5.23, n=47), FilP Δ4x7 (5.94 µm, SD=2.07, n=144) and FilP Δ4x7 2x11 (7.23 µm, SD=2.39, n=95) are much longer than the control *E. coli* carrying the pET28 plasmid (2.17 µm). The *E. coli* cells expressing FilP Δtail were even longer than the FilP expressing cells (10.88 µm), whereas both the FilP Δ4x7 and FilP Δ4x7 2x11 expressing cells were shorter than the FilP expressing cells (Figure 6.5.1). To test for statistical significance, measurements were compared using a two-tailed T-test with a 95% confidence level. This revealed that these measurements were all statistically different to both the control cells carrying pET28 and to cells expressing FilP. Visually, FilP Δtail, FilP Δ4x7 and FilP Δ4x7 2x11 all appeared to be largely consisting of cells which lacked the segmented features visible in phase contrast of cells when FilP was over expressed (Figure 6.3.2, Figure 6.5.1).

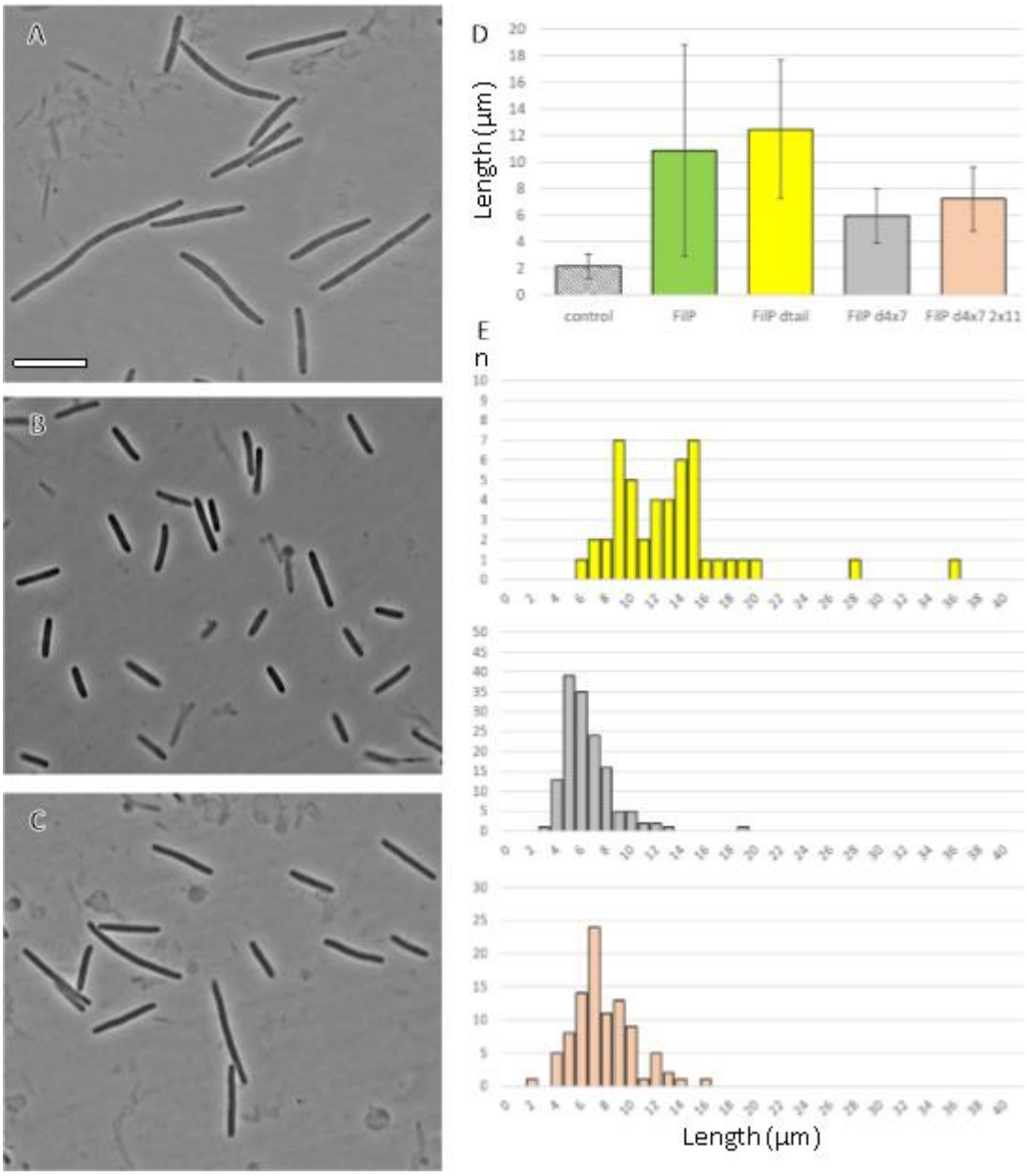

Figure 6.5.1 Monitoring of *E. coli* cells expressing FilP Δtail, FilP Δ4x7, and FilP Δ4x7 2x11 grown on cellophane using epi-fluorescence microscopy.

E. coli cells grown for 2 hrs after they were placed on cellophane covered solid LB media containing 1 mM IPTG to express His-FilP Δtail, Δ4x7, and Δ4x7 2x11. **(A)** phase contrast microscopy images of *E. coil* BL21 pLysS pET28 FilP Δtail. **(B)** phase contrast images of *E. coil* BL21 pLysS pET28 FilP Δ4x7. **(C)** phase contrast images of *E. coil* BL21 pLysS pET28 FilP Δ4x7 2x11. Scale bar 10 µm applies to all images. **(D)** Comparisons of the average lengths of cells of the control, cells expressing FilP, FilP Δtail, FilP Δ4x7 and FilP Δ4x7 2x11. Error bars represent standard deviation. **(E)** Histogram of the length of cells expressing FilP Δtail (top), FilP Δ4x7 (middle) and FilP Δ4x7 2x11 (bottom).

6.6 *E. coli* expressing miniFilP, miniFilP Δtail, and miniFilP Δ4x7

E. coli cells expressing miniFilP, the FilP variant that lacked the middle of the coil 2 sub-domain, and its C-terminally truncated derivatives, miniFilP Δtail and miniFilP Δ4x7 (Figure 5.3.1) were also visualised to assess whether these variants had the capacity to elongate the cells when grown on the surface of cellophane compared to cells expressing FilP.

Cells were grown to mid exponential phase in LB liquid medium and transferred to cellophane covered solid LB medium containing the inducer, IPTG. After 2 hrs induction, cells expressing miniFilP and those expressing miniFilP Δtail were greatly elongated compared to the cells carrying the pET28 plasmid, similarly to cells expressing FilP (Figure 6.6.1).

As stated previously, control *E. coli* cells carrying pET28 grown on cellophane have an average length of 2.17 µm. Cell length was much longer when expressing miniFilP (5.95 µm, SD= 3.33, n=297), miniFilP Δtail (11.08 µm, SD=10.20, n=133) and miniFilP Δ4x7 (4.98 µm, SD=2.39, n=248). To test for statistical significance, measurements were compared using a two-tailed T-test with a 95% confidence level. This revealed that these measurements were all statistically different to the control cells carrying pET28. *E. coli* cells expressing miniFilP and miniFilP Δ4x7 were statistically different to that of the length of cells expressing FilP. The average length of cells expressing miniFilP Δtail was statistically not different to the length of cells expressing FilP. Visually, miniFilP and miniFilP Δtail appeared as both segmented and non-segmented cells whereas miniFilP Δ4x7 appeared largely non-segmented (Figure 6.6.1).

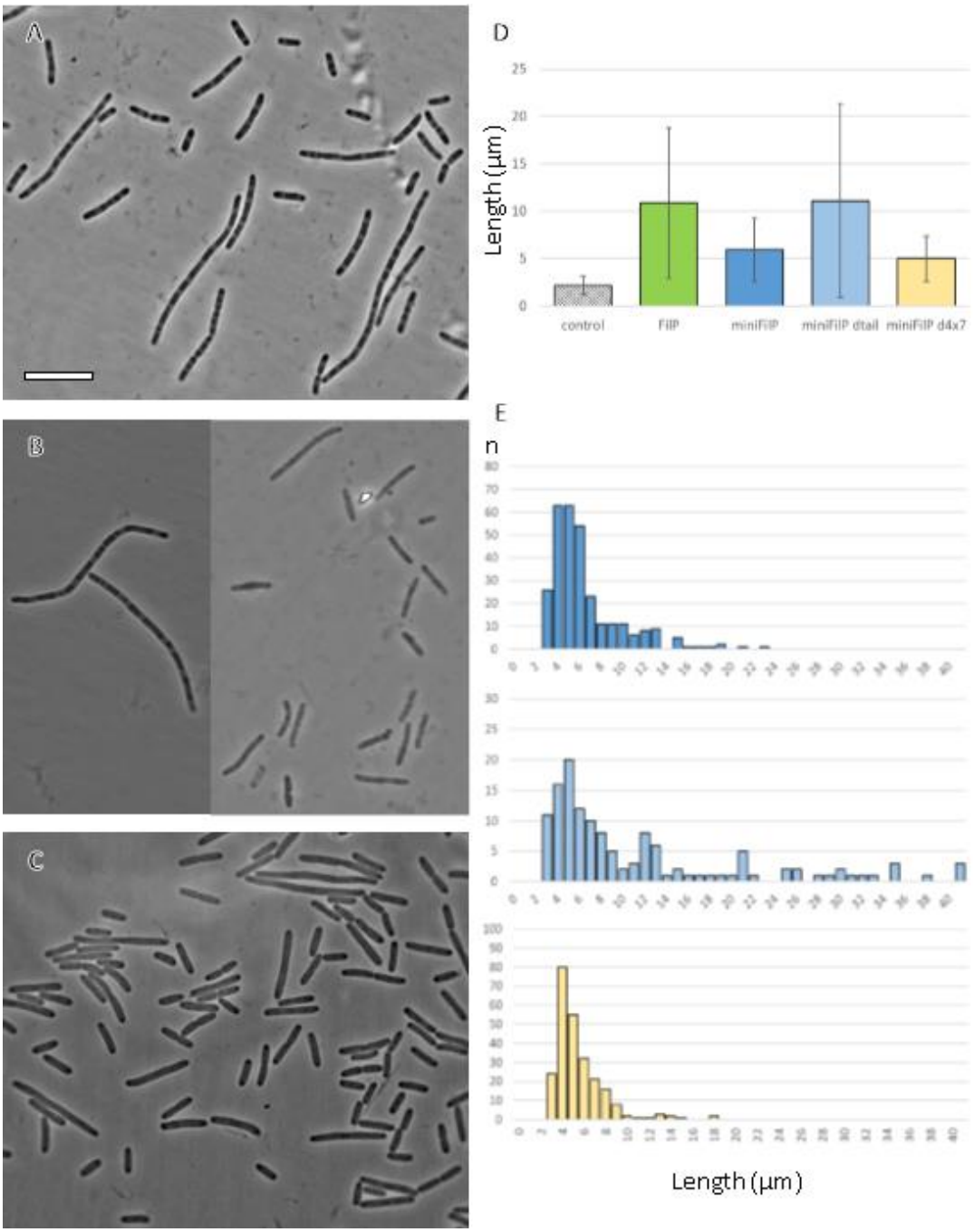

Figure 6.6.1 Monitoring of *E. coli* cells expressing miniFilP, miniFilP Δtail, and miniFilP Δ4x7 grown on cellophane using epi-fluorescence microscopy.

E. coli cells grown for 2 hrs after they were placed on cellophane covered solid LB media containing 1 mM IPTG to express His-miniFilP, miniFilP Δtail and miniFilP Δ4x7. **(A)** phase contrast images of *E. coil* BL21 pLysS pET28 miniFilP. **(B)** phase contrast images of *E. coil* BL21 pLysS pET28 miniFilP Δtail. **(C)** phase contrast images of *E. coil* BL21 pLysS pET28 miniFilP Δ4x7. Scale bar 10 µm applies to all images. **(D)** Comparisons of the average lengths of cells of the control, cells expressing FilP, miniFilP, miniFilP Δtail and miniFilP Δ4x7. Error bars represent standard deviation. **(E)** Histogram of the length of cells expressing miniFilP (top), miniFilP Δtail (middle) and miniFilP Δ4x7 (bottom).

6.7 *E. coli* cells expressing FilPN, FilPC and FilPT

E. coli cells which were expressing FilPN, FilPC and FilPT were observed by epi-fluorescence microscopy when grown on cellophane overnight after induction with IPTG (Figure 6.7.1). Overexpression of FilPC and FilPT generated elongated cells (Figure 6.7.1), whereas preliminary results from cells expressing FilPN generated cells which were like the control (data not shown). FilPT also generated an abundance of the ball shaped cells.

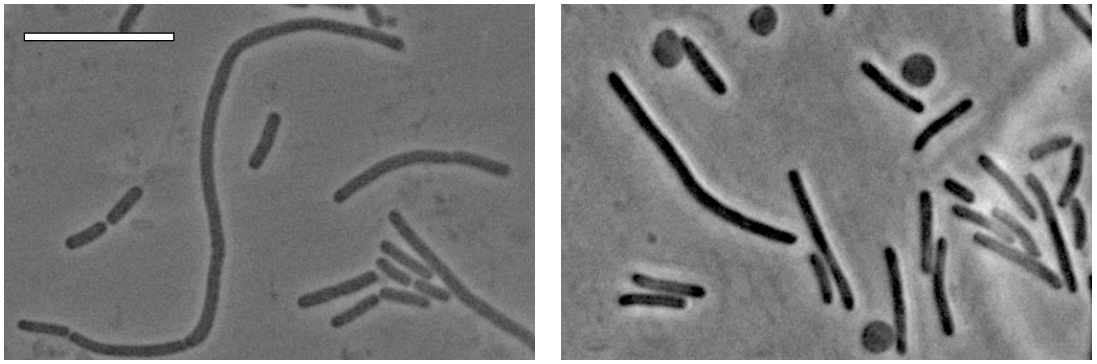

Figure 6.7.1 Monitoring of *E. coli* cells expressing FilPC and FilPT grown on cellophane using epi-fluorescence microscopy.

E. coli cells grown for 2 hrs after they were placed on cellophane covered solid LB media containing 1 mM IPTG to express His-FilPC and His-FilPT. **(left)** phase contrast image of *E. coil* BL21 pLysS pET28 FilPC. **(right)** phase contrast image of *E. coil* BL21 pLysS pET28 FilPT. Scale bar 10 µm applies to all images.

6.8 *E. coli* cells expressing FilP-mCherry

E. coli cells expressing a C-terminally mCherry tagged FilP protein were analysed by epi-fluorescence microscopy to assess whether the FilP-mCherry fusion had the same effect on the *E. coli* cells as that of the non-tagged FilP. In addition, the fluorescent tag allowed visualisation of the cellular localisation within *E. coli* cells in comparison to the chromosomal material and the sites of cell wall synthesis, as assessed using DAPI (nucleic acid stain) and WGA (cell wall stain) respectively.

Cells expressing FilP-mCherry were elongated and looked very similar to cells expressing non-tagged FilP (Figure 6.3.2, Figure 6.8.1). The average length for cells expressing FilP-mCherry (13.39 µm, SD=7.44, n=89) was longer than that for FilP alone (10.88 µm). To test for statistical significance, measurements were compared using a two-tailed T-test with a 95% confidence level. This revealed that these measurements were statistically different.

The cells expressing FilP-mCherry appeared segmented as was seen with cells expressing FilP, although there were some smooth cells too. When viewed with fluorescence microscopy the mCherry fluorescence was found at places where darker segments were seen in the phase contrast image (Figure 6.8.1). In contrast, nucleic acids accumulated in the FilP free areas that were phase bright. This is very similar to the pattern observed in *E. coli* expressing FilP (Figure 6.3.2). The alternating pattern of FilP-mCherry and chromosome staining does not appear to be very regular in size (Figure 6.8.1). Chromosome staining was always discontinuous throughout the elongated cells. This indicates that there is distinct compartmentalisation within these elongated cells expressing FilP-mCherry, and the presence of the FilP-mCherry assemblies excluded the nucleic acids, presumably the chromosomes at those places. With cells expressing the FilP protein without the mCherry tag, PI staining revealed that the chromosomes were often also in this distinct pattern. The sites of new cell wall incorporation revealed that here the WGA stained relatively evenly along the sides of the cell (Figure 6.8.1). While most of the older cells had these internal compartmentalisations, there were also cells whereby the chromosome stain stretched along the length of the cell in the same time FilP mCherry also generated a continuous signal along the cells (Figure 6.8.1C). This suggests that initially cells can accommodate both FilP polymers and the chromosomes, perhaps when levels of FilP are lower, then as FilP becomes more extensive the exclusion

zones appear. In cells expressing FilP which appeared segmented, areas where the chromosome was present sometimes appeared to be unhealthy (Figure 6.3.2D) and bulging as if about to burst while areas which did not stain for nucleic acids were not.

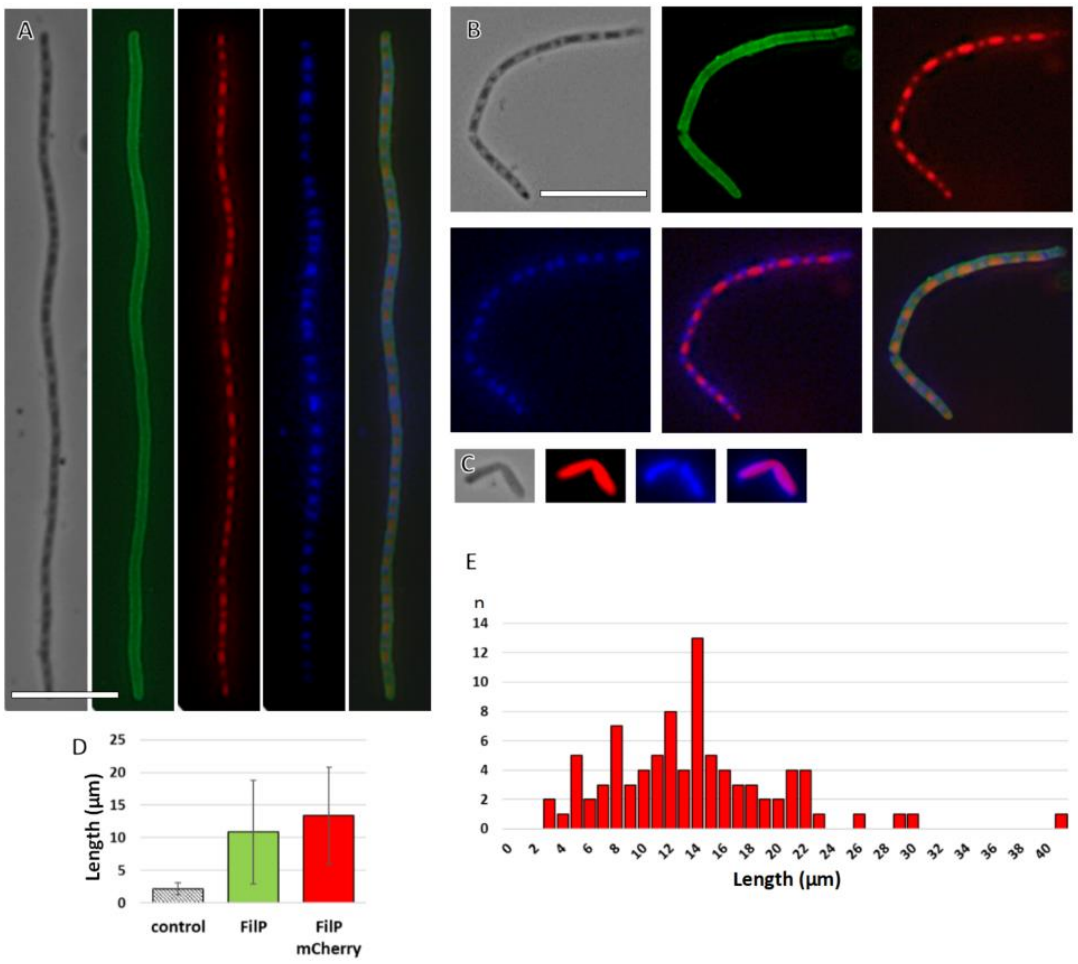

Figure 6.8.1 Monitoring of *E. coli* cells expressing FilP-mCherry grown on cellophane using epi-fluorescence microscopy.

E. coli cells grown for 2 hrs after they were placed on cellophane covered solid LB media containing 1 mM IPTG to express His-FilP-mCherry. Phase contrast and fluorescence microscopy images of *E. coil* BL21 pLysS pET28 FilP-mCherry. **(A)** left phase contrast image; green wheat germ agglutinin (WGA) stain for cell wall; red mCherry fluorescence; blue 4',6-diamidino-2-phenylindole (DAPI) stain for DNA; overlayed image of WGA, mCherry and DAPI (right). **(B)** Top left phase contrast image; top middle green wheat germ agglutinin (WGA) stain for cell wall; top right red mCherry fluorescence; bottom left blue 4',6-diamidino-2-phenylindole (DAPI) stain for DNA; bottom middle overlayed image of mCherry and DAPI; bottom right overlayed image of WGA, mCherry and DAPI. **(C)** left phase contrast, PI, DAPI, PI and DAPI overlayed right. Scale bars 10 µm applies to all images. **(D)** Comparisons of the average lengths of cells of the control, cells expressing FilP, and cells expressing FilP-mCherry. Error bars represent standard deviation. **(E)** Histogram of the length of cells expressing FilP-mCherry.

6.9 *E. coli* cells expressing 2CC51

2CC51 is a 102 amino acid motif of the coil 2 sub-domain of FilP and is predicted to consist of two 51-mer repeat sequences. Cells expressing this small fragment of FilP were grown after induction by IPTG on the surface of cellophane and beside glass coverslips on solid LB medium. Cells expressing 2CC51 grown on the surface of cellophane appeared to exist in many forms and were unlike the control cells expressing pET28 or the cells expressing FilP. Many of the cells lysed and appeared unhealthy (Figure 6.9.1). Some of the cells were club shaped with one end fatter than the other. Many cells also appeared as spheres which appeared to be lysing suggesting that the presence of 2CC51 promoted changes in the cell wall of *E. coil* (Figure 6.9.1). Cells which appeared to be healthier did not conform to the rod shape which would be expected from an *E. coli* cell (Figure 6.9.1). Cells were observed which appeared to almost have a stalk at one or both ends, and infrequently cells which appeared to have branched (Figure 6.9.1). The average length of the cells expressing 2CC51 grown on cellophane was 3.00 µm (SD=2.31, n=216) which is slightly longer than the control cells carrying pET28 at 2.18 µm. To test for statistical significance, measurements were compared using a two-tailed T-test with a 95% confidence level. This revealed that these measurements were statistically different. The length of cells expressing 2CC51 were also statistically different to cells expressing FilP.

Staining of the chromosomal material of these cells using PI revealed that the chromosomal material spread largely evenly within most cells. In a few cells, there were areas that lacked the chromosomal material and in some cells areas of lighter and darker PI staining (Figure 6.9.1). Staining of the cell walls with WGA revealed that there were areas of the misshapen cells which stained brighter than others, indicating sites where new cell wall material was being incorporated. The stalk structure observed in some cells appeared much brighter on the images. Some cells stained consistently around all sides with WGA and some cells, notably in cells which appear to be branching, had a brighter WGA stain at the tips of the cells.

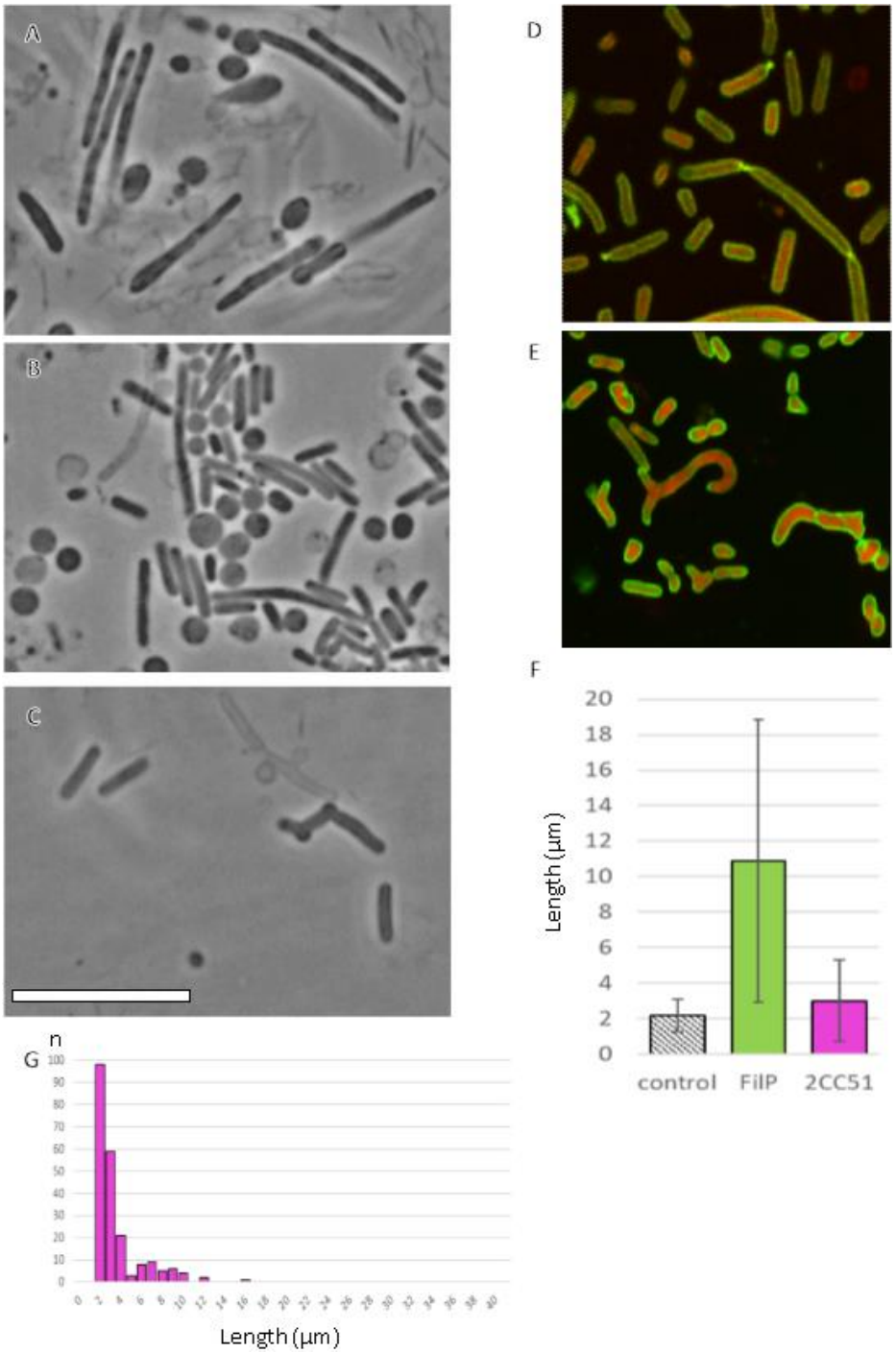

Figure 6.9.1 Monitoring of *E. coli* cells expressing 2CC51 grown on cellophane using epi-fluorescence microscopy.

E. coli cells grown for 2 hrs after they were placed on cellophane covered solid LB media containing 1 mM IPTG to express His-2CC51. Phase contrast and fluorescence microscopy images of *E. coil* BL21 pLysS pET28 2CC51. **(A), (B), (C)** phase contrast images showing different cell morphologies grown on cellophane. Scale bars 10 µm. **(D), (E)** Epi-fluorescence microscopy images: green wheat germ agglutinin (WGA) stain for cell wall; red propidium iodide (PI) stain for chromosomal material overlayed. Grown next to glass coverslips. Scale bar 10 µm applies to all images. **(F)** Comparisons of the average lengths of cells of the control, cells expressing FilP, and cells expressing 2CC51 (all on cellophane). Error bars represent standard deviation. **(G)** Histogram of the length of cells expressing 2CC51 when grown on cellophane.

The 2CC51 variant had a very different and striking affect compared to the other FilP variants tested. *E. coli* cells expressing 2CC51 did increase the length but only slightly (2.2 µm - 3.0 µm). However, cells expressing 2CC51 generated unusual shapes and features as well as many round cells and high levels of lysis (Figure 6.9.1). This indicates that the small 2CC51 coiled-coil fragment of FilP was seriously impacting the internal workings of the cells. The most interesting feature were cells which appeared to be branching, although these appeared rarely. *E. coli* cells are known to grow by lateral growth whereby the new cell material is inserted along the lateral side of the cells. This method of growth does not allow for branching of cells, unlike polar growth which is exhibited by *S. coelicolor*. Where polar growth is exhibited, the ability of cell wall material to be inserted at the tips of the hyphae allows for directional growth and branching by instigating a new pole. In these *E. coli* cells which are exhibiting a branching phenotype, it appears that the lateral growth normally exhibited had been disrupted by the presence of the 2CC51 fragment. If this is the case, the other odd shapes observed with the 2CC51 variant could also be attributed to the disruption of the normal function new cell wall material insertion. The staining patterns of cells expressing 2CC51 also appear to support this hypothesis. The tips of the branching cell (or stalk like structure) stained more intensely than the rest of those cells. The WGA stain stains sites of new cell wall incorporation more intensely. This observation, therefore, potentially indicates that the normal function of lateral growth within these cells has been severely interrupted by the 2CC51 fragment. In some cells, the mode of growth appears more like polar than lateral. This finding could potentially be very interesting and novel. My results here suggest that a small, 102 amino acid coiled-coil fragment of a protein has the potential to interact within a normally lateral growth cell to implement a change whereby polar growth is exhibited. Which proteins 2CC51 interacts with within *E. coli* would be fascinating to study. Studying this further and identifying these interactions may give important clues as to how cells divide and grow.

6.10 Analysing width measurements for the *E. coli* cells expressing FilP and FilP variants.

E. coli cells expressing FilP and FilP variants were initially characterised by their dramatic increase in length. However, upon further analysis it became apparent that the cells expressing FilP and grown on the surface of cellophane-covered solid LB medium were not only significantly longer than *E. coli* cells carrying pET28, but their width also when compared to the control. The average widths were 0.80 µm (SD=0.12, n=47), 0.80 µm (SD=0.09, n=131), 0.80 µm (SD=0.13, n=366) and 1.04 µm (SD=0.16, n=218) for control cells in liquid culture, cells expressing FilP in liquid culture, control cells on cellophane and cells expressing FilP on cellophane respectively (Figure 6.3.1). To test for statistical significance, measurements were compared using a two-tailed T-test with a 95% confidence level. This revealed that these cells expressing FilP grown on cellophane were statistically different than either cells grown in liquid or cells that carried the empty plasmid.

Analysis of the widths of the cells expressing the different FilP variants revealed that not only the length of these cells increased, but the widths also increased (Figure 6.10.1). Cells expressing FilP, miniFilP, FilP Δtail and FilP Δ4x7 had average widths which were statistically the same at the 95% confidence level with results at 1.04 µm (SD=0.16, n=218), 1.05 µm (SD=0.12, n=297), 1.08 µm (SD=0.08, n=47), and 1.04 µm (SD=0.14, n=95) respectively. Cells expressing FilP Δ4x7 2x11, miniFilP Δtail, miniFilP Δ4x7 and FilP Δlinker all had widths which were close to 1 µm but were not statistically the same as cells expressing FilP with 0.99 µm (SD=0.14, n=95), 0.98 µm (SD=0.09, n=133), 1.08 µm (SD=0.09, n=248), and 0.98 µm (SD=0.08, n=74) respectively. Cells expressing FilP-mCherry and 2CC51 on the other hand had widths which were smaller than the rest of the variants. Cells expressing FilP-mCherry had an average width of 0.85 µm (SD=0.11, n=89) while 2CC51 had an average width of 0.76 µm (SD= 0.10, n=216). The widths for these two variants are much closer to that of the average width of the control (0.80 µm) than that for the full FilP (1.04 µm) although they are statistically different to both.

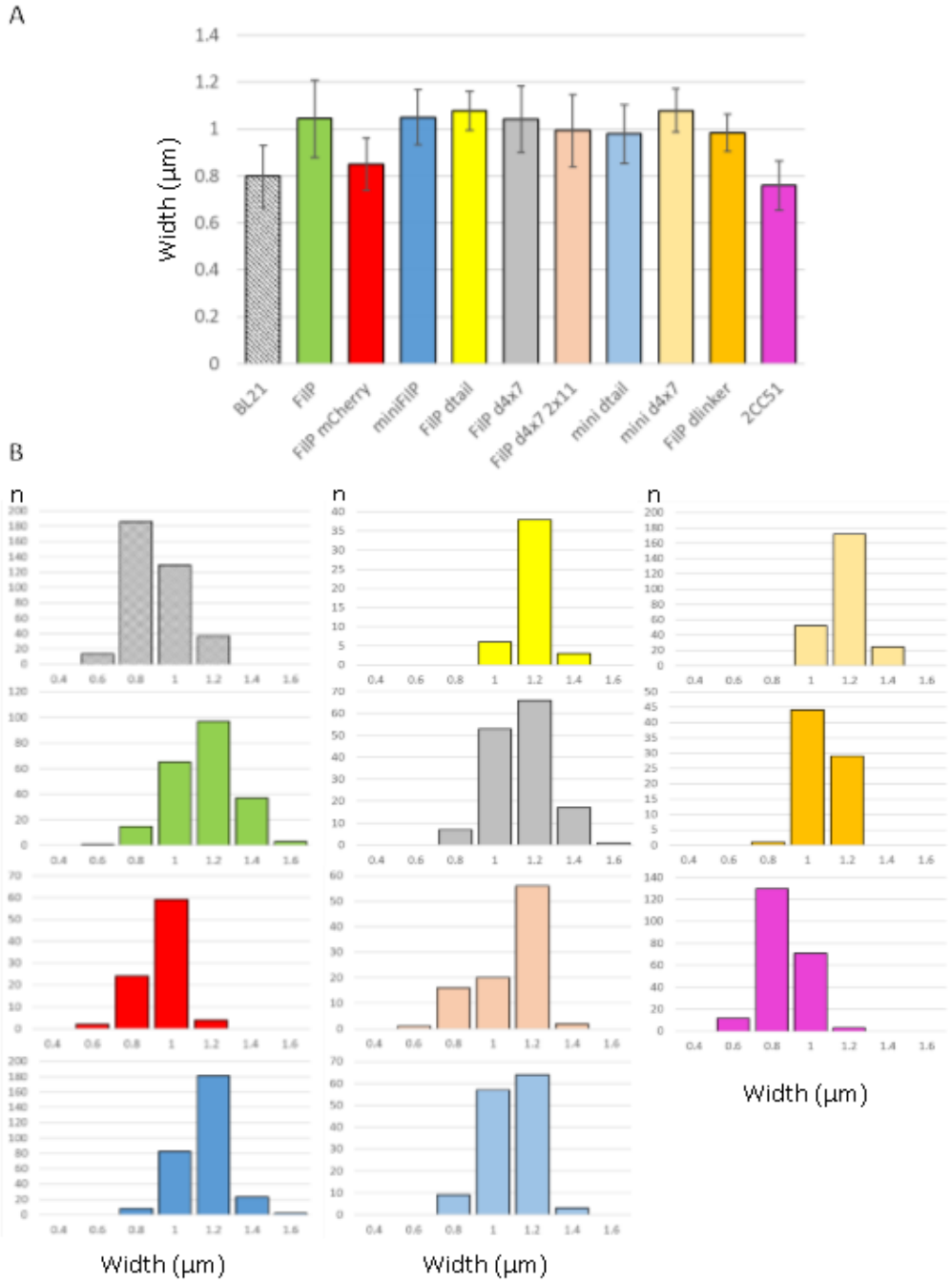

Figure 6.10.1 *E. coli* cells expressing FilP variants widths comparison

E. coli cells grown for 2 hrs after they were placed on cellophane covered solid LB media containing 1 mM IPTG to express His-FiP variants. **(A)** Comparisons of the average widths of cells of the control, cells expressing FilP, FilP-mCherry, miniFilP, FilP Δtail, FilP Δ4x7, FilP Δ4x7 2x11, miniFilP Δtail, miniFilP Δ4x7, FilP Δlinker, and 2CC51. Error bars represent standard deviation. **(B)** Histogram of the width of cells expressing FilP variants. Control (left top), cells expressing FilP (left second), FilP-mCherry (left third), miniFilP (left bottom), FilP Δtail (middle top), FilP Δ4x7 (middle second), FilP Δ4x7 2x11 (middle third), miniFilP Δtail (middle bottom), miniFilP Δ4x7 (right top), FilP Δlinker (right second), and 2CC51 (right third).

Overall cells expressing FilP variants were wider than that of the control and the FilP variants were similar in width for cells expressing FilP. Cells expressing 2CC51 and FilP-mCherry were the exception here. While cells expressing FilP-mCherry were longer than the control, the average width was closer to that of the control than it was to the FilP expressing cells. This difference with FilP-mCherry in its width but not its length is intriguing. The increased length, as with FilP, implies that the mCherry tag is not affecting the ability of FilP to change the length morphology of the cell. However, the lack of increase in width as seen with FilP indicates the potential that the C-terminal mCherry tag is affecting its ability to change the morphology of the cell with regards to its width. One possible explanation for this is that the mCherry tag inhibits the interaction of FilP with some *E. coli* component and that it is this interaction in the un-tagged version which is driving this width increase.

6.11 Summary

In summary, overexpression of FilP into *E. coli* cells increased cell length and width, but only when grown on a specific solid surface. Growth in liquid culture yielded cells which were slightly longer in length but the same in width as the control cells (Figure 6.3.1). This extreme elongation observed on solid media in contrast to the liquid culture indicates that the cells are mechanosencing the environment and are growing differently on solid material than suspended in liquid culture when FilP is present.

Analysis of the FilP variants expressed in *E. coli* cells grown on cellophane in comparison to the control carrying only the pET28 vector and to the cells expressing full length FilP revealed that none of the FilP variants resembled exactly the control and all FilP variants tested influenced the morphology of the cells in some way (Figure 6.3.2, Figure 6.4.1, Figure 6.5.1, Figure 6.6.1, Figure 6.7.1, Figure 6.8.1, Figure 6.9.1). Cells expressing miniFilP, FilP Δtail, FilP Δ4x7, FilP Δ4x7 2x11, miniFilP Δtail, miniFilP Δ4x7 and FilP Δlinker all had an increased length compared to the control, although these average lengths did vary and were not exactly the same as that for FilP (Figure 6.3.2, Figure 6.4.1, Figure 6.5.1, Figure 6.6.1, Figure 6.7.1, Figure 6.8.1, Figure 6.9.1). Overnight observations of these variants revealed that they were all continuing to grow longer. This increase in length and width of the cells suggests that the expression of FilP within these cells is influencing the internal workings of the cell in some way to generate these elongated cells. The absence of this dramatic increase in cell length or width when grown in liquid culture raises an interesting difference between liquid culture and those grown on solid media with cellophane. These results suggest that, in the presence of FilP, growth on solid media means that the cells are mechanosensing the environment in someway which is affecting the way the FilP within the cell affects the phenotype of the cell. Although the mechanism of how this would occur is unclear.

FilPC and FilPT expressing cells observed after overnight growth on cellophane revealed that these were also capable of forming elongated cells (Figure 6.7.1) although preliminary results show that FilPN appeared to be similar to the control. This suggests FilPN is the only variant which did not have any effect on the cell morphology. This indicates that the production of the head and coil 1 of FilP is not responsible for the elongation phenomenon, though these preliminary results need confirming. The 2CC51 variant, though a small increase

in length was observed, did not form the extreme elongation seen with the other variants (Figure 6.9.1). This indicates that this 102 amino acid stretch of 51-mer repeats of coiled-coil from the coil 2 domain of FilP is not capable of producing this elongation on its own. Expression of 2CC51 had a dramatic effect on the morphology of the cells (Figure 6.9.1), even though the average length did not increase by much. The severe defects seen with this variant when expressed within *E. coli* cells indicates that this short fragment is likely to be interacting with proteins within the *E. coli* and interfering with the cell machinery and potentially interfering with the cell division and lateral growth mechanisms.

FilP-mCherry when expressed in *E. coli* was the only variant which elongated the cells but did not increase the width (Figure 6.8.1, Figure 6.10.1). This raises the possibility that the mCherry tag is interfering with the ability of FilP to increase the width of the cells, but not the width. Fluorescence microscopy of the mCherry tag revealed that, in the elongated cells, the FilP-mCherry signal and the chromosome stain alternated along the length of the cell (Figure 6.8.1).

The segmented pattern observed with the phase contrast microscopy was seen to differentiate between areas of phase bright and phase dark segments. Interestingly, lighter areas corresponded to patches where we found strong PI staining, indicating the presence of nucleic acids (Figure 6.3.2). On the other hand, phase dark areas coincided with patches where FilP mCherry accumulated (Figure 6.8.1). In cells expressing FilP which appeared segmented, areas where the chromosome was present sometimes appeared to be unhealthy (Figure 6.3.2D) and bulging as if about to burst while areas which did not stain for nucleic acids were not. This indicates that perhaps in the absence of FilP, the cell is not able to cope with this elongation and that it is only due to the internal cytoskeleton of FilP stabilising the cell wall that it is able to maintain intact.

The elongation of *E. coli* cells has been previously noted. Cells where there were physical constraints to growth resulted elongated cells to fill those microchambers without dividing (Takeuchi et al., 2005). Elongated cells have also been observed a number of times where the cell division proteins have been mutated in some way. Elongated *E. coli* cells have been observed in cells: with reduced concentrations of FtsZ (El-Hajj and Newman, 2015); FtsZ temperature sensitive mutants which elongate when grown at high temperatures; a *metK* mutant grows 2-4 times longer than normal cells, it stops dividing when slowly starved of S-

adenosylmethionine but continues to elongate and generates imperfectly segregated nuclei and no visible restriction (Newman et al., 1998); cell division mutants (strain MNR2 or *ftsZ84* mutants) made no septum at all and S-adenosylmethionine starved cells made partial septa incorporating FtsZ, ZipA and FtsA but continued to elongate (Wang et al., 2005); where the SOS response had been triggered due to DNA damage which generated large and non-viable cells with no width increase (Jones and Holland, 1984); and cells treated with the antibiotic aztreonam, which blocks division by inhibiting the FtsI protein which is involved in the formation of the septal ring, formed elongated cells which were large and non-viable (Wang et al., 2005). These are all indications that the elongation of the *E. coli* cells in these cases are due to the malfunctioning of the cell division machinery. A further elongated *E. coli* observation was reported with the same strain, BL21(DE3). Expression of the S-layer proteins (S-layer proteins cover the cell wall of many prokaryotes and are mostly comprised of protein and glycoprotein monomers (Bahl et al., 1997; Sára and Sleytr, 2000; Sidhu and Olsen, 1997)) of *Lysinibacillus sphaericus* JG-A12 generated elongated cells. As with the FilP variants described, a repeated pattern with the fluorescent microscopy indicated that the S-layer proteins had distinct gaps within the fluorescence pattern and that the DNA stain revealed that the chromosomal material lied within these breaks in expressed protein fluorescence (Lederer et al., 2011).

The fact that *E. coli* has been previously observed to form these elongated cells after interference with the cell division machinery indicates that, in these instances, the cells are able to elongate but not divide, which leads to the elongated cells. The introduction of the S-layer protein is of particular interest because it does not have any obvious interference with the cell division machinery. It has been suggested that the Gram-negative *E. coli* are incorporating this S-layer protein from the Gram-positive *L. sphaericus* into its own cell wall which is stabilising the cell and inhibiting division, though not all cells were observed to be long (Lederer et al., 2011) although this sounds unlikely. This is the only other example to my knowledge where introduction of a foreign protein into *E. coli* cells was observed to cause an elongation of the cell. However this experiment appeared to be conducted in liquid culture. The observed extreme elongation of FilP was not present in the liquid culture as presented in this chapter. Proteins are often expressed in *E. coli* for purification purposes, however, it would not be common practice to observe them under a microscope. *E. coli* is grown in liquid culture

for expression of proteins, so even if they were to be looked at microscopically, it would be unlikely that anyone would think to grow them on solid media. It is therefore possible that there are other proteins which have the same affect when grown on solid media which have been overlooked. However, experiments with *E. coli* cells expressing DivIVA and Scy (both proteins of the TIPOC from *S. coelicolor*) did not yield any elongated cells and they were comparable to the control (data not shown here). This indicates that these elongated cells on cellophane are likely to be directly linked to the expression of FilP. Given that FilP is involved with the polar growth of the cells within *S. coelicolor* and that the previously observed elongations involved disruption of the cell division machinery, it appears likely that FilP is interfering with this in someway and preventing cell division. Fluorescently tagged FilP in *Streptomyces* has been previously shown to be present in immature and still growing aerial hyphae but not in mature spore chains (Bagchi et al., 2008). This suggests that the disassembly of FilP is required for cell division to occur.

7 Characterisation of a *filP* knockout and localisation of FilP mCherry within *S. coelicolor*

7.1 Introduction

S. coelicolor exhibits a more complex life cycle than most other bacteria, as it does not divide by binary fission, but by filamentous growth. Initially, ovoid spores which contain a single chromosome begin to germinate and germ tubes are formed (Jyothikumar et al., 2008). These germ tubes contain multiple chromosomes and grow, by polarised growth, into a network of vegetative mycelium by tip extension and branching. Branching is essential for exponential growth of the hyphae as the rate of single tip extension is limited. In the vegetative mycelium, cell division does not occur. Mutants which are developmentally halted in this stage of development appear as shiny colonies and are termed 'bald mutants' (Flärdh and Buttner, 2009; McCormick and Flärdh, 2012). In response to lack of nutrients, aerial mycelium are formed by extension into the air (Kelemen and Buttner, 1998). Aerial mycelium grow as multi-genomic hyphae with less branching than in vegetative hyphae. Mutants which are developmentally halted in this stage appear as fuzzy white colonies and are termed 'white mutants'. Once growth has ceased, septa are placed at equal spacing along the hyphae with a single chromosome in each pre-spore compartment. This leads to unigenomic spores and the cycle starts again (Flärdh and Buttner, 2009) (Figure 1.15.1).

Polar growth, in bacteria, refers to the insertion of new cell wall material at the poles of the cell, as opposed to on the lateral walls. In *S. coelicolor*, the sites for polarisation are selected using positional markers, followed by recruitment of a complex assembly called the Tip Organising Centre (TIPOC). The TIPOC is a multiprotein assembly which is present at the tip of actively growing hyphae and orientates the cytoskeletal filaments (Holmes et al., 2013). There are three main proteins involved in the TIPOC: Scy, DivIVA and FilP. All three of these proteins have been implicated in growth and branching.

The final protein in the TIPOC is FilP which is an intermediate filament like protein. The *filP* gene lies directly downstream to that of *scy* and they are similar except FilP is smaller (311 amino acids) and has a differing role within the cell (Bentley et al., 2002; Walshaw et al., 2010). FilP was identified initially as a homologue for a protein in *Streptomyces reticuli* which had an

affinity to avicel, a crystalline form of cellulose. This led to the name AbpS (avicel binding protein) (Walter et al., 1998). It was then identified again when looking for proteins similar to Crescentin from *Caulobacter crescentus* which is responsible for the curvature of the organism. The protein was then characterised by its relationship to growth and cytoskeletal-like properties and so, its name was changed to FilP (filamentous intermediate-like protein) (Bagchi et al., 2008).

Strains lacking FilP have been observed to have a relatively mild phenotype. When grown on solid media, a FilP knockout has been seen to lag approximately a day behind a wild-type control in terms of when it sporulates (Bagchi et al., 2008). Microscopically, when grown on either solid media or in liquid culture, the hyphae of the FilP knockout mutant appeared much more meandering that the wild-type (Bagchi et al., 2008; Fröjd and Flärdh, 2019).

Localisations of FilP have produced some varying results. A FilP-EGFP fusion protein was used to observe its localisation in a *filP* knockout background as well as with a wild-type copy present (Bagchi et al., 2008). In the knockout background they observed prominent fluorescent filamentous structures in the vegetative hyphae. FilP was also observed in immature and still growing aerial hyphae but not in mature spore chains (Bagchi et al., 2008). With a copy of the wild-type *filP* expressed, the localisation of the FilP-EGFP fusion was seen to be different in that it was observed in nearly all tips of young hyphae as well as a tip distant regions (Bagchi et al., 2008).

Immunolocalisation revealed that during early growth nearly all hyphae fluoresced in the apical regions with the signal strongest just behind the tip where DivIVA signal appears (Fuchino et al., 2013; Javadi et al., 2019). Long cables were also observed asymmetrically along one side of the hyphae as well as sights of new branch points were marked by bright fluorescence. In hyphae which were no longer growing this apical gradient was replaced by a uniform intensity along the hyphae (Fuchino et al., 2013).

Localisation using a FilP mCherry fusion protein in *Streptomyces venezuelae*, with a wild-type copy of *filP* present showed that the localisation appeared to be irregular spots or patches along the hyphae with no distinct apical gradients (Fröjd and Flärdh, 2019). However, treatment with formaldehyde produced distinctive zones of fluorescence just subapical of the tips. The inference from this was that the handling of cells and interference with its growth

was a source of discrepancy between the results observed with immunofluorescence in comparison to those observed with non-fixed samples with fluorescent protein fusions (Fröjd and Flärdh, 2019).

Strains with only the *filP-EGFP* or *filP-mCherry* and no wild-type copy of *filP* displayed a *filP* knockout phenotype (Bagchi et al., 2008; Fröjd and Flärdh, 2019). However, strains with both the *filP* fusion gene and a wild-type copy displayed wild-type characteristics.

Aims

In this chapter a characterisation of the *filP* knockout mutant is presented along with a localisation study of FilP in *Streptomyces coelicolor* using mCherry, a constitutively fluorescent, monomeric, red fluorescent protein which is derived from *Discosoma sp*. (Shaner et al., 2004).

- Macroscopic analysis of colonies for the *filP* knockout strain will be compared to the M145 wild-type strain when grown on solid media with and without cellophane.
- Microscopic analysis of the *filP* knockout phenotype when grown with and without cellophane.
- Utilisation of a modified version of the REDIRECT© protocol (Gust et al., 2002), a PCR based approach to knock out gene function in *S. coelicolor*. Our experiment modifies this to fuse mCherry carboxy-terminally to FilP.
- Microscopic analysis of the FilP mCherry localisation with strains which carry a copy of *filP mCherry* as its lone *filP*, and a strain which carries a wild-type *filP* in addition to the *filP mCherry* fusion.

7.2 FilP knockout macroscopic phenotype

A *filP* knockout was previously generated (Holmes, 2012) using a modified REDIRECT© PCR-targeting system (Gust et al., 2002). The *filP* gene in the 8F4 cosmid was replaced with the apramycin resistance cassette (*aac(3)IV*). This was then moved into *S. coelicolor* by conjugation with *E. coli* (Holmes, 2012).

Initial observations of the colonies of the *filP* knockout compared to the M145 parent strain did not reveal any dramatic differences between the two. However, after growth on SFM for around six days around 38 percent of the colonies of the *filP* knockout strain appeared to have a split in them. After seven days every colony of the *filP* knockout strain had this characteristic split in them (Table 7.2.1, Figure 7.2.1). The M145 colonies can often be observed to have a slight crack or dip running through the centre of the colony, however very few of these colonies actually split. After 11 days growth on SFM, the M145 strain had only around 16% of colonies which split (Table 7.2.1). Apart from this distinctive splitting of the colonies, at the macroscopic level the *filP* knockout strain appears to grow at a similar rate to the M145 strain. Observations of colonies when grown on cellophane show that none split for either the M145 of *filP* knockout strain (Table 7.2.1).

Table 7.2.1 Percentage of split colonies for M145 and *ΔfilP* on SFM with and without cellophane (cello).

	4 days	6 days	7 days	8 days	11 days	13 days
M145 SFM	0%	0%	0%	0%	16%	16%
M145 SFM + cello	0%	0%	0%	0%	0%	0%
ΔfilP SFM	0%	38%	100%	100%	100%	100%
ΔfilP SFM + cello	0%	0%	0%	0%	0%	0%

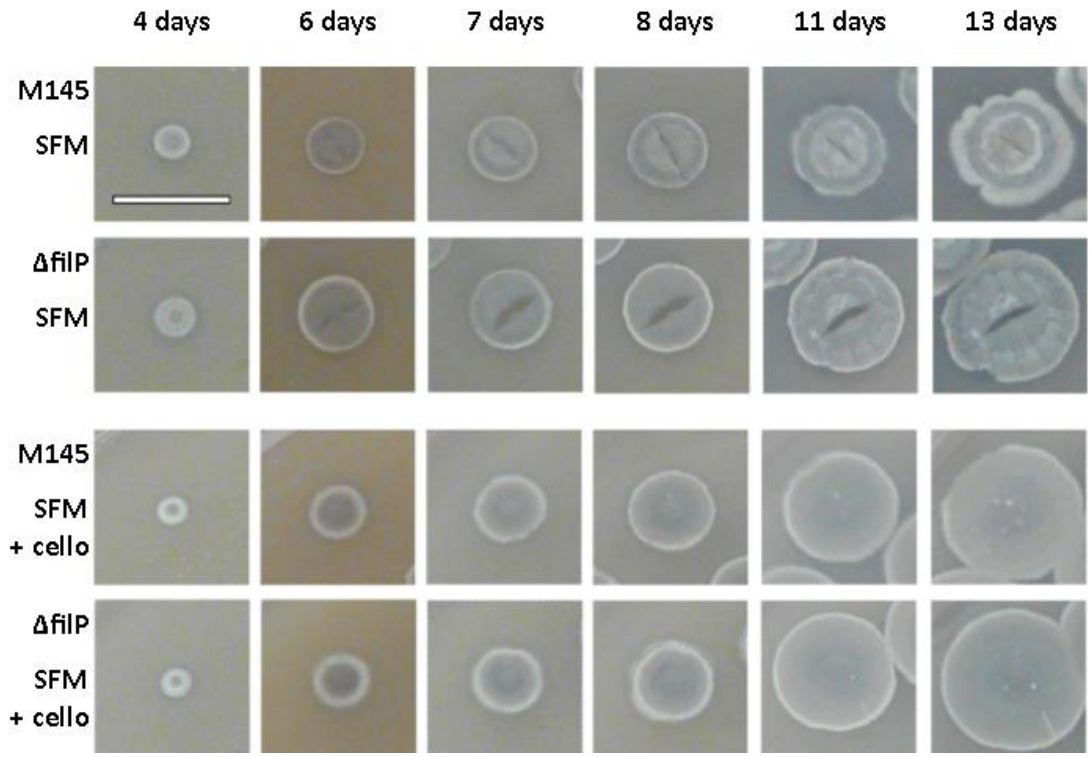

Figure 7.2.1 *filP* knockout and M145 colony development.

Colony development of M145 and *ΔFilP* strains on SFM with and without cellophane (cello). Scale bar 10 mm applies to all images.

Measurement of the diameters of the colonies revealed that *filP* knockout colonies were always more spread than the M145 equivalent colonies both with and without cellophane (Figure 7.2.2). It also shows that the colonies grown without cellophane are more spread for both strains at earlier growth times. Whereas at later growth times, colonies on cellophane are more spread. This is true for both the M145 and the *filP* knockout strain. For the M145 strain, the point at which the cellophane colonies overtake the SFM colonies in spread is at around seven days growth, which is earlier than the *filP* knockout colonies where this occurs after 8 days growth (Figure 7.2.2).

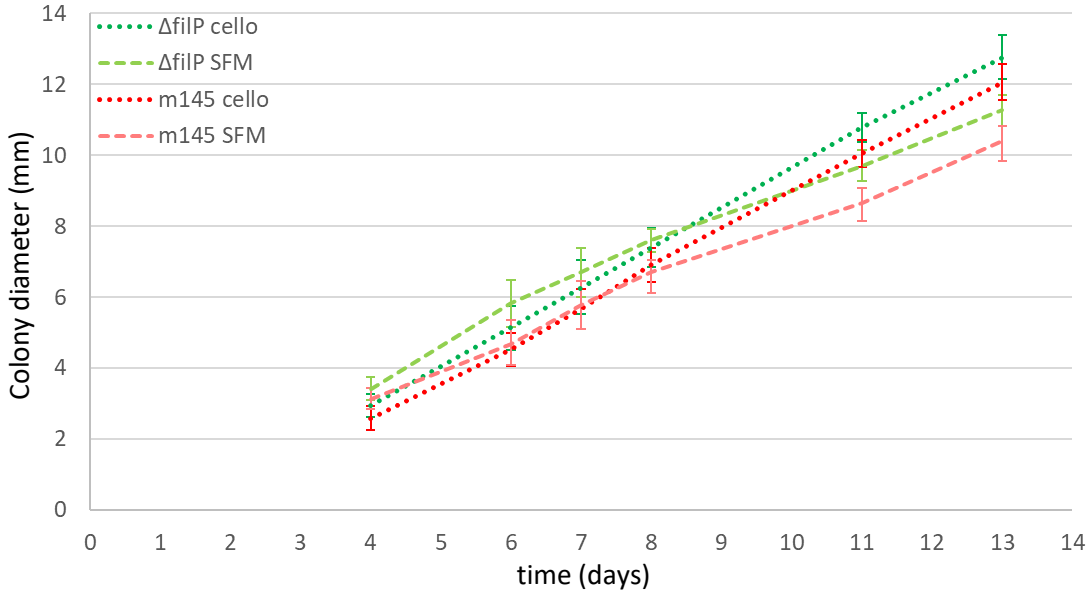

Figure 7.2.2 Colony spread for M145 and *filP* knockout strains.

Colony spread for M145 and *ΔfilP* strains with and without cellophane (cello). Colony spread as measured by the diameter of the colonies. Green dotted line *ΔfilP* strain on SFM and cellophane. Light green dashed line *ΔfilP* strain on SFM only. Red dotted line M145 strain on SFM and cellophane. Pink dashed line M145 strain on SFM only. Error bars standard deviation.

The macroscopic observations of the colonies indicate that the *filP* knockout strain is potentially less stable in its construction compared to the M145 strain. This is due to the splitting of all the colonies for the *filP* knockout strain compared to only a few for the M145 strain. It should be noted that the homologue of FilP, AbpS, from *S. reticulii* was shown to be able to bind to avicel. Both avicel and cellophane are forms of cellulose, so it might be possible that FilP is able to bind to the cellophane and causing some affect which we then see the difference too when FilP is absent. Colonies of the *filP* knockout strain were also observed to have a larger diameter than those of the M145 strain. This could be also due to a lack of stability within the colony as it spreads out farther rather than going down far into the medium or up into the air. However, in our hands, the *filP* knockout strain did not appear to have the around a day delay in sporulation as has been previously reported (Bagchi et al., 2008). Why this would be is unclear.

7.3 *filP* knockout microscopic phenotype

Microscopic visualisation of both M145 and the *filP* knockout strains revealed that there is a subtle difference between the strains when grown on SFM media and against a glass coverslip. The hyphae of the *filP* knockout strain appear to be much more meandering than in comparison to the M145 strain (Figure 7.3.1, Figure 7.3.2). The meandering nature of the hyphae appeared to persist in all stages of growth. Comparison of the DNA (as visualised by propidium iodine staining) and cell wall (as visualised by wheat germ agglutinin staining) between the two strains did not reveal any obvious distinctions (Figure 7.3.1, Figure 7.3.2).

In contrast, when these strains are grown on cellophane, the strains became indistinguishable (Figure 7.3.3). This is due to the hyphae of the M145 strain also being of a meandering nature. On cellophane both strains appear to meander equally. The DNA and cell wall staining here did also not reveal any obvious differences between the two.

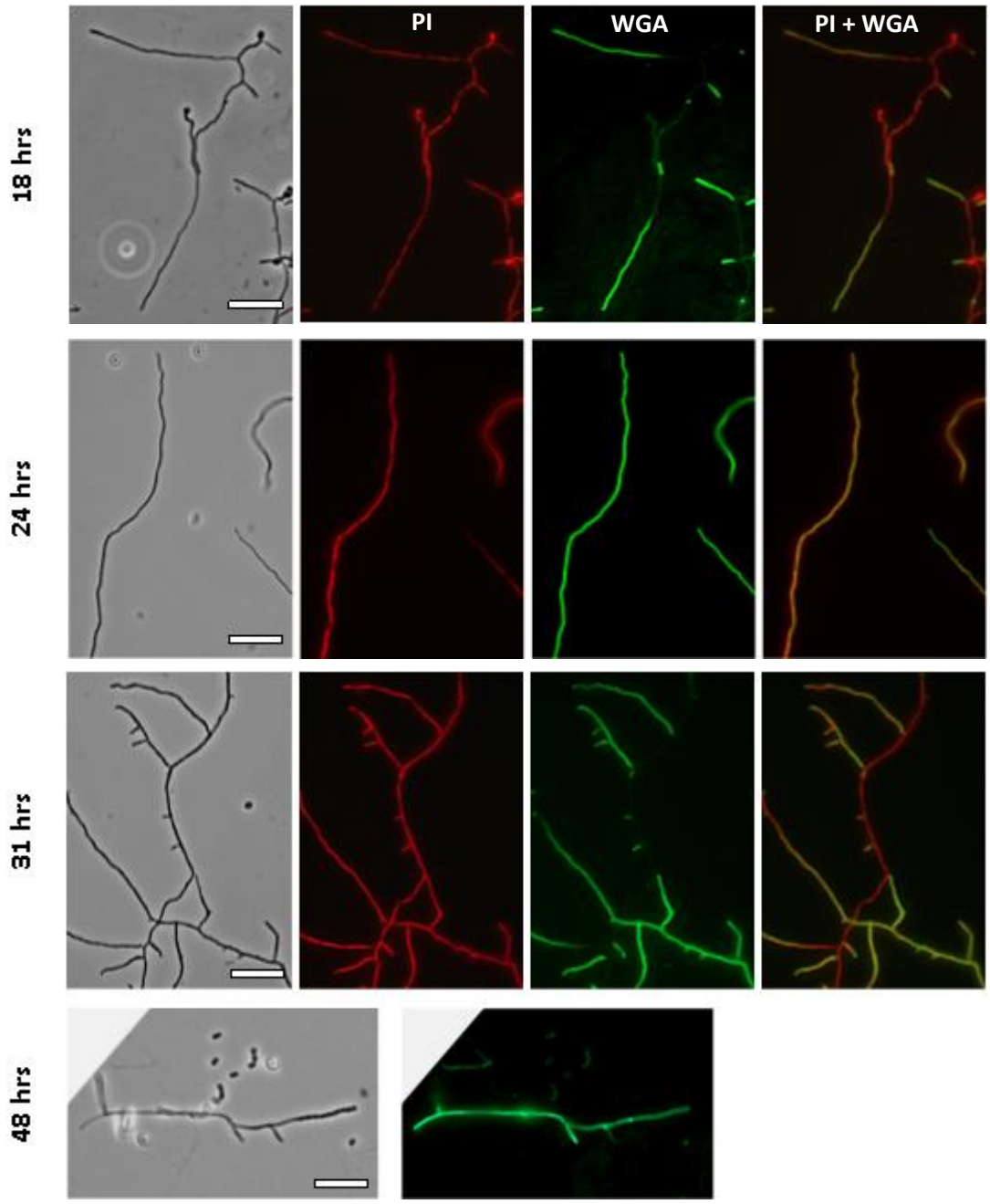

Figure 7.3.1 M145 strain grown against a glass coverslip.

M145 SFM coverslip microscopy. Development of the M145 strain on SFM against a glass coverslip. Phase contrast images (left), propidium iodide (PI) stain for chromosomal material (red), wheat germ agglutinin (WGA) stain for cell wall (green) and overlaid PI and WGA images (right). Scale bar represents 10 µm.

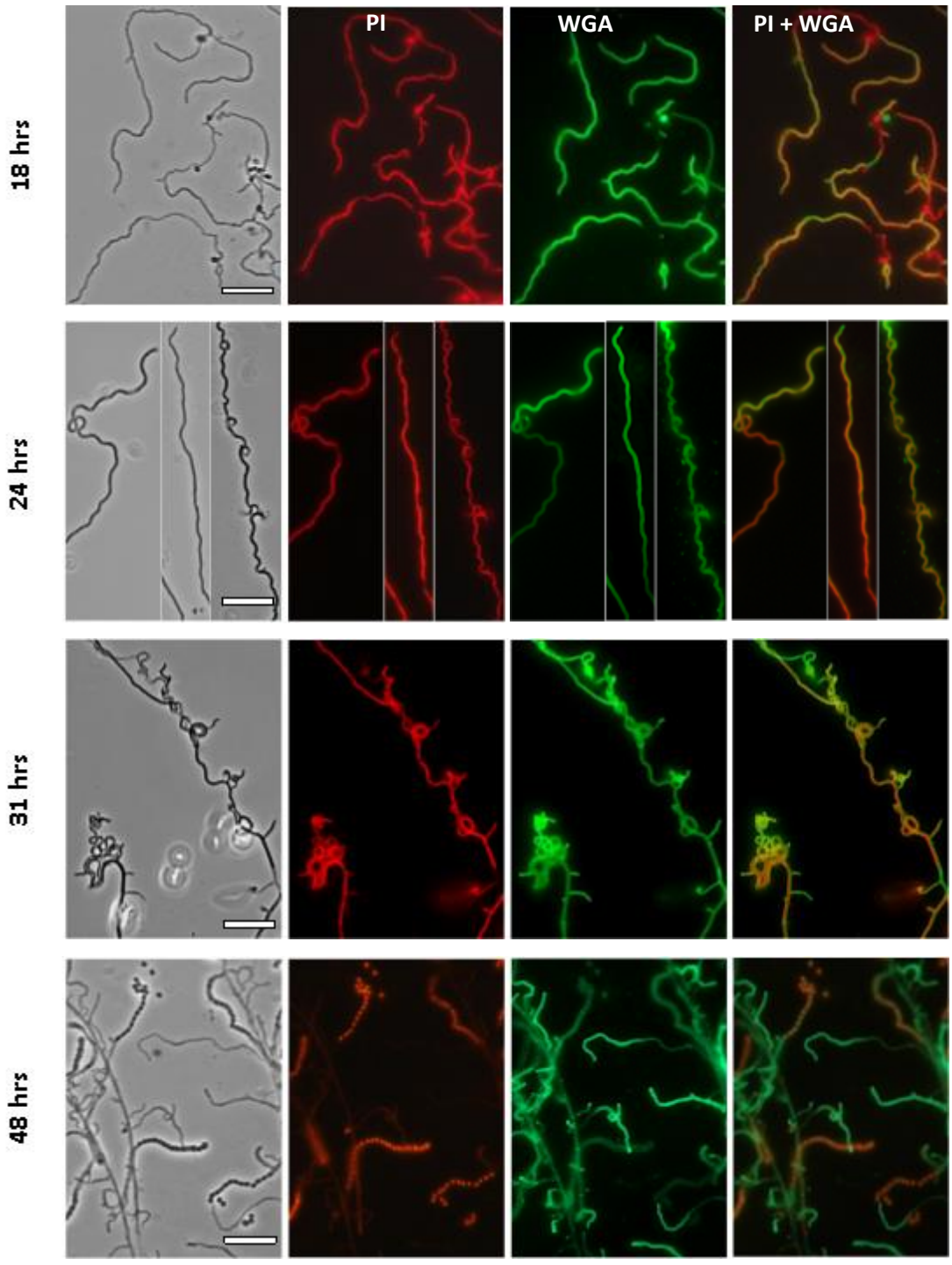

Figure 7.3.2 *filP* knockout strain grown against a glass coverslip.

ΔFilP SFM coverslip microscopy. Development of the *ΔfilP* strain on SFM against a glass coverslip. Phase contrast images (left), propidium iodide (PI) stain for chromosomal material (red), wheat germ agglutinin (WGA) stain for cell wall (green) and overlaid PI and WGA images (right). Scale bar represents 10 µm.

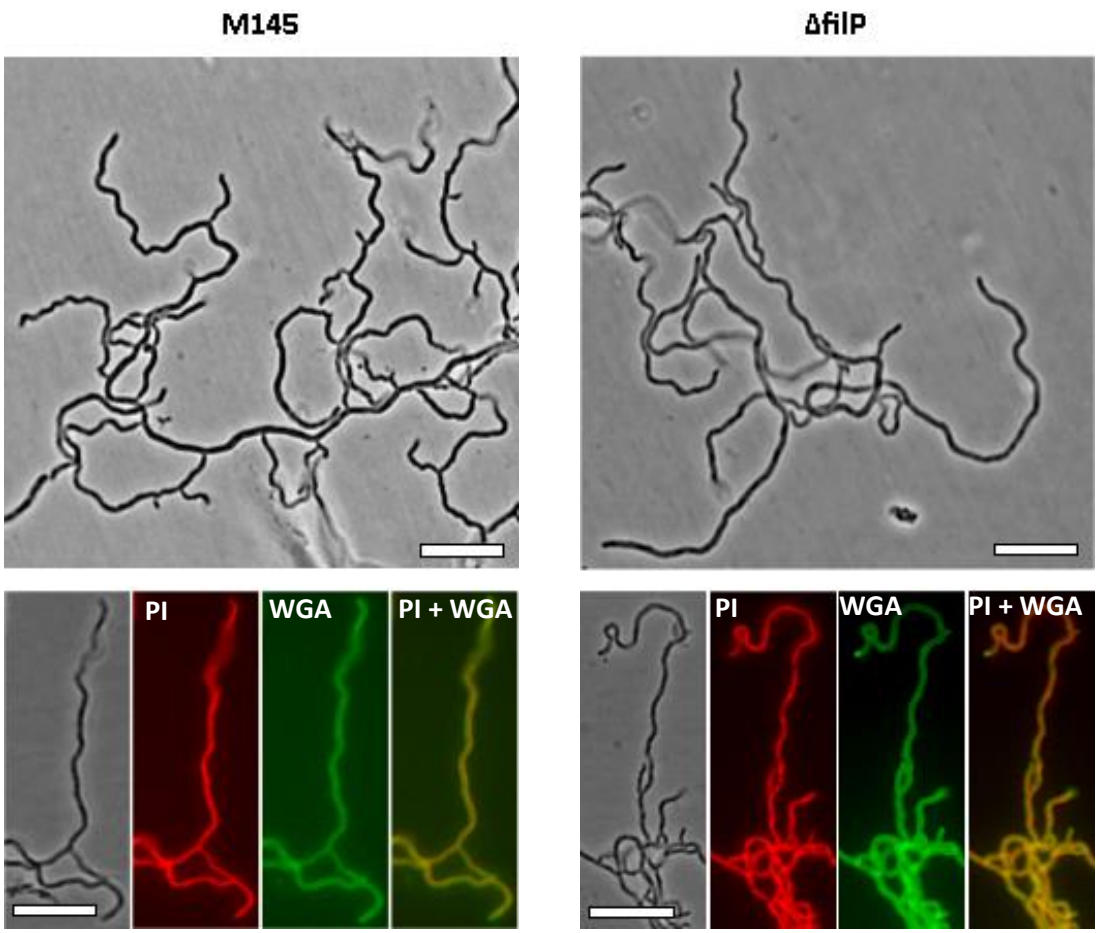

Figure 7.3.3 M145 and *filP* knockout strains grown on top of cellophane.

M145 and *ΔfilP* SFM cellophane microscopy. M145 and *ΔfilP* strains on SFM topped with cellophane. Phase contrast images (large image and bottom left for each), propidium iodide (PI) stain for chromosomal material (red), wheat germ agglu

The meandering nature of the hyphae for the *filP* knockout strain when grown on SFM with a coverslip is the same as the previously reported phenotype (Bagchi et al., 2008; Fröjd and Flärdh, 2019). This meandering nature also indicates that, perhaps, the hyphae are lacking some strength and stability. This implies that *filP* is fulfilling this role within the M145 strain and is stabilising the hyphae and allowing the hyphae to grow relatively straight. However, both the M145 and the *filP* knockout strain display this meandering phenotype when grown on cellophane. This raises the interesting possibility that *filP* is not providing stability within hyphae when it is on cellophane.

7.4 Generation of FilP mCherry knock-in construct in *E. coli*

To observe the localisation of FilP in *S. coelicolor*, a FilP mCherry translational fusion was created and expressed from its native location in the chromosome as the only copy of *filP* or in combination with a wild-type copy of *filP*. To express the *mCherry*, it was fused to the 3' end of the *filP* gene. This was done using an extended PCR cassette which allows the insertion of the *mCherry-ApraR* cassette at the 3' end of the gene via recombination (Figure 7.4.1). The inclusion of an apramycin resistance gene (*ApraR*) in the cassette allows for selection of the generated fusion.

The extended *mCherry-ApraR* cassette was generated by PCR using the primers FilP FP Pro NOV FRW and FilP FP KO REV in such a way that the product had 40 nucleotide extensions corresponding to the targeted genome location. The PCR product was analysed on a 0.7% agarose gel (Figure 7.4.2). The bright band in lane 4 and 5 corresponds to the 2.1 kbp PCR product corresponding to the extended mCherry cassette for targeting to the *filP* gene.

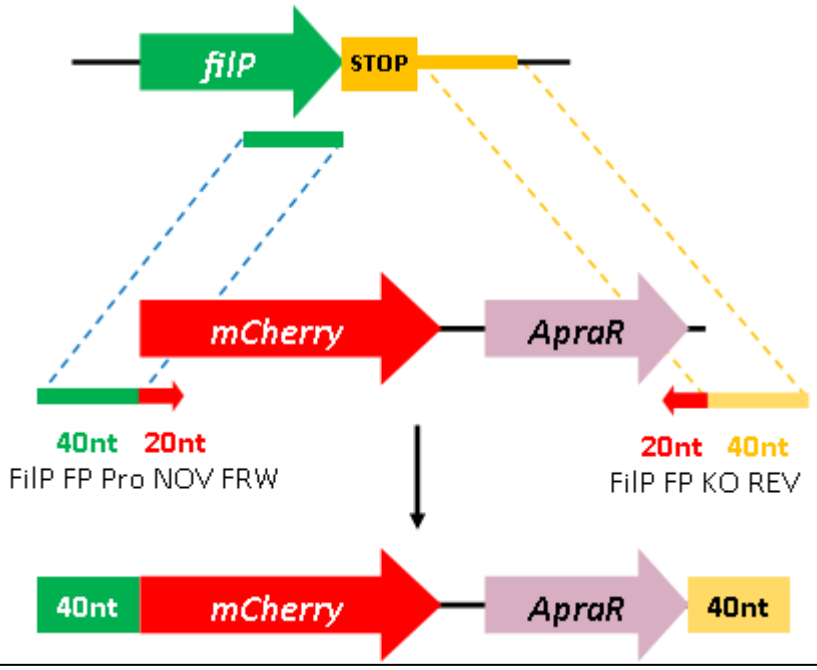

Figure 7.4.1 Design of the mCherry-ApraR cassette.

Design of the mCherry-ApraR cassette for delivering successful recombination at the 3' end of the *filP* gene. Primers FilP FP Pro NOV FRW and FilP FP KO REV containing sequences from both the *filP* and *mCherry-ApraR* cassette were used to generate an extended cassette.

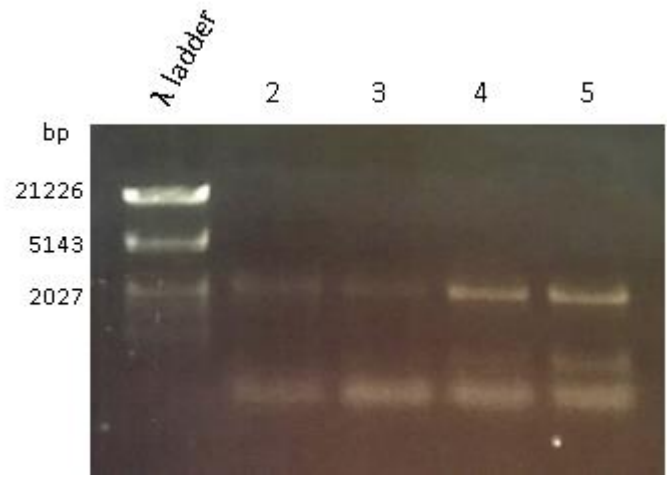

Figure 7.4.2 Gel electrophoresis of the mCherry-ApraR cassette with FilP localisation extension.

Lambda DNA digested with *Eco*RI and *Hind*III, sizes shown in bp. Lanes 2, 3, 4 and 5 replicates and show the FilP specific PCR cassette.

Once the extended *mCherry-ApraR* cassette targeted to the *filP* gene was obtained through PCR, it was electroporated into *E. coli* BW25113 cells which contained the 8F4 cosmid. The 8F4 cosmid contains the region of the *S. coelicolor* which encodes for FilP and nearby genes. Recombination between the 4 nucleotide overlap of the extensions to the cassette and of the corresponding regions at the 3' end of the *filP* gene in the 8F4 cosmid generated a *filP-mCherry* fusion. This was selected for by plating the *E. coli* cells on the LB containing apramycin. The cosmid DNA was extracted from one of these colonies displaying apramycin resistance, and subsequently digested using restriction enzymes *Eco*RI and *Xba*I to determine whether the *mCherry-ApraR* cassette was correctly inserted into the 3' end of the *filP* gene. Theoretical fragment lengths for the *Eco*RI/*Xba*I reaction were determined by constructing restriction maps of the 8F4 cosmid and the 8F4/*filP::filP-mCherry-ApraR* (Figure 7.4.3).

The gel image of the restriction digest of 8F4 cosmid and the 8F4/*filP::filP-mCherry-ApraR* with *Eco*RI and *Xba*I (Figure 7.4.4) confirm the successful incorporation of the *mCherry-ApraR* cassette onto the 3' end of the *filP* gene in the 8F4 cosmid. The gel image confirms three fragments for the 8F4 cosmid at 17417 bp, 7542 bp and 8914 bp. The fragments generated from the larger 8F4/*filP::filP-mCherry-ApraR* confirms that two of these fragments, 17417 bp and 7542 bp, seen in 8F4 remain unchanged. However the 8914 bp fragment seen with the 8F4 cosmid is no longer present in the 8F4/*filP::filP-mCherry-ApraR* cosmid and is replaced by

three different fragments. The smaller 2644 bp and 1301 bp fragments are indicated with red arrows to aid detection. The 7063 bp fragment however runs together with the 7542 bp fragment which is in both the 8F4 cosmid and the 8F4/*filP::filP-mCherry-ApraR* cosmid. However this band is brighter in the 8F4/*filP::filP-mCherry-ApraR* than with the 8F4 cosmid and indicates that this fragment is indeed present within this band. The presence of these bands within the 8F4/*filP::filP-mCherry-ApraR* when digested with *Eco*RI and *Xba*I suggests that the cassette was successfully inserted in the correct location.

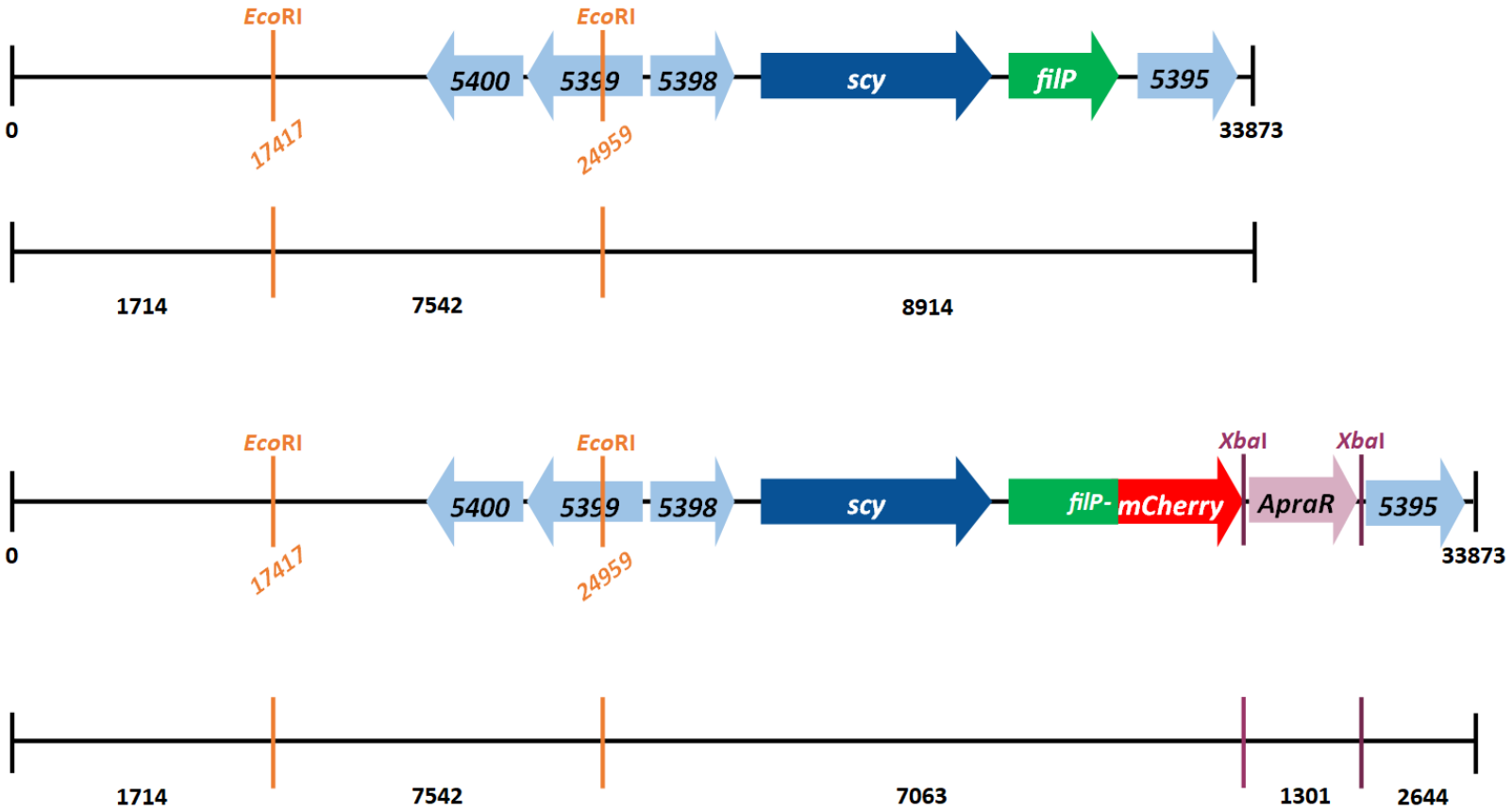

Figure 7.4.3 Restriction maps of the 8F4 cosmid and the 8F4/filP::filP-mCherry-ApraR cosmid.

Restriction maps of the 8F4 cosmid and the 8F4/filP::filP-mCherry-ApraR cosmid. Cosmid drawing is not to scale. *Eco*RI restriction sites are marked with orange dashes, with position (in bp) given. *Xba*I restriction sites are marked with purple dashes. Fragment sizes of *Eco*RI/*Xba*I double digest presented in map B in bp.

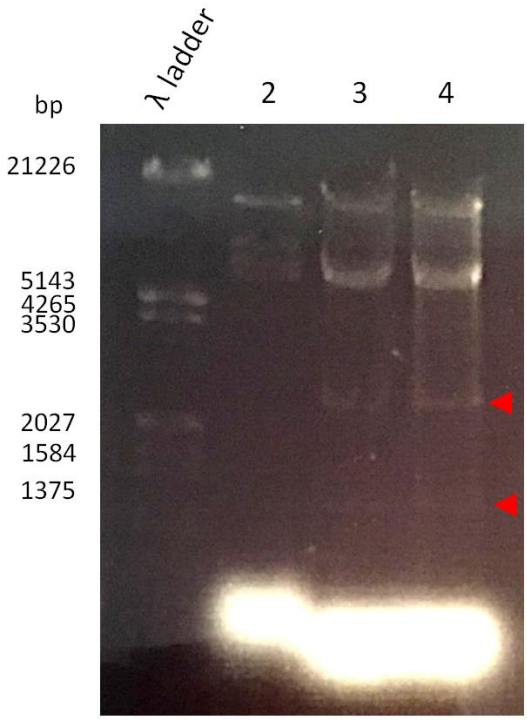

Figure 7.4.4 Restriction digest of 8F4 cosmid and the 8F4/*filP::filP-mCherry-ApraR* with *Eco*RI and *Xba*I.

Restriction digest of 8F4 cosmid and the 8F4/*filP::filP-mCherry-ApraR* with *Eco*RI and *Xba*I. 8F4 cosmid (lane 2) and 8F4/*filP::filP-mCherry-ApraR* (lanes 3 & 4). Ladder is lambda DNA digested with *Eco*RI and *Hind*III with fragment sizes given in bp. Red arrows show position of 2644 bp and 1301 bp bands.

The 8F4/*filP::filP-mCherry-ApraR* cosmid was subsequently transformed into *E. coli* ET12567 using electroporation. *E. coli* ET 12567 is methylation deficient and was used to move the cosmid DNA into *S. coelicolor* M145 by conjugation. Two possible recombination events were possible within the exconjugants. The single crossover events would result in the bacterium possessing the *filP mCherry* gene along with another copy of the wild-type 8F4 cosmid. These colonies would display resistance to both apramycin and kanamycin. Double crossover events would result in the bacterium possessing only the *filP mCherry* gene. These colonies would only display resistance to apramycin. Replica plating onto LB containing nalidixic acid and kanamycin as well as onto LB containing nalidixic acid and apramycin was used to determine colonies which were single or double crossovers. Nalidixic acid was included to kill *E. coli* cells after conjugation. Spores were collected from both types of crossover. Both single and double crossover colonies appeared wild-type in appearance and both types where characterised using microscopy.

7.5 Microscopic localisation of FilP mCherry in the wild-type strain

Both the double crossover and single crossover strains of *S. coelicolor* M145/ *filP:: filP-mCherry-ApraR* were used to monitor the localisation patterns of FilP mCherry throughout the life cycle of *S. coelicolor*. Spores of these strains were inoculated onto SFM media and microscopy slides were inserted at an approximate 70° angle to the top of the media. Samples were grown at 30°C before fixing with methanol and staining with WGA (wheat germ agglutinin) which stains for the cell wall. Samples were visualised during different stages of development.

The first sample was taken after 18 hours growth to allow visualisation of FilP mCherry localisation during early vegetative growth (Figure 7.5.1, Figure 7.5.2). For both the single and double crossover strains, the FilP mCherry is present throughout the length of the hyphae with patches of brighter fluorescence. The spore from which these germinated has a bright FilP mCherry fluorescence as does a patch located just behind the hyphal tip.

A second sample was taken after 24 hrs to assess the FilP mCherry localisation during vegetative growth and branching (Figure 7.5.1, Figure 7.5.2). This revealed that FilP mCherry was localising in patches along the length of the hyphae. Here, there did not appear to be a brighter patch just behind the hyphal tip in most cases. This is true for both the single and double crossover strains. However, there was more variation in fluorescence intensity with the double crossover strain, in that some hyphae appeared to have much brighter fluorescence than others. The single crossover strain appeared much more uniform in that respect.

A third sample was taken after around 32 hours to visualise the FilP mCherry localisation in aerial hyphae prior to septation and sporulation (Figure 7.5.1, Figure 7.5.2). For both double and single crossover strains the aerial hyphae revealed to have patches of fluorescence along the length of the hyphae. There often appeared to be a particularly bright patch of fluorescence immediately behind the hyphal tip. A final sample was taken after 48 hours to localise FilP mCherry in hyphae undergoing septation and sporulation (Figure 7.5.1, Figure 7.5.2). In both the single and double crossover strains, FilP mCherry was present between septa as well as in spores.

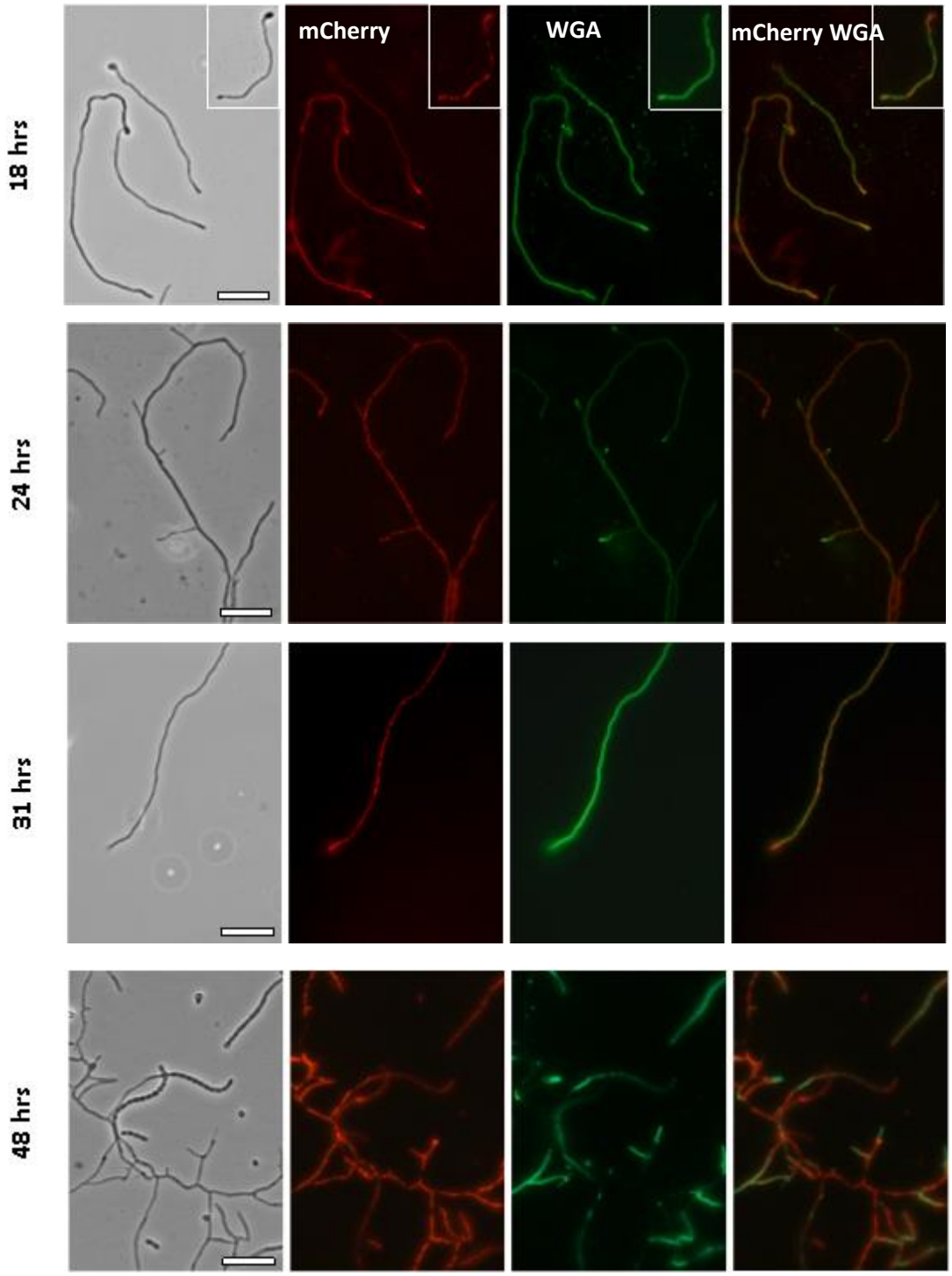

Figure 7.5.1 Monitoring FilP mCherry localisation in a single crossover strain.

Single crossover strains of *S. coelicolor* M145/ *filP:: filP-mCherry-ApraR* grown on SFM next to a glass coverslip. Phase contrast images (left), FilP mCherry (red), wheat germ agglutinin (WGA) stain for cell wall (green) and overlaid PI and WGA images (right). Scale bar represents 10 µm.

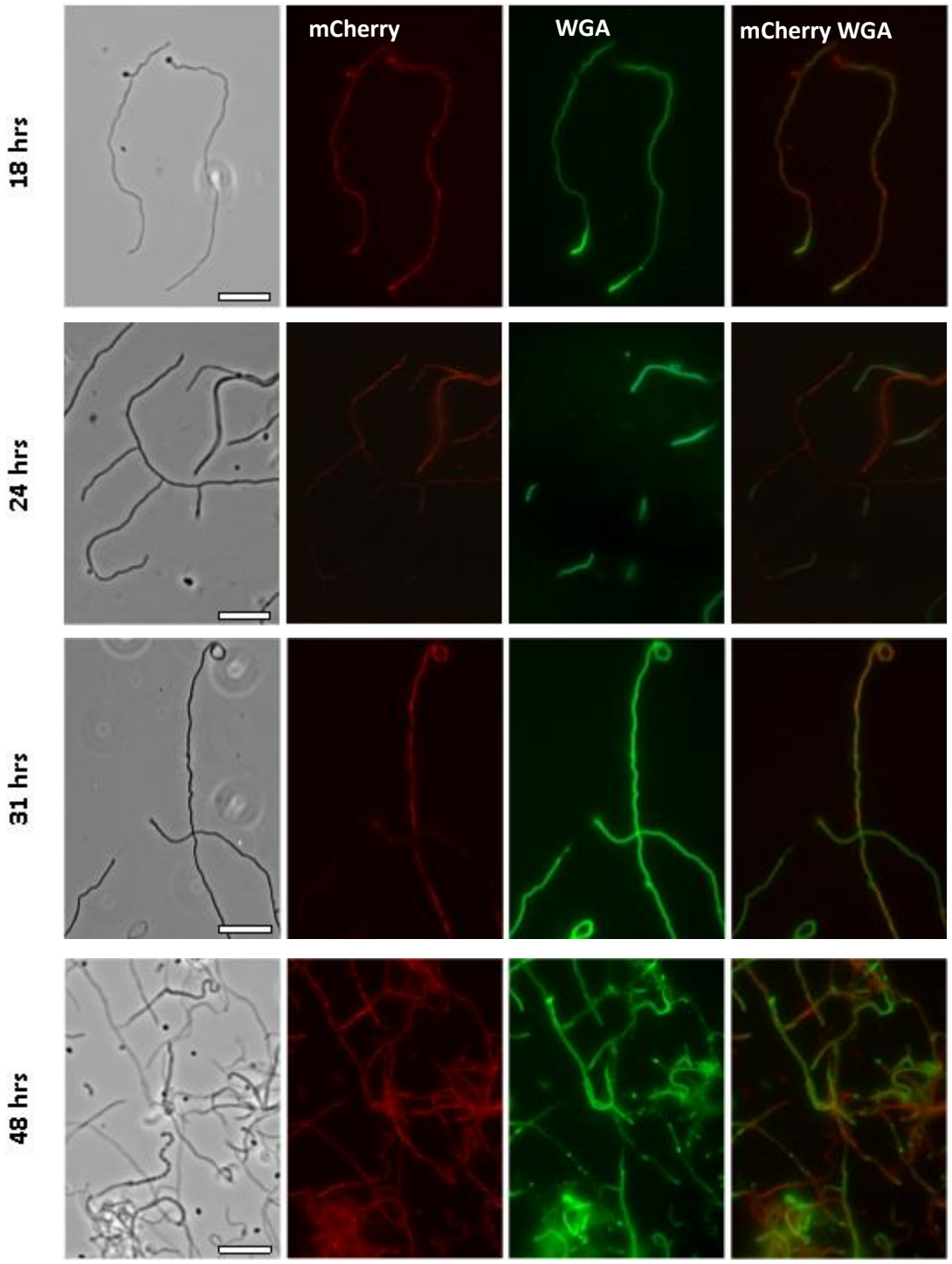

Figure 7.5.2 Monitoring FilP mCherry localisation in a double crossover strain.

Double crossover strains of *S. coelicolor* M145/ *filP:: filP-mCherry-ApraR* grown on SFM next to a glass coverslip. Phase contrast images (left), FilP mCherry (red), wheat germ agglutinin (WGA) stain for cell wall (green) and overlaid PI and WGA images (right). Scale bar represents 10 µm.

Comparison of the single crossover (Figure 7.5.1) and double crossover (Figure 7.5.2) strains revealed that they both show very similar localisation patterns for each stage of development. However, the double crossover strain, which only contains FilP mCherry and no wild-type copy, had slightly patchier fluorescence that the single crossover strain, which also contains a wild-type copy of FilP. The fluorescence of the double crossover also had more variations in the fluorescence strength between hyphae where the single crossover appeared more consistent. The appearance of the hyphae for the single crossover appeared like that of the wildype. However, the hyphae for the double crossover appeared to be more meandering than the wild-type. This meandering was in a similar way to that of the FilP knockout however was not as strong. It appears to be between the wild-type and the complete knock out. This indicates that the addition of the mCherry to the c terminal of the protein could be partially blocking the function of FilP in some way.

When both the double and single crossover strains of *S. coelicolor* M145/ *filP:: filP-mCherry-ApraR* were grown on cellophane (Figure 7.5.3), the localisation of FilP mCherry appeared quite different from those observed when grown against a glass coverslip. When grown on cellophane the localisation patterns of the single and double crossover strains were very similar to one another (Figure 7.5.3). However, this pattern was quite different to that observed on the coverslip. Here the pattern is that there are very bright spots of FilP mCherry localisation which are very punctate, and the rest of the hyphae does not appear to contain FilP mCherry. The localisation of these points does not appear to be at any particular place along the hyphae. Very few of the hyphae have FilP mCherry localisation just behind the hyphal tip.

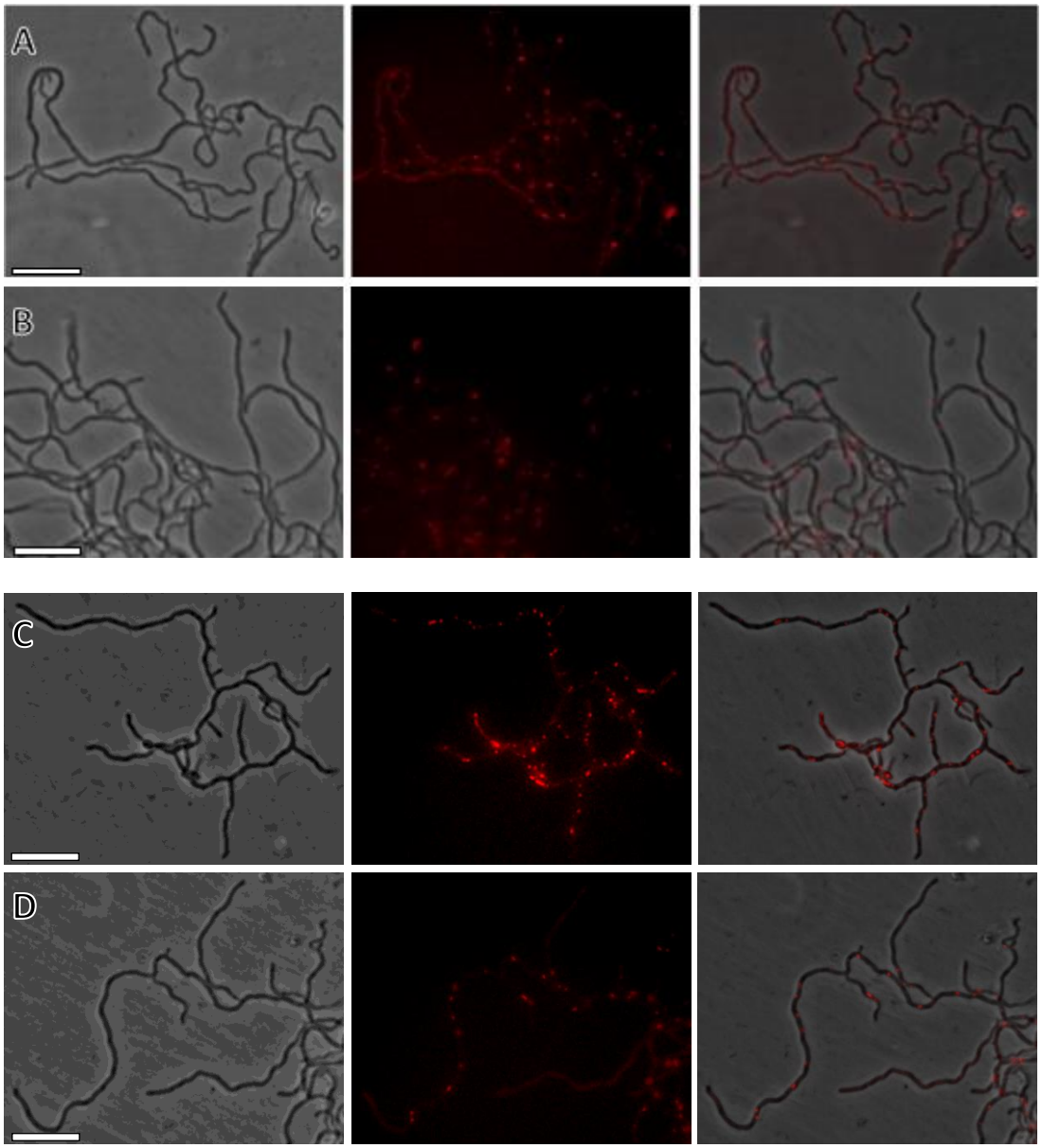

Figure 7.5.3 Monitoring FilP mCherry localisation in double and single crossover strains when grown on cellophane.

Double **(A)**, **(B)** and single **(C)**, **(D)** crossover strains of *S. coelicolor* M145/ *filP::filP-mCherry-ApraR* grown on SFM with cellophane. Phase contrast images (left), propidium iodide (PI) FilP mCherry (red) and overlaid PI and phase contrast images (right). Scale bar represents 10 µm.

The distinct difference in patterning of FilP mCherry localisation between coverslip and cellophane growth indicates that there is likely to be a difference in expression of FilP dependant on the substrate surface. The localisation with the coverslips appeared along most of the length of the hyphae, even if it was patchy in places. When grown on cellophane, the

patterning is much more confined to distinct points and is not present along the length of the hyphae. This knowledge, combined with the meandering phenotype observed on cellophane, indicates that FilP is not utilised by the hyphae to strengthen it and allow it to grow straight when grown on cellophane. Although, that there are discrete patches of FilP mCherry localisation when grown on cellophane indicates that FilP is still present in the hyphae at least in a small quantity when growing on cellophane.

Localisation of FilP mCherry within our strains did not reveal the same apical focused localisation which has previously been observed (Bagchi et al., 2008; Fröjd and Flärdh, 2019; Fuchino et al., 2013; Javadi et al., 2019). However, this was often observed with fixation with formaldehyde. When cells were viewed without formaldehyde fixation the localisation appeared as irregular spots or patches along the hyphae with no distinct apical gradients (Javadi et al., 2019) which was much like what was observed here. Our fixation of cells with methanol does not appear to have the same affect which the formaldehyde fixation was observed to have. Our methanol fixation and staining did not appear to alter the FilP mCherry localisation compared to cells viewed without.

Comparison of the hyphae of the single and double crossover versions of the strain *S. coelicolor* M145/ *filP:: filP-mCherry-ApraR* shows that the double crossover meanders when grown against a coverslip. This is in a similar way to that observed for the FilP knockout strain, although it is not as severe in the double crossover. This indicates that the double crossover (which contains only a FilP mCherry version of FilP) is not likely to be fully functional and the mCherry tag is affecting the ability of FilP in some way. That it is not as bad as the knockout phenotype indicates that it is only impairing its ability rather than abolishing its functionality completely. The single crossover version contains both a FilP mCherry version of FilP as well as a wild-type version. This strain appears like the M145 wild-type and the inclusion of a wild-type FilP appears to be allowing the hyphae to behave in a wild-type manor despite the presence of FilP mCherry. Comparison of the localisation patterns of the single and double crossover shows that they are very similar with only some mild differences in the consistency of brightness of fluorescence with the double crossover being patchier.

8 Discussion

8.1 FilP as an Intermediate Filament

Domain organisation of FilP

Eukaryote intermediate filaments are defined by six criteria: intermediate filaments can self-assemble into higher order structures without the requirement for cofactors; intermediate filaments have a tripartite structure with a head and tail domain flanking a central rod domain; the rod domain is coiled-coil in nature; the rod domain is 310 or 350 amino acids for a cytoplasmic or nuclear intermediate filament respectively; the rod domain consists of three sub-domains; and the coil 2 subdomain contains a characteristic stutter.

FilP fulfils the first three requirements. It has been shown to self-assemble into higher order structures without the requirement for cofactors (Figure 3.3.2, Figure 3.3.12), it has a tripartite structure with head and tail domains flanking the central rod domain and this rod domain is coiled-coil in nature. However, FilP has a slightly shorter rod domain of only 270 aa. Current sub-domain assignment (Walshaw et al., 2010) also suggests that FilP has two sub-domains, and not three (Figure 1.10.1). However, our assignments of heptad and hendecad repeats (Figure 8.1.1) suggested that there is a potentially non coiled-coil motif in the centre of coil 2 which could in fact be a second linker. Only further structural studies will establish the exact sub-domain organisation of FilP. The last criteria of an intermediate filament, the inclusion of a stutter in the middle of coil 2 sub-domain, is difficult to assess due to the many hendecad repeats in the coil 2 subdomain of FilP. Overall, FilP appears to largely fit with the definition of eukaryotic intermediate filaments but does fall short of the strict length characteristics.

Comparison of the Higher Order Structures of FilP to those of Eukaryotic Intermediate Filaments

Comparison of FilP to established intermediate filaments in their higher order structures revealed that FilP was able to form the rope like structure (Figure 3.3.2) which resemble that of the eukaryotic intermediate filaments such as vimentin after 1 hour in assembly buffer (Herrmann and Aebi, 2004; Figure 1.7.2). This rope structure has been shown

here for the first time, as previous studies demonstrated striated and lace structures (Bagchi et al., 2008; Fuchino et al., 2013; Javadi et al., 2019). The average width of eukaryote intermediate filament rope structures is around 10 nm (Herrmann and Aebi, 2004) which is comparable to the 15.5 nm rope width we observed of FilP in 50 mM Tris pH7.0 (Figure 3.3.7). This indicates that FilP is similar to eukaryotic intermediate filaments and can form similar higher order associations generating rope filaments supporting the idea that FilP is an intermediate filament like protein.

The striated structure that was also observed (Figure 3.3.12) which resembles that of the 'paracrystaline' structure observed for the type V intermediate filaments (lamins) (Figure 1.7.2). Lamins are able to form both the rope and striated structures. This further lends itself to the idea that FilP is an intermediate filament like protein and that it is potentially more like members of the lamin family than the other, cytoplasmic, intermediate filaments.

A further higher order structure, a lace-like structure has been observed before when FilP was dialysed slowly against 50 mM Tris pH7.0 (Fuchino et al., 2013). However, we observed a much less defined lace structure in 50 mM Tris pH8.0 and pH8.5 (Figure 3.3.3), but not in pH7.0. We also observed a lace like structure which appeared more defined with visible nodes and protein linking between them with the FilP variants FilPC and FilP Δlinker (Figure 5.3.2, Figure 5.4.3). This lace structure is so far unique as it has not been observed for any eukaryotic intermediate filament protein.

That FilP is able to form higher order structures that greatly resemble those generated by eukaryotic intermediate filaments adds to the argument that FilP is an intermediate filament like protein. In addition, FilP can also form a lace/ interconnected network structure which has not been observed for intermediate filaments.

Comparing Essential Regions of Intermediate Filaments to FilP

For vimentin and lamin, motif that are essential for the formation of higher order structures have been assessed to be the first four heptad repeats of the coil 1 subdomain and the last five heptad repeats of the coil 2 subdomain (red boxes, Figure 8.1.1). These regions have conserved amino acid sequences across intermediate filaments (Kapinos et al., 2010;

Köster et al., 2015). Our analysis of FilP variants revealed that the entire coil 1 subdomain was not essential for the formation of higher order structures as FilPC (lacking coil 1) was able to form some striated structures and a lace network as well as large, unstriated structures. The somewhat lower propensity for striated structures may indicate that the coil 1 subdomain aids lateral assembly in FilP. This is in contrast to that of vimentin and lamin where an essential region is located in the first four heptad repeats of the coil 1 subdomain (Figure 8.1.1; Kapinos et al., 2010; Köster et al., 2015). This is a discrepancy between that found for vimentin and lamin and that of FilP. The second essential region of vimentin and lamin for higher order assemblies is found at the C terminus of the rod domain (Figure 8.1.1; Kapinos et al., 2010; Köster et al., 2015). The final five heptad repeats of the coil 2 subdomain of vimentin and lamin are essential. This corresponds to the C terminus of the coil 2 of FilP (Figure 4.2.1). We found that FilP Δ4x7 variant was no longer able to form the characteristic striation observed with wild-type FilP (Figure 5.5.3). Instead, FilP Δ4x7 formed large structures which lacked definition and an occasional striated section where this striation had a shorter unit length than wild-type FilP (Figure 5.5.2). This indicates that the final four heptad repeats of FilP are also essential for the formation of the wild-type higher order assemblies although their absence still allowed assemblies of different morphology. With further deletion of the two hendecad repeats adjacent to the four heptads as well, the ability of the FilP Δ4x7 2x11 variant to form any type of higher order assembly was completely abolished. This suggests that the final four heptads and the final two hendecad repeats, are essential for the ability of FilP to form higher order structures. This region corresponds to the region identified as essential in both vimentin and lamin (Figure 8.1.1) and strengthens the argument that FilP is an intermediate filament like protein.

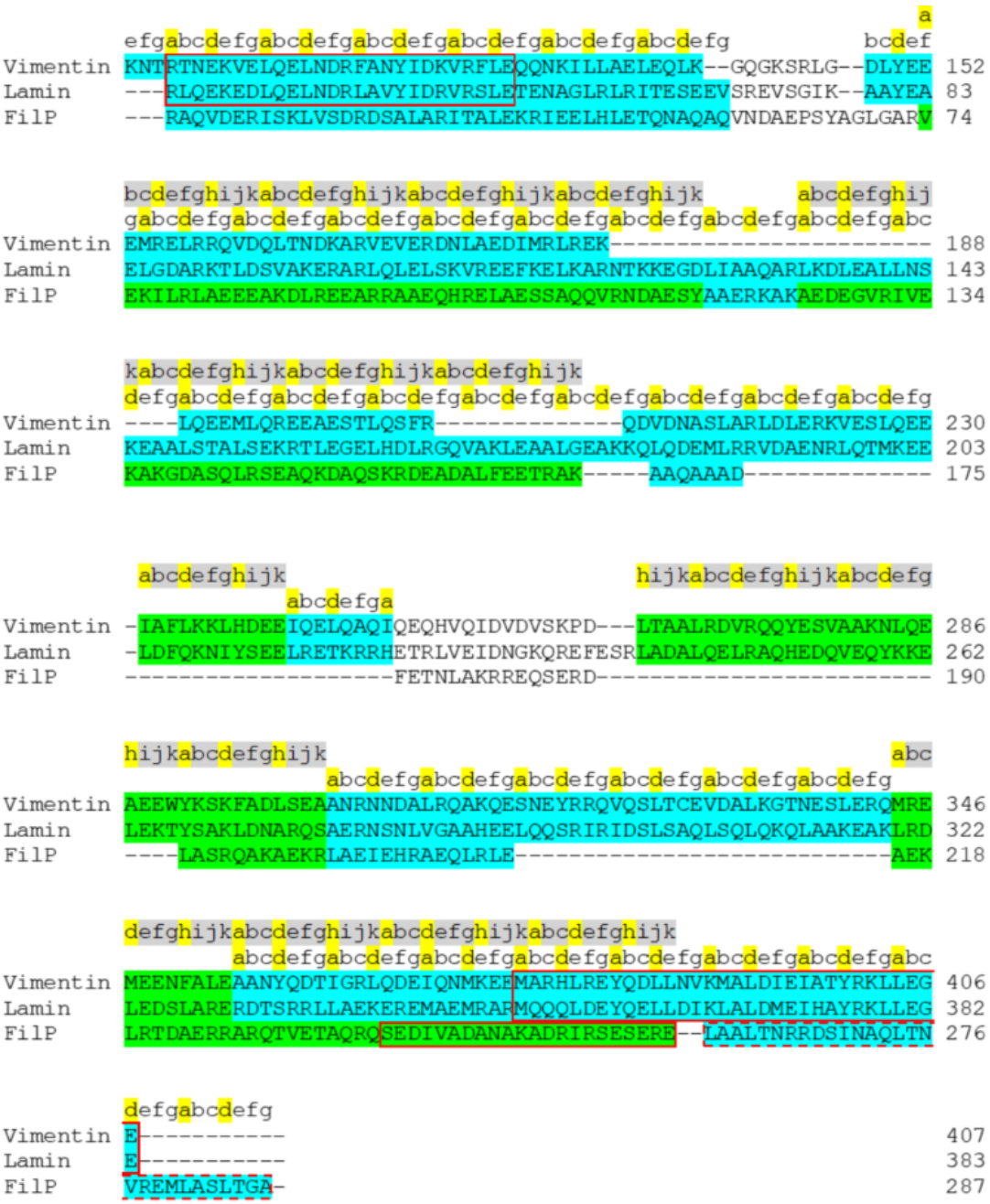

Figure 8.1.1 Sequence alignment of vimentin (*Mus musculus*), lamin (*Homo sapiens*) and FilP(*Streptomyces coelicolor*) rod domains.

Top line (grey highlight) hendecad repeat lettering. Second line heptad repeat lettering. Blue highlight heptad repeat, green highlight hendecad repeat, yellow highlight hydrophobic positions. Head and tail domain sequences are not shown. Heptad and hendecad motifs assigned to vimentin and lamin as designated by Chernyatina et al (A. a Chernyatina et al., 2015). Red boxes on vimentin and lamin indicate areas of highly conserved residues (Kapinos et al., 2010; Köster et al., 2015). Solid red box on FilP indicates area thought to be essential for the formation of higher order structures. Red dashed box on FilP indicates area which is thought to aid the higher order assembly, though it is not strictly essential for higher order structures to form, it is essential for the regular striated pattern normally seen with FilP in 50 mM Tris pH7.0. Uniprot number vimentin: P20152, lamin: W8QEH3.

Comparison of the different FilP variants we have studied to those generated for the intermediate filaments vimentin and lamin as well as the bacterial intermediate filament crescentin, corresponding deletions had very similar affects on their ability to generate higher order assemblies. Vimentin that lacked the tail domain was able to form ropes like the wild-type but its cellular localisation was affected (Rogers et al., 1995). A tail-less variant of lamin formed striated structures and ropes like the wild-type but with a higher propensity to form ropes (Heitlinger et al., 1992; Sasse et al., 1997). A tail-less variant of crescentin formed structures like wild-type but its cellular localisation was affected (Cabeen et al., 2011). Here we showed that tail-less FilP formed assemblies with striated patterns which were indistinguishable from those formed by FilP suggesting that the tail domain is not essential for the formation of higher order assemblies of FilP, vimentin, lamin or crescentin. Headless variants of lamin showed an ability to form the striated structure but not the rope (Heitlinger et al., 1992, 1991; Karabinos et al., 2003; Sasse et al., 1997; Stuurman et al., 1996). Removal of the head domain in crescentin showed ropes which were able to form *in vitro* but were not observed *in vivo* (Cabeen et al., 2011, 2009). The *Streptomyces* FilPC variant lacked the head domain as well as the coil 1 subdomain. Although FilPC and the other headless variants are not directly comparable due to the extra deletion of coil 1, FilPC was still able to form striated structures and no rope was observed as was seen for lamin. The head and tail domains of lamin were not important for the formation dimers and of the striated structure, although the head domain was essential for the formation of rope structure (Heitlinger et al., 1992, 1991; Karabinos et al., 2003; Sasse et al., 1997; Stuurman et al., 1996). This is very similar to what we observed although it should be noted that no rope structure was observed for any of the FilP variants generated. However, rope structures of FilP were observed only at aa specific pH and most of the FilP variants have different pIs so it is conceivable that the buffer condition used for the FilP variants never mimicked the same condition that was the 50 mM Tris pH7.0 buffer for FilP. Despite this, comparison of our variants of FilP and those of vimentin, lamin and crescentin share similarities and indicate that they may behave in a similar way.

8.2 A New Proposed Orientation of FilP in the Different Higher Order Assemblies

An assembly of FilP into the higher order striated structure has been proposed by (Javadi et al., 2019). They propose a head to head assembly of FilP dimers which allow assembly into higher order structures with the coil 1 subdomains approximately overlapping each other with a further overlap at the C terminus (Figure 8.2.1). First, I have adopted their model including the detailed domain organisation of FilP. Whilst our data is consistent with a head to head assembly, however, our data does not support the model that is presented for several reasons. The primary reason why this assembly is not possible is that we found FilPC, which lacks the head domain and coil 1 subdomain (Figure 5.3.1), to still be able to form striations and lace structures which have the same unit length as that of FilP (Figure 5.3.2, Figure 5.3.3). This indicates that the coil 1 subdomain I does not directly control the unit length of the striated pattern. Also, removal of the linker subdomain would result in shortened unit length according to the model by Javadi et al., 2019. However, this is not the case as the FilP Δlinker variant generated striated patterns with a longer unit length than that of FilP (Figure 5.4.3, Figure 5.4.4). Finally, in the Javadi model the N terminal overlap of coil 1 and the C terminal overlap do not appear to have different protein density. However, in the striated structure the white, protein dense stripe arises from the N terminal region, as indicated by FilP mCherry experiments (Figure 5.6.2, Figure 5.6.3). This indicates that this area is much more protein dense than the C terminal overlap. The reasons described above lead us to propose a different association of FilP into higher order assemblies in the striated patterns.

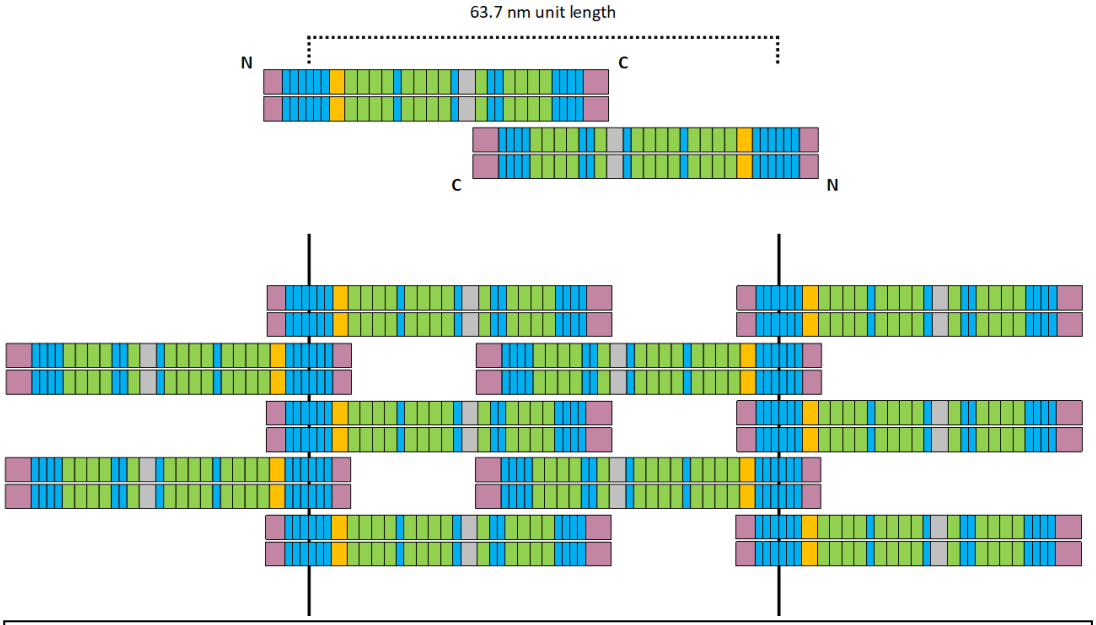

Figure 8.2.1 FilP Assembly from Javadi et al.

FilP parallel in-register dimers with antiparallel tetramers showing overlap at the C terminus of the rod domain. Further assembly as described by Javadi et al. *(Javadi et al., 2019)* where the coil 1 subdomain of the rod domains overlap. Head and tail (purple), linker (yellow), non-coiled motif (grey), heptad repeats (blue) hendecad repeats (green). Scale to length if all α-helical in nature.

New proposed model for FilP assembly

Due to the FilPC variant successfully generating both striations and lace with the same unit length as that of FilP (Figure 5.3.2, Figure 5.3.3), it is inferred that the coil 1 subdomain is not involved in controlling the unit length of the striated pattern. We speculate that the linker between coil1 and coil 2 could allow a turn, positioning the coil 1 subdomain alongside the N terminus of the coil 2 subdomain, which would be consistent with the fact that coil 1 does not control the unit length of the striated pattern (Figure 8.2.2). This would also explain the protein dense streaks when viewed by TEM as coil 1 and the N terminus of coil 2 would generate protein density at least twice than at places where the C termini of coil 2 overlap. We have generated some calculations based on the predicted lengths of alpha-helices to assess whether our new proposed model was compatible with the measured unit length of the

striated patterns. Calculations of the length of FilP in this structure whereby the second half of the linker subdomain (which is present in FilPC) and the coil 2 subdomain were assumed to be alpha helical. This consists of 222 amino acids. In alpha helices, there is 0.15 nm between each amino acid along the length of the helices. This produces 222 x 0.15 = 33.3 nm which is the calculated length of the coil 2 subdomain. For a repeating pattern which would establish a consistent unit length, there would be an overlap between the two antiparallel dimers which is (predicted length of FilP coil 2 domain x 2) - unit length observed by TEM= overlap. (33.3 nm x 2) - 63.7 nm = 2.9 nm. Therefore, the overlap is 2.9 nm or 19 amino acids. These overlap amino acids need to be split between both termini and therefore there is no sufficient overlap to indicate a strong interaction. Therefore, we argue that this assembly does not appear likely either.

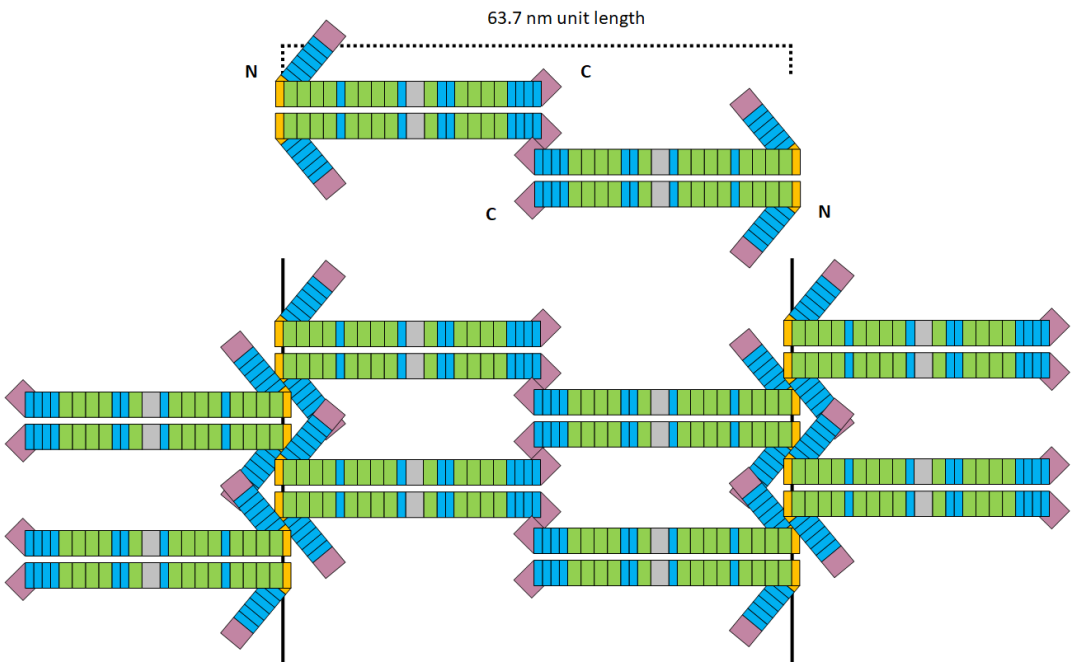

Figure 8.2.2 New proposed FilP assembly.

FilP parallel in-register dimers with antiparallel tetramers showing overlap at the C terminus of the rod domain. Further assembly with the reorientation of coil 1 subdomain to make the unit length. Head and tail (purple), linker (yellow), non-coiled motif (grey), heptad repeats (blue) hendecad repeats (green). Scale to length if all α-helical in nature.

We then considered non-coiled motif we predicted in the centre of coil 2 (Figure 5.3.1). This motif is 15 amino acids long and is therefore predicted to be 2.25 nm long if it is coiled-coil. If this was linear, then this increases to around 5.25 nm in length assuming that the average distance between amino acids is 0.35 nm. This increase in the length of the non-coiled motif increases the length of an individual dimer by 3 nm and therefore gives 8.9 nm overlap, a 6 nm increase, which is the equivalent of 59 amino acids overlap (Figure 8.2.3). This gives much more leeway with the overlaps at each end and would allow for the stronger interactions needed to form these assemblies. However, it is unlikely that this non-coiled motif is completely linear and therefore is likely to lie somewhere between the structure where it was predicted to be α-helical (Figure 8.2.2) and linear (Figure 8.2.3).

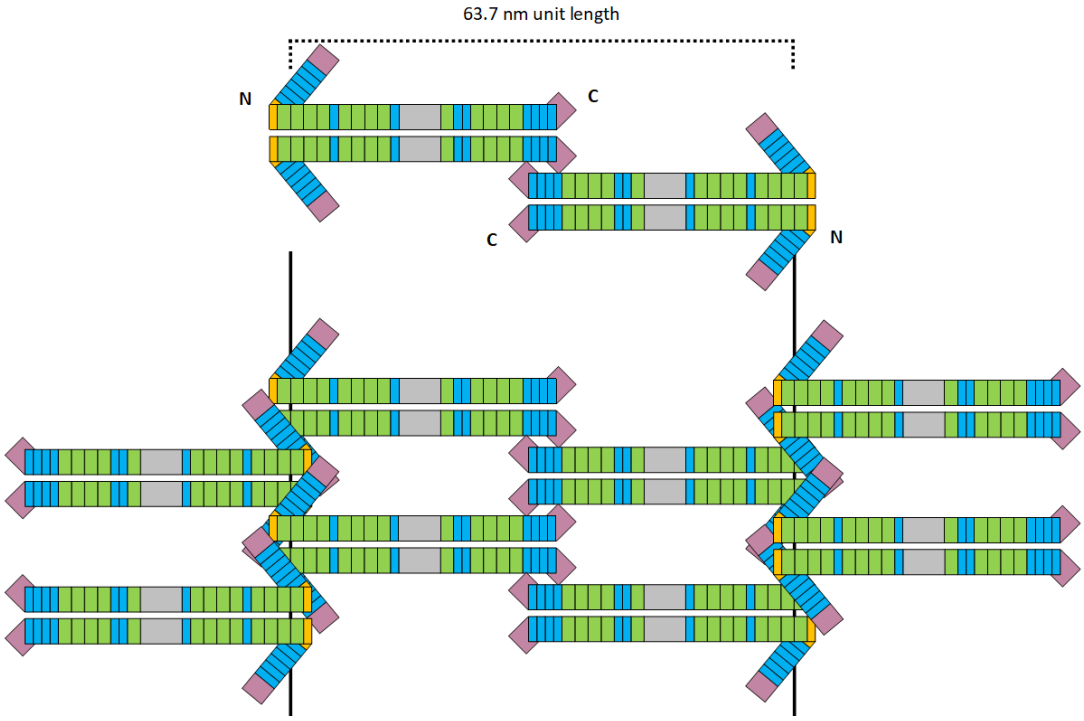

Figure 8.2.3 FilP assembly with a linear non-coiled motif.

FilP parallel in-register dimers with antiparallel tetramers showing overlap at the C terminus of the rod domain. The coil 1 subdomain is pulled back and the non-coiled motif in coil 2 (grey) extended to be linear rather than α-helical. Head and tail (purple), linker (yellow), non-coiled motif (grey), heptad repeats (blue) hendecad repeats (green). Scale to length if all α-helical in nature (except non-coiled motif in grey).

Using the variant miniFilP, it may be possible to estimate the length of non-coiled motif of FilP. MiniFilP forms higher order structures which are remarkably similar to that of FilP despite it lacking a large region of the coil 2 subdomain which includes the potentially non-coiled motif (Figure 5.3.1). MiniFilP forms striated structures with a much shorter unit length than that of FilP (19.2 nm rather than 63.7 nm) (Figure 5.4.1, Figure 5.4.2). The shortened coil 2 subdomain of FilP (and the second half of the linker included in FilPC) is 80 amino acids in length. Assuming this is α helical as before, this comes out as 12 nm in length (80 x 0.15 nm). The overlap of these dimers was calculated to be 4.8 nm ((12 nm x 2) - 19.2 nm) (Figure 8.2.4). This assembly leaves a small overlap at either end of the coil 2 subdomain which looks like it might be more substantial and could sustain the higher order assemblies of FilP.

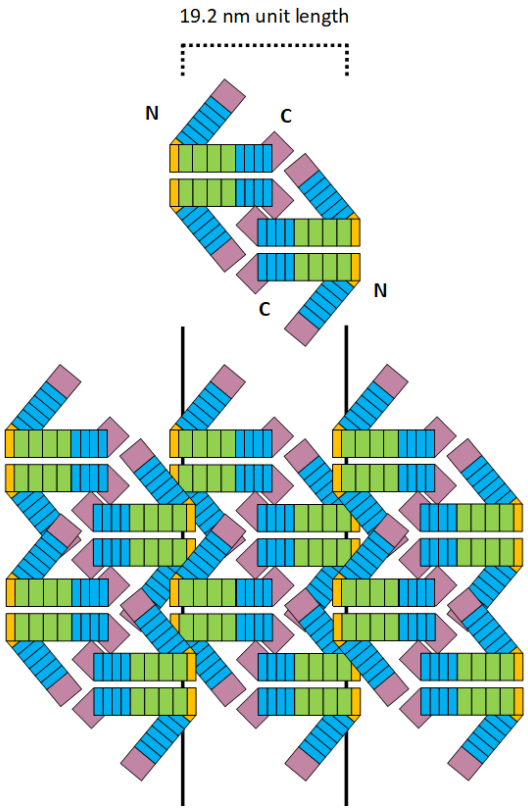

Figure 8.2.4 MiniFilP assembly

MiniFilP parallel in-register dimers with antiparallel tetramers showing overlap at the C terminus of the rod domain. Further assembly such that the coil 1 subdomain is pulled back to make the unit length. Head and tail (purple), linker (yellow), heptad repeats (blue) hendecad repeats (green). Scale to length if all α-helical in nature.

This overlap of 4.8 nm of miniFilP lies between the 2.9 nm and 8.9 nm overlaps which were the limits for the non-coiled motif being α-helical and linear respectively in FilP. Because miniFilP lacks this non-coiled-coil motif, it can be assumed that the overlap calculation is more reliable than that for FilP with this non-coiled-coil motif. If this same overlap is applied to FilP, the non-coiled motif would need to be 3.20 nm in length which lies between that of 2.25 nm calculated if it is α-helical and 5.25 nm if it is linear. As with miniFilP, this proposed assembly generates a good overlap at each end with the first hendecad coils of the coil 2 subdomain interacting in the protein dense N terminal stripe, and the last two heptad repeats of the coil 2 subdomain interacting at the C terminus (Figure 8.2.5).

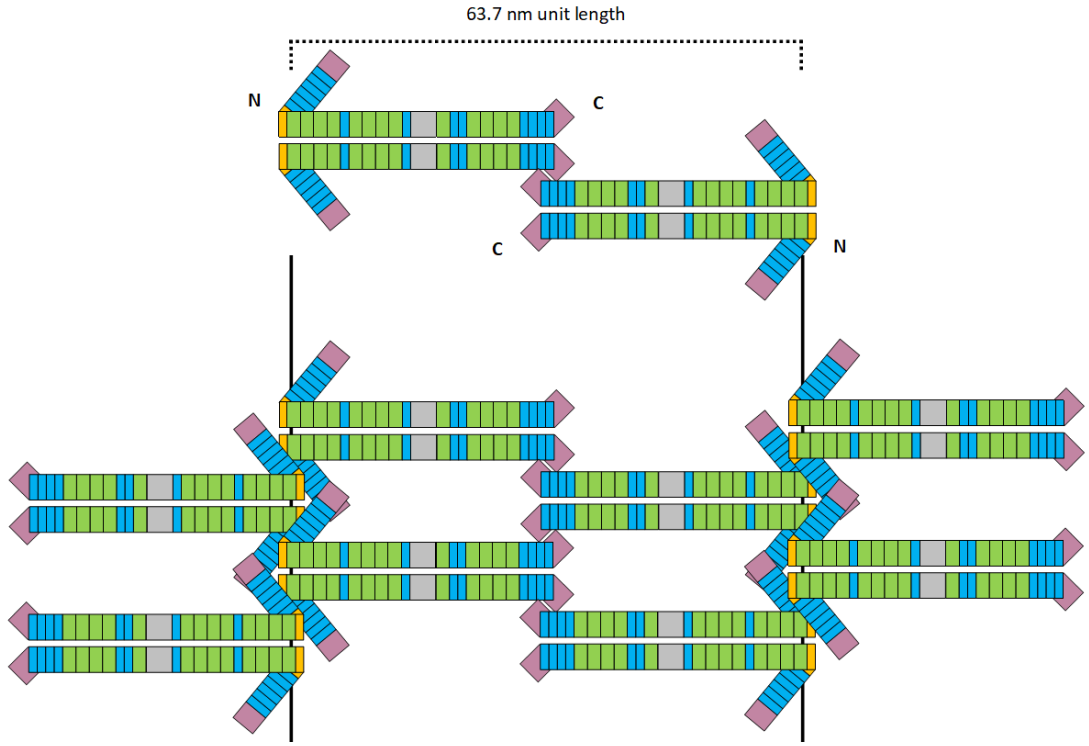

Figure 8.2.5 FilP assembly with same overlap as miniFilP

FilP parallel in-register dimers with antiparallel tetramers showing overlap at the C terminus of the rod domain. Further assembly such that the coil 1 subdomain is pulled back to make the unit length with the non-coiled motif the length such that the overlap is the same as that with miniFilP. Head and tail (purple), linker (yellow), heptad repeats (blue) hendecad repeats (green). Scale to length if all α-helical in nature.

It was previously found that in 20 mM ethanolamine pH11.0 rod structures were observed by TEM (Javadi et al., 2019). These were measured to be 37 nm in length (Javadi et

al., 2019) which is close to the around 40 nm predicted length for that of the rod domain of FilP. This does question whether the coil 1 domain is pulled back in the homodimer. If it was completely pulled back, the length of those rods would have been around 34 nm by our calculations including the proposed length of the non-coiled region. This could cast some doubt onto this proposed assembly, however it is possible that this pulling back of the coil 1 subdomain only occurs when further assembly occurs.

This proposed assembly is consistent with the findings from the sequential shortenings of FilP. The FilP Δtail variant was able to form higher order structures and striations like that of FilP with the same unit length (Figure 5.5.1, Figure 5.5.2). This indicated that the tail domain of FilP was not essential for the formation of higher order structures and this proposed assembly does not require the interaction of the tail domain for assembly or unit length. A further shortening of FilP such that it was lacking the tail domain and the last four heptad repeats of the coil 2 subdomain failed to generate striated structures with the same unit length as FilP (Figure 5.5.3, Figure 5.5.2). However, it was able to form some higher order assemblies without defined striations, an occasional striation was also observed, although this had a much shorter unit length than that of FilP. From the proposed assembly, the last four heptad repeats of the coil 2 subdomain should be essential for the formation of higher order assemblies and of the unit length. This FilP Δ4x7 variant concurs with this to an extent in that it is no longer able to form the same striation unit length as that observed with FilP, although it was still able to form large higher order assemblies and an occasional shorter periodicity. This implies that this variant is forming a slightly different assembly to that proposed here, although it confirms that the deletion of the last four heptads of FilP does remove its ability to form the 63.7 nm unit length striations which characterise FilP. The FilP Δ4x7 2x11 variant is another further subsequent deletion whereby the last two hendecads of the coil 2 subdomain are also removed. This variant failed to produce any higher order structures which concurs with the proposed assembly due to its lacking of the last four heptads of the coil 2 subdomain. Where the variant lacking the 4x7 was still able to produce some higher order structures but not the FilP striations, this variant also lacking the 2x11 was not able to form any type of higher order assemblies. This indicates that the 2x11 motif is important in that formation of unstriated or short unit length higher order assemblies occasionally observed with FilP Δ4x7.

Sequential shortenings of miniFilP did not have quite the same results as that of FilP. Removing the tail domain of miniFilP did not, as expected, have no visible affect on the unit length and higher order structure of miniFilP. Instead, large unstriated curled filaments were observed (Figure 5.5.4). Why this would be the case is unclear and indicates that, at least in miniFilP, the tail domain is important for generating the striated structure seen with miniFilP. Subsequent deletion of the last four heptads of the coil 2 subdomain failed to produce any higher order assemblies, indicating that they are important for the formation of the assembly which leads to the curled filaments observed with miniFilP Δtail, although this is unclear how.

The variant which lacks the linker subdomain between the coil 1 and coil 2 sub-domains, FilP Δlinker, formed striations and, more commonly, lace structures which had a unit length which was larger than that of FilP, despite it having fewer amino acids (Figure 5.4.3, Figure 5.4.4). In our model the linker might have important role in the reorientation of the coil 1 subdomain. The lack of this linker might straighten the coil 1 and coil 2 subdomains to align and forma a long coil (Figure 8.2.6) generating a longer unit length.

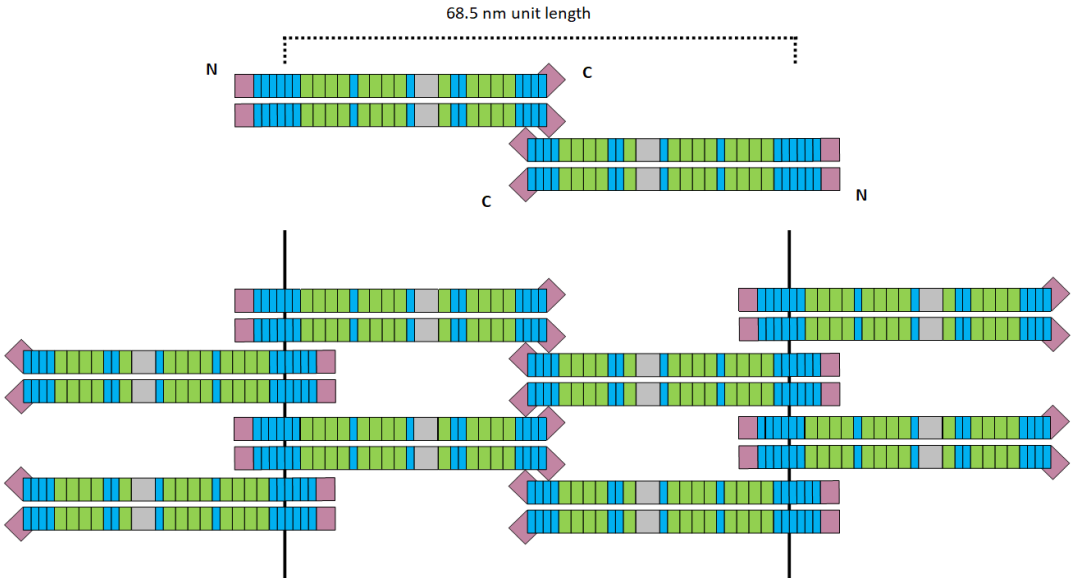

Figure 8.2.6 FilP Δlinker assembly.

FilP Δlinker parallel in-register dimers with antiparallel tetramers showing overlap at the C terminus of the rod domain. Further assembly to make the unit length. Head and tail (purple), linker (yellow), heptad repeats (blue) hendecad repeats (green). Scale to length if all α-helical in nature.

FilPC and FilP Δlinker are both variants that had an abundance of lace structure. Both of these lack the reorientation of the coil 1 subdomains, FilPC because it lacks them and FilP Δlinker because it cannot re-orientate them. This indicates that variants which lack these folded back arms are more likely to form the lace structure than the striated pattern. The lace structure appears to have a much lower requirement for lateral interactions than the striated structure and could indicate that the lack of coil 1 folded back arms reduces the ability for lateral interactions and therefore the lace structure is more readily observed. This raises the question of whether the coil 1 subdomain reorientation potentially aids the lateral interactions of the FilP assembly.

Confirmation that the protein dense white stripe is generated from the N terminus of FilP was established using the data obtained by the extra stripe in the FilP mCherry variant, it is possible to state that the protein dense white stripe of the FilP striation is likely to be that of the N terminus. This is due to the secondary stripe observed with the FilP mCherry variant (Figure 5.6.2, Figure 5.6.3) being of larger width than that of the stripe in the wild-type FilP measurements. This secondary stripe within the FilP mCherry variant must be composed of the mCherry tag which is located at the C terminus of FilP. Therefore, the C terminus of FilP would not normally be positioned in the protein dense stripes that are created by the N terminus of FilP (Figure 8.2.7).

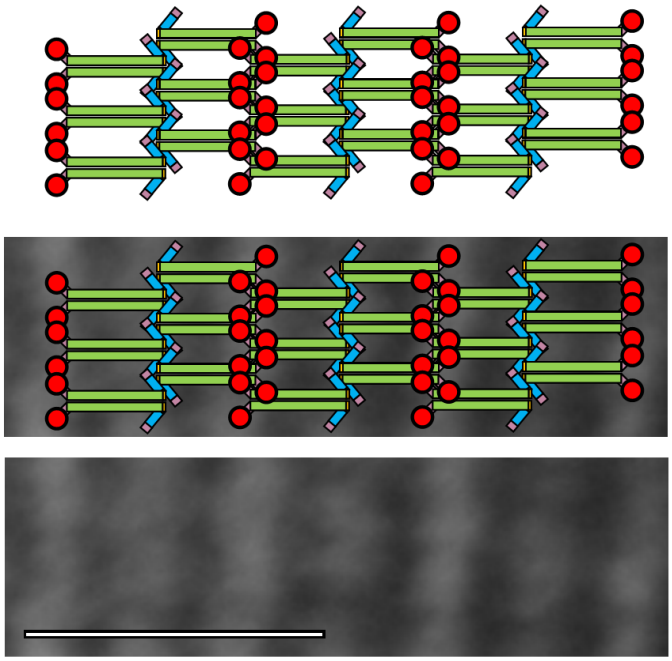

Figure 8.2.7 FilP mCherry proposed higher order assembly.

FilP mCherry parallel in-register dimers assembly in a head to head manner to generate a wider white stripe which is comprised of the N terminal of FilP, and a narrower white stripe which is composed of the mCherry fluorescent tag. FilP mCherry in 50 mM Tris pH7.0 viewed by TEM, negatively stained by Ammonium Molybdate pH7.0.

Further confirmation of this came from the nanogold staining of FilP, where the nanogold particles located either side of the stripe which indicated that the N terminal histidine tag is located either side of the stripe, but not directly on it (Figure 5.8.1). The implications from this are that the N terminal of the protein lies close to the protein sense white stripe, and potentially that the head domain and/or coil 1 subdomain lie within the stripe. For the nanogold particles to bind in a line either side of the minor stripe, N terminal histidine tags must be present at either side of the stripe. This indicates that the protein is aligned in both directions with the histidine tags sticking out each end (Figure 8.2.8) and further indicates that the interaction is in a head to head manner.

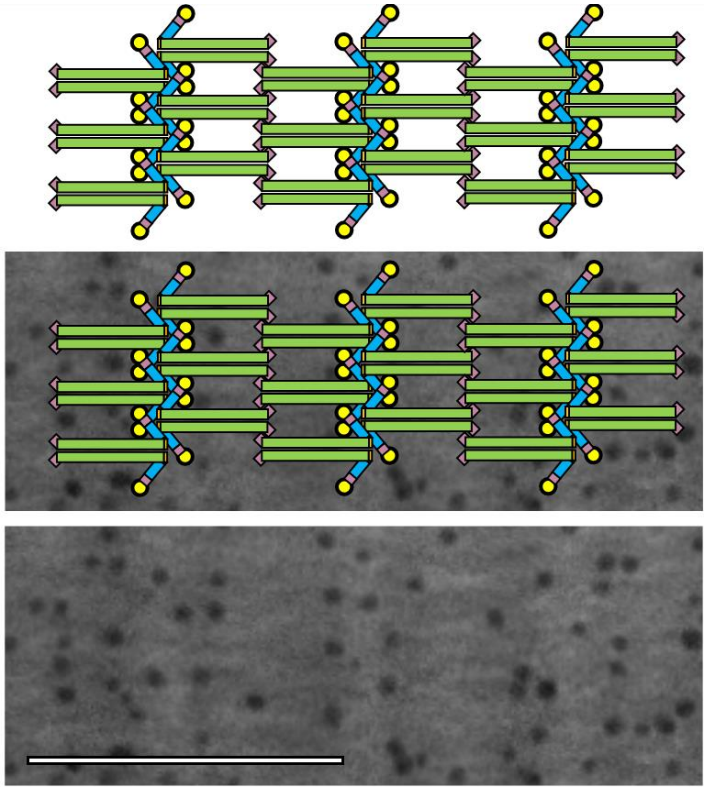

Figure 8.2.8 Proposed FilP higher order assembly with His-tag pattern shown.

FilP parallel in-register dimers with antiparallel tetramers showing overlap at the C terminus of the rod domain. Further assembly in the head to head manner shown with histidine tags (yellow) in the alignment as indicated by the nanogold particle staining experiment whereby the N terminal histidine tags were visualised by the addition of nanogold particles which bound to the histidine tags and were located on either side of the protein dense white stripe. TEM image of His-FilP striations in 50 mM Tris pH7.0 with nanogold particles (black dots) and Methylamine vanadate pH8.0 staining. Scale bar: 100 nm.

This head to head association differs from that stated in the literature for intermediate filaments which state a head to tail association. However, the structure for which this has been assessed is for the rope like structure more commonly seen in eukaryotic intermediate filaments. The head to tail association for those intermediate filaments which do form striations has not been assessed when forming the striated structure, only the rope structure.

It is possible that the head to tail association established for intermediate filaments applies only to the rope structure (Figure 8.2.10). In that case, a head to head association is required for the formation of a striated structure. Crystallisation of a fragment of vimentin which contained the coil 1A, the linker and part of coil 1B showed the coil 1A helices to be spread apart in an 'open' configuration as opposed to the 'closed' configuration seen with

other crystallisations. This coil 1A has also been shown to be important for the formation of head to tail associations. The N terminus of coil 1A has been shown to interact with the C terminus of coil 2 (Chernyatina et al., 2012). It has also been proposed that the vimentin 'open' and 'closed' structures may present different configurations of assembly of higher order structures (Meier et al., 2009; Smith et al., 2002). This opening of the coil 1A subdomain in vimentin as well as the closed formation could indicate that the same could be possible with FilP. The indications that the coil 1A is not essential for the formation of the striated structure lead to the exclusion of it from the unit length calculations with the assumption that it is in an 'open' state much like that as seen with vimentin. Speculatively, it is possible that the 'open' configuration could be necessary for the striation assembly and head to head binding, and that a 'closed' configuration could be necessary for the for head to tail assembly and the rope structure formation, although this is highly speculative and further work would need to be done to assess this.

For the network or lace structure which others observed clearly with FilP (Fuchino et al., 2013; Javadi et al., 2019) and we observed in a less obvious way (Figure 3.3.3), we also observed something like this with both FilPC which had a unit length comparable with that of FilP and FilPC striations (Figure 5.3.2, Figure 5.3.3) as well as with FilP Δlinker which had an increased unit length compared to FilP (Figure 5.4.3, Figure 5.4.4). This lace structure was often seen in combination with that of a striated structure and it could sometimes be seen merging from one into another. This combined with the same unit length leads to the conclusion that the formation of the lace structure and the striated structure are not very different from one another and only the lateral interactions or lack of makes the difference between the two structures. This has led to the proposition of a further assembly structure which answers how this lace network could be formed (Figure 8.2.9, Figure 8.2.10).

This head to head association has recently also been proposed (Javadi et al., 2019). They observed a whiter stripe when the FilP was N-terminally histidine tagged compared to a non-tagged version. They concluded that the white stripe of the striated pattern was comprised of the N terminal of FilP, and from this surmised the head to head nature of the interactions as we did. However, they did not propose an assembly for the lace/network structure.

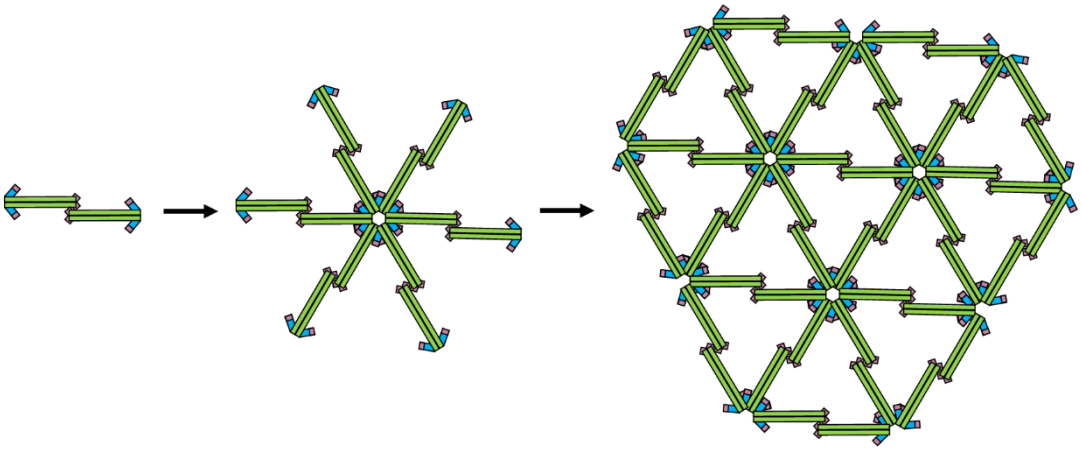

Figure 8.2.9 Proposed higher order assembly for FilP lace structure.

FilP parallel in-register dimers with antiparallel tetramers showing overlap at the C terminus of the rod domain. Further assembly in the head to head manner shown into a lace structure.

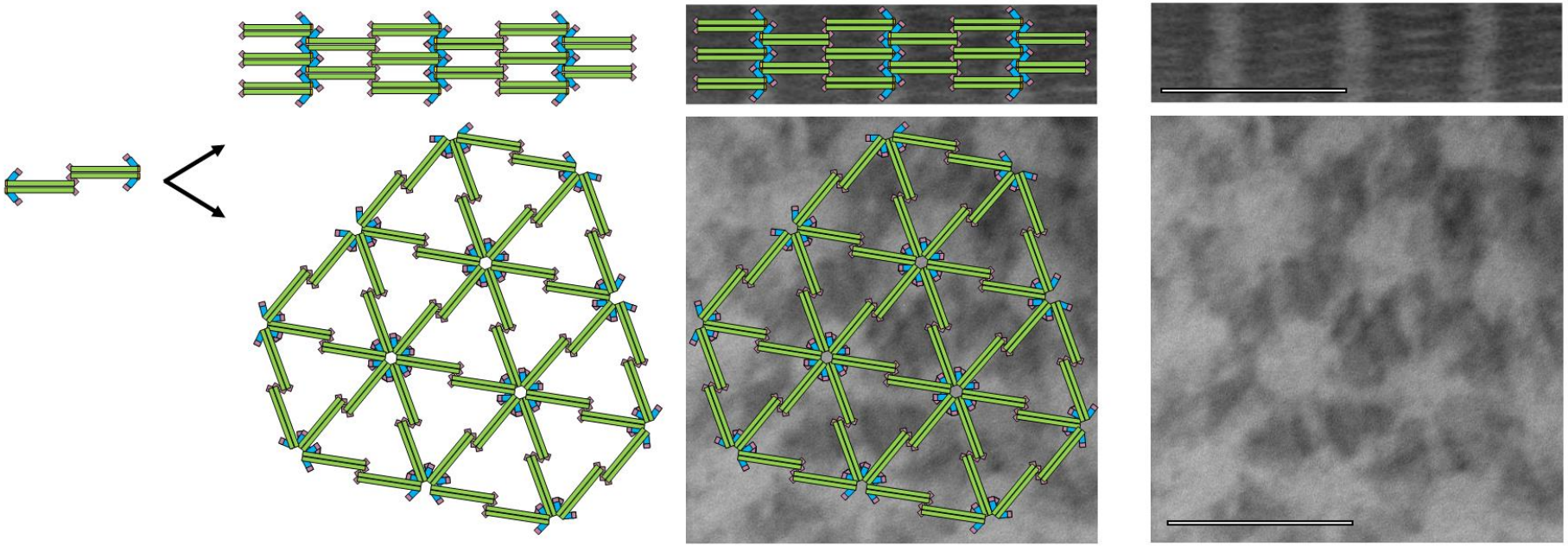

Figure 8.2.10 Proposed assemblies of FilP to form the three higher order structures.

FilP parallel in-register dimers with antiparallel tetramers showing overlap at the C terminus of the rod domain. Further assembly in a head to head manner leads to striations (with lateral interactions) or lace (with out lateral interactions). Striation: FilP in 50 mM Tris, 5 mM $MgCl_2$ pH7.0. Lace: FilPC in 50 mM Tris pH7.0. Scale bar represents 100 nm.

This elementary tetramer which we are proposing here appears strikingly similar to that of a crystal structure for a DivIVA tetramer (Figure 8.2.11; Oliva et al., 2010). Our model also has the N termini folded back in a similar way to this (Figure 8.2.5). There are a few obvious differences including the size of the folded back section, as well as the 'open' nature of the C termini as a method of interaction between the dimers. DivIVA is a coiled-coil protein much like FilP although it has not been shown to form any further higher order structures than the tetramer.

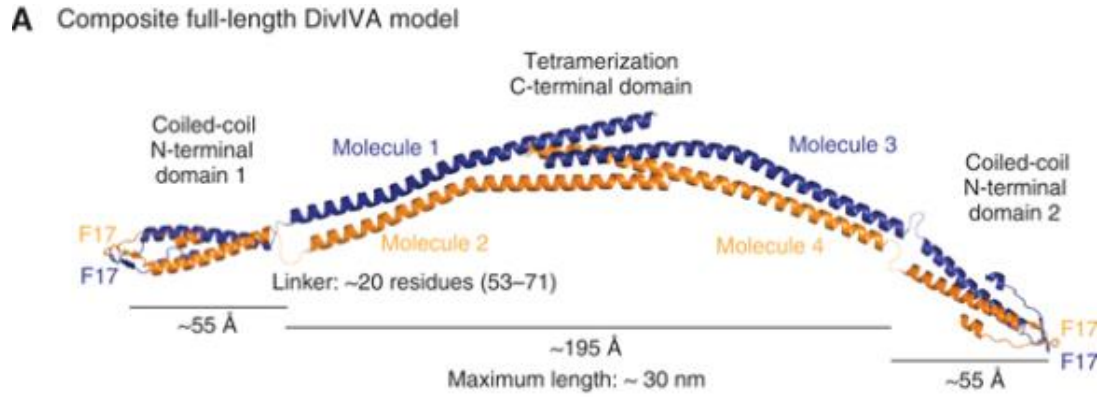

Figure 8.2.11 DivIVA tetramer model.

Model combining crystal structures of N and C terminal domains of *Bacillus subtilis* DivIVA to show tetramer arrangement (Oliva et al., 2010).

8.3 Role of FilP in *Streptomyces* Hyphae

FilP mCherry

Purified FilP mCherry was able to form large, striated higher order assemblies which appeared like that of FilP (Figure 5.6.2) and the unit length of these striations remained statistically the same (Figure 5.6.3). This indicates that the fluorescent mCherry tag is not affecting the ability of FilP to form higher order striated structures. When FilP mCherry was expressed in *E. coli*, the cells elongated in a similar way to that of cells expressing FilP without the fluorescent tag (Figure 6.3.2; Figure 6.8.1). This again indicated that FilP mCherry was able to function in the same way as FilP. Although, the width of the cells expressing FilP increased in comparison to the control, the FilP mCherry cells did not increase in width from the control (Figure 6.10.1). This indicates that the addition of the fluorescent tag is potentially interfering with the way FilP interacts with other proteins within cells. When FilP mCherry was observed as the lone copy of FilP in an *S. coelicolor* mutant, the hyphae had a slight meandering phenotype which was similar to that of the *filP* knockout mutant (Figure 7.3.2; Figure 7.5.1). This indicated that the FilP mCherry was not able have the same function and to complement the FilP knockout. Altogether, this indicates that FilP mCherry is able to form higher order assemblies in much the same way as that of FilP, however the mCherry tag is interfering with its ability to function in completely the same way within the cell. This could indicate that FilP is able to interact with other proteins within cells and that the addition of the mCherry tag is prohibiting this and therefore affecting the function.

8.4 Summary

The biological role of FilP

Streptomyces strains lacking FilP have been observed to have a relatively subtle phenotype. When grown on solid media, a *filP knockout* has been seen to lag approximately a day behind a wild-type control in terms of when it sporulates (Bagchi et al., 2008). Microscopically, when grown on either solid media or in liquid culture, the hyphae of the *filP knockout* mutant appeared much more meandering that the wild-type (Bagchi et al., 2008; Fröjd and Flärdh, 2019; Figure 1.10.2). *filP knockout*s have also been shown to have a reduced rigidity of the cell wall at the hyphal tips as was shown by atomic force microscopy and the distorted growth morphology suggests a mechanical role in controlling cell shape (Bagchi et al., 2008).

Localisations of FilP have produced some varying results. A FilP-EGFP fusion protein was used to observe its localisation in a FilP knockout background as well as with a wild-type copy present (Bagchi et al., 2008). In the knockout background they observed prominent fluorescent filamentous structures in the vegetative hyphae. FilP was also observed in young and still growing aerial hyphae but not in mature spore chains (Bagchi et al., 2008). With a copy of the wild-type FilP expressed, the localisation of the FilP-EGFP fusion was seen to be different in that it was observed in nearly all tips of young hyphae as well as a tip distant regions (Bagchi et al., 2008). Immunolocalisation revealed that during early growth nearly all hyphae fluoresced in the apical regions with the signal strongest just behind the tip where DivIVA signal appears (Fuchino et al., 2013; Javadi et al., 2019; Figure 1.10.2). Long cables were also observed asymmetrically along one side of the hyphae as well as sights of new branch points were marked by bright fluorescence. In hyphae which were no longer growing this apical gradient was replaced by a uniform intensity along the hyphae (Fuchino et al., 2013).

Localisation using a FilP mCherry fusion protein in *Streptomyces venezuelae*, with a wild-type copy of *filP* present showed that the localisation appeared to be irregular spots or patches along the hyphae with no distinct apical gradients (Fröjd and Flärdh, 2019) (Figure 1.10.2). However, treatment with formaldehyde produced distinctive zones of fluorescence just subapical of the tips. The inference from this was that the handling of cells and interference with its growth was a source of discrepancy between the results observed with

immunofluorescence in comparison to those observed with non-fixed samples with fluorescent protein fusions (Fröjd and Flärdh, 2019).

Strains with only the FilP-EGFP or FilP-mCherry and no wild-type copy of FilP displayed a *filP* knockout phenotype. However, strains with both the FilP fusion protein and a wild-type copy displayed wild-type characteristics (Bagchi et al., 2008; Fröjd and Flärdh, 2019).

After osmotic upshift, which was achieved by moving hyphae grown on a cellophane onto a plate containing sucrose which *S. coelicolor* cannot catabolise, growth of the hyphae ceased for 2 to 3 hours. After this lag, growth resumed with new branches emerging from the lateral hyphal wall with only 12% restarting growth at the tips and 77% regrowth exclusively at the lateral sites (Fuchino et al., 2016). This affect was also observed with NaCl-containing media. Osmotic downshift and acid stress did not have the same affect with regrowth occurring at the existing tips. FilP and DivIVA were observed to persist at the tips of existing hyphae throughout the lag phase but delocalise from these arrested tips prior to regrowth. Scy was present at the hyphal tips during the lag phase but also persisted at the arrested tips once branching and new growth resumed. Mutants which lacked FilP or Scy still had this same affect and therefore, neither FilP or Scy are thought to be required for the reprogramming of cell polarity (Fuchino et al., 2016).

The meandering phenotype for the *filP* knockout (Bagchi et al., 2008) was something which was consistent with our findings (Figure 7.3.2) when grown on agar against a glass coverslip. However, when grown on cellophane, we found that the hyphae of the wild-type meandered to the same extent as that of the *filP* knockout strain (Figure 7.3.3) which had not previously been observed. It had also previously been observed that the *filP* knockout strain was developmentally delayed compared to the wild-type (Bagchi et al., 2008), however this was not what we observed and they appeared to be very similar in their development rates (Figure 7.2.2). The only differences which were obvious at a macroscopic level was the characteristic crack which ran through the colonies of the *filP* knockout strain but was only present in a few of the wild-type colonies (Figure 7.2.1).

Localisation of FilP mCherry within our strains did not reveal the same apical focused localisation which has previously been observed (Bagchi et al., 2008; Fröjd and Flärdh, 2019; Fuchino et al., 2013; Javadi et al., 2019). However, this was often observed with fixation with

formaldehyde. When cells were viewed without formaldehyde fixation the localisation appeared as irregular spots or patches along the hyphae with no distinct apical gradients (Javadi et al., 2019) which was much like what was observed here (Figure 7.5.1, Figure 7.5.2, Figure 7.5.3). Our fixation of cells with methanol does not appear to have the same affect which the formaldehyde fixation was observed to have. Our methanol fixation and staining did not appear to alter the FilP mCherry localisation compared to cells viewed without.

A variety of higher order structures have been observed for FilP

FilP has been previously purified and visualised *in vitro* using transmission electron microscopy (TEM) and scanning electron microscopy (SEM). Previously observed structures included a smooth rope-like filament with a diameter of around 60 nm which constituted the less frequent type, and striated filaments which branched and had a varying diameter (Bagchi et al., 2008*;* Figure 1.10.3A, B). These striated filaments visually resembled those seen with nuclear lamins (Stuurman et al., 1998; Figure 1.7.2). Other structures observed included some striated structures surrounding a dominant lace like structure (Fuchino et al., 2013; Figure 1.10.3C, D). Recent observations at pH6.8 showed striated structures (Javadi et al., 2019) which closely resembled previously seen striations (Bagchi et al., 2008; Figure 1.10.3E). They also observed that with addition of both monovalent and divalent cations a hexagonal mesh lacework was observed which more closely resembled what was observed by Fuchino et al., 2013 (Figure 1.10.3F). These additions of magnesium, potassium and sodium ions increased the solubility of the proteins (Javadi et al., 2019). Differing pHs were also found to alter the appearance of the higher order assemblies of FilP. In citric acid pH3.9 the structures were observed to have the same unit length but vague banding patterns and thin bundles (Figure 1.10.3 G). It is speculated that the low pH altered the charge of FilP which could affect the lateral alignment of protofilaments and explain the less pronounced banding pattern (Javadi et al., 2019). FilP in Tris pH8.8 formed fewer and less condensed filaments compared with assembly buffer at pH6.8 (Figure 1.10.3H). FilP in Etanolamine pH11 no filaments were observed but rod shaped polymer units were seen (Figure 1.10.3 I). In a Hepes buffer FilP displays a 'bead on a string' look (Figure 1.10.3J). These are around 60 nm apart and from this it is suggested that the primary stage of assembly is two FilP rods interacting tail to tail (Javadi et al., 2019).

FilP higher order assembly as described above has been seen with an N-terminally histidine tagged FilP. A C-terminally histidine tagged-FilP formed smooth filaments as well as striated filaments which had a smaller unit length to the banding pattern at around 28 nm as opposed to the around 60 nm banding pattern for N terminally histidine tagged FilP (Javadi et al., 2019). This C-terminally histidine tagged FilP failed to complement a FilP knockout strain, where the N-terminally tagged version did (Javadi et al., 2019). The histidine tags associated with the N terminal made major band more defined, where with C terminal histidine tags the minor band became denser. This gave the appearance of a half unit length (Javadi et al., 2019). Non-tagged FilP was observed at low concentrations to form striated filaments with a unit length of around 19 nm. At higher concentrations it formed striations with a larger unit length of around 54 nm similarly to that of the N-terminally histidine tagged version (Javadi et al., 2019). It is speculated that the additional 18 amino acids which were introduced with the tagged version are likely to be the cause of the 6 nm difference between the tagged and un-tagged versions (Javadi et al., 2019). Use of nano-gold staining to identify where the histidine tag lies within the striated structure revealed that, for the N terminally tagged version, this was in the major band. The C-terminally tagged version had less specific localisation and the addition of the nanogold appeared to disassemble the structures. The non-tagged version of FilP showed a faint affinity for FilP which was also present in the other versions. This indicated that the FilP heads were gathered in the electron dense major band of the striated structure with the C-terminal tail to tail interactions between them (Javadi et al., 2019).

In our first round of observations by TEM in 50 mM Tris pH7.0 we reliably saw rope structures as the main structure with some striations (Figure 3.3.2), however in a second round of observations separated by time, we observed striated filaments in vast majority and only saw rope structures once more (Figure 3.3.12). This is different to what had previously been observed where a lace structure was observed in 50 mM Tris pH7.0 (Fuchino et al., 2013), although in 50 mM Tris pH6.8 a striated structure had also been observed (Javadi et al., 2019). This variation in structures seen under the same conditions highlights that the protein is likely to be sensitive in its nature of forming higher order structures to a factor which is as yet unknown.

Addition of cations pushed the structures towards the striated structure and appeared to increase the lateral associations (Figure 3.3.6, Figure 3.3.9). This is contrary to

previous findings where an increase in solubility of the protein was observed with increased cations as well as a shifting from a striated structure to an hexagonal meshwork lace (Javadi et al., 2019). Why there would be this discrepancy is unclear and further highlights that there is likely to be a factor which affects structure of higher order assemblies of FilP which we have not yet elucidated.

Previous staining of FilP with 1.8 nm nanogold beads and imaged with cryo-EM revealed that the N terminally histidine tagged FilP showed nanogold localisation specifically in the vicinity of the protein dense stripes (Figure 5.8.2; Javadi et al., 2019). The difference between our findings and theirs is that our 5 nm nanogold appeared to flank the stripe where theirs localised to it. This is a subtle difference which could be due to the different sized nanogold beads used, although both our findings indicate that this protein dense white stripe is the location of the N-terminal histidine tag.

Are *in vitro* findings relevant *in vivo*?

It is difficult to assess whether the structures observed *in vitro* are relevant *in vivo.* Previously in our lab, *E. coli* BL21 overexpressing FilP was seen by TEM to have large striations within it as has also been observed recently (Javadi et al., 2019). This indicates that these striated structures are able to form inside *E. coli*, but this is not where the protein is native in *S. coelicolor* hyphae. It is also from overexpression where the concentrations of FilP are very high. It is estimated that the cellular concentration of FilP is around 63 μg/ml (Javadi et al., 2019). The concentrations of FilP protein which we mainly used was 30 μM which is 1080 μg/ml, much higher than the estimated cellular concentration. We also observed structures at 20 μM and 2 μM. Though the 20 μM is still far higher than this at 720 μg/ml, 2 μM FilP protein is comparable with that estimated at 72 μg/ml. With this concentration of FilP protein, large striated structures were still observed (Figure 3.3.12) which indicates that this is potentially still possible within the cell. To further confirm this, ideally further systematic alterations of the concentrations would be achieved and at lower concentrations which go below this estimated cellular concentration.

Structures of FilP are highly variable and unreliable

The structures of FilP which have been observed in 50 mM Tris pH7.0 appear highly variable. Initial experiments observed predominantly rope structures with occasional lace nodes and striations (Figure 3.3.2). This was then separated in time with striated structures only being found and ropes only occasionally (Figure 3.3.12) despite searching by altering dialysis parameters as well as purified protein age and various other factors. These same buffer concentrations have also been previously observed to generate a lace structure (Fuchino et al., 2013) as well as a striated structure which was observed at pH6.8 (Javadi et al., 2019). This variation in structures seen under the same conditions highlights that the protein is likely to be sensitive in its nature of forming higher order structures to a factor which is as yet unknown.

Also confusingly, (during the time when we were able to see ropes and lace) addition of cations pushed the structures towards the striated structure and appeared to increase the lateral associations (Figure 3.3.6, Figure 3.3.9). This is again contrary to other findings whereby increased cations caused an increase in solubility of the protein as well as a shifting from a striated structure to an hexagonal meshwork lace (Javadi et al., 2019). Where cations appear to increase lateral interactions in this study, it decreased it in theirs. Why there would be this discrepancy is unclear and further highlights that there is likely to be a factor which affects structure of higher order assemblies of FilP which we have not yet elucidated.

References

Adams, D.W., Errington, J., 2009. Bacterial cell division: Assembly, maintenance and disassembly of the Z ring. Nat. Rev. Microbiol. https://doi.org/10.1038/nrmicro2198

Adams, D.W., Wu, L.J., Errington, J., 2015. Nucleoid occlusion protein N oc recruits DNA to the bacterial cell membrane . EMBO J. 34, 491–501. https://doi.org/10.15252/embj.201490177

Aebi, U., Cohn, J., Buhle, L., Gerace, L., 1986. The nuclear lamina is a meshwork of intermediate-type filaments. Nature 323, 560–564. https://doi.org/10.1038/323560a0

Aldridge, B.B., Fernandez-Suarez, M., Heller, D., Ambravaneswaran, V., Irimia, D., Toner, M., Fortune, S.M., 2012. Asymmetry and aging of mycobacterial cells lead to variable growth and antibiotic susceptibility. Science (80-.). 335, 100–104. https://doi.org/10.1126/science.1216166

Arslana, M., Qin, Z., Buehler, M.J., 2011. Coiled-coil intermediate filament stutter instability and molecular unfolding. Comput. Methods Biomech. Biomed. Engin. 14, 483–489. https://doi.org/10.1080/10255842.2011.560147

Atta, H.M., 2015. Biochemical studies on antibiotic production from Streptomyces sp.: Taxonomy, fermentation, isolation and biological properties. J. Saudi Chem. Soc. 19, 12–22. https://doi.org/10.1016/j.jscs.2011.12.011

Ausmees, N., Kuhn, J.R., Jacobs-Wagner, C., 2003. The bacterial cytoskeleton: An intermediate filament-like function in cell shape. Cell 115, 705–713. https://doi.org/10.1016/S0092-8674(03)00935-8

Aziz, A., Hess, J.F., Budamagunta, M.S., Voss, J.C., Kuzin, A.P., Huang, Y.J., Xiao, R., Montelione, G.T., FitzGerald, P.G., Hunt, J.F., 2012. The structure of vimentin linker 1 and rod 1B domains characterized by site-directed spin-labeling electron paramagnetic resonance (SDSL-EPR) and X-ray crystallography. J. Biol. Chem. 287, 28349–28361. https://doi.org/10.1074/jbc.M111.334011

Bagchi, S., Tomenius, H., Belova, L.M., Ausmees, N., 2008. Intermediate filament-like proteins in bacteria and a cytoskeletal function in Streptomyces. Mol. Microbiol. 70, 1037–50. https://doi.org/10.1111/j.1365-2958.2008.06473.x

Baltz, R.H., 2007. Antimicrobials from Actinomycetes: Back to the Future. Microbiol. 2, 125–131.

Barák, I., Wilkinson, A.J., 2007. Division site recognition in Escherichia coli and Bacillus subtilis. FEMS Microbiol. Rev. https://doi.org/10.1111/j.1574-6976.2007.00067.x

Ben-Harush, K., Wiesel, N., Frenkiel-Krispin, D., Moeller, D., Soreq, E., Aebi, U., Herrmann, H., Gruenbaum, Y., Medalia, O., 2009. The Supramolecular Organization of the C. elegans Nuclear Lamin Filament. J. Mol. Biol. 386, 1392–1402. https://doi.org/10.1016/j.jmb.2008.12.024

Bentley, S., Chater, K., Cerdeño-Tárraga, a-M., Challis, G.L., Thomson, N.R., James, K.D., Harris, D.E., Quail, M. a, Kieser, H., Harper, D., Bateman, a, Brown, S., Chandra, G., Chen, C.W., Collins, M., Cronin, a, Fraser, a, Goble, a, Hidalgo, J., Hornsby, T., Howarth, S., Huang, C.-H., Kieser, T., Larke, L., Murphy, L., Oliver, K., O'Neil, S., Rabbinowitsch, E., Rajandream, M., Rutherford, K., Rutter, S., Seeger, K., Saunders, D., Sharp, S., Squares, R., Squares, S., Taylor, K., Warren, T., Wietzorrek, a, Woodward, J., Barrell, B.G., Parkhill, J., Hopwood, D. a, 2002. Complete genome sequence of the model actinomycete Streptomyces coelicolor A3(2). Nature 417, 141–147. https://doi.org/10.1038/417141a

Bernhardt, T.G., De Boer, P.A.J., 2005. SlmA, a nucleoid-associated, FtsZ binding protein required for blocking septal ring assembly over chromosomes in E. coli. Mol. Cell 18, 555–564. https://doi.org/10.1016/j.molcel.2005.04.012

Bibb, M.J., 2013. Understanding and manipulating antibiotic production in actinomycetes. Biochem Soc Trans 41, 1355–1364. https://doi.org/10.1042/BST20130214\rBST20130214 [pii]

Billings, G., Ouzounov, N., Ursell, T., Desmarais, S.M., Shaevitz, J., Gitai, Z., Huang, K.C., 2014. De novo morphogenesis in L-forms via geometric control of cell

growth. Mol. Microbiol. 93, 883–896. https://doi.org/10.1111/mmi.12703

Bisson-Filho, A.W., Hsu, Y.P., Squyres, G.R., Kuru, E., Wu, F., Jukes, C., Sun, Y., Dekker, C., Holden, S., VanNieuwenhze, M.S., Brun, Y. V., Garner, E.C., 2017. Treadmilling by FtsZ filaments drives peptidoglycan synthesis and bacterial cell division. Science (80-.). 355, 739–743. https://doi.org/10.1126/science.aak9973

Bornhorst, J.A., Falke, J.J., 2000. Purification of Proteins Using Polyhistidine Affinity Tags. Methods Enzym. 245–254. https://doi.org/10.1016/j.pep.2011.08.022

Bramhill, D., Thompson, C.M., 1994. GTP-dependent polymerization of Escherichia coli FtsZ protein to form tubules. Proc. Natl. Acad. Sci. U. S. A. 91, 5813–5817. https://doi.org/10.1073/pnas.91.13.5813

Bramkamp, M., van Baarle, S., 2009. Division site selection in rod-shaped bacteria. Curr. Opin. Microbiol. https://doi.org/10.1016/j.mib.2009.10.002

Brangwynne, C.P., MacKintosh, F.C., Kumar, S., Geisse, N.A., Talbot, J., Mahadevan, L., Parker, K.K., Ingber, D.E., Weitz, D.A., 2006. Microtubules can bear enhanced compressive loads in living cells because of lateral reinforcement. J. Cell Biol. 173, 733–741. https://doi.org/10.1083/jcb.200601060

Brown, J.H., Cohen, C., Parry, D. a D., 1996. Heptad breaks in alpha-helical coiled coils: Stutters and stammers. Proteins Struct. Funct. Genet. 26, 134–145. https://doi.org/10.1002/(SICI)1097-0134(199610)26:2<134::AID-PROT3>3.0.CO;2-G

Brown, P.J.B., De Pedro, M.A., Kysela, D.T., Van Der Henst, C., Kim, J., De Bolle, X., Fuqua, C., Brun, Y. V., 2012. Polar growth in the Alphaproteobacterial order Rhizobiales. Proc. Natl. Acad. Sci. U. S. A. 109, 1697–1701. https://doi.org/10.1073/pnas.1114476109

Budamagunta, M.S., Hess, J.F., Fitzgerald, P.G., Voss, J.C., 2007. Describing the structure and assembly of protein filaments by EPR spectroscopy of spin-labeled side chains. Cell Biochem. Biophys. https://doi.org/10.1007/s12013-007-0035-4

Cabeen, M.T., Charbon, G., Vollmer, W., Born, P., Ausmees, N., Weibel, D.B., Jacobs-Wagner, C., 2009. Bacterial cell curvature through mechanical control of cell growth. EMBO J. 28, 1208–1219. https://doi.org/10.1038/emboj.2009.61

Cabeen, M.T., Herrmann, H., Jacobs-Wagner, C., 2011. The domain organization of the bacterial intermediate filament-like protein crescentin is important for assembly and function. Cytoskeleton 68, 205–219. https://doi.org/10.1002/cm.20505

Cabeen, M.T., Jacobs-Wagner, C., 2005. Bacterial cell shape. Nat. Rev. Microbiol. https://doi.org/10.1038/nrmicro1205

Carballido-López, R., Errington, J., 2003. A dynamic bacterial cytoskeleton. Trends Cell Biol. https://doi.org/10.1016/j.tcb.2003.09.005

Carballido-López, R., Formstone, A., Li, Y., Ehrlich, S.D., Noirot, P., Errington, J., 2006. Actin Homolog MreBH Governs Cell Morphogenesis by Localization of the Cell Wall Hydrolase LytE. Dev. Cell 11, 399–409. https://doi.org/10.1016/j.devcel.2006.07.017

Cha, J.H., Stewart, G.C., 1997. The divIVA minicell locus of Bacillus subtilis. J. Bacteriol. 179, 1671–1683. https://doi.org/10.1128/jb.179.5.1671-1683.1997

Chater, K.F., 1993. Genetics of Differentiation in Streptomyces. Annu. Rev. Microbiol. 47, 685–711. https://doi.org/10.1146/annurev.mi.47.100193.003345

Chernyatina, A. a, Guzenko, D., Strelkov, S. V, 2015. Intermediate filament structure: the bottom-up approach. Curr. Opin. Cell Biol. 32C, 65–72. https://doi.org/10.1016/j.ceb.2014.12.007

Chernyatina, A.A., Guzenko, D., Strelkov, S. V., 2015. Intermediate filament structure: The bottom-up approach. Curr. Opin. Cell Biol. https://doi.org/10.1016/j.ceb.2014.12.007

Chernyatina, A.A., Nicolet, S., Aebi, U., Herrmann, H., Strelkov, S. V., 2012. Atomic

structure of the vimentin central α-helical domain and its implications for intermediate filament assembly. Proc. Natl. Acad. Sci. U. S. A. 109, 13620–13625. https://doi.org/10.1073/pnas.1206836109

Chernyatina, A.A., Strelkov, S. V., 2012. Stabilization of vimentin coil2 fragment via an engineered disulfide. J. Struct. Biol. 177, 46–53. https://doi.org/10.1016/j.jsb.2011.11.014

Cho, H., McManus, H.R., Dove, S.L., Bernhardt, T.G., 2011. Nucleoid occlusion factor SlmA is a DNA-activated FtsZ polymerization antagonist. Proc. Natl. Acad. Sci. U. S. A. 108, 3773–3778. https://doi.org/10.1073/pnas.1018674108

Cho, H., Uehara, T., Bernhardt, T.G., 2014. Beta-lactam antibiotics induce a lethal malfunctioning of the bacterial cell wall synthesis machinery. Cell 159, 1300–1311. https://doi.org/10.1016/j.cell.2014.11.017

Crick, F.H.C., 1953. The packing of-helices: simple coiled-coils. Acta Crystallogr. 6, 689–697.

Dale, J.W., Greenaway, P.J., 1985. The use of alkaline phosphatase to prevent vector regeneration. Methods Mol. Biol. 2, 231–236. https://doi.org/10.1385/0-89603-064-4:231

Daniel, R. a., Errington, J., 2003. Control of cell morphogenesis in bacteria: Two distinct ways to make a rod-shaped cell. Cell 113, 767–776. https://doi.org/10.1016/S0092-8674(03)00421-5

Datsenko, K.A., Wanner, B.L., 2000. One-step inactivation of chromosomal genes in Escherichia coli K-12 using PCR products. Proc. Natl. Acad. Sci. U. S. A. 97, 6640–6645. https://doi.org/10.1073/pnas.120163297

Davidson, P.M., Lammerding, J., 2014. Broken nuclei - lamins, nuclear mechanics, and disease. Trends Cell Biol. https://doi.org/10.1016/j.tcb.2013.11.004

Defeu Soufo, H.J., Graumann, P.L., 2006. Dynamic localization and interaction with other Bacillus subtilis actin-like proteins are important for the function of MreB. Mol. Microbiol. 62, 1340–1356. https://doi.org/10.1111/j.1365-

2958.2006.05457.x

Ditkowski, B., Holmes, N., Rydzak, J., Donczew, M., Bezulska, M., Ginda, K., Kędzierski, P., Zakrzewska-Czerwińska, J., Kelemen, G.H., Jakimowicz, D., 2013. Dynamic interplay of ParA with the polarity protein, Scy, coordinates the growth with chromosome segregation in Streptomyces coelicolor. Open Biol. 3. https://doi.org/10.1098/rsob.130006

Dittmer, T., Misteli, T., 2011. The lamin protein family. Genome Biol. 12. https://doi.org/10.1186/gb-2011-12-5-222

Doherty, a J., Ashford, S.R., Brannigan, J. a, Wigley, D.B., 1995. A superior host strain for the over-expression of cloned genes using the T7 promoter based vectors. Nucleic Acids Res. 23, 2074–2075. https://doi.org/10.1093/nar/23.11.2074

Doherty, G.J., McMahon, H.T., 2008. Mediation, modulation, and consequences of membrane-cytoskeleton interactions. Annu. Rev. Biophys. https://doi.org/10.1146/annurev.biophys.37.032807.125912

Domínguez-Cuevas, P., Porcelli, I., Daniel, R.A., Errington, J., 2013. Differentiated roles for MreB-actin isologues and autolytic enzymes in Bacillus subtilis morphogenesis. Mol. Microbiol. 89, 1084–1098. https://doi.org/10.1111/mmi.12335

Domínguez-Escobar, J., Chastanet, A., Crevenna, A.H., Fromion, V., Wedlich-Söldner, R., Carballido-López, R., 2011. Processive movement of MreB-associated cell wall biosynthetic complexes in bacteria. Science (80-.). 333, 225–228. https://doi.org/10.1126/science.1203466

Dominguez, R., Holmes, K.C., 2011. Actin structure and function. Annu. Rev. Biophys. 40, 169–186. https://doi.org/10.1146/annurev-biophys-042910-155359

El-Hajj, Z.W., Newman, E.B., 2015. An Escherichia coli mutant that makes exceptionally long cells. J. Bacteriol. 197, 1507–1514. https://doi.org/10.1128/JB.00046-15

Erickson, H.P., 1997. FtsZ, a tubulin homologue in prokaryote cell division. Trends Cell Biol. https://doi.org/10.1016/S0962-8924(97)01108-2

Erickson, H.P., 1995. FtsZ, a prokaryotic homolog of tubulin? Cell. https://doi.org/10.1016/0092-8674(95)90486-7

Erickson, H.P., Anderson, D.E., Osawa, M., 2010. FtsZ in Bacterial Cytokinesis: Cytoskeleton and Force Generator All in One. Microbiol. Mol. Biol. Rev. 74, 504–528. https://doi.org/10.1128/mmbr.00021-10

Erickson, H.P., Taylor, D.W., Taylor, K.A., Bramhill, D., 1996. Bacterial cell division protein FtsZ assembles into protofilament sheets and minirings, structural homologs of tubulin polymers. Proc. Natl. Acad. Sci. U. S. A. 93, 519–523. https://doi.org/10.1073/pnas.93.1.519

Errington, J., 2015. Bacterial morphogenesis and the enigmatic MreB helix. Nat. Rev. Microbiol. https://doi.org/10.1038/nrmicro3398

Errington, J., 2003. Regulation of endospore formation in Bacillus subtilis. Nat. Rev. Microbiol. 1, 117–126. https://doi.org/10.1038/nrmicro750

Fjærvik, E., Zotchev, S.B., 2005. Biosynthesis of the polyene macrolide antibiotic nystatin in Streptomyces noursei. Appl. Microbiol. Biotechnol. https://doi.org/10.1007/s00253-004-1802-4

Flärdh, K., 2003a. Essential role of DivIVA in polar growth and morphogenesis in Streptomyces coelicolor A3(2). Mol. Microbiol. 49, 1523–1536. https://doi.org/10.1046/j.1365-2958.2003.03660.x

Flärdh, K., 2003b. Growth polarity and cell division in Streptomyces. Curr. Opin. Microbiol. https://doi.org/10.1016/j.mib.2003.10.011

Flärdh, K., Buttner, M.J., 2009. Streptomyces morphogenetics: dissecting differentiation in a filamentous bacterium. Nat. Rev. Microbiol. 7, 36–49. https://doi.org/10.1038/nrmicro1968

Fletcher, D.A., Mullins, R.D., 2010. Cell mechanics and the cytoskeleton. Nature 463, 485–492. https://doi.org/10.1038/nature08908

Flitney, E.W., Kuczmarski, E.R., Adam, S.A., Goldman, R.D., 2009. Insights into the mechanical properties of epithelial cells: the effects of shear stress on the assembly and remodeling of keratin intermediate filaments. FASEB J. 23, 2110–2119. https://doi.org/10.1096/fj.08-124453

Fröjd, M.J., Flärdh, K., 2019. Apical assemblies of intermediate filament-like protein FilP are highly dynamic and affect polar growth determinant DivIVA in Streptomyces venezuelae. Mol. Microbiol. 112, 47–61. https://doi.org/10.1111/mmi.14253

Fuchino, K., Bagchi, S., Cantlay, S., Sandblad, L., Wu, D., Bergman, J., Kamali-Moghaddam, M., Flärdh, K., Ausmees, N., 2013. Dynamic gradients of an intermediate filament-like cytoskeleton are recruited by a polarity landmark during apical growth. Proc. Natl. Acad. Sci. U. S. A. 110, E1889-97. https://doi.org/10.1073/pnas.1305358110

Fuchino, K., Flärdh, K., Dyson, P., Ausmees, N., 2016. Cell-biological studies of osmotic shock response in *Streptomyces*. J. Bacteriol. JB.00465-16. https://doi.org/10.1128/JB.00465-16

Fultz, B., Howe, J.M., 2008. Transmission electron microscopy and diffractometry of materials, Transmission Electron Microscopy and Diffractometry of Materials. https://doi.org/10.1007/978-3-540-73886-2

Garner, E.C., Bernard, R., Wang, W., Zhuang, X., Rudner, D.Z., Mitchison, T., 2011. Coupled, circumferential motions of the cell wall synthesis machinery and MreB filaments in B. subtilis. Science (80-.). 333, 222–225. https://doi.org/10.1126/science.1203285

Gitai, Z., Dye, N.A., Reisenauer, A., Wachi, M., Shapiro, L., 2005. MreB actin-mediated segregation of a specific region of a bacterial chromosome. Cell 120, 329–341. https://doi.org/10.1016/j.cell.2005.01.007

Gruber, M., Lupas, A.N., 2003. Historical review: Another 50th anniversary - New periodicities in coiled coils. Trends Biochem. Sci. https://doi.org/10.1016/j.tibs.2003.10.008

Gust, B., Kieser, T., Chater, K., 2002. PCR targeting system in Streptomyces coelicolor A3(2).

Hajduk, I. V., Rodrigues, C.D.A., Harry, E.J., 2016. Connecting the dots of the bacterial cell cycle: Coordinating chromosome replication and segregation with cell division. Semin. Cell Dev. Biol. https://doi.org/10.1016/j.semcdb.2015.11.012

Hanahan, D., 1983. Studies on transformation of Escherichia coli with plasmids. J. Mol. Biol. 166, 557–580. https://doi.org/10.1016/S0022-2836(83)80284-8

Harbury, P.B., Zhang, T., Kim, P.S., Alber, T., 1993. A Switch Between Two-, Three-, and Four- Stranded Coiled Coils in GCN4 Leucine Zipper Mutants. Science (80-.). 262, 1401–1407. https://doi.org/10.1007/s11214-005-8072-z

Harry, E., Monahan, L., Thompson, L., 2006. Bacterial Cell Division: The Mechanism and Its Precison. Int. Rev. Cytol. https://doi.org/10.1016/S0074-7696(06)53002-5

Hayat, M.A., 2000. Chapter seven: Negative staining, in: Principles and Tehniques of Electron Microscopy. Biological Applications. 4-Th Edition. pp. 367–399.

Heald, R., Nogales, E., 2002. Microtubule dynamics. J. Cell Sci. https://doi.org/10.4081/ejh.2012.br5

Heitlinger, E., Peter, M., Häner, M., Lustig, A., Aebi, U., Nigg, E.A., 1991. Expression of chicken lamin B2 in Escherichia coli: Characterization of its structure, assembly, and molecular interactions. J. Cell Biol. 113, 485–495. https://doi.org/10.1083/jcb.113.3.485

Heitlinger, E., Peter, M., Lustig, A., Villiger, W., Nigg, E.A., Aebi, U., 1992. The role of the head and tail domain in lamin structure and assembly: Analysis of bacterially expressed chicken Lamin A and truncated B2 lamins. J. Struct. Biol. 108, 74–91. https://doi.org/10.1016/1047-8477(92)90009-Y

Hempel, A.M., Wang, S.B., Letek, M., Gil, J.A., Flärdh, K., 2008. Assemblies of DivIVA mark sites for hyphal branching and can establish new zones of cell wall

growth in Streptomyces coelicolor. J. Bacteriol. 190, 7579–7583. https://doi.org/10.1128/JB.00839-08

Henning, U., Rehn, K., Hoehn, B., 1973. Cell envelope and shape of Escherichia coli K12. Proc. Natl. Acad. Sci. U. S. A. 70, 2033–6.

Herrmann, H., Aebi, U., 2004. Intermediate filaments: molecular structure, assembly mechanism, and integration into functionally distinct intracellular Scaffolds. Annu. Rev. Biochem. 73, 749–89. https://doi.org/10.1146/annurev.biochem.73.011303.073823

Herrmann, H., Häner, M., Brettel, M., Ku, N.O., Aebi, U., 1999. Characterization of distinct early assembly units of different intermediate filament proteins. J. Mol. Biol. 286, 1403–1420. https://doi.org/10.1006/jmbi.1999.2528

Herrmann, H., Häner, M., Brettel, M., Müller, S. a, Goldie, K.N., Fedtke, B., Lustig, A., Franke, W.W., Aebi, U., 1996. Structure and assembly properties of the intermediate filament protein vimentin: the role of its head, rod and tail domains. J. Mol. Biol. 264, 933–953. https://doi.org/10.1006/jmbi.1996.0688

Herrmann, H., Häner, M., Brettel, M., Müller, S.A., Goldie, K.N., Fedtke, B., Lustig, A., Franke, W.W., Aebi, U., 1996. Structure and assembly properties of the intermediate filament protein vimentin: The role of its head, rod and tail domains. J. Mol. Biol. 264, 933–953. https://doi.org/10.1006/jmbi.1996.0688

Hesse, M., Magin, T.M., Weber, K., 2001. Genes for intermediate filament proteins and the draft sequence of the human genome: novel keratin genes and a surprisingly high number of pseudogenes related to keratin genes 8 and 18. J. Cell Sci. 114, 2569–75.

Holden, S.J., Pengo, T., Meibom, K.L., Fernandez, C.F., Collier, J., Manley, S., 2014. High throughput 3D super-resolution microscopy reveals Caulobacter crescentus in vivo Z-ring organization. Proc. Natl. Acad. Sci. U. S. A. 111, 4566–4571. https://doi.org/10.1073/pnas.1313368111

Holmes, N., 2012. The Streptomyces cytoskeletal protein (Scy), a key component of the Tip Organising Centre of Streptomyces coelicolor. University of East Anglia.

Holmes, N. a, Walshaw, J., Leggett, R.M., Thibessard, A., Dalton, K. a, Gillespie, M.D., Hemmings, A.M., Gust, B., Kelemen, G.H., 2013. Coiled-coil protein Scy is a key component of a multiprotein assembly controlling polarized growth in Streptomyces. Proc. Natl. Acad. Sci. U. S. A. 110, E397-406. https://doi.org/10.1073/pnas.1210657110

Holy, T.E., Leibler, S., 1994. Dynamic instability of microtubules as an efficient way to search in space. Pro. Natl. Aca. Sci., USA 91, 5682–5685. https://doi.org/10.1073/pnas.91.12.5682

Hopwood, D.A., Bibb, M., Chater, K., Bruton, C.J., Kieser, H., Lydiate, D.J., Smith, C.P., Ward, J.M., Schrempf, H., 1985. Genetic Manipulation of Streptomyces. A Laboratory Manual. John Innes Foundation, Norwich.

Howard, J., Hyman, A.A., 2003. Dynamics and mechanics of the microtubule plus end. Nature. https://doi.org/10.1038/nature01600

Javadi, A., Söderholm, N., Olofsson, A., Flärdh, K., Sandblad, L., 2019. Assembly mechanisms of the bacterial cytoskeletal protein FilP. Life Sci. alliance 2, 1–15. https://doi.org/10.26508/lsa.201800290

Jones, C.A., Holland, I.B., 1984. Inactivation of essential division genes, ftsA, ftsZ, suppresses mutations at sfiB, a locus mediating division inhibition during the SOS response in E. coli. EMBO J. 3, 1181–1186. https://doi.org/10.1002/j.1460-2075.1984.tb01948.x

Jones, L.J.F., Carballido-López, R., Errington, J., 2001. Control of cell shape in bacteria: Helical, actin-like filaments in Bacillus subtilis. Cell 104, 913–922. https://doi.org/10.1016/S0092-8674(01)00287-2

Jyothikumar, V., Tilley, E.J., Wali, R., Herron, P.R., 2008. Time-lapse microscopy of Streptomyces coelicolor growth and sporulation. Appl. Environ. Microbiol. 74, 6774–6781. https://doi.org/10.1128/AEM.01233-08

Kang, C.M., Nyayapathy, S., Lee, J.Y., Suh, J.W., Husson, R.N., 2008. Wag31, a homologue of the cell division protein DivIVA, regulates growth, morphology and polar cell wall synthesis in mycobacteria. Microbiology 154, 725–735.

https://doi.org/10.1099/mic.0.2007/014076-0

Kapinos, L.E., Schumacher, J., Mücke, N., Machaidze, G., Burkhard, P., Aebi, U., Strelkov, S. V., Herrmann, H., 2010. Characterization of the Head-to-Tail Overlap Complexes Formed by Human Lamin A, B1 and B2 “Half-minilamin” Dimers. J. Mol. Biol. 396, 719–731. https://doi.org/10.1016/j.jmb.2009.12.001

Karabinos, A., Schünemann, J., Meyer, M., Aebi, U., Weber, K., 2003. The single nuclear lamin of Caenorhabditis elegans forms in vitro stable intermediate filaments and paracrystals with a reduced axial periodicity. J. Mol. Biol. 325, 241–247. https://doi.org/10.1016/S0022-2836(02)01240-8

Kawai, Y., Asai, K., Errington, J., 2009. Partial functional redundancy of MreB isoforms, MreB, Mbl and MreBHp in cell morphogenesis of Bacillus subtilis. Mol. Microbiol. 73, 719–731. https://doi.org/10.1111/j.1365-2958.2009.06805.x

Kelemen, G.H., 2017. Intermediate filaments supporting cell shape and growth in bacteria. Subcell. Biochem. 84, 161–211. https://doi.org/10.1007/978-3-319-53047-5_6

Kelemen, G.H., Brian, P., Flärdh, K., Chamberlin, L., Chater, K.F., Buttner, M.J., 1998. Developmental regulation of transcription of whiE, a locus specifying the polyketide spore pigment in Streptomyces coelicolor A3(2). J. Bacteriol. 180, 2515–2521. https://doi.org/10.1128/jb.180.9.2515-2521.1998

Kelemen, G.H., Buttner, M.J., 1998. Initiation of aerial mycelium formation in Streptomyces. Curr. Opin. Microbiol. 1, 656–662. https://doi.org/10.1016/S1369-5274(98)80111-2

Kieser, T., Bibb, M.J., Buttner, M.J., Chater, K.F., Hopwood, D.A., 2000. Practical *Streptomyces* genetics. John Innes Found. Norwich, Engl. 3, 260–261. https://doi.org/10.2436/im.v3i4.9291

Klapper, M., Exner, K., Kempf, A., Gehrig, C., Stuurman, N., Fisher, P.A., Krohne, G., 1997. Assembly of A- and B-type lamins studied in vivo with the baculovirus system. J. Cell Sci. 110, 2519–2532.

Köster, S., Weitz, D.A., Goldman, R.D., Aebi, U., Herrmann, H., 2015. Intermediate filament mechanics in vitro and in the cell: from coiled coils to filaments, fibers and networks. Curr. Opin. Cell Biol. 32, 82–91. https://doi.org/10.1016/j.ceb.2015.01.001

Kruse, T., Bork-Jensen, J., Gerdes, K., 2005. The morphogenetic MreBCD proteins of Escherichia coli form an essential membrane-bound complex. Mol. Microbiol. 55, 78–89. https://doi.org/10.1111/j.1365-2958.2004.04367.x

Kühnel, K., Jarchau, T., Wolf, E., Schlichting, I., Walter, U., Wittinghofer, A., Strelkov, S. V., 2004. The VASP tetramerization domain is a right-handed coiled coil based on a 15-residue repeat. Proc. Natl. Acad. Sci. U. S. A. 101, 17027–17032. https://doi.org/10.1073/pnas.0403069101

Lederer, F.L., Günther, T.J., Raff, J., Pollmann, K., 2011. E. coli filament formation induced by heterologous S-layer expression. Bioeng. Bugs 2, 178–181. https://doi.org/10.4161/bbug.2.3.15418

Levin, P.A., Margolis, P.S., Setlow, P., Losick, R., Sun, D., 1992. Identification of Bacillus subtilis genes for septum placement and shape determination. J. Bacteriol. 174, 6717–6728. https://doi.org/10.1128/jb.174.21.6717-6728.1992

Lin, Y. -S, Kieser, H.M., Hopwood, D.A., Chen, C.W., 1993. The chromosomal DNA of Streptomyces lividans 66 is linear. Mol. Microbiol. 10, 923–933. https://doi.org/10.1111/j.1365-2958.1993.tb00964.x

Loose, M., Mitchison, T.J., 2014. The bacterial cell division proteins ftsA and ftsZ self-organize into dynamic cytoskeletal patterns. Nat. Cell Biol. 16, 38–46. https://doi.org/10.1038/ncb2885

Lupas, a, 1996. Coiled coils: new structures and new functions. Trends Biochem. Sci. 21, 375–382. https://doi.org/10.1016/S0968-0004(96)90126-7

Lupas, A., Van Dyke, M., Stock, J., 1991. Predicting coiled coils from protein sequences. Science (80-.). 252, 1162–1164. https://doi.org/10.1126/science.252.5009.1162

Lutkenhaus, J., 2007. Assembly Dynamics of the Bacterial MinCDE System and Spatial Regulation of the Z Ring. Annu. Rev. Biochem. 76, 539–562. https://doi.org/10.1146/annurev.biochem.75.103004.142652

MacNeil, D.J., Gewain, K.M., Ruby, C.L., Dezeny, G., Gibbons, P.H., MacNeil, T., 1992. Analysis of Streptomyces avermitilis genes required for avermectin biosynthesis utilizing a novel integration vector. Gene 111, 61–68. https://doi.org/10.1016/0378-1119(92)90603-M

Madeira, F., Park, Y.M., Lee, J., Buso, N., Gur, T., Madhusoodanan, N., Basutkar, P., Tivey, A.R.N., Potter, S.C., Finn, R.D., Lopez, R., 2019. The EMBL-EBI search and sequence analysis tools APIs in 2019. Nucleic Acids Res. 47, W636–W641. https://doi.org/10.1093/nar/gkz268

Marston, A.L., Thomaides, H.B., Edwards, D.H., Sharpe, M.E., Errington, J., 1998. Polar localization of the MinD protein of Bacillus subtilis and its role in selection of the mid-cell division site. Genes Dev. 12, 3419–3430. https://doi.org/10.1101/gad.12.21.3419

Mazza, P., Noens, E.E., Schirner, K., Grantcharova, N., Mommaas, A.M., Koerten, H.K., Muth, G., Flärdh, K., Van Wezel, G.P., Wohlleben, W., 2006. MreB of Streptomyces coelicolor is not essential for vegetative growth but is required for the integrity of aerial hyphae and spores. Mol. Microbiol. 60, 838–852. https://doi.org/10.1111/j.1365-2958.2006.05134.x

McCormick, J.R., Flärdh, K., 2012. Signals and regulators that govern Streptomyces development. FEMS Microbiol. Rev. https://doi.org/10.1111/j.1574-6976.2011.00317.x

McCormick, J.R., Su, E.P., Driks, A., Losick, R., 1994. Growth and viability of Streptomyces coelicolor mutant for the cell division gene ftsZ. Mol. Microbiol. 14, 243–254. https://doi.org/10.1111/j.1365-2958.1994.tb01285.x

McIntosh, J.R., Morphew, M.K., Grissom, P.M., Gilbert, S.P., Hoenger, A., 2009. Lattice Structure of Cytoplasmic Microtubules in a Cultured Mammalian Cell. J. Mol. Biol. 394, 177–182. https://doi.org/10.1016/j.jmb.2009.09.033

Meier, M., Padilla, G.P., Herrmann, H., Wedig, T., Hergt, M., Patel, T.R., Stetefeld, J., Aebi, U., Burkhard, P., 2009. Vimentin Coil 1A-A Molecular Switch Involved in the Initiation of Filament Elongation. J. Mol. Biol. 390, 245–261. https://doi.org/10.1016/j.jmb.2009.04.067

Meniche, X., Otten, R., Siegrist, M.S., Baer, C.E., Murphy, K.C., Bertozzi, C.R., Sassetti, C.M., 2014. Subpolar addition of new cell wall is directed by DivIVA in mycobacteria. Proc. Natl. Acad. Sci. U. S. A. 111. https://doi.org/10.1073/pnas.1402158111

Mitchison, T., Kirschner, M., 1984. Dynamic instability of microtubule growth. Nature 312, 237–242. https://doi.org/10.1038/312237a0

Morgenstein, R.M., Bratton, B.P., Nguyen, J.P., Ouzounov, N., Shaevitz, J.W., Gitai, Z., 2015. RodZ links MreB to cell wall synthesis to mediate MreB rotation and robust morphogenesis. Proc. Natl. Acad. Sci. U. S. A. 112, 12510–12515. https://doi.org/10.1073/pnas.1509610112

Morgenstein, R.M., Bratton, B.P., Shaevitz, J.W., Gitai, Z., 2017. RodZ promotes MreB polymer formation and curvature localization to determine the cylindrical uniformity of E. coli shape. bioRxiv. https://doi.org/10.1101/226290

Mukherjee, A., Lutkenhaus, J., 1998. Dynamic assembly of FtsZ regulated by GTP hydrolysis. EMBO J. 17, 462–469. https://doi.org/10.1093/emboj/17.2.462

Mukherjee, A., Lutkenhaus, J., 1994. Guanine nucleotide-dependent assembly of FtsZ into filaments. J. Bacteriol. https://doi.org/10.1128/jb.176.9.2754-2758.1994

Mukherjee, P., Sureka, K., Datta, P., Hossain, T., Barik, S., Das, K.P., Kundu, M., Basu, J., 2009. Novel role of Wag31 in protection of mycobacteria under oxidative stress. Mol. Microbiol. 73, 103–119. https://doi.org/10.1111/j.1365-2958.2009.06750.x

Newman, E.B., Budman, L.I., Chan, E.C., Greene, R.C., Lin, R.T., Woldringh, C.L., D'ari, R., 1998. Lack of S-adenosylmethionine results in a cell division defect in Escherichia coli. J. Bacteriol. 180, 3614–3619.

https://doi.org/10.1128/jb.180.14.3614-3619.1998

Nguyen, L., Scherr, N., Gatfield, J., Walburger, A., Pieters, J., Thompson, C.J., 2007. Antigen 84, an effector of pleiomorphism in Mycobactenum smegmatis. J. Bacteriol. 189, 7896–7910. https://doi.org/10.1128/JB.00726-07

Nicolet, S., Herrmann, H., Aebi, U., Strelkov, S. V., 2010. Atomic structure of vimentin coil 2. J. Struct. Biol. 170, 369–376. https://doi.org/10.1016/j.jsb.2010.02.012

Nogales, E., Downing, K.H., Amos, L.A., Löwe, J., 1998. Tubulin and FtsZ form a distinct family of GTPases. Nat. Struct. Biol. 5, 451–458. https://doi.org/10.1038/nsb0698-451

Oliva, M.A., Halbedel, S., Freund, S.M., Dutow, P., Leonard, T.A., Veprintsev, D.B., Hamoen, L.W., Löwe, J., 2010. Features critical for membrane binding revealed by DivIVA crystal structure. EMBO J. 29, 1988–2001. https://doi.org/10.1038/emboj.2010.99

Olshausen, P. V., Defeu Soufo, H.J., Wicker, K., Heintzmann, R., Graumann, P.L., Rohrbach, A., 2013. Superresolution imaging of dynamic MreB filaments in B. subtilis - A multiple-motor-driven transport? Biophys. J. 105, 1171–1181. https://doi.org/10.1016/j.bpj.2013.07.038

Ouzounov, N., Nguyen, J.P., Bratton, B.P., Jacobowitz, D., Gitai, Z., Shaevitz, J.W., 2016. MreB Orientation Correlates with Cell Diameter in Escherichia coli. Biophys. J. 111, 1035–1043. https://doi.org/10.1016/j.bpj.2016.07.017

Pan, S.H., Malcolm, B. a., 2000. Reduced background expression and improved plasmid stability with pET vectors in BL21 (DE3). Biotechniques 29, 1234–1238. https://doi.org/10.2144/000113156

Parry, D.A.D., 2006. Hendecad repeat in segment 2A and linker L2 of intermediate filament chains implies the possibility of a right-handed coiled-coil structure. J. Struct. Biol. 155, 370–4. https://doi.org/10.1016/j.jsb.2006.03.017

Parry, D.A.D., Steinert, P.M., 1999. Intermediate filaments: Molecular architecture,

assembly, dynamics and polymorphism. Q. Rev. Biophys. https://doi.org/10.1017/S0033583500003516

Parry, D.A.D., Steinert, P.M., 1992. Intermediate filament structure. Curr. Opin. Cell Biol. 4, 94–98. https://doi.org/10.1016/0955-0674(92)90064-J

Pauling, L., Corey, R.B., 1951. Configurations of Polypeptide Chains With Favored Orientations Around Single Bonds: Two New Pleated Sheets. Proc. Natl. Acad. Sci. U. S. A. 37, 729–40. https://doi.org/10.1073/pnas.37.11.729

Petersen, B., Petersen, T.N., Andersen, P., Nielsen, M., Lundegaard, C., 2009. A generic method for assignment of reliability scores applied to solvent accessibility predictions. BMC Struct. Biol. 9. https://doi.org/10.1186/1472-6807-9-51

Pichoff, S., Lutkenhaus, J., 2005. Tethering the Z ring to the membrane through a conserved membrane targeting sequence in FtsA. Mol. Microbiol. 55, 1722–1734. https://doi.org/10.1111/j.1365-2958.2005.04522.x

Pichoff, S., Lutkenhaus, J., 2002. Unique and overlapping roles for ZipA and FtsA in septal ring assembly in Escherichia coli. EMBO J. 21, 685–693. https://doi.org/10.1093/emboj/21.4.685

Pilhofer, M., Ladinsky, M.S., McDowall, A.W., Petroni, G., Jensen, G.J., 2011. Microtubules in Bacteria: Ancient tubulins build a five-protofilament homolog of the eukaryotic cytoskeleton. PLoS Biol. 9. https://doi.org/10.1371/journal.pbio.1001213

Pollard, T.D., Borisy, G.G., 2003. Cellular motility driven by assembly and disassembly of actin filaments. Cell. https://doi.org/10.1016/S0092-8674(03)00120-X

Redenbach, M., Kieser, H.M., Denapaite, D., Eichner, A., Cullum, J., Kinashi, H., Hopwood, D.A., 1996. A set of ordered cosmids and a detailed genetic and physical map for the 8 Mb Streptomyces coelicolor A3(2) chromosome. Mol. Microbiol. 21, 77–96. https://doi.org/10.1046/j.1365-2958.1996.6191336.x

Reimold, C., Soufo, H.J.D., Dempwolff, F., Graumann, P.L., 2013. Motion of variable-length MreB filaments at the bacterial cell membrane influences cell morphology. Mol. Biol. Cell 24, 2340–2349. https://doi.org/10.1091/mbc.E12-10-0728

Rodrigues, C.D.A., Harry, E.J., 2012. The min system and nucleoid occlusion are not required for identifying the division site in bacillus subtilis but ensure its efficient utilization. PLoS Genet. 8. https://doi.org/10.1371/journal.pgen.1002561

Rogers, K.R., Eckelt, A., Nimmrich, V., Janssen, K.P., Schliwa, M., Herrmann, H., Franke, W.W., 1995. Truncation mutagenesis of the non-alpha-helical carboxyterminal tail domain of vimentin reveals contributions to cellular localization but not to filament assembly. Eur J Cell Biol 66, 136–150.

Romberg, L., Levin, P.A., Drive, O.B., 2017. Poised at the Edge of Stability. Annu. Rev. Microbiol. 57, 125–154. https://doi.org/10.1146/annurev.micro.57.012903.074300.Assembly

Salje, J., van den Ent, F., de Boer, P., Löwe, J., 2011. Direct Membrane Binding by Bacterial Actin MreB. Mol. Cell 43, 478–487. https://doi.org/10.1016/j.molcel.2011.07.008

Santos-Beneit, F., Roberts, D.M., Cantlay, S., McCormick, J.R., Errington, J., 2017. A mechanism for FtsZ-independent proliferation in Streptomyces. Nat. Commun. 8. https://doi.org/10.1038/s41467-017-01596-z

Sasse, B., Lustig, a, Aebi, U., Stuurman, N., 1997. In vitro assembly of Drosophila lamin Dm0--lamin polymerization properties are conserved. Eur. J. Biochem. 250, 30–8.

Schlicke, M., Brakmann, S., 2005. Expression and purification of histidine-tagged bacteriophage T7 DNA polymerase. Protein Expr. Purif. 39, 247–253. https://doi.org/10.1016/j.pep.2004.10.022

Schmidt, A., Hall, M.N., 1998. Signaling to the actin cytoskeleton. Annu. Rev. Cell Dev. Biol. https://doi.org/10.1146/annurev.cellbio.14.1.305

Schwedock, J., McCormick, J.R., Angert, E.R., Nodwell, J.R., Losick, R., 1997. Assembly of the cell division protein FtsZ into ladder-like structures in the aerial hyphae of *Streptomyces coelicolor*. Mol. Microbiol. 25, 847–858. https://doi.org/10.1111/j.1365-2958.1997.mmi507.x

Shaner, N.C., Campbell, R.E., Steinbach, P.A., Giepmans, B.N.G., Palmer, A.E., Tsien, R.Y., 2004. Improved monomeric red, orange and yellow fluorescent proteins derived from Discosoma sp. red fluorescent protein. Nat. Biotechnol. 22, 1567–1572. https://doi.org/10.1038/nbt1037

Shi, H., Bratton, B.P., Gitai, Z., Huang, K.C., 2018. How to Build a Bacterial Cell: MreB as the Foreman of E. coli Construction. Cell. https://doi.org/10.1016/j.cell.2018.02.050

Shi, H., Colavin, A., Bigos, M., Tropini, C., Monds, R.D., Huang, K.C., 2017. Deep Phenotypic Mapping of Bacterial Cytoskeletal Mutants Reveals Physiological Robustness to Cell Size. Curr. Biol. 27, 3419–3429.e4. https://doi.org/10.1016/j.cub.2017.09.065

Sieger, B., Schubert, K., Donovan, C., Bramkamp, M., 2013. The lipid II flippase RodA determines morphology and growth in Corynebacterium glutamicum. Mol. Microbiol. 90, 966–982. https://doi.org/10.1111/mmi.12411

Smith, T.A., Strelkov, S. V., Burkhard, P., Aebi, U., Parry, D.A.D., 2002. Sequence comparisons of intermediate filament chains: Evidence of a unique functional/structural role for coiled-coil segment 1A and linker L1, in: Journal of Structural Biology. pp. 128–145. https://doi.org/10.1006/jsbi.2002.4438

Soellner, P., Quinlan, R.A., Franke, W.W., 1985. Identification of a distinct soluble subunit of an intermediate filament protein: Tetrameric vimentin from living cells. Proc. Natl. Acad. Sci. U. S. A. 82, 7929–7933. https://doi.org/10.1073/pnas.82.23.7929

Stanton, R.A., Gernert, K.M., Nettles, J.H., Aneja, R., 2011. Drugs that target dynamic microtubules: A new molecular perspective. Med. Res. Rev. 31, 443–481. https://doi.org/10.1002/med.20242

Strauss, M.P., Liew, A.T.F., Turnbull, L., Whitchurch, C.B., Monahan, L.G., Harry, E.J., 2012. 3D-SIM Super Resolution Microscopy Reveals a Bead-Like Arrangement for FtsZ and the Division Machinery: Implications for Triggering Cytokinesis. PLoS Biol. 10. https://doi.org/10.1371/journal.pbio.1001389

Strelkov, S. V., Herrmann, H., Geisler, N., Lustig, A., Ivaninskii, S., Zimbelmann, R., Burkhard, P., Aebi, U., 2001. Divide-and-conquer crystallographic approach towards an atomic structure of intermediate filaments. J. Mol. Biol. 306, 773–781. https://doi.org/10.1006/jmbi.2001.4442

Strelkov, S. V., Herrmann, H., Geisler, N., Wedig, T., Zimbelmann, R., Aebi, U., Burkhard, P., 2002. Conserved segments 1A and 2B of the intermediate filament dimer: Their atomic structures and role in filament assembly. EMBO J. 21, 1255–1266. https://doi.org/10.1093/emboj/21.6.1255

Strelkov, S. V, Herrmann, H., Aebi, U., 2003. Molecular architecture of intermediate filaments. Bioessays 25, 243–51. https://doi.org/10.1002/bies.10246

Studier, F.W., Moffatt, B.A., 1986. Use of bacteriophage T7 RNA polymerase to direct selective high-level expression of cloned genes. J. Mol. Biol. 189, 113–130. https://doi.org/10.1016/0022-2836(86)90385-2

Stuurman, N., Heins, S., Aebi, U., 1998. Nuclear lamins: Their structure, assembly, and interactions. J. Struct. Biol. 122, 42–66. https://doi.org/10.1006/jsbi.1998.3987

Stuurman, N., Sasse, B., Fisher, P. a, 1996. Intermediate filament protein polymerization: molecular analysis of Drosophila nuclear lamin head-to-tail binding. J. Struct. Biol. 117, 1–15. https://doi.org/10.1006/jsbi.1996.0064

Sui, H., Downing, K.H., 2010. Structural basis of interprotofilament interaction and lateral deformation of microtubules. Structure 18, 1022–1031. https://doi.org/10.1016/j.str.2010.05.010

Swiss Institute of Bioinformatics, 2015. ExPASy - Compute pI/Mw tool. ExPASy Bioinforma. Resour. Portal.

Swulius, M.T., Chen, S., Jane Ding, H., Li, Z., Briegel, A., Pilhofer, M., Tocheva, E.I., Lybarger, S.R., Johnson, T.L., Sandkvist, M., Jensen, G.J., 2011. Long helical filaments are not seen encircling cells in electron cryotomograms of rod-shaped bacteria. Biochem. Biophys. Res. Commun. 407, 650–655. https://doi.org/10.1016/j.bbrc.2011.03.062

Szwedziak, P., Wang, Q., Freund, S.M., Löwe, J., 2012. FtsA forms actin-like protofilaments. EMBO J. 31, 2249–2260. https://doi.org/10.1038/emboj.2012.76

Takeuchi, S., Diluzio, W.R., Weibel, D.B., Whitesides, G.M., 2005. Controlling the shape of filamentous cells of Escherichia coli. Nano Lett. 5, 1819–1823. https://doi.org/10.1021/nl0507360

The International Pharmacopoeia, 2015. 19th WHO Model List of Essential Medicines. Http://Www.Who.Int/Medicines/Publications/Essentialmedicines/En. https://doi.org/10.1016/S1473-3099(14)70780-7

Tonthat, N.K., Milam, S.L., Chinnam, N., Whitfill, T., Margolin, W., Schumacher, M.A., 2013. SlmA forms a higher-order structure on DNA that inhibits cytokinetic Z-ring formation over the nucleoid. Proc. Natl. Acad. Sci. U. S. A. 110, 10586–10591. https://doi.org/10.1073/pnas.1221036110

Ultee, E., Briegel, A., Claessen, D., 2020. Formation of wall-less cells in Kitasatospora viridifaciens requires cytoskeletal protein FilP in oxygen-limiting conditions. bioRxiv 2020.05.26.116947. https://doi.org/10.1101/2020.05.26.116947

van den Ent, F., Amos, L.A., Löwe, J., 2001. Prokaryotic origin of the actin cytoskeleton. Nature 413, 39–44. https://doi.org/10.1038/35092500

Van den Ent, F., Amos, L.A., Löwe, J., 2001. Prokaryotic origin of the actin cytoskeleton. Nature 413, 39–44. https://doi.org/10.1038/35092500

van den Ent, F., Izoré, T., Bharat, T.A.M., Johnson, C.M., Löwe, J., 2014. Bacterial actin MreB forms antiparallel double filaments. Elife 2014.

https://doi.org/10.7554/eLife.02634

Van Teeffelen, S., Wang, S., Furchtgott, L., Huang, K.C., Wingreen, N.S., Shaevitz, J.W., Gitai, Z., 2011. The bacterial actin MreB rotates, and rotation depends on cell-wall assembly. Proc. Natl. Acad. Sci. U. S. A. 108, 15822–15827. https://doi.org/10.1073/pnas.1108999108

Varley, A.W., Stewart, G.C., 1992. The divIVB region of the Bacillus subtilis chromosome encodes homologs of Escherichia coli septum placement (MinCD) and cell shape (MreBCD) determinants. J. Bacteriol. 174, 6729–6742. https://doi.org/10.1128/jb.174.21.6729-6742.1992

Vollmer, W., Blanot, D., De Pedro, M.A., 2008. Peptidoglycan structure and architecture. FEMS Microbiol. Rev. https://doi.org/10.1111/j.1574-6976.2007.00094.x

Wachi, M., Doi, M., Tamaki, S., Park, W., Nakajima-Iijima, S., Matsuhashi, M., 1987. Mutant isolation and molecular cloning of mre genes, which determine cell shape, sensitivity to mecillinam, and amount of penicillin-binding proteins in Escherichia coli. J. Bacteriol. 169, 4935–4940. https://doi.org/10.1073/pnas.0921

Walshaw, J., Gillespie, M.D., Kelemen, G.H., 2010. A novel coiled-coil repeat variant in a class of bacterial cytoskeletal proteins. J. Struct. Biol. 170, 202–215. https://doi.org/10.1016/j.jsb.2010.02.008

Walter, S., Rohde, M., Machner, M., Schrempf, H., 1999. Electron microscopy studies of cell-wall-anchored cellulose (Avicel)- binding protein (AbpS) from Streptomyces reticuli. Appl. Environ. Microbiol. 65, 886–892. https://doi.org/10.1128/aem.65.3.886-892.1999

Walter, S., Schrempf, H., 2003. Oligomerization, membrane anchoring, and cellulose-binding characteristics of AbpS, a receptor-like Streptomyces protein. J. Biol. Chem. 278, 26639–26647. https://doi.org/10.1074/jbc.M212792200

Walter, S., Wellmann, E., Schrempf, H., 1998. The cell wall-anchored Streptomyces reticuli Avicel-binding protein (AbpS) and its gene. J. Bacteriol. 180, 1647–

1654.

Wang, S., Arellano-Santoyo, H., Combs, P.A., Shaevitz, J.W., 2010. Actin-like cytoskeleton filaments contribute to cell mechanics in bacteria. Proc. Natl. Acad. Sci. U. S. A. 107, 9182–9185. https://doi.org/10.1073/pnas.0911517107

Wang, S., Arends, S.J.R., Weiss, D.S., Newman, E.B., 2005. A deficiency in S-adenosylmethionine synthetase interrupts assembly of the septal ring in Escherichia coli K-12. Mol. Microbiol. 58, 791–799. https://doi.org/10.1111/j.1365-2958.2005.04864.x

Wang, X., Lutkenhaus, J., 1996. FtsZ ring: The eubacterial division apparatus conserved in archaebacteria. Mol. Microbiol. 21, 313–320. https://doi.org/10.1046/j.1365-2958.1996.6421360.x

Who, 2013. Global Tuberculosis Report 2013. World Heal. Organ. 306. https://doi.org/10.3917/spub.092.0139

Wiche, G., 1998. Role of plectin in cytoskeleton organization and dynamics. J. Cell Sci. 111, 2477–2486. https://doi.org/10.1096/fj.08-124453

Williams, D.B., Carter, C.B., 1996. The Transmission Electron Microscopy, in: Transmission Electron Microscopy. pp. 3–17.

Wu, L.J., Errington, J., 2012. Nucleoid occlusion and bacterial cell division. Nat. Rev. Microbiol. 10, 8–12. https://doi.org/10.1038/nrmicro2671

Wu, L.J., Errington, J., 2004. Coordination of cell division and chromosome segregation by a nucleoid occlusion protein in Bacillus subtilis. Cell 117, 915–925. https://doi.org/10.1016/j.cell.2004.06.002

Yang, X., Lyu, Z., Miguel, A., McQuillen, R., Huang, K.C., Xiao, J., 2017. GTPase activity-coupled treadmilling of the bacterial tubulin FtsZ organizes septal cell wall synthesis. Science (80-.). 355, 744–747. https://doi.org/10.1126/science.aak9995

Yao, Q., Jewett, A.I., Chang, Y., Oikonomou, C.M., Beeby, M., Iancu, C. V, Briegel, A., Ghosal, D., Jensen, G.J., 2017. Short FtsZ filaments can drive asymmetric cell

envelope constriction at the onset of bacterial cytokinesis. EMBO J. 36, 1577–1589. https://doi.org/10.15252/embj.201696235

Yu, X.C., Margolin, W., 1999. FtsZ ring clusters in min and partition mutants: Role of both the Min system and the nucleoid in regulating FtsZ ring localization. Mol. Microbiol. 32, 315–326. https://doi.org/10.1046/j.1365-2958.1999.01351.x

Yu, Y., Zhou, J., Gueiros-Filho, F.J., Kearns, D.B., Jacobson, S.C., 2021. Noc corrals migration of FtsZ protofilaments during cytokinesis in bacillus subtilis. MBio 12, 1–14. https://doi.org/10.1128/mBio.02964-20

Zhang, L., Willemse, J., Claessen, D., Van Wezel, G.P., 2016. SepG coordinates sporulation-specific cell division and nucleoid organization in Streptomyces coelicolor. Open Biol. 6. https://doi.org/10.1098/rsob.150164

Zwerger, M., Jaalouk, D.E., Lombardi, M.L., Isermann, P., Mauermann, M., Dialynas, G., Herrmann, H., Wallrath, L., Lammerding, J., 2013. Myopathic lamin mutations impair nuclear stability in cells and tissue and disrupt nucleo-cytoskeletal coupling. Hum. Mol. Genet. 22, 2335–2349. https://doi.org/10.1093/hmg/ddt079